Resource Allocation and Adaptive Antennas in Cellular Communications

by

Paulo Cardieri

Dissertation submitted to the Faculty
of the Virginia Polytechnic Institute and State University
in partial fulfillment of the requirements for the degree of

Doctor of Philosophy
in
Electrical and Computer Engineering

Committee:

Theodore S. Rappaport (Chairman)
Jeff H. Reed
Ahmad Safaai-Jazi
William H. Tranter
Brian D. Woerner
Werner Kohler - Department of Mathematics
Norman C. Beaulieu - Queen's University - Canada

September 15, 2000
Blacksburg, Virginia

Keywords: Resource Allocation, Channel Allocation, Adaptive Antennas, Power Control, Simulation of Cellular Networks, Log-normal Distribution.

Resource Allocation and Adaptive Antennas in Cellular Communications

Paulo Cardieri

(ABSTRACT)

The rapid growth in demand for cellular mobile communications and emerging fixed wireless access has created the need to increase system capacity through more efficient utilization of the frequency spectrum, and the need for better grade of service. In cellular systems, capacity improvement can be achieved by reducing co-channel interference. Several techniques have been proposed in literature for mitigating co-channel interference, such as adaptive antennas and power control. Also, by allocating transmitter power and communication channels efficiently (resource allocation), overall co-channel interference can be maintained below a desired maximum tolerable level, while maximizing the carried traffic of the system.

This dissertation presents investigation results on the performance of base station adaptive antennas, power control and channel allocation, as techniques for capacity improvement. Several approaches are analyzed. Firstly, we study the combined use of adaptive antennas and fractional loading factor, in order to estimate the potential capacity improvement achieved by adaptive antennas.

Next, an extensive simulation analysis of a cellular network is carried out aiming to investigate the complex interrelationship between power control, channel allocation and adaptive antennas. In the first part of this simulation analysis, the combined use of adaptive antennas, power control and reduced cluster size is analyzed in a cellular system using fixed channel allocation. In the second part, we analyze the benefits of combining adaptive antennas, dynamic channel allocation and power control. Two representative channel allocation algorithms are considered and analyzed regarding how efficiently they transform reduced co-channel interference into higher carried traffic. Finally, the spatial filtering capability of adaptive antennas is used to allow several users to share the same channel within the same cell. Several allocation algorithms combined with power control are analyzed.

Funded by the Conselho Nacional de Desenvolvimento Científico e Tecnológico (CNPq) of Brazil and MPRG Affiliates Program.

Acknowledgments

I could not have completed my dissertation without the support and help from several people. First, my sincere appreciation goes to my advisor, Professor Theodore S. Rappaport, who has provided invaluable support and encouragement over the past several years. I also would like to thank my committee members for their help and support.

I wish to express my gratitude to all my friends and colleagues in the Mobile and Portable Radio Research Group, for creating a friendly and stimulating atmosphere, especially to Hao Xu, Christos Kontogeorgakis, Greg Durgin, Max Robert, Neiyer Correal, Neal Patwari, Praveen Sheethalnath, Vikas Kukshya, Jason Aron, Ben Henty and Narayan Iyengar. In addition to students, I would like to thank all the staff and associates of MPRG. Especially, I would like to thank the assistance of Aurelia Scharnhorst and Cindy Reifsnider.

Financial support from Conselho Nacional de Desenvolvimento Científico e Tecnológico (CNPq) of Brazil, and MPRG Industrial Affiliates program is gratefully acknowledged. Without this funding, it would not have been possible to complete this dissertation. I also wish to thank the constant support from Fundação Centro de Pesquisa e Desenvolvimento (CPqD), from Brazil.

Most of all, I would like to thank my mother Nilze, my father Sebastião, my sisters Elisabete and Miriam, my brother Sergio and my lovely fiancee Monica, for their continuous encouragement, understanding and unfailing support.

Contents

List of Figures

List of Tables

Chapter 1

Introduction

1.1 Cellular Communication System

The rapid growth in demand for cellular mobile communications and emerging fixed wireless access have created the need to increase system capacity through more efficient utilization of the frequency spectrum, and the need for better grade of service. Even though cellular systems using different access techniques (such as FDMA, TDMA and CDMA) differ from each other in several key aspects, all cellular systems have in common the fundamental *tradeoff between system capacity and link quality*, which can be exploited to increase the system capacity. System capacity refers to the amount of traffic a system can handle. Link quality is usually measured in terms of *bit error rate* (*BER*), in digital systems, or the ratio of desired signal to interference signal (*SIR*). Before discussing how capacity in cellular systems can be improved, a brief description of the most common access techniques is presented.

In analog systems, such as AMPS [1], FDMA (Frequency Division Multiple Access) is used and the entire spectrum allocated to the service area is divided into channels of appropriate bandwidth, and users transmit on different frequencies. In AMPS, for example, voice channels have a bandwidth of 30 kHz. Channel reuse is employed in order to increase system capacity, as described subsequently. In TDMA (Time Division Multiple Access), used in digital system, such as IS-136 and GSM [1], the entire spectrum is divided into channels, as in FDMA systems. However, in TDMA systems, several users can use the same frequency channel. Each user is assigned a time-slot of a frame and transmits its time-slot at a given time. For example, in the IS-136 digital system, channels have a bandwidth of 30 kHz, and a single channel can support up to three users (three time-slots per frame). As

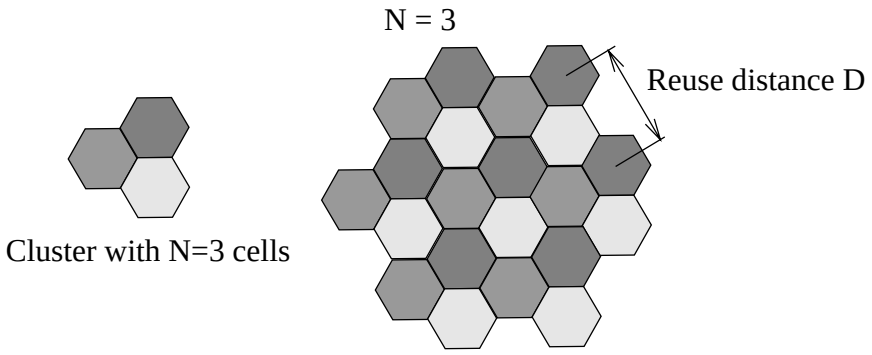

Figure 1.1: Cell clustering in cellular communication systems: Cluster with $N = 3$ cells.

in FDMA, channels and time-slots in TDMA systems are reused over the coverage area in order to improve system capacity. In CDMA systems, such as IS-95 [1], which are based on spread spectrum transmission, all users within a cell share the same frequency band at the same time and the users are separated by assigning them different spreading codes [1].

Therefore, all access techniques have in common that capacity improvement is achieved by reusing channels throughout the entire service area. Channel reuse, however, creates *co-channel interference*. A link using a particular channel in a cell, interferes with other links reusing that particular channel, degrading transmission quality. Thus, it is well accepted that capacity of cellular systems is interference limited, as discussed next.

In TDMA and FDMA systems, adjacent cells of the service area are grouped into clusters of an appropriate number N of cells [1], as shown in Figure 1.1 for cluster size $N = 3$. The entire set of channels available in the system is divided into N subsets of channels, and each subset is assigned to a cell in the cluster. As this pattern is replicated over all clusters in the coverage area, channels are reused, increasing system capacity and creating co-channel interference. The shortest distance between the centers of two cells sharing a given channel is called *reuse distance* D. For hexagonal shape for the cells, $D = \sqrt{3N}R$, where R is the cell radius [1]. Therefore, the smaller the cell cluster size N, the larger the number of channels available in the cell, which means higher maximum carried traffic. However, reduction in cell cluster size increases co-channel interference, since the reuse distance D decreases. A straightforward technique for increasing system capacity is to decrease cell cluster size, while controlling the increased co-channel interference.

The approach for assigning channels to cells described above is called *fixed channel assignment*. A base station can assign to calls only channels from its subset of channels. Fixed channel assignment guarantees that a call served on any channel of a given subset of channels

will present a link quality above the performance specification. The performance specification refers to the minimum tolerable ratio of desired signal to co-channel interference (*SIR*). Therefore, reuse distance in fixed channel allocation is defined on a subset of channels basis.

Since the desired and interference signals vary within the cell, due to shadow fading, user mobility, etc, many calls will have *SIR* larger than the minimum tolerable, while other calls will have lower *SIR*. Calls experiencing high *SIR* could be allocated channels with smaller reuse distance. A *dynamic channel allocation* technique based on interference level can be used to allocate channels to calls such that the reuse distance is minimized and, consequently, improving system capacity.

It is clear that, in both fixed or dynamic channel allocation scenarios for TDMA and FDMA systems, reduction in co-channel interference can be traded for capacity enhancement, that is, for more users in the system.

In CDMA system (Code Division Multiple Access), as mentioned before, all users transmit on the same wideband channel and each user is assigned a spreading code [1]. Therefore, each user adds to the total interference in the system, and system capacity is limited by the interference produced by in-cell co-channel users. As for TDMA/FDMA systems, system capacity in CDMA system can be enhanced by mitigating co-channel interference.

As one can expect, all access techniques have in common that the transmitted power plays an important role in the total co-channel interference. Excessive transmitted power only adds to the interference with users sharing the same channel. Therefore, along with the communication channel set, transmitted power is an important *resource* in cellular system, since the allocation strategy adopted affects the overall system capacity.

We conclude that, regardless of the access technique used, co-channel interference reduction in wireless cellular systems can be traded for capacity improvement. Two approaches can be used for controlling co-channel interference: In the first approach, the interference produced by a link with other co-channel links is mitigated. For example, base station adaptive antennas (narrow beam antennas) can significantly mitigate co-channel interference. By steering narrowbeams toward the desired users and significantly low antenna gains toward the undesired users, the overall co-channel interference can be reduced.

In the second approach, resources in a cellular system, namely transmitted power and communication channels, are appropriately allocated, such that the overall interference is maintained below a desired maximum tolerable level, while maximizing the carried traffic in the system

In this dissertation, the interrelationship between resource allocation algorithms, namely power control and channel allocation, and adaptive antennas is investigated. Power control and channel allocation have been extensively studied for application in cellular systems. Also, it is well known that adaptive antennas are efficient techniques for reducing co-channel interference. However, little has been done aiming to investigate how power control, channel allocation and adaptive antennas interrelate to each other. In a combined application of power control, adaptive antennas, channel allocation, the role of adaptive antennas and power control is to reduce co-channel interference, allowing channels to be reused more often throughout the entire cellular system. Dynamic channel allocation algorithms, on the other hand, attempts to organize the channel reuse. Reduced co-channel interference, provided by the use of adaptive antennas or power control, is expected to help the channel allocation algorithm to allocate channels more efficiently. In this dissertation, we investigate, by extensive simulation, how efficiently channel allocation algorithms transform reduced interference into higher carried traffic.

Most of the studies carried out on application of resource allocation algorithms (such as power control and channel allocation) use the resulting capacity improvement, in terms of carried traffic, as a measure of the performance of such algorithms. Capacity improvement is, in fact, an important performance measure of resource allocation algorithms. However, a detailed analysis of such algorithms and their combination, reveals that there is always a price to be paid for capacity improvement. In general, capacity improvement is at the expense of degradation of other performance parameters, such as the number of required intracell handoffs. In this dissertation we also investigate the negative side effects of resource allocations algorithms and their combinations.

1.2 Outline

The remainder of this dissertation is organized as follows. Chapter 2 introduces adaptive antennas in mobile communications. The benefits of adaptive antennas in mobile communications are briefly discussed, followed by an introduction to optimal beamforming techniques. Since the operation of adaptive antennas is based on spatial filtering, spatial properties of wireless communications channels are also discussed in this chapter. Macrocell and microcell spatial channel models are presented. Based on spatial filtering properties of adaptive antennas, co-channel interference reduction and the consequent system capacity improvement are

discussed. Some representative studies on capacity improvement using adaptive antennas in TDMA, FDMA and CDMA cellular systems are reviewed.

A statistical analysis of co-channel interference in mobile communications is presented in Chapter 3. The total cochannel interference signal received at a given location is generally modeled as a sum of lognormally distributed signals [1, 2]. It is well accepted that the distribution of a sum of lognormally distributed random variables can be approximated by a log-normal distribution. We analyze the accuracy of two methods for computing the mean value and standard deviation of a sum of log-normal random variables, namely Fenton-Wilkinson's and Schwartz & Yeh's methods, when the summands (individual interference signals) have different mean values and standard deviations.

In Chapter 4, we analyze the effectiveness of reducing co-channel interference using *narrowbeam adaptive antennas* with the *fractional loading factor*. As discussed in Chapter 2, narrowbeam adaptive antennas mitigate co-channel interference by steering narrow beams in the direction of the desired mobile stations, and significant side lobe attenuation in the direction of undesired users. The fractional loading factor technique exploits the fact that interference is related to the loading factor, p_{ch}, which defines the probability that a given channel is in use within a cell. As shown in Chapter 4, it is possible to increase capacity by manyfold, by decreasing the cluster size (i.e. increasing frequency reuse), although the proper combination of antenna specifications and fractional loading are surprisingly non-intuitive. We show that large capacity gains with respect to a reference cellular system ($N = 7$, 3 sectors per cell) can be obtained by combining narrowbeam antennas and a fractional loading factor.

In Chapter 6, we discuss important aspects of channel allocation and power control, from system capacity improvement perspectives. We also present an extensive literature search on joint power control and channel allocation. Representative works on combined power control and adaptive antennas and channel allocation strategies combined with adaptive antennas are also presented.

In the remaining chapters of this dissertation, we concentrate on an extensive simulation analysis of combined use of power control, adaptive antennas and channel allocation algorithms.

In Chapter 7, we describe the main features of the cellular network simulation used in the analysis presented in the subsequent Chapters 8 through 10.

Chapter 8 presents results of performance analysis of a cellular system using fixed channel

allocation, base station adaptive antennas, power control and reduced cluster size. Cluster size reduction increases the number of channels allocated to each cell, but degrades the link quality, due to high co-channel interference levels. Adaptive antennas and power control are then used to mitigate the increased interference. Simulation results show that the use of power control allows the use of a less complex antenna required to achieve a given capacity improvement.

In Chapter 9, we analyze the benefits of combining adaptive antennas, dynamic channel allocation and power control. We will focus our attention on dynamic channel allocation algorithms based on interference. The performance of such algorithms depends on the level of interference experienced by the channels. By combining channel allocation with interference reduction techniques, such as adaptive antennas and power control, one expects to improve the performance of such allocation algorithms. Different channel allocation strategies transform the reduced interference into higher carried traffic in different ways. This chapter aims to analyze how efficiently two representative channel allocation algorithms transform the reduced interference level into higher carried traffic and higher performance.

The spatial filtering capability of adaptive antennas can be used to allow several users to share the same channel within the same cell, using the so called *Spatial Division Multiple Access Technique* (SDMA). It is well known that the channel allocation strategy used in SDMA systems plays an important role in the performance of such systems. In Chapter 10, we present the analysis of some representative allocation algorithms for SDMA systems. Some of the algorithms analyzed are specially designed for SDMA systems, while others do not explicitly exploit the SDMA mechanism. Also, we analyze the performance of such allocation algorithms when power control is used.

Finally, Chapter 11 summarizes the contributions of this dissertation and outlines future areas to be investigated.

Chapter 2

Adaptive Antennas in Cellular Communication Systems

2.1 Introduction

Adaptive antennas for cellular systems can significantly increase system capacity and improve performance. As we will see in this chapter, adaptive antennas can reduce co-channel interference, which can be traded for system capacity improvement. The benefits of adaptive antennas are based on spatial filtering and the performance of such antennas is highly dependent on the spatial characteristics of the radio propagation channel.

This chapter aims to review the basic concepts of array antennas and beamforming techniques. We also review spatial channel models and describe the differences between macrocell and microcell environments from the point of view of spatial channel models. Finally, some representative studies on capacity improvement using adaptive antennas are reviewed and discussed.

2.2 Performance Improvement Using an Array Antenna

Before introducing the concepts of adaptive antennas and beamforming, we briefly describe the performance improvement using array antennas in cellular communication systems.

- *Reduction in Co-channel Interference*

  In the transmit mode, base station adaptive antennas can focus radiated energy in

the region the desired mobile is located, reducing the interference in other directions. Also, nulls can be steered towards co-channel mobiles, providing further reduction in co-channel interference. In the receive mode, a high antenna gain can be steered toward the desired signal, reducing the interference received from other co-channel mobiles. Note that, in both modes, some information about the desired mobile is required, such as its location. In the receive mode, a reference signal correlated with the transmitted signal by the mobile can also be used to determine the mobile location.

- *System Capacity Improvement*

  System capacity refers to the amount of traffic a given system can handle. System capacity can be improved by using adaptive antennas, based on two approaches. In the first approach, the reduction in co-channel interference due to the use of base station adaptive antennas can be traded for more users in the cell. For example, in TDMA/FDMA systems, the reduction in co-channel interference may be sufficient to allow cluster size reduction, increasing the number of channels per cell. In CDMA systems, the use of adaptive antennas allows users to transmit less power, reducing the multiple access interference, which, in turn, increases the number of users in the cell.

  In the second approach, a base station adaptive antenna can be used to *create* additional channels in the cell, by spatial filtering. By steering narrow beams towards mobiles, in-cell mobiles can share the same channel, provided that they are sufficiently distant (in angle) from each other. This technique is often called *Spatial Division Multiple Access* (SDMA) and is discussed in Chapter 6.

  Results of studies on capacity improvement based on both approaches are discussed in Section 2.6.

- *Reduction in Delay Spread*

  By forming narrow beams in certain directions and nulls in others, adaptive antennas can reduce delay spread. In the receive mode, when a beam is steered towards the main signal, multipath components impinging upon the antenna from directions other than the direction of the main signal are attenuated. In the transmit mode, the energy is focused in the desired direction, reducing multipath reflections that cause the delay spread.

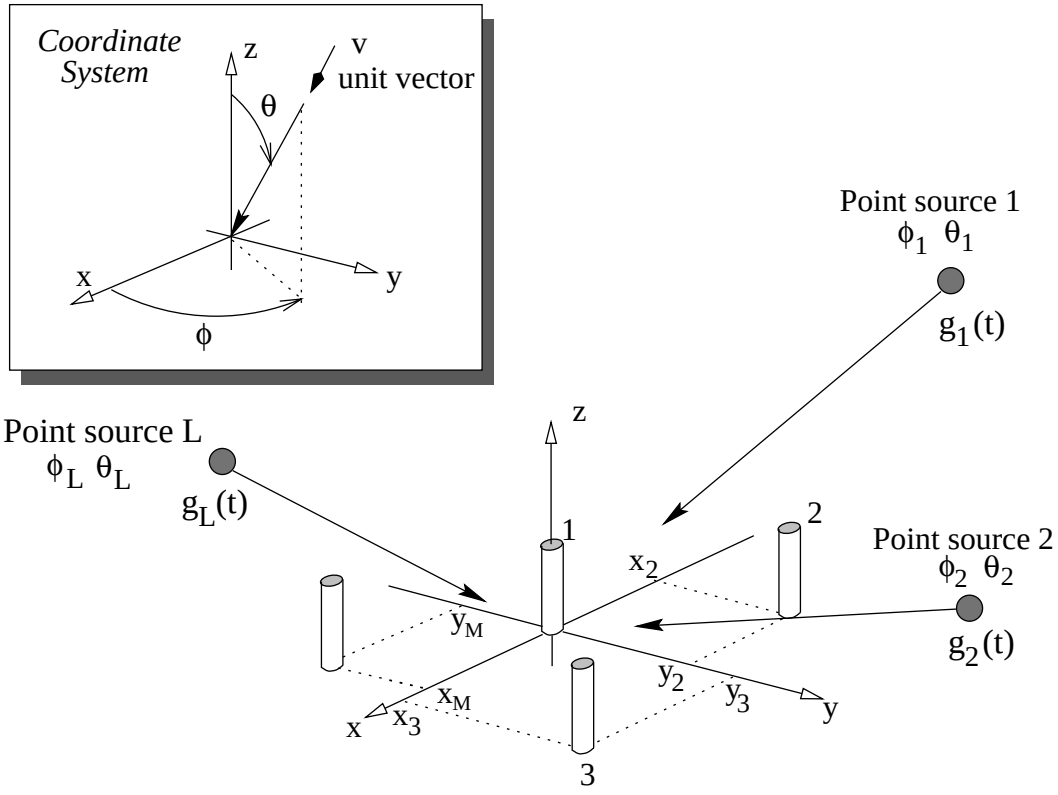

Figure 2.1: Antenna Array with M elements in a media of L point sources.

2.3 Beamforming Techniques

2.3.1 Signal Model

We present in this section a brief description of the basic concepts of array antennas and beamforming, following Godara in [14].

Consider an array of M omnidirectional elements in the far field of L uncorrelated point sources of frequency f_0, as shown in Figure 2.1. Assume that the origin of the coordinate system corresponds to the *time reference*, so that the plane wave from the l-th source in direction (ϕ_l, θ_l) reaches the origin at time $t = 0$. Therefore, the same plane wave impinges upon the m-th element at time $\tau_{m,l}$

$$\tau_{m,l} = \frac{\mathbf{u}_m \cdot \mathbf{v}(\phi_l, \theta_l)}{c}, \tag{2.1}$$

where $\cdot$ represents the inner product, $\mathbf{u}_m$ is the position vector of the m-th element, $\mathbf{v}(\phi_l, \theta_l)$ is the unit vector in direction (ϕ_l, θ_l) and c is the speed of light. Using rectangular coordinates,

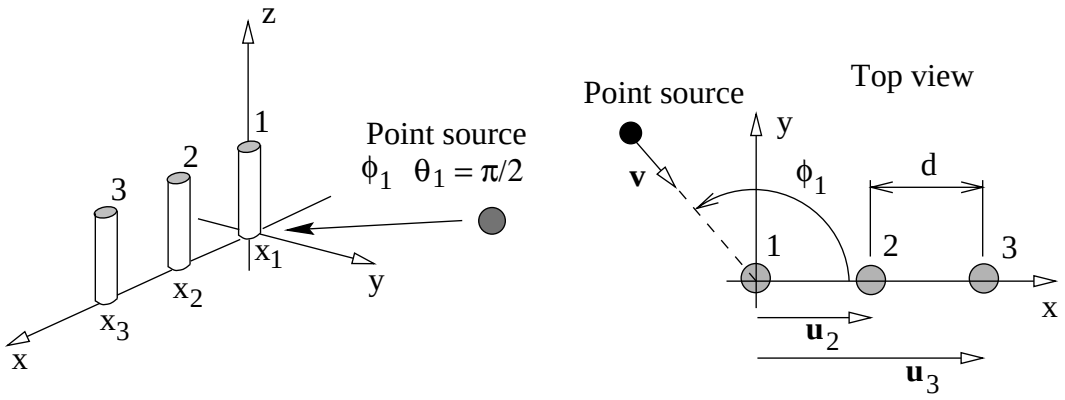

Figure 2.2: Three-element linear array.

we have:

$$\mathbf{v}(\phi_l, \theta_l) = \cos\phi_l \ \sin\theta_l \ \hat{x} + \sin\phi_l \ \sin\theta_l \ \hat{y} + \cos\theta_l \ \hat{z}, \tag{2.2}$$

and

$$\mathbf{u}_m = x_m \ \hat{x} + y_m \ \hat{y} + z_m \ \hat{z}, \tag{2.3}$$

where (x_m, y_m, z_m) is the location of the m-th antenna element. Thus, the delay $\tau_{m,l}$ can be expressed as:

$$\tau_{m,l} = \frac{1}{c}\left(x_m \ \cos\phi_l \ \sin\theta_l + y_m \ \sin\phi_l \ \sin\theta_l + z_m \ \cos\theta_l\right). \tag{2.4}$$

Since the distance between the base station and the mobiles are usually much larger than the base station antenna height, it is usually assumed that $\theta_l \approx \pi/2$.

Consider a simple example shown in Figure 2.2, where a uniformly spaced linear array with three identical isotropic antenna elements is depicted. The interelement spacing d is usually chosen to be equal half the wavelength of the received signal, λ. A point source is located in the direction (ϕ_1, θ_1), and, for simplicity, we assume that $\theta_1 = \pi/2$. Thus, $\mathbf{v} = \cos\phi_1 \ \hat{x} + \sin\phi_1 \ \hat{y}$. The position vectors are, therefore,

$$\mathbf{u}_1 = 0, \qquad \mathbf{u}_2 = d \ \hat{x}, \qquad \mathbf{u}_3 = 2d \ \hat{x}. \tag{2.5}$$

Using (2.1) and assuming, for example, $f = 1.9$ GHz and $d = \lambda/2 \approx 15.8$ cm, we have

$$\tau_{1,1} = 0, \qquad \tau_{2,1} = 0.263\cos\phi_1 \text{ ns} \qquad \tau_{3,1} = 0.526\cos\phi_1 \text{ ns} \tag{2.6}$$

The time delays between the signals received at different element antennas will be maximum when the distances between the elements, *seen from the direction of propagation* ϕ_1, are maximum, that is, for $\phi_1 = 0$ or $\phi_1 = 180^o$.

Let $g_l(t)$ denote the physical bandpass signal transmitted by the point source l:

$$g_l(t) = \Re\{m_l(t)e^{\jmath 2\pi f_0 t}\}, \tag{2.7}$$

where $m_l(t)$ is the *complex envelope* of $g_l(t)$ amd $\Re\{.\}$ represents the real part of $\{.\}$. Also, let $q_{m,l}(t)$ denote the signal induced by the point source l on the m-th element. Assuming that the distances between the array elements are small enough, such that the amplitude differences between the signals received at different elements are negligible, and recalling that the antenna elements are omnidirectional, we can write:

$$q_{m,l}(t) = g_l(t - \tau_{m,l}). \tag{2.8}$$

Using complex envelope representation:

$$\begin{aligned} q_{m,l}(t) &= \Re\{m_l(t-\tau_{m,l})e^{\jmath 2\pi f_0(t-\tau_{m,l})}\} \\ &= \Re\{\underbrace{m_l(t)e^{-\jmath 2\pi f_0\tau_{m,l}}}_{complex\ envelope}\ e^{\jmath 2\pi f_0 t}\}. \end{aligned} \tag{2.9}$$

Note that, we have assumed in (2.9) that the bandwidth of the signal $m_l(t)$ is narrow enough such that the approximation $m_l(t) \approx m_l(t - \tau_{m,l})$ is valid.

Thus, the complex envelope of the signal induced by the l-th source on the m-th element, $r_{m,l}(t)$, is a phase shifted version of the transmitted signal $m_l(t)$:

$$\begin{aligned} r_{m,l}(t) &= m_l(t)e^{-\jmath 2\pi f_0\tau_{m,l}} \\ &= m_l(t)e^{-\jmath\Delta\psi_m(\theta_l,\phi_l)}. \end{aligned} \tag{2.10}$$

The phase shift $\Delta\psi_m(\theta,\phi)$ can be written in terms of the element location (x_m, y_m, z_m) and source direction (ϕ_l, θ_l):

$$\begin{aligned} \Delta\psi_m(\theta_l,\phi_l) &= 2\pi f_0\tau_{m,l} \\ &= \frac{2\pi f_0}{c}\left(x_m\ \cos\phi_l\ \sin\theta_l + y_m\ \sin\phi_l\ \sin\theta_l + z_m\ \cos\theta_l\right) \\ &= \beta\left(x_m\ \cos\phi_l\ \sin\theta_l + y_m\ \sin\phi_l\ \sin\theta_l + z_m\ \cos\theta_l\right), \end{aligned} \tag{2.11}$$

where $\beta = 2\pi f_0/c$. Note that $\Delta\psi_0(\theta_l,\phi_l) = 0$, since we are assuming that $\tau_{0,l} = 0$, for all l.

Since we have L sources, the complex envelope of the total received signal at the antenna element m is

$$\begin{aligned} x_m(t) &= \sum_{l=1}^{L} r_{m,l}(t) + \eta_m(t) \\ &= \sum_{l=1}^{L} m_l(t)e^{-\jmath\Delta\psi_m(\theta_l,\phi_l)} + \eta_m(t), \end{aligned} \tag{2.12}$$

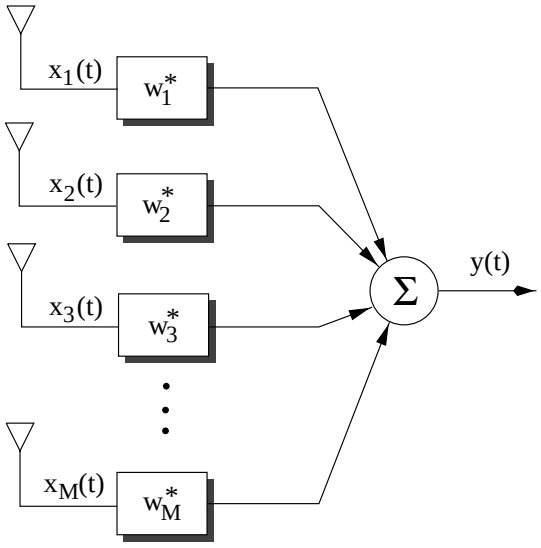

Figure 2.3: Antenna Array.

where $\eta_m(t)$ is the background random noise, assumed to be white with zero mean and variance σ_η^2. We also assume that $\eta_m(t)$ and $\eta_n(t)$ are uncorrelated for $m \neq n$.

Consider now that each signal $x_m(t)$ is multiplied by a complex weight w_m and summed, as shown in Figure 2.3, to form the output of the array, denoted by $y(t)$,

$$y(t) = \sum_{m=1}^{M} w_m^* \, x_m(t) = \mathbf{w}^H \, \mathbf{x}, \tag{2.13}$$

where $*$ denotes the complex conjugate and H denotes the complex conjugate transpose of a vector or matrix. The vectors $\mathbf{x}$ and $\mathbf{w}$, referred to as the *array signal vector* and *array weight vector*, respectively, are:

$$\mathbf{x} = [x_1(t) \; x_2(t) \; \cdots x_M(t)]^T, \tag{2.14}$$

$$\mathbf{w} = [w_1 \; w_2 \; \cdots w_M]^T, \tag{2.15}$$

where T denotes the transpose of a vector or matrix. The array signal vector $\mathbf{x}$ can also be written as:

$$\mathbf{x} = \sum_{l=1}^{L} m_l(t)\mathbf{a}(\theta_l, \phi_l) + \mathbf{n}(t), \tag{2.16}$$

where

$$\mathbf{n} = [\eta_1(t) \; \eta_2(t) \; \cdots \eta_M(t)]^T, \tag{2.17}$$

and $\mathbf{a}_l$ is the *steering vector* or *array response vector* associated with the l-th source or direction (ϕ_l, θ_l):

$$\mathbf{a}(\theta_l, \phi_l) = [1 \;\; e^{-\jmath\Delta\psi_2(\theta_l,\phi_l)} \;\; \cdots \;\; e^{-\jmath\Delta\psi_M(\theta_l,\phi_l)}]^T. \tag{2.18}$$

The m-th element of $\mathbf{a}(\theta_l, \phi_l)$ denotes the phase shift of the signal available at the m-th antenna element, relative to the phase of the signal at the reference antenna element. To simplify the notation, we will use hereinafter $\mathbf{a}(\theta_l, \phi_l) = \mathbf{a}_l$.

The mean output power of the array is given by:

$$\begin{aligned} P(\mathbf{w}) &= E\{y(t)\, y^*(t)\} \\ &= \mathbf{w}^H \mathbf{R}\, \mathbf{w}, \end{aligned} \tag{2.19}$$

where $E\{.\}$ denotes the expectation operator and $\mathbf{R}$ is the *array correlation matrix*, defined as:

$$\mathbf{R} = E\{\mathbf{x}\, \mathbf{x}^H\}. \tag{2.20}$$

Using (2.14) and (2.12), and assuming that the signals $m_l(t)$ and $m_k(t)$ are uncorrelated for $l \neq k$, the element R_{ij} of $\mathbf{R}$ can be written as:

$$\begin{aligned} R_{ij} &= E\left\{ \left(\sum_{l=1}^{L} m_l(t) e^{-\jmath \Delta\psi_i(\theta_l,\phi_l)} \right) \left(\sum_{l=1}^{L} m_l^*(t) e^{\jmath \Delta\psi_j(\theta_l,\phi_l)} \right) \right\} + E\left\{ \eta_i(t) \eta_j^*(t) \right\} \\ &= \sum_{l=1}^{L} E\{|m_l(t)|^2\} e^{-\jmath \Delta\psi_i(\theta,\phi)}\, e^{\jmath \Delta\psi_j(\theta,\phi)} + \sigma_\eta^2\, \delta_{ij}, \end{aligned} \tag{2.21}$$

where

$$\delta_{ij} = \begin{cases} 1 & \text{for } i = j \\ 0 & \text{otherwise.} \end{cases} \tag{2.22}$$

Using (2.18) in (2.21), the matrix $\mathbf{R}$ can be written as:

$$\mathbf{R} = \sum_{l=1}^{L} p_l\, \mathbf{a}_l\, \mathbf{a}_l^H + \sigma_\eta^2 \mathbf{I}. \tag{2.23}$$

where $p_l = E\{|m_l(t)|^2\}$ is the power of the l-th source.

Consider now that there is only one point source, that is, $L = 1$. Therefore, the array output $y(t)$ is:

$$\begin{aligned} y(t) &= \sum_{m=1}^{M} w_m^*\, m_1(t) e^{-\jmath \Delta\psi_m(\theta_1,\phi_1)} + \eta_m(t) \\ &= m_1(t) \sum_{m=1}^{M} w_m^*\, e^{-\jmath \Delta\psi_m(\theta_1,\phi_1)} + \eta_m(t) \\ &= m_1(t)\, f(\theta_1, \phi_1) + \eta_m(t), \end{aligned} \tag{2.24}$$

where

$$f(\theta, \phi) = \sum_{m=1}^{M} w_m^*\, e^{-\jmath \Delta\psi_m(\theta,\phi)} \tag{2.25}$$

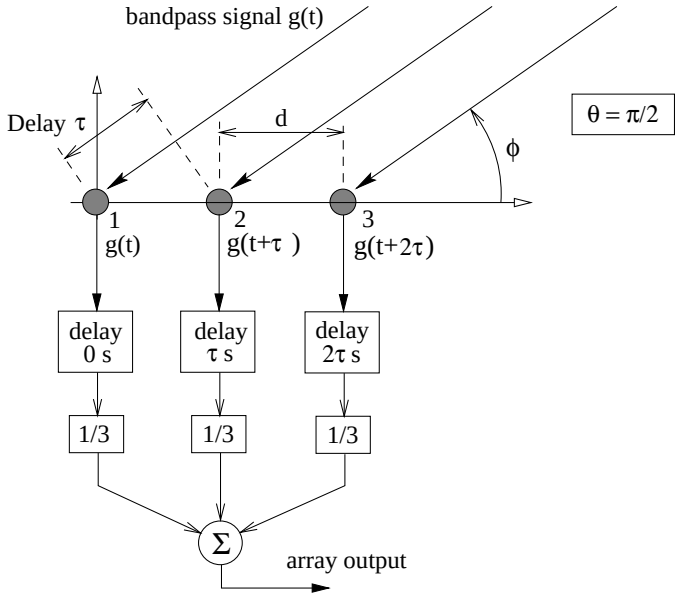

Figure 2.4: Antenna Array with $M = 3$ elements and one point source.

is called the *array factor*. The array factor is the ratio of the array output signal $y(t)$ to the total signal impinging upon the array, as a function of the direction (θ, ϕ). The *radiation pattern* of the array, denoted by $F(\theta, \phi)$, is the product of the array factor $f(\theta, \phi)$ and the antenna element radiation pattern $g_a(\theta, \phi)$

$$F(\theta, \phi) = f(\theta, \phi) g_a(\theta, \phi). \tag{2.26}$$

By adjusting the weight coefficients w_m, we can "form" beams or nulls such that signals received from a certain direction are maximized or minimized, as illustrated in the following examples.

Examples of Beamforming

Consider that a bandband signal $g(t)$ of frequency f_0 impinges upon a 3-element linear antenna array from direction $(\theta = \pi/2, \phi)$, as shown in Figure 2.4. Assuming that the elements are omnidirectional and element 1 is the reference, the signals received at each element is a delayed replica of the transmitted signal $g(t)$:

$$\begin{aligned} \text{element 1} &\Rightarrow g(t) \\ \text{element 2} &\Rightarrow g(t+\tau) \\ \text{element 3} &\Rightarrow g(t+2\tau) \end{aligned}$$

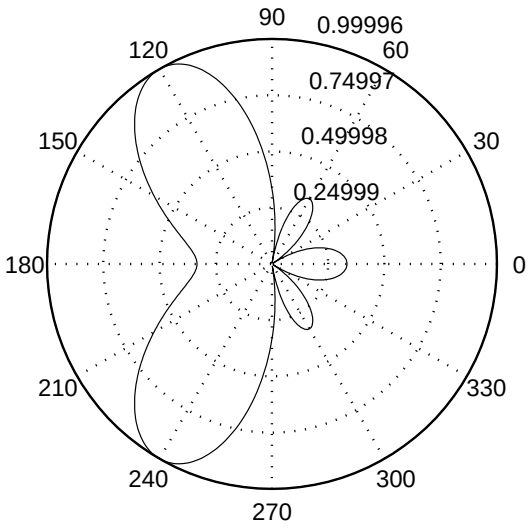

Figure 2.5: Radiation pattern of a 3-element linear array, whose coefficients are adjusted in order to produce a main lobe steered toward $\phi = 120^o$.

where τ, using (2.11), is:

$$\tau = \frac{d\ \cos\phi}{c}, \tag{2.27}$$

and d is the inter-element spacing. The transmitted signal $m(t)$ can be recovered at the array output by introducing additional delays in each element signal, as shown in Figure 2.4. Using complex envelope representation, the coefficients w_m should be:

$$w_1 = \frac{1}{3}, w_2 = \frac{1}{3}\ e^{-\jmath 2\pi f_0 \tau} \quad \text{and} \quad w_3 = \frac{1}{3}\ e^{-\jmath 2\pi f_0 2\tau}, \tag{2.28}$$

so that the output signal $y(t)$ is:

$$\begin{aligned} y(t) &= \sum_{m=1}^{3} w_m^* m(t) e^{\jmath 2\pi f_0 (m-1)\tau} \\ &= m(t), \end{aligned} \tag{2.29}$$

where $m(t)$ is the complex envelope of $g(t)$. For example, consider a point source located in direction $\phi = 120^o$ and $\theta = \pi/2$. Assuming that the array elements are omnidirectional, the amplitude of the array radiation pattern is shown in Figure 2.5.

Likewise, the weights w_m can be adjusted in order to null signals impinging upon an array from certain directions. Consider, for example, that L signals $m_l(t)$ impinge upon a M-element array and we desire to null signals $m_2(t), m_3(t), \cdots, m_L(t)$, while steering a unity

array response towards signal $m_1(t)$. The array weight vector $\mathbf{w}$ must, therefore, satisfy the following conditions:

$$\begin{aligned} \mathbf{w}^H\mathbf{a}_1 &= 1 \\ \mathbf{w}^H\mathbf{a}_l &= 0 \quad \text{for } l = 2, 3, \cdots, L, \end{aligned} \tag{2.30}$$

or, in matrix notation

$$\mathbf{w}^H\mathbf{A} = \mathbf{e}_1^T, \tag{2.31}$$

where $\mathbf{A}$ is a matrix composed by all steering vectors

$$\mathbf{A} = [\mathbf{a}_1\ \mathbf{a}_2\ \cdots\ \mathbf{a}_L], \tag{2.32}$$

and $\mathbf{e} = [1\ \ 0\ \cdots\ 0]$. If the number of elements in the array, M, is equal to the number of signals we want to null out, $L-1$, $\mathbf{A}$ is a square matrix. Assuming that all steering vectors are linearly independent, the solution for the weight vector is:

$$\mathbf{w}^H = \mathbf{e}_1^T\ \mathbf{A}^{-1}. \tag{2.33}$$

If $M < L-1$, then $\mathbf{A}$ is not a square matrix. Post-multiplying both sides of (2.31) by $\mathbf{A}^H$, we obtain

$$\mathbf{w}^H\mathbf{A}\mathbf{A}^H = \mathbf{e}_1^T\mathbf{A}^H \tag{2.34}$$

where $\mathbf{A}\mathbf{A}^H$ is a square matrix, and $\mathbf{w}^H$ is, therefore,

$$\mathbf{w}^H = \mathbf{e}_1^T\mathbf{A}^H(\mathbf{A}\mathbf{A}^H)^{-1}. \tag{2.35}$$

As an example, consider three signals with equal powers impinging upon a 4 element linear antenna array, with angles $\phi_1 = 30^o$, $\phi_2 = 60^o$ and $\phi_3 = 150^o$, and $\theta_1 = \theta_2 = \theta_3 = \pi/2$. The element spacing is $d = \lambda/2$. The radiation pattern of the array, adjusted to receive signals from direction $\phi_1 = 30^o$, but null out the signals from $\phi_2 = 60^o$ and $\phi_3 = 150^o$, is shown in Figure 2.6.

We reviewed in this section the basic concepts of beamforming. In few words, by adjusting the coefficients w_m, we can "form" beams or nulls such that signals received from a certain direction are maximized or minimized at the array output. In the next section we present three optimal approaches for computing the coefficients w_m (beamforming) which minimize a given cost function. In the approaches presented in the next section, a beam or null is formed towards a particular direction, giving the antenna the ability to *adaptively* change its radiation according to the environment. Another approach for beamforming is based on forming a set of *fixed* beams steered towards predefined directions. Fixed beam systems are discussed in Section 2.4.

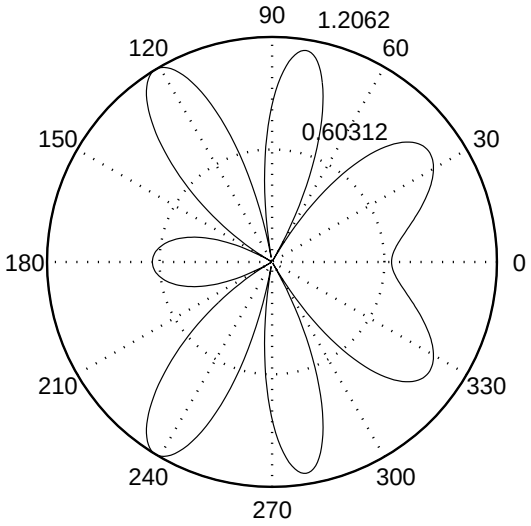

Figure 2.6: Radiation pattern of a 4-element linear array, receiving signal from $\phi_1 = 30^o$ and nulling out signals from $\phi_2 = 60^o$ and $\phi_3 = 150^o$.

2.3.2 Optimal Beamforming

Minimum Mean Square Error (MMSE)

Consider again a M-element array immersed in an environment where there is one desired signal $m_1(t)$, arriving at the array with the angle (ϕ_1, θ_1), and $L-1$ interfering signals $m_l(t)$, $l = 2, 3, \cdots, L$, impinging upon the array with angles (ϕ_l, θ_l). The array signal vector, $\mathbf{x}(t)$, is:

$$\begin{aligned} \mathbf{x}(t) &= m_1(t)\mathbf{a}_1 + \sum_{l=2}^{L} m_l(t)\mathbf{a}_l \\ &= \mathbf{z}(t) + \mathbf{u}(t), \end{aligned} \tag{2.36}$$

where $\mathbf{z} = m_1(t)\mathbf{a}_1$ and $\mathbf{u} = \sum_{l=2}^{L} m_l(t)\mathbf{a}_l$. Let us assume that a *reference* signal $d(t)$, that closely enough represents $m_1(t)$, can be generated at the receiver. The weights of the array can be chosen in order to minimize the *mean square error* (MSE) between the array output, $y(t)$, and the reference sinal, $d(t)$:

$$\begin{aligned} J(\mathbf{w}) &= E\{[d(t) - y(t)]^2\} \\ &= E\{[d(t) - \mathbf{w}^H\mathbf{x}(t)]^2\} \\ &= E\{d^2(t)]\} - 2\mathbf{w}^H\mathbf{r} + \mathbf{w}^H\mathbf{R}\mathbf{w}, \end{aligned} \tag{2.37}$$

where $\mathbf{r} = E\{\mathbf{x}\ d(t)^*\}$ is the cross-correlation vector between the array signal vector and the reference signal, and $\mathbf{R}$ is the correlation matrix, given by (2.20). The optimum weight vector $\mathbf{w}_{opt}$ can be computed by setting the derivative of $J(\mathbf{w})$ with respect to $\mathbf{w}^*$ equal to zero. In order to compute the derivative of $J(\mathbf{w})$, we use the following rules of differentiation with respect to a vector [15]:

$$\begin{aligned} \frac{\partial}{\partial \mathbf{w}^*}(\mathbf{w}^H\mathbf{R}\mathbf{w}) &= 2\mathbf{R}\mathbf{w}, \\ \frac{\partial}{\partial \mathbf{w}^*}(\mathbf{w}^H\mathbf{c}) &= 2\mathbf{c}, \\ \frac{\partial}{\partial \mathbf{w}^*}(\mathbf{c}^H\mathbf{w}) &= 0. \end{aligned} \tag{2.38}$$

where $\mathbf{c}$ is an arbitrary vector.

Therefore,

$$\begin{aligned} \frac{\partial}{\partial \mathbf{w}^*}J(\mathbf{w}) &= -2\mathbf{r} + 2\mathbf{R}\mathbf{w} \\ &= 0. \end{aligned} \tag{2.39}$$

Thus,

$$\mathbf{w}_{opt} = \mathbf{R}^{-1}\mathbf{r}. \tag{2.40}$$

Ideally, the reference signal is equal to the desired signal $m_1(t)$, and, assuming the messages $m_l(t)$ are uncorrelated with one another, $\mathbf{r}$ is:

$$\begin{aligned} \mathbf{r} &= E\{[m_1(t)\mathbf{a}_1 + \mathbf{u}(t)]m_1^*(t)\} \\ &= E\{[|m_1(t)|^2\}\mathbf{a}_1 \\ &= p_1\mathbf{a}_1. \end{aligned} \tag{2.41}$$

Therefore, (2.40) can be rewritten as

$$\mathbf{w}_{opt} = p_1\mathbf{R}^{-1}\mathbf{a}_1. \tag{2.42}$$

Further, using (2.23), the matrix $\mathbf{R}$ can be expressed as:

$$\begin{aligned} \mathbf{R} &= p_1\ \mathbf{a}_1\ \mathbf{a}_1^H + \sum_{l=1}^{L} p_l\ \mathbf{a}_l\ \mathbf{a}_l^H + \sigma_\eta^2\mathbf{I} \\ &= p_1\ \mathbf{a}_1\ \mathbf{a}_1^H + \mathbf{R}_u. \end{aligned} \tag{2.43}$$

Using a special case of *matrix inversion lemma*, known as *Woodbury's Identity* [16], we have

$$\mathbf{R}^{-1} = \mathbf{R}_u^{-1} + \frac{p_1\mathbf{R}_u^{-1}\mathbf{a}_1\ \mathbf{a}_1^H\mathbf{R}_u^{-1}}{1 + p_1\mathbf{a}_1^H\mathbf{R}_u^{-1}\mathbf{a}_1}. \tag{2.44}$$

Post-multiplying both sides of (2.44) by $\mathbf{a}_1$

$$\begin{aligned}\mathbf{R}^{-1}\mathbf{a}_1 &= \mathbf{R}_u^{-1}\mathbf{a}_1 - \frac{\mathbf{R}_u^{-1}\mathbf{a}_1\,(p_1\mathbf{a}_1^H\mathbf{R}_u^{-1}\mathbf{a}_1)}{1+p_1\mathbf{a}_1^H\mathbf{R}_u^{-1}\mathbf{a}_1} \\ &= \frac{p_1\mathbf{R}_u^{-1}\mathbf{a}_1}{1+p_1\mathbf{a}_1^H\mathbf{R}_u^{-1}\mathbf{a}_1}. \end{aligned} \tag{2.45}$$

Using (2.45) in (2.42), the MSE solution can be written as [16]

$$\mathbf{w}_{opt} = \beta_{MSE}\mathbf{R}_u^{-1}\mathbf{a}_1 \tag{2.46}$$

$$\beta_{MSE} = \frac{p_1}{1+p_1\mathbf{s}^H\mathbf{R}_u^{-1}\mathbf{s}}. \tag{2.47}$$

Maximum Signal-to-Interference Ratio (MSIR)

Another criterion for selecting array weights is based on maximizing the *Signal-to-Interference Ratio* (*SIR*) at the array output. The array output signal $y(t)$ can be expressed as:

$$y(t) = \mathbf{w}^H\mathbf{z}(t) + \mathbf{w}^H\mathbf{u}(t), \tag{2.48}$$

where $\mathbf{z}(t) = m_1(t)\mathbf{a}_1$ is the portion of the $\mathbf{x}(t)$ corresponding to the desired signal $m_1(t)$, and $\mathbf{u}(t) = \sum_{l=2}^{L} m_l(t)\mathbf{a}_l$ is the total interference signal.

The signal-to-interference ratio is defined as the ratio of the portion of the power of $y(t)$ corresponding to the desired signal, denoted by σ_z^2, to the portion of the power of $y(t)$ corresponding to the interference signal, denoted by σ_u^2:

$$SIR = \frac{\sigma_z^2}{\sigma_u^2} = \frac{E\{|\mathbf{w}^H\mathbf{z}(t)|^2\}}{E\{|\mathbf{w}^H\mathbf{u}(t)|^2\}} = \frac{\mathbf{w}^H\mathbf{R}_z\mathbf{w}}{\mathbf{w}^H\mathbf{R}_u\mathbf{w}}, \tag{2.49}$$

where $\mathbf{R}_z = E\{\mathbf{z}(t)\mathbf{z}^H(t)\}$ and $\mathbf{R}_u = E\{\mathbf{u}(t)\mathbf{u}^H(t)\}$. Setting the derivative of *SIR* with respect to $\mathbf{w}$ equal to zero, we obtain:

$$\frac{\partial}{\partial\mathbf{w}^*}SIR = \frac{(\mathbf{w}^H\mathbf{R}_u\mathbf{w})\,\mathbf{R}_z\mathbf{w} - (\mathbf{w}^H\mathbf{R}_z\mathbf{w})\,\mathbf{R}_u\mathbf{w}}{(\mathbf{w}^H\mathbf{R}_u\mathbf{w})^2} = 0, \tag{2.50}$$

or

$$\mathbf{R}_z\mathbf{w} = \frac{\mathbf{w}^H\mathbf{R}_z\mathbf{w}}{\mathbf{w}^H\mathbf{R}_u\mathbf{w}}\mathbf{R}_u\mathbf{w}. \tag{2.51}$$

Pre-multiplying both sides of (2.51) by $\mathbf{R}_u^{-1}$, we obtain

$$\mathbf{R}_u^{-1}\mathbf{R}_z\mathbf{w} = \frac{\mathbf{w}^H\mathbf{R}_z\mathbf{w}}{\mathbf{w}^H\mathbf{R}_u\mathbf{w}}\mathbf{w}. \tag{2.52}$$

Computing $\mathbf{w}$ from (2.52) is a generalized eingenvalue problem. The scalar $\frac{\mathbf{w}^H\mathbf{R}_z\mathbf{w}}{\mathbf{w}^H\mathbf{R}_u\mathbf{w}} = SIR$ is bounded by the eigenvalues of $\mathbf{R}_u^{-1}\mathbf{R}_z$:

$$\lambda_{min} \leq \frac{\mathbf{w}^H\mathbf{R}_z\mathbf{w}}{\mathbf{w}^H\mathbf{R}_u\mathbf{w}} \leq \lambda_{max}, \tag{2.53}$$

where λ_{min} and λ_{max} are the minimum and maximum eigenvalues of $\mathbf{R}_u^{-1}\mathbf{R}_z$. Therefore, the maximum SIR is achieved when $\mathbf{w}_{opt}$ is equal to the eigenvector of $\mathbf{R}_u^{-1}\mathbf{R}_z$ corresponding to λ_{max}:

$$\mathbf{R}_u^{-1}\mathbf{R}_z\mathbf{w}_{opt} = \lambda_{max}\mathbf{w}_{opt}. \tag{2.54}$$

Recalling that $\mathbf{R}_z = p_1\mathbf{s}\,\mathbf{s}^H$, we have [16]

$$\mathbf{w}_{opt} = \beta_{MSIR}\mathbf{R}_u^{-1}\mathbf{a}_1. \tag{2.55}$$

where

$$\beta_{MSIR} = \frac{p_1\mathbf{s}^H\mathbf{w}_{opt}}{SIR}. \tag{2.56}$$

In this method, we must know the statistics of the interference (matrix $\mathbf{R}_u$) and angle-of-arrival of the desired signal, in order to construct the matrix $\mathbf{R}_z$.

Minimum Variance (MV)

In the Minimum Variance criterion, we compute the weight vector $\mathbf{w}$ that minimizes the variance, or power, of the output signal $y(t)$

$$\begin{aligned} P(\mathbf{w}) &= E\{y(t)\,y^*(t)\} \\ &= \mathbf{w}^H\mathbf{R}\,\mathbf{w}. \end{aligned} \tag{2.57}$$

Using $\mathbf{x}(t) = \mathbf{z}(t) + \mathbf{u}(t)$, we can rewrite (2.57) as

$$P(\mathbf{w}) = \underbrace{\mathbf{w}^H\mathbf{R}_z\,\mathbf{w}}_{\text{desired signal term}} + \underbrace{\mathbf{w}^H\mathbf{R}_u\,\mathbf{w},}_{\text{interference term}} \tag{2.58}$$

where $\mathbf{R}_z$ and $\mathbf{R}_u$ are the autocorrelation matrices of the desired signal $\mathbf{z}(t)$ and total interference signal $\mathbf{u}(t)$, respectively. The minimization of $P(\mathbf{w})$ can be accomplished by minimizing the interference term in $P(\mathbf{w})$, $\mathbf{w}^H\mathbf{R}_u\,\mathbf{w}$.

To ensure that the desired signal $\mathbf{z}(t)$ is going to be preserved by the array, we impose the condition that the response of the array to $\mathbf{z}(t)$ is an arbitrary constant ζ:

$$\mathbf{w}^H\mathbf{a}_1 = \zeta. \tag{2.59}$$

Therefore, we have the following constrained optimization problem:

$$\begin{aligned} \min_{\mathbf{w}} \quad & \mathbf{w}^H \mathbf{R}_u \, \mathbf{w} \\ \text{subject to} \quad & \mathbf{w}^H \mathbf{a}_1 - \zeta = 0. \end{aligned} \tag{2.60}$$

We solve this problem using the *Method of Lagrange Multipliers* as follows. First, we convert the problem of constrained minimization into one of unconstrained minimization by introducing the complex Lagrange multiplier λ_L. Define the real-valued function $h(\mathbf{w})$:

$$h(\mathbf{w}) = \mathbf{w}^H \mathbf{R}_u \, \mathbf{w} + \Re\{\lambda_L^*(\mathbf{w}^H \mathbf{a}_1 - \zeta)\}. \tag{2.61}$$

Next, we minimize $h(\mathbf{w})$ with respect to $\mathbf{w}$, which can be accomplished by setting the derivative $\partial h / \partial \mathbf{w}^*$ to zero:

$$\frac{\partial h}{\partial \mathbf{w}^*} = \frac{\partial}{\partial \mathbf{w}^*}(\mathbf{w}^H \mathbf{R}_u \, \mathbf{w}) + \frac{\partial}{\partial \mathbf{w}^*}\Re\{\lambda_L^*(\mathbf{w}^H \mathbf{a}_1 - \zeta)\} = \mathbf{0}. \tag{2.62}$$

Using the rules for differentiation with respect to a vector, we have:

$$\frac{\partial}{\partial \mathbf{w}^*}(\mathbf{w}^H \mathbf{R}_u \, \mathbf{w}) = \mathbf{R}_u \, \mathbf{w}, \tag{2.63}$$

and

$$\begin{aligned} \frac{\partial}{\partial \mathbf{w}^*}\Re\{\lambda_L^*(\mathbf{w}^H \mathbf{a}_1 - \zeta)\} &= \frac{\partial}{\partial \mathbf{w}^*}[\lambda_L^*(\mathbf{w}^H \mathbf{a}_1 - \zeta) - \lambda_L(\mathbf{a}_1^H \mathbf{w} - \zeta)] \\ &= \frac{\partial}{\partial \mathbf{w}^*}[\lambda_L^* \mathbf{w}^H \mathbf{a}_1 - \lambda_L \mathbf{a}_1^H \mathbf{w} + \jmath\zeta\Im\{\lambda_L\}] \\ &= \lambda_L^* \frac{\partial}{\partial \mathbf{w}^*}(\mathbf{w}^H \mathbf{a}_1) + \lambda_L \frac{\partial}{\partial \mathbf{w}^*}(\mathbf{a}_1^H \mathbf{w}) \\ &= \lambda_L^* \mathbf{a}_1, \end{aligned} \tag{2.64}$$

where $\Im\{.\}$ denotes the imaginary part of $\{.\}$. Substituting (2.63) and (2.64) into (2.62) we have:

$$\mathbf{R}_u \, \mathbf{w} = \lambda_L^* \mathbf{a}_1, \tag{2.65}$$

or

$$\mathbf{w}_{opt} = \lambda_L^* \mathbf{R}_u^{-1} \mathbf{a}_1. \tag{2.66}$$

In order to determine λ_L^*, we pre-multiply (2.66) by the transposed complex conjugate of the steering vector of the desired signal, $\mathbf{a}_1^H = \mathbf{a}^H(\theta_1, \phi_1)$

$$\mathbf{a}_1^H \mathbf{w}_{opt} = \lambda_L^* \mathbf{a}_1^H \mathbf{R}_u^{-1} \mathbf{a}_1. \tag{2.67}$$

Noting that $\mathbf{w}_{opt}^H \mathbf{a}_1 = \mathbf{a}_1^H \mathbf{w}_{opt} = \zeta$, we have

$$\lambda_L^* = \frac{\zeta}{\mathbf{a}_1^H \mathbf{R}_u^{-1} \mathbf{a}_1}, \tag{2.68}$$

and, finally

$$\mathbf{w}_{opt} = \frac{\zeta \mathbf{R}_u^{-1} \mathbf{a}_1}{\mathbf{a}_1^H \mathbf{R}_u^{-1} \mathbf{a}_1}, \tag{2.69}$$

or,

$$\mathbf{w}_{opt} = \beta_{MV} \mathbf{R}_u^{-1} \mathbf{a}_1, \tag{2.70}$$

where

$$\beta_{MV} = \frac{\zeta \mathbf{R}_u^{-1} \mathbf{a}_1}{\mathbf{a}_1^H}. \tag{2.71}$$

In practice, where the determination of $\mathbf{R}_u$ may not be available, the autocorrelation $\mathbf{R}$ of total array signal vector $\mathbf{x}$ may be used to compute $\mathbf{w}$. In this case, $\mathbf{w}_{opt}$ is:

$$\mathbf{w}_{opt} = \frac{\zeta \mathbf{R}^{-1} \mathbf{a}_1}{\mathbf{a}_1^H \mathbf{R}^{-1} \mathbf{a}_1}. \tag{2.72}$$

Comparison

Note that, in all approaches the optimum weights are given by equations in the form:

$$\mathbf{w}_{opt} = \beta \mathbf{R}_u^{-1} \mathbf{a}_1 \tag{2.73}$$

where β assumes the values β_{MSE}, β_{MSIR} or β_{MV}, depending on the approach adopted. It is interesting to note that all three approaches result the same *SIR* [16]:

$$\begin{aligned} SIR = \frac{\sigma_z^2}{\sigma_u^2} &= \frac{\mathbf{w}_{opt}^H \, \mathbf{R}_z \, \mathbf{w}_{opt}}{\mathbf{w}_{opt}^H \, \mathbf{R}_u \, \mathbf{w}_{opt}} \\ &= \frac{\beta^2 \, \mathbf{a}_1^H \mathbf{R}_u^{-1} \, \mathbf{R}_z \, \mathbf{R}_u^{-1} \mathbf{a}_1}{\beta^2 \, \mathbf{a}_1^H \mathbf{R}_u^{-1} \, \mathbf{R}_u \, \mathbf{R}_u^{-1} \mathbf{a}_1} \\ &= \frac{\mathbf{a}_1^H \mathbf{R}_u^{-1} \, p_1 \mathbf{s} \mathbf{a}_1^H \, \mathbf{R}_u^{-1} \mathbf{a}_1}{\mathbf{a}_1^H \, \mathbf{R}_u^{-1} \mathbf{a}_1} \\ &= p_1 \mathbf{a}_1^H \mathbf{R}_u^{-1} \, \mathbf{s}. \end{aligned} \tag{2.74}$$

As already noted, the differences between the approaches are the information needed to compute the quantities involved in the computation. The differences between the requirements of each approach make a particular approach more suitable for a particular situation, as discussed subsequently.

- **Minimum Mean Error Square:** A disadvantage of this method is that a reference signal $d(t)$ is required. However, in TDMA cellular systems, such as IS-136 and GSM [1], each time slot includes a syncronization sequence that can be used as the reference signal for adaptive array weight aquisition. Another disadvantage of the MMSE approach arises from the fact that it is not possible to implement ensemble averaging, as required to obtain $\mathbf{R}$ and $\mathbf{r}$, in a practical application. Thus, ergodicity and stationarity must be assumed when implementing an algorithm based on MMSE [15]. The advantage of this approach is that no direction of arrival information is required.

- **Maximum *SIR*:**

  In this method, we must estimate matrix $\mathbf{R}_u$ (interference signal) and $\mathbf{R}_z$ (desired signal). These matrices can be estimated by using the expressions

$$\begin{aligned} \mathbf{R}_z &= \sum_{l=2}^{L} p_l \, \mathbf{a}_l \, \mathbf{a}_l^H \\ \mathbf{R}_z &= p_1 \, \mathbf{a}_1 \, \mathbf{a}_1^H, \end{aligned} \tag{2.75}$$

  which require estimates of the angle of arrival of the desired signal and interfering signals.

- **Minimum Variance:**

  This method doe not require the knowledge of the angle of arrival of the interferences, but it requires the angle of arrival of the desired signal.

2.4 Switched Beam Systems

In Section 2.3.2, we presented beamforming techniques based on forming a beam or null towards any particular direction. Another approach for beamforming is based on forming a set of *fixed* beams, steered towards predefined directions, and selecting a beam for transmittion or reception based on a beam-selection algorithm. In the *receive mode*, the switched beam system selects the beam that provides the best reception of a particular signal. In the *transmit mode*, the beam selected is the one that better illuminates the region where the desired receiver is located. Figure 2.7 shows a switched beam system in the receive mode with M fixed beams. The output $\mathbf{y} = [y_1(t) \; y_2(t) \cdots y_M(t)]^T$ of the *Beamforming Network*

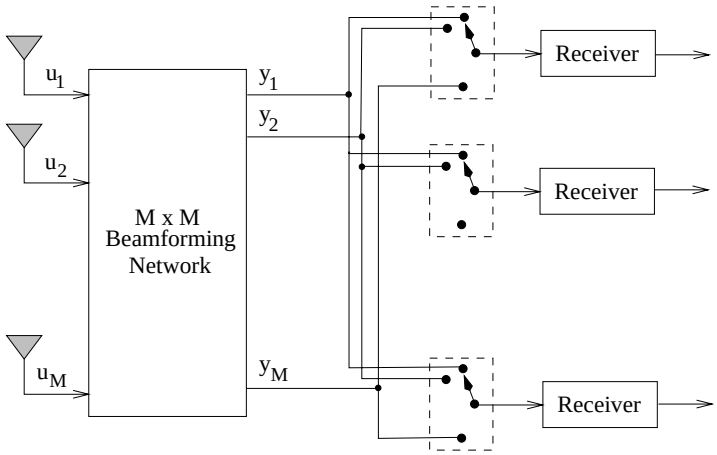

Figure 2.7: Switched Beam System.

is (see Figure 2.7)

$$\mathbf{y} = \mathbf{T}^H \mathbf{u}(t), \tag{2.76}$$

where

$$\mathbf{T} = [\mathbf{w}_1 \ \mathbf{w}_2 \ \cdots \mathbf{w}_M]. \tag{2.77}$$

The m-th output $y_m(t)$ corresponds to the output of an array with weight vector $\mathbf{w}_m$ and, consequently, wiht a particular radiation pattern. Fixed beamforming can be implemented by using the *Butler* matrix [17]. An example of the radiation pattern of a fixed beamforming using the Butler matrix with 4 antenna elements is shown in Figure 2.8.

The advantage of switched beam systems is the low complexity compared to the complexity of fully adaptive antennas. Also, the integration of a switched beam system in an existing cellular system requires few modification in the cellular system.

2.5 Vector Channel Impulse Response

In the analysis of adaptive antenna systems, it is important to understand the spatial properties of the wireless communication channel, since these properties will have a strong impact on the performance of adaptive antenna systems. Classically, channel models provide information on signal power level distribution, Doppler shifts of the received signals and time delay spread. When antenna array is incorporated to the transmission system, additional spatial information on the RF propagation channel must be provided by the channel model.

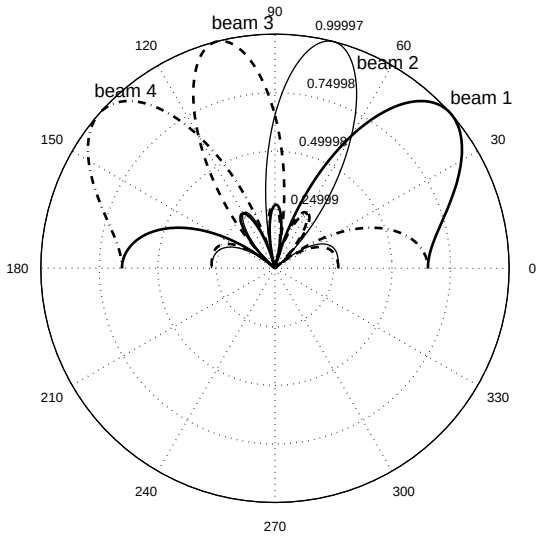

Figure 2.8: Radiation pattern of a fixed beamforming system with four beams and using Butler matrix.

In this section, we introduce the *vector channel impulse response*, that is used to characterize the wireless channel, where each multipath component arrives from a discrete direction at a discrete time delay. Also, channel models including spatial properties information are presented. Portions of this section are based on [6].

Consider a simplified multipath environment depicted in Figure 2.9. Each signal component experiences a different path environment, which will determine the amplitude $A_{l,k}$, carrier phase shift $\varphi_{l,k}$, time delay $\tau_{l,k}$, angle-of-arrival (AOA) $\phi_{l,k}$, and Doppler shift f_d of the l-th signal component of the k-th mobile. In general, each of these signal parameters will be time-varying. Representing the RF channel as a time-variant channel and using a baseband complex envelope representation, the channel response for mobile 1 has classically been represented as:

$$h_1(t,\tau) = \sum_{l=0}^{L(t)} A_{l,1} \exp[j\varphi_{l,1}]\delta(t - \tau_{l,1}(t)). \tag{2.78}$$

where $L(t)$ is the number of multipath components and the other variables have already been defined. The amplitude $A_{l,k}$ of the multipath components is usually modeled as a Rayleigh distributed random variable, while the phase $\varphi_{l,k}$ is uniformly distributed.

The time-varying nature of a wireless channel is caused by the motion of objects in the channel. A measure of the time rate of change of the channel is the Doppler power spectrum, introduced by M. J. Gans in 1972 [18]. The Doppler power spectrum provides us

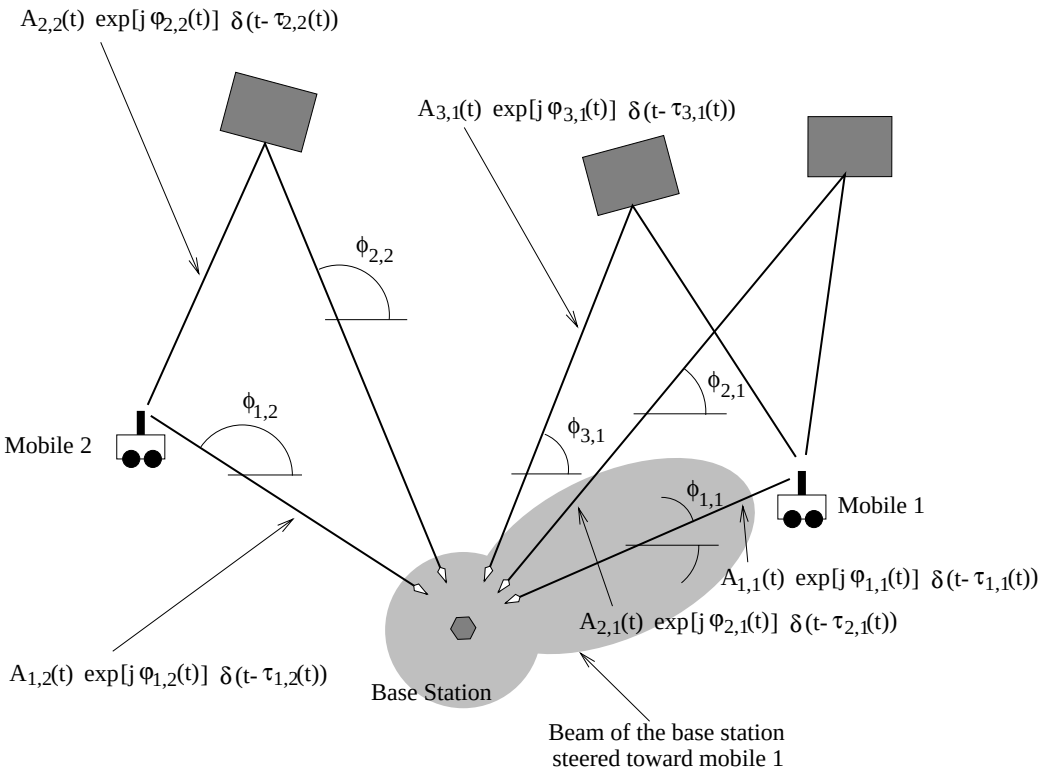

Figure 2.9: Multipath propagation channel.

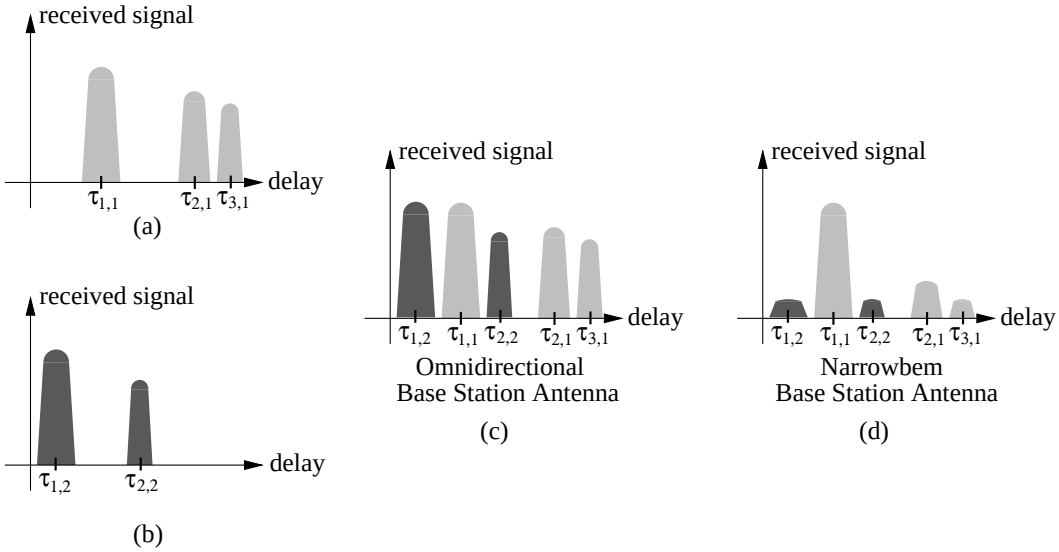

Figure 2.10: Channel impulse responses for mobiles 1 and 2: (a) received signal from mobile 1 at the base station; (b) received signal from mobile 2 at the base station; (c) combined received signal from mobiles 1 and 2 at the base station, assuming omindirectional base station antenna; (d) received signal at the base station when a narrow beam steered toward mobile 1 is employed.

with statistical information on the variation of the frequency of a tone received by a mobile traveling at speed v. Based on the flat fading channel model developed by R. H. Clarke in 1968, Gans assumed that the received signal at the mobile station came from all directions and was uniformly distributed

Assuming that both mobiles in Figure 2.9 are transmitting narrow pulses on the same channel and the base station is omnidirectional, the signal received at the base station is a combination of all multipath components of signal transmitted by all mobiles, as shown in Figure 2.10. However, when a narrow beam is steered toward mobile 1, multipath components are attenuated, as also shown in Figure 2.10.

The channel model in (2.78) does not consider the AOA of each multipath component shown in Figures 2.9 and 2.10. For narrowband signals, the AOA may be included into the *vector channel impulse response* using

$$\mathbf{h}_1(t,\tau) = \sum_{l=0}^{L(t)} A_{l,1}\mathbf{a}(\theta_{l,1},\phi_{l,1})\exp[\jmath\varphi_{l,1}]\delta(t-\tau_{l,1}(t)). \tag{2.79}$$

where $\mathbf{a}(\theta,\phi)$ is the steering vector, defined in (2.18).

If the differences between the path delays $\tau_{l,1}(t)$ of multipath components are very small compared with the channel symbol duration, the channel is call a *narrowband channel* and

the fading is said to be *flat*. Therefore, the approximation

$$\tau_{l,1}(t) \approx \tau_{0,k}(t) \quad \text{for all } l \tag{2.80}$$

is valid and the vector channel impulse response $\mathbf{h}_1(t,\tau)$ may be expressed by

$$\begin{aligned} \mathbf{h}_1(t,\tau) &= \delta(t-\tau_{0,1}(t)) \sum_{l=0}^{L(t)} A_{l,1} \exp[\jmath\varphi_{l,1}]\ \mathbf{a}(\theta_{l,1},\phi_{l,1}) \\ &= \delta(t-\tau_{0,1}(t))\ \mathbf{b}_1(t), \end{aligned} \tag{2.81}$$

where $\mathbf{b}_1(t)$ is given by

$$\mathbf{b}_1(t) = \sum_{l=0}^{L(t)} A_{l,1} \exp[\jmath\varphi_{l,1}]\ \mathbf{a}(\theta_{l,1},\phi_{l,1}) \tag{2.82}$$

and is called the *spatial signature* of the channel for mobile 1.

The spatial channel impulse response given in expression (2.79) is a summation of several multipath components, each of which has its own amplitude, phase, and AOA. The distribution of these parameters depends on the type of environment. In particular, the angle spread of the channel is known to be a function of both the environment and the base station antenna heights. Next, we describe macrocell and microcell environments and discuss how the environment affects the signal parameters.

2.5.1 Macrocell Environment

Figure 2.11 shows the channel on the forward link for a macrocell environment. It is usually assumed that the scatterers surrounding the mobile station are about the same height as or are higher than the mobile. This implies that the received signal at the mobile antenna arrives from all directions after bouncing from the surrounding scatterers as illustrated in Figure 2.11.

Under these conditions, Gans' assumption that the AOA is uniformly distributed over $[0, 2\pi]$ is valid. The classical Rayleigh fading envelope with deep fades approximately $\lambda/2$ apart emanates from this model [1].

However, the AOA of the received signal at the base station is quite different. In a macrocell environment, typically, the base station is deployed higher than the surrounding scatterers. Hence, the received signals at the base station result from the scattering process in the vicinity of the mobile station, as shown in Figure 2.12. The multipath components at the base station are restricted to a smaller angular region, BW, and the distribution of the

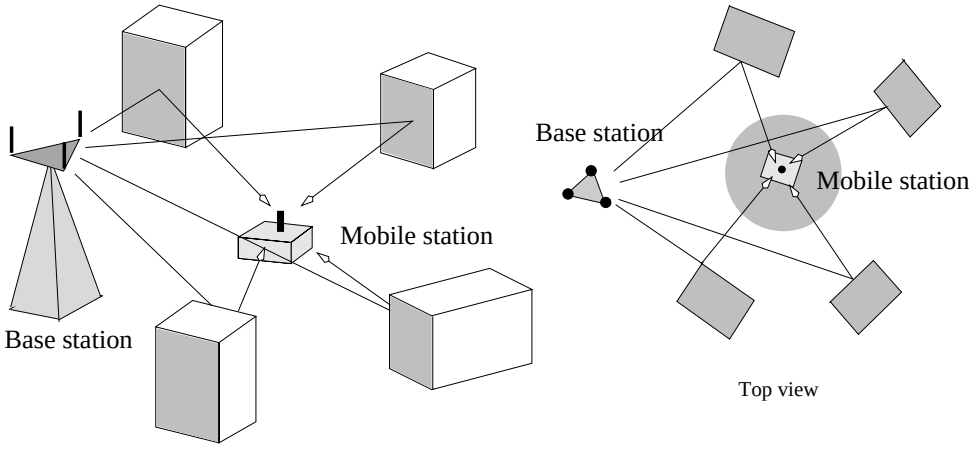

Figure 2.11: Macrocell environment - mobile station perspective.

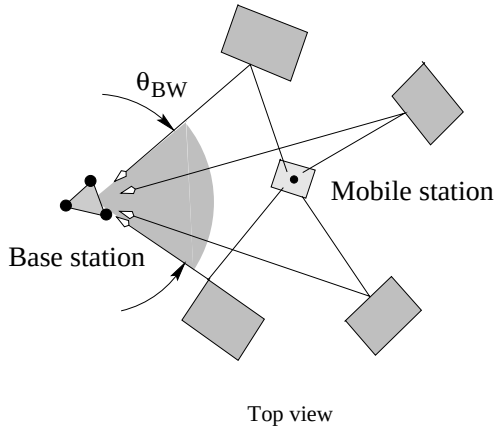

Figure 2.12: Macrocell environment - base station perspective.

AOA is no longer uniform over $[0, 2\pi]$. Other AOA distributions are presented later in this chapter. The base station model of Figure 2.11 was used to develop the theory and practice of base station diversity in today's cellular systems and has led to rules of thumb for the spacing of diversity antennas on cellular towers [4].

2.5.2 Microcell Environment

In the microcell environment, the base station antenna is usually mounted at the same height as the surrounding objects. This implies that the scattering spread of the AOA of the received signal at the base station is larger than in the macrocell case since the scattering process also happens in the vicinity of the base station. Thus, as the base station antenna is lowered, the tendency is for the multipath AOA spread to increase. This change in the behavior of the received signal is very important as far as antenna array applications are concerned. Studies have shown that statistical characteristics of the received signal are functions of the angle spread. Lee [4] and Adachi [19] found that the correlation between the signals received at two base station antennas increases as the angle spread decreases. This section has presented some of the physical properties of a wireless communication channel. A mathematical expression that describes the time-varying spatial channel impulse response was given in equation (2.79).

In the next section, two models that provide information about the spatial channel are presented.

2.5.3 Geometrically Based Single Bounce Circular Model - Macrocell Model

This model is based on the assumption that, in a macrocell environment, there will be no signal scattering from locations near the base station antenna, as discussed in Section 2.5.1. The geometry of this model is presented in Figure 2.13. Scatterers are assumed to be re-radiating elements whereby the plane wave, on arrival, is reflected to the mobile antenna, without the influence from other scatterers [20]. Also, it is assumed that the scatterers are uniformly distributed within radius R_C about the mobile. The transmitter-receiver (T-R) distance is D_0. It can be shown that the probability density function (PDF) of the angle of

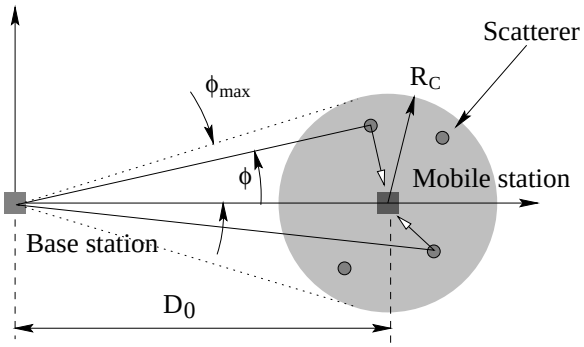

Figure 2.13: Illustration of the Geometrically Based Single Bounce Circular Model.

arrival ϕ of the multipath components at the base station is:

$$f_\phi(\phi) = \begin{cases} \frac{2D_0 \cos\phi \sqrt{D_0^2 \cos^2\phi - D_0^2 + R_C^2}}{\pi R_C^2} & , \quad -\phi_{max} \leq \phi \leq \phi_{max} \\ 0 & , \quad \text{otherwise.} \end{cases} \tag{2.83}$$

where $\phi_{max} = \sin^{-1}(R_C/D_0)$.

Figure 2.14 shows the PDF $f_\phi(\phi)$ for $D_0 = 5$ km and radius of scatterers R_C of 200 m, 500 m and 1 km.

2.5.4 Geometrically Based Single Bounce Elliptical Model - Microcell Model

This model assumes that the base station antenna is usually mounted at the same height as the surrounding objects and, therefore, there will be signal scattering from locations near both the base station and mobile station antennas. The geometry of this model is shown in Figure 2.15, where the base station and the mobile are located at the foci of an ellipse. Assuming that the line-of-sight path is not obstructed, the first multipath components arrives at a time $\tau_0 = D_0/c$, where D_0 is the T-R distance and c is the speed of light.

Consider that a multipath component arrives at time τ_i (also called the *time-of-arrival* (TOA)) at the base station, as shown in Figure 2.15. Assuming that this component is the result of a single bounce, the scatterer that causes the reflection lies on an ellipse with major and minor axes $2a_i$ and $2b_i$, respectively, where:

$$a_i = c\tau_i/2 \quad \text{and} \quad b_i = \sqrt{a_i^2 - D_0^2/4}. \tag{2.84}$$

Using the properties of ellipse geometry and assuming that the scatterers are uniformly distributed over the ellipse, we can show that the PDF of the angle-of-arrival ϕ of multipath

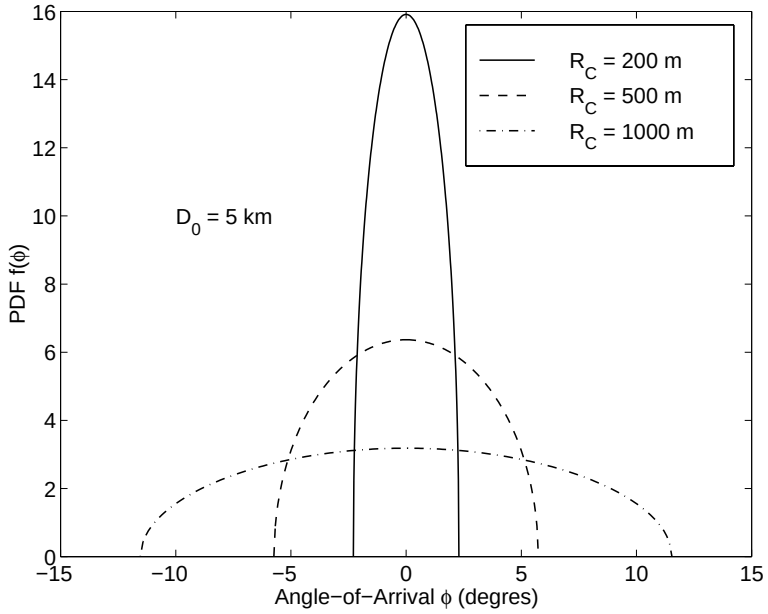

Figure 2.14: Probability Density Function of the angle-of-arrival ϕ of the multipath components received at the base station for the Geometrically Based Single Bounce Circular Model: T-R distance is 5 km.

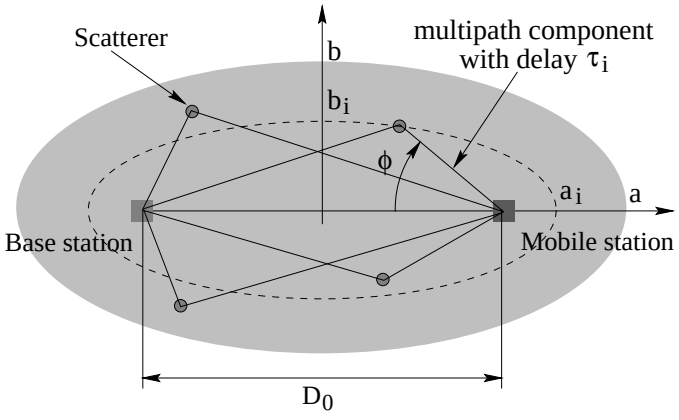

Figure 2.15: Illustration of the Geometrically Based Single Bounce Elliptical Model.

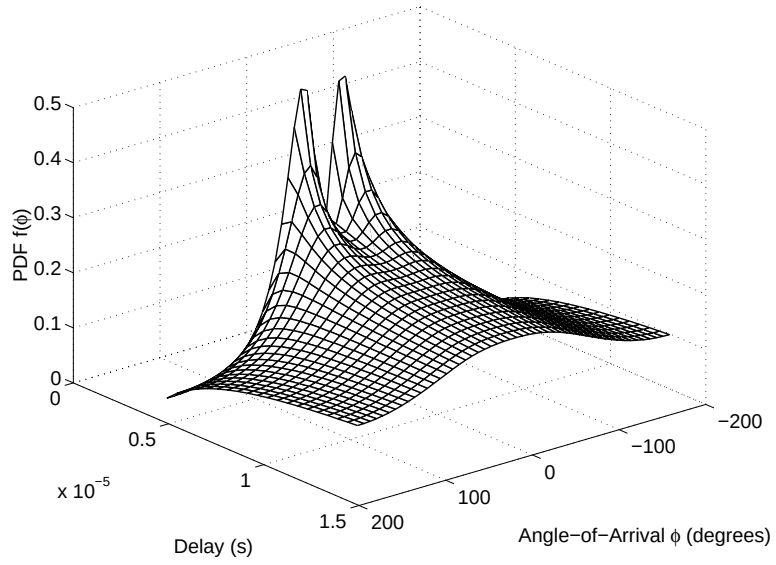

Figure 2.16: Probability Density Function of the angle-of-arrival ϕ of the multipath components conditioned on multipath delay for Geometrically Based Single Bounce Elliptical Model: T-R distance is 1 km.

components arriving at a time τ_i is [15]:

$$f_{\phi,r_i}(\phi, r_i) = \frac{(r_i^2 - 1)^{3/2}(r_i^2 - 2r\cos\phi + 1)}{\pi(2r_i^2 - 1)(r - cos\phi)^3} \quad \text{for} \quad -\pi \leq \phi \leq \pi, \tag{2.85}$$

where $r_i = \tau_i/\tau_0$ is the normalized multipath delay. Figure 2.16 shows $f_{\phi,r_i}(\phi, r_i)$ for a T-R distance of 1 km.

Assuming that the maximum multipath delay is τ_m, we can show that the probability density function of the multipath delay τ is [15]:

$$f_\tau(\tau) = \frac{c}{D_0\gamma}\frac{2(c\tau/D_0)^2 - 1}{\sqrt{\tau/D_0)^2 - 1}} \quad \text{for} \quad \tau_0 \leq \tau \leq \tau_m \tag{2.86}$$

where $\gamma = \tau_m/\tau_0\sqrt{(\tau_m/\tau_0)^2 - 1}$. The maximum delay spread τ_m determines the delay spread and angle spread of the channel.

2.6 Capacity Improvement by Using Adaptive Antennas

Adaptive antennas can be used in TDMA/FDMA cellular systems to reduce co-channel interference *from other cells*, allowing cluster size reduction and system capacity improvement. Additionally, adaptive antennas can be used to allow channel reuse within the cell. In CDMA systems, on the other hand, adaptive antennas are used to reduce interference from *in-cell* co-channel users, since in-cell interference is the major limiting factor of system capacity in such systems.

In the following, we present some representative studies on cellular capacity enhancement using adaptive antennas. Different approaches for increasing system capacity are used in these studies, but all based on the spatial filtering capability of antenna arrays.

2.6.1 TDMA and FDMA Cellular Systems

Before presenting studies that analyze system capacity improvement by using adaptive antennas, we discuss how array antennas are able to improve system capacity in FDMA/TDMA cellular systems. The formulas presented can be used to predict capacity improvement when array antennas are used. This description follows in part the approach proposed by Lopez [21]. We consider the forward link, but the same approach can be used for the reverse link.

Consider the forward link of a cellular system with cluster size N and cell radius R. The base stations are equipped with omnidirectional antennas. In the present analysis, we consider only the first tier of co-channel cells. The area mean signal-to-interference ratio (SIR) at a mobile located at the cell boundary is

$$\begin{aligned} SIR_{omni} &= \frac{1}{6}\left(\frac{R}{D}\right)^{\gamma} \\ &= \frac{1}{6}\,(3N)^{\gamma/2}, \end{aligned} \tag{2.87}$$

where we have assumed that all distances between the interfering base stations in the first tier and the mobile where the SIR is measured are equal to the reuse distance $D = \sqrt{3N}R$. The parameter γ is the path loss exponent, usually assumed to be between 3 and 4.

Consider now that the base stations are equipped with switched-beam antennas that are able to form any number m of ideal beams, with beamwidth $BW = 2\pi/m$. The antenna gain within the beamwidth is equal to the gain of the omnidirectional antenna, and zero outside

the beamwidth. Assuming that the co-channel interference from interfering base stations is uniformly distributed over $[0, 2\pi]$, the *SIR* at the mobile located at the cell boundary is

$$\begin{aligned} SIR_{nb} &= \frac{1}{6}\,(3N)^{\gamma/2}\,\frac{2\pi}{BW} \\ &= \frac{m}{6}\,(3N)^{\gamma/2}. \end{aligned} \tag{2.88}$$

Therefore, the *SIR* at the mobile can be improved by increasing the number of beams in the antenna. The improvement in the *SIR* achieved by using narrowbeams may be sufficient to reduce the cell cluster size. Assume that the minimum tolerable *SIR* is equal to 23.4 dB, which is the *SIR* (computed using (2.88)) in a conventional system using cluster size $N = 7$ and 3 sectors ($m = 3$ beams) with $BW = 120^o$. For a particular number of beams m, the smallest cluster size N that guarantees $SIR \geq 23.4$ dB is computed using

$$N = \frac{1}{3}\,\left(\frac{6\,SIR}{m}\right)^{2/\gamma}\Bigg|_{SIR=220.5=23.4\;dB}. \tag{2.89}$$

Its worth noting that, for cells with hexagonal shapes, N assumes only the values $N = i^2 + ij + j^2$, where i and j are non-negative integers. Therefore, $N = 1, 3, 4, 7, 9, 12, 13, \cdots$. Figure 2.17(a) shows the minimum cluster size required to guarantee $SIR \geq 23.4$ dB, for several values of m and $\gamma = 4$. It is interesting to note that, increasing the number of beams from $m = 3$ to $m = 8$ is not enough to reduce the cluster size. The reason is that the correponding increase in *SIR* is not sufficient to allow cluster size reduction from $N = 7$ to $N = 4$ and maintain $SIR \geq 23.4$ dB.

Reduction in cell cluster size increases system capacity, since more channels are assigned to each cell. However, additional capacity improvement can be achieved by maximizing the trunking efficiency. Conventional cellular systems, such as AMPS, employ cells with three sectors (or beams) and the available channels in the cell are equally divided among the sectors to form three *trunks*. The advantage of forming trunks is that no control among the sector is required to allocate a channel to a call. However, trunking (i.e. dividing the channel available in the cell into subsets) reduces the maximum carried traffic by the cell. In a multibeam base station antenna, trunking efficiency is maximized if any given beam can use any channel available in the cell. Assume that $N_S = 395$ channels are available in the entire cellular system under consideration. Therefore, $N_c = 395/N$ channels are available in each cell, where N is the cluster size shown in Figure 2.17(a). Assume also that, on average, a user generates a traffic of 0.03 Erlangs. Figure 2.17(b) shows the maximum number of users when m antenna beams are used at the base stations. We see that, in addition to the

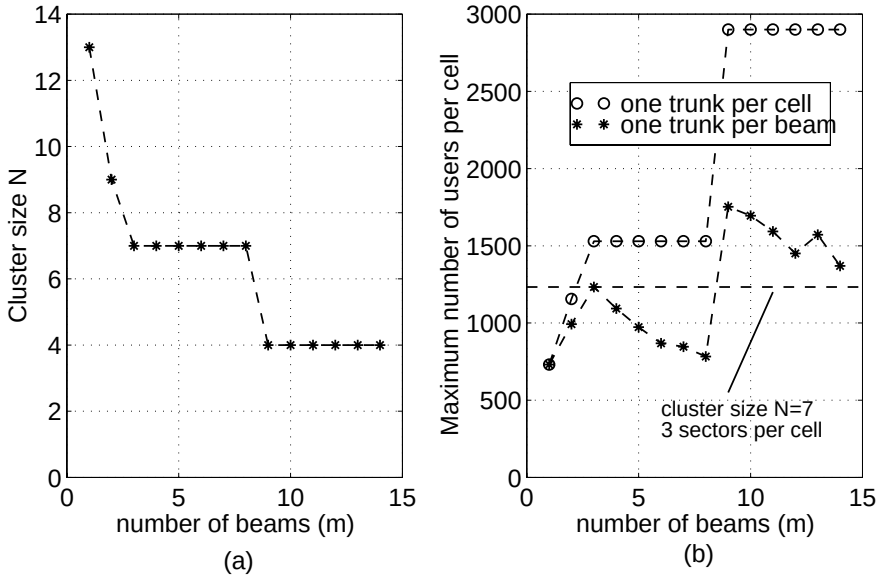

Figure 2.17: (a) Minimum cluster size required to guarantee $SIR \geq 23.4$ dB, when base station antennas with m beams are employed; (b) Maximum number of users per cell when m beams are used at the base stations.

capacity improvement achieved by reducing cell cluster size (when possible), capacity can be improved by forming only one trunk. Even though the analysis presented above is rather simplified, some basic concepts regarding how array antennas can reduce cluster size and improve system capacity could be discussed. An extensive study on capacity improvement by combining narrowbeam antennas with fractional loading factor is presented in Chapter 4. Several other studies based on capacity improvement achieved by reducing cluster size and controlling the increased co-channel interference using adaptive antennas can be found in the literature. We describe some of these studies next.

Swales *et. al* [22] studied the capacity improvement in a TDMA cellular system with base stations equipped with adaptive antennas on the foward link. The adaptive antennas are assumed to be ideal, with beamwidth $BW = 2\pi/m$, where m is the number of beams formed in the array, and no side lobe level ($SLL = -\infty$ dB). It is also assumed that any mobile is perfectly tracked by its serving base station. Channels are assigned to the base stations following the fixed channel allocation approach (see Chapter 6). The capacity improvement is measured in terms of increase in spectrum efficiency E, defined in [22] as the number of

channels per bandwidth per area:

$$E = \frac{B_t/B_c}{B_t N A} \quad \frac{\text{number of channels}}{\text{MHz/km}^2}, \tag{2.90}$$

where B_t is the total bandwidth available in the system in MHz, B_c is the channel spacing in MHz and A is the cell area in km^2. N is the cluster size required to guarantee that the interference level does not exceed a maximum tolerable level. Since the interference level is a random variable, it is necessary to introduce the concept of *outage probability* P_o, defined as the probability that the signal-to-interference ratio is lower than a threshold SIR_0. In order to guarantee a minimum link quality, it is usually required that $P_o \leq 10\%$. In [22], $P_o = 1\%$ is used and only the first tier of co-channel cells is considered. The capacities of systems using adaptive antennas and omnidirectional antennas at the base stations are compared. If the systems to be compared employ the same transmission system (same modulation technique and channel spacing), and same cell area, the efficiency is then proportional to the inverse of the cluster size N. Thus, the spectrum efficiency improvement achieved by using adaptive antennas is the ratio G

$$G = \frac{E_{adapt}}{E_{omni}} = \frac{N_{adapt}}{N_{omni}}, \tag{2.91}$$

where N_{omni} is the cluster size of the system employing omnidirectional base station antennas, while N_{adapt} is the cluster size of the system employing adaptive antennas. The propagation channel model in [22] includes the path loss (path exponent $n = 4$), Rayleigh fading and shadowing fading (shadowing standard deviation of 6 dB). An analytical approach is then used to compute the required cluster size when base station adaptive antennas with m beams are used, such that the outage probability is below 1%. Figure 2.18 shows the spectrum efficiency improvement G, computed using (2.91), as a function of the number of beams m formed by the base station adaptive antennas, for $SIR_0 = 8$ and 20 dB. We see that, for instance, the use of 8-beam adaptive antennas at the base stations increases the spectrum efficiency by almost 300%. The results presented in [22] demonstrate the benefits of adaptive antennas in TDMA systems.

In [22], capacity improvement is obtained by reducing cluster size and controlling the increased co-channel interference by using adaptive antennas at the base stations. In [23], Zetterberg *et. al* investigate capacity improvement by reusing channels within the cells, in addition to the cluster size reduction approach. In the study presented in [23], each 120^o sector of the cell (a *subcell*) is covered by a M-element antenna array on the foward link. Each element of the array is an ideal sectorized antenna with a sector of 120^o. The

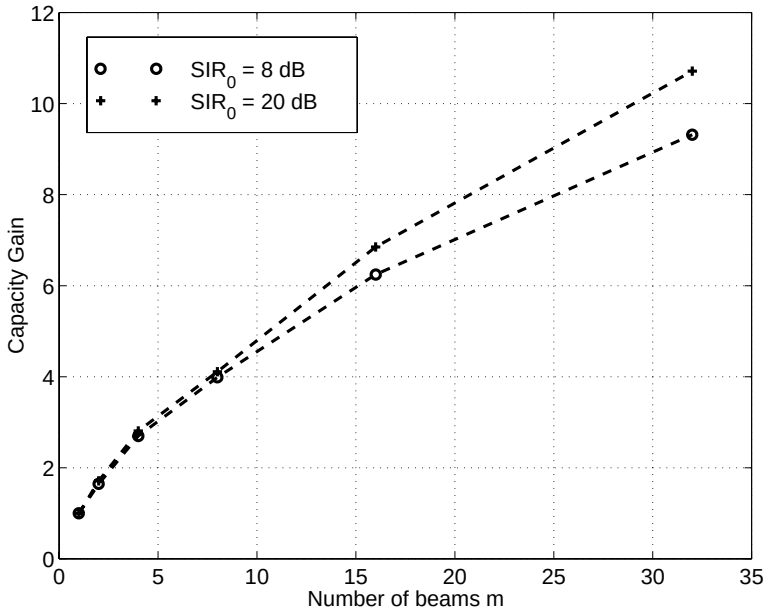

Figure 2.18: Relative spectrum efficiency, with respect to the spectrum efficiency of the reference system (omnidirectional base station antennas), as a function of the number of beams, for outage probability 1% [22].

weights of the array are adjusted in order to maximize the transmitted power towards the desired mobile and minimize the transmitted power towards in-cell co-channel mobiles. The angular positions of the desired and in-cell co-channel mobiles are assumed to be known by the base station. Note that no attempt to reduce the co-channel interference at the mobile in other cells is made. A *channel allocator* is used to allocate d in-cell users on each of the channels available in the cell. The strategy used for the channel allocator is such that the users sharing a particular channels are uniformly distributed over $[0, 2\pi]$. The propagation channel model includes path loss (path loss exponent $n = 4$), shadowing fading (shadowing standard deviation of 6 dB) and Rayleigh fading. The angles of departure of the multipath components are modeled as Gaussian random variables, with angular spread σ_A. The number of mobiles d and the angular spread σ_A are simulation parameters. The capacity of a cellular system employing the proposed base station antenna array transmission system is compared with the capacity of a reference system. The reference system employs cluster size $N = 4$, 3-sectorized cells and allocates only one mobile on each channel ($d = 1$). The outage probability in the reference system, for threshold $SIR_0 = 9$ dB, is estimated to be 2.65%, which is deemed to be the minimum acceptable performance that must be achieved

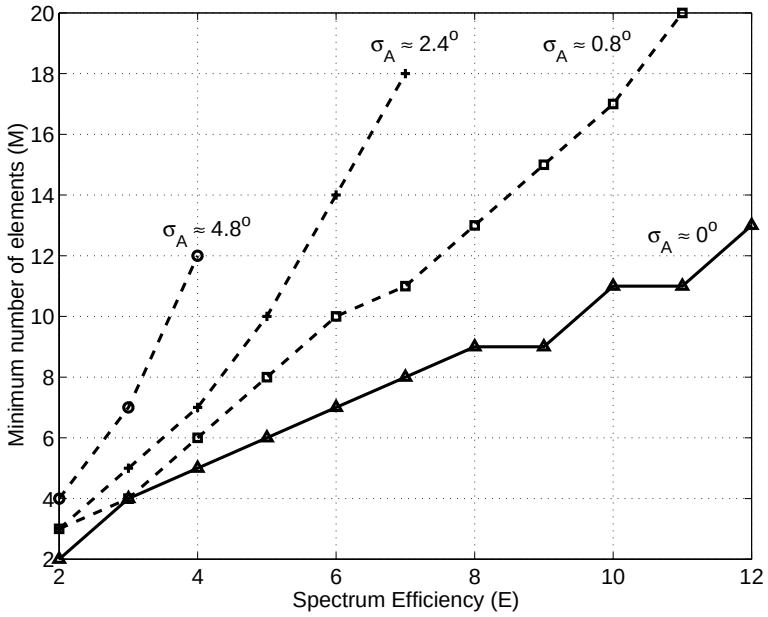

Figure 2.19: Minimum number of antenna elements required to achieve an outage probability of 2.65% as a function of spectrum efficiency E for $N = 4$ [23].

when using base station adaptive antennas. The capacity improvement analysis is based on the spectrum efficiency E, defined in [23] as

$$E = 4\,\frac{d}{C}. \tag{2.92}$$

Thus, $E = 1$ for the reference system. Simulation results have shown that, for all M (number of elements in the array) in the range $\{1, \cdots, 20\}$ and for outage probability less than 2.65%, the maximum spectrum efficiency is achieved for cluster size $N = 4$. However, a given spectrum efficiency requires a minimum number of antenna elements, which depends on the angular spread σ_A, as shown in Figure 2.19. We see that the number of elements required rapidly increases as the angular spread σ_A increases. For example, in order to increase system capacity by 500% (6 times) with respect to the capacity of the reference system, 7 elements are required when $\sigma_A \approx 0^o$. However, if σ_A is about 2.4^o, the number of elements required increases to 14. Therefore, the performance highly depends on the propagation environment.

2.6.2 CDMA Cellular Systems

In CDMA systems, adaptive antennas are used to reduce interference from *in-cell* co-channel users, since in-cell interference is the major limiting factor of system capacity in such systems.

Table 2.1: The maximum number of users supported at $Pr\{BER > 10^{-2}\} < 10\%$ as a function of the number of multipath components L and number of elements M in the array antennas, for switched beam (SB) and optimum beamforming (OB): wideband case [24].

L	**Number of users supported**				
	omni	$M = 6$ SB	$M = 6$ OB	$M = 12$ SB	$M = 12$ OB
1	14	31	> 31	> 31	> 31
2	10	23	> 31	> 31	> 31
10	4	15	23	20	29
30	0	6	10	13	20

Liberti *et. al* [24] presented an analysis of a CDMA cellular system with spreading gain $N = 31$ and using base station adaptive antennas with M elements on the reverse link. Both optimum beamforming (OB), based on the minimum mean square error criterion, and switched beam (SB) approaches are considered. The Geometrically Based Single Bounce Elliptical Model, discussed in Section 2.5.4, was adopted, with L multipath components for each user. Both *narrowband* and *wideband* cases are considered. In the narrowband case, all multipath components arrive with delays which are very small compared to a chip and are assumed to be correlated with one another. On the other hand, in the wideband case, the multipath components are uncorrelated with one another, due to sufficient difference in the propagation delays. The path loss assumed is $n = 3$ and no out-of-cell interference is considered. It is also assumed that the total received power from each user is the same, that is, power control is perfect. The capacity of the system is computed based on the outage probability, which is defined in [24] as the probability that a raw bit error rate (BER) exceeds 10^{-2}. Thus, the capacity of the system is defined as the maximum number of users that can be supported at an outage probability of less than 10%.

Table 2.1 shows the number of users for the wideband case (uncorrelated multipath components). We can see that system capacity increases as the number of antenna elements increases. Note also that an OB system performs better than a SB system for the same number of antenna elements. As expected, system capacity degrades as the number of multipath components L increases, especially for a small number of antenna elements.

Table 2.2 shows the performance of the SB and OB systems for the narrowband case (correlated multipath environment). We see that, unlike for the wideband case shown in

Table 2.2: The maximum number of users supported at $Pr\{BER > 10^{-2}\} < 10\%$ as a function of the number of multipath components L and number of elements M in the array antennas, for switched beam (SB) and optimum beamforming (OB): narrowband case [24].

L	**Number of users supported**				
	omni	$M = 6$ SB	$M = 6$ OB	$M = 12$ SB	$M = 12$ OB
1	14	31	> 31	> 31	> 31
2	4	23	> 31	> 31	> 31
10	0	6	> 31	25	> 31
30	0	12	> 31	14	> 31

Table 2.1, the performance of the OB system does not degrade as the number of multipath components increases. Also, the capacity improvement achieved by increasing the number of elements for the SB systems in the narrowband case is not as large as it is for the wideband case.

Several other important studies on capacity improvement using adaptive antennas can be found in literature. In the following, we summarize some of them, with their main conclusions and results.

Reference	**Description**
[25]	Winter *et. al* show, by Monte Carlo evaluation, that a three-element base station antenna increases the signal-to-interference-plus-noise ratio (*SINR*) by 9.2 dB in the reverse link IS-54 digital cellular system. Increasing the number of elements in the array to four and five, the *SINR* increases 12.4 dB and 15 dB, respectively. Based on the observed *SIR* improvement, it is claimed that, with a three-element antenna, the capacity of the IS-54 cellular system can improve 100%, with respect to a conventional cellular system using cluster size $N = 7$ and omnidirectional antennas. It is also noted that with a two-element antenna and dynamic channel allocation, a cluster size of 4 is possible. The dynamic channel allocation would reallocate channels, when the adaptive antenna cannot sufficiently mitigate the co-channel interference.

Reference	Description
[26]	In the U.S. TDMA digital cellular system IS-136, a carrier is shared by three users (three time-slots per carrier) and the base station output power on each carrier must be kept at a constant level for the full duration of the frame. Therefore, individual beamforming on the reverse link for each time slot is not possible. Hagerman and Mazuer investigated reverse link beamforming on a carrier basis, combined with *beam packing*. With beam packing, mobiles close to each other (similar angle-of-arrival) are allocated time-slots on the same carrier. When beam packing is not used, a carrier is transmitted in several beams, increasing the total co-channel interference, and reducing the beamforming gain. The IS-136 system is simulated with cluster size $N = 4$, three-sectorized cells and four beams per cell. Results show that, assuming that $P[SIR < 18\text{dB}] < 10\%$ is required, the use of beam packing doubles the served traffic (number of users/cell/channel). As expected, the gain achieved by using beam packing increases as the traffic increases.
[27]	Petrus *et. al* analyze the capacity improvement achieved using base station adaptive antennas for AMPS system. The analysis is based on outage probability. It is shown that SDMA is not possible in an AMPS system. A cell cluster size of four can be achieved using a 5 element array and a cluster size of three is possible if a 8-element array is used.
[28]	The performance of switched-beam for cellular systems is analyzed by Ho *et. al*. Both forward and reverse links are analyzed and it is observed that the performance improvement in the reverse link is not uniform over the entire cell area. It has been shown that switched-beams are robust to imperfect power control. The trunking degradation caused by narrowbeam sectoring is also investigated and a variety of trunkpool techniques is analyzed.

2.7 Conclusions

We introduced in this chapter the basic concepts of adaptive antennas and beamforming techniques. The performance of adaptive antennas are highly dependent on the spatial characteristics of the propagation channel. Therefore, channel propagation models must include spatial information, such as angle-of-arrival, time-of-arrival, angle spread, etc. We discuss in this chapter the differences between microcell and macrocell propagation channel environments, from the point of view of spatial characteristics. Two spatial channel models are reviewed.

Adaptive antennas can reduce co-channel interference in cellular systems, increasing system capacity. In FDMA/TDMA cellular systems, reduction in co-channel interference allow cell cluster size reduction, increasing system capacity. Additionally, adaptive antennas can be use to allow channel reuse within the cell, increasing even more system capacity. In CDMA system, adaptive antennas are used to reduce interference from *in-cell* co-channel users, since in-cell interference is the major limiting factor of system capacity in such systems. We also reviewed in this chapter some representative studies on system capacity enhancement using adaptive antennas in cellular systems.

Chapter 3

Statistical Analysis of Co-channel Interference in Cellular Communication Systems

3.1 Introduction

Co-channel interference is generally recognized as one of the factors that limits the capacity and transmission quality in wireless communications. An appropriate understanding of the statistical behavior of the co-channel interference is extremely important when analyzing and designing multi-user wireless systems or for exploring techniques that mitigate the undesirable effects of co-channel interference.

The performance of wireless communications systems operating under the effects of co-channel interference has been extensively studied [29]-[32]. Co-channel interference in a wireless system occurs, for example, when a mobile simultaneously receives signals from co-channel base stations. In this instance, one co-channel forward link is the desired signal, and the other co-channel signals are received as interference and compose the total co-channel interference at the receiver.

In wireless communications, the statistical characterization of the desired or interference signals involves mainly two propagation effects: *small scale fading*, induced by multipath over a local area, and *shadowing* (large scale fading), induced by random attenuators of the local mean signal, such as trees, buildings and terrain [1, 33]. Measurements have shown that the local mean signal level in a wireless communications system [34, 35] can be accurately model

as a lognormal random variable (RV). When expressed in decibel units, the local mean signal level follows a normal variation and it is characterized by an area mean value and standard deviation, both in dB. The area mean value is a function of particular parameters, such as the transmitter to receiver separation (T-R) distance, transmitter power levels and antenna gains, while the shadowing standard deviation depends on the physical environment. In the general case of system design or simulation, the effects of small fading and shadowing fading must be taken into consideration, although, in some cases, shadowing of the desired and interference signals is the main source of performance degradation. For example, spatial diversity, spread spectrum, and coding and interleaving techniques have been extensively employed to combat the effects of small scale fading [1, 33, 4], such that received signals are mainly dependent on large scale channel variations. In the analysis presented in this work, we assume that the small scale fading effects are averaged out and only shadowing fading and path loss are considered.

Based on the assumption that the received signals are affected by shadowing fading and path loss only, the total co-channel interference is therefore modeled as a composition of individual interference signals, whose local mean power levels follow lognormal variation. It is usually assumed that the phase shift observed in each individual interference signal varies significantly due to scattering, such that we can assume that the signals add incoherently (e.g. their powers add) when averaged over the local area. Therefore, the total co-channel interference received at a given location is modeled as the *sum* of lognormally distributed signals.

It is well accepted that the distribution of the sum of lognormal RVs can be approximated by another lognormal distribution [36]-[37], and several methods have been proposed for computing the mean value and standard deviation in decibel units of the resulting lognormal distribution. Wilkinson's [36] and Schwartz and Yeh's methods [38] are among the most popular methods, and several studies have been published on both methods [36]-[37], comparing the estimated distribution functions (DFs) and moments of the sum. While Wilkinson's and Schwartz and Yeh's methods allow the individual signals in the sum to have different mean values and standard deviations in decibel units, previous works have surprisingly assumed that all the summands have identical means and standard deviations. However, practical situations where the individual interference signals have *different* mean values and *different* standard deviations occur very often in wireless communications, and will become more important as future wireless systems proliferate. Since the mean values of

the interference signals depend on parameters such as the T-R distance and antenna gains, the area means of each signal differ significantly if the distances and the antenna patterns are significantly different. Furthermore, it is likely that each interference has a different standard deviation about the area mean, due to different physical shadow environments. A typical situation where interference signals have different area means and standard deviations occurs in indoor wireless communications systems in multifloored buildings. Measurements have shown [39, 40] that the standard deviation in decibel units of the signal received at a given location depends on the number of floors separating the transmitter and receiver. When analyzing the performance and capacity of wireless systems, the assumption that all interference signals have the same mean and standard deviation may be used for a first-order prediction. However, for more accurate capacity and performance predictions of emerging in-building and microcell wireless systems, a more accurate description of the statistics of the individual interference signals is required, by considering the appropriate values of mean and standard deviation of each individual interference signal.

In this chapter, we present an accuracy analysis of Schwartz & Yeh's and Wilkinson's methods for the general case, when the individual interference signals that compose the total interference have *different* mean values and *different* standard deviations. We show that the accuracy of Wilkinson's method, unlike for Schwartz & Yeh's method, is very sensitive to the difference between the mean values and standard deviations of the individual interference signals, and the number of signals in the sum.

The analysis presented in this work is based on comparing the estimates of the mean and standard deviation of the sum computed using each method [41, 42]. In many applications, such as the simulation of wireless communications systems, we are interested in the mean value and standard deviation of the sum of the interference signals, rather than the distribution function of the sum, for simplified analysis of outage, frame error rate, capacity or other system performance parameters.

The remainder of this chapter is organized as follows. Section 3.2 briefly reviews Wilkinson's and Schwartz & Yeh's methods. Section 3.3 compares the mean values and standard deviations of the total interference signal computed using both methods, for a wide range of statistical distributions of the individual co-channel interference signals. Section 3.4 concludes the chapter.

3.2 Sum of Lognormal Random Variables

Consider that N interference signals arrive at the receiver from co-channel mobiles or base stations. Assuming that the effects of small scale fading are averaged out, the local mean power level I_i of the i-th signal undergoes lognormal variation. Using decibel units, the local mean power level can be modeled as [1, 33]

$$X_i = 10 \log_{10} I_i = m_{X_i} + \chi_i \quad \text{(in dBm)}, \tag{3.1}$$

where m_{X_i} is the area mean power (or, alternatively, average large-scale propagation path loss) and χ_i is a zero-mean normally distributed RV in dB with standard deviation σ_{X_i}, also in dB, due to the shadowing caused by large obstacles [1, 33]. The area mean m_{X_i} is usually modeled as a function of the T-R separation d_i, path loss exponent γ, transmitted power $P_{T,i}$, in dBm, and transmitter and receiver antenna gains $G_{T,i}$ and $G_{R,i}$, both in dB

$$m_{X_i} = P_{T,i} + G_{T,i} + G_{R,i} - 10\gamma \log_{10} d_i \quad \text{(in dBm)}. \tag{3.2}$$

Under the reasonable assumption that the individual signals I_i add incoherently, the total interference signal is modeled as the sum of N lognormally distributed signals

$$I = \sum_{i=1}^{N} I_i. \tag{3.3}$$

It is well accepted that the distribution of I can be approximated by another lognormal distribution [36]-[37], or, equivalently, that $X = 10 \log_{10} I$ follows a normal distribution. Assuming that the sum I is lognormally distributed, which is a fair assumption based on numerous and well known empirical and analytical studies, Wilkinson's [36] and Schwartz and Yeh's methods [38] compute the mean m_X and standard deviation σ_X of X.

In the derivation of these two methods, it is convenient to use the natural logarithm instead of the logarithm with base 10 to define the normal RV that corresponds to a lognormal RV. Thus, define the normal RV Y_i as

$$Y_i = \ln I_i, \quad \text{(logarithmic units)} \tag{3.4}$$

with mean value m_{Y_i} and standard deviation σ_{Y_i} given, respectively, by

$$m_{Y_i} = \lambda \, m_{X_i} \;\text{ and }\; \sigma_{Y_i} = \lambda \, \sigma_{X_i}, \quad \text{(logarithmic units)} \tag{3.5}$$

where $\lambda = \ln(10)/10$. Note that $Y_i = \lambda X_i$.

Using (3.4) and recalling that we are approximating the distribution of I by a lognormal distribution, we have

$$I = e^{Y_1} + e^{Y_2} + \cdots + e^{Y_N} \approx e^Z = 10^{X/10}, \tag{3.6}$$

where Z (in logarithmic units) and X (in dB) are normally distributed, and $Z = \lambda X$. Wilkinson's and Schwartz & Yeh's methods then compute the mean value and standard deviation of Z (m_Z and σ_Z) or X (m_X and σ_X) from the mean values and standard deviations of the summands Y_i, as shown subsequently.

For generality, it is useful to assume that the individual signals I_i may be correlated to each other. This correlation may be due to the fact that shadowing loss is caused by large objects surrounding the mobiles or base stations. Therefore, even signals coming from different directions may be attenuated by the same obstacles, leading to correlation among the received signals. Also, uncorrelated shadowing is simply a specific case for the general correlated shadowing assumption. Therefore, in order to consider the correlated interference signals case, let us define the correlation coefficient r_{ij} of Y_i and Y_j by

$$r_{ij} = \frac{E\{(Y_i - m_{Y_i})(Y_j - m_{Y_j})\}}{\sigma_{Y_i}\, \sigma_{Y_j}}. \tag{3.7}$$

Since Y_i is a scaled version of X_i, r_{ij} is also the correlation coefficient of X_i and X_j.

3.2.1 Wilkinson's Method

According to Wilkinson's method, the mean value and standard deviation of Z in (3.6) are determined by matching the first and second moments of I with those of $I_1 + I_2 + \cdots + I_N$. For the first moment, we have

$$E\{e^Z\} = E\{e^{Y_1} + e^{Y_2} + \cdots + e^{Y_N}\}. \tag{3.8}$$

The moments in (3.8) are evaluated by observing that, for a normal RV u with mean value m_u and variance σ_u^2, and any integer n, we have [13]

$$E\{e^{nu}\} = \exp(nm_u + \frac{1}{2}n^2\sigma_u^2). \tag{3.9}$$

Therefore,

$$E\{e^Z\} = \exp(m_Z + \sigma_Z^2/2), \tag{3.10}$$

and

$$E\{e^{Y_1} + e^{Y_2} + \cdots + e^{Y_N}\} = \sum_{i=1}^{N} \exp(m_{Y_i} + \sigma_{Y_i}^2/2). \tag{3.11}$$

Using (3.10) and (3.11) in (3.8), we have

$$\exp(m_Z + \sigma_Z^2/2) = \sum_{i=1}^{N} \exp(m_{Y_i} + \sigma_{Y_i}^2/2) = u_1. \tag{3.12}$$

The summation in (3.12), henceforth denoted by u_1, is a function of the mean values m_{Y_i} and standard deviations σ_{Y_i} of the summands Y_i, which are assumed to be known.

Now, matching the second moments of I and $I_1 + I_2 + \cdots + I_N$, we have

$$E\{e^{2Z}\} = E\{(e^{Y_1} + e^{Y_2} + \cdots + e^{Y_N})^2\}. \tag{3.13}$$

Using again the property (3.9) in both sides of (3.13), we obtain

$$\begin{aligned} \exp(2m_Z + 2\sigma_Z^2) &= \sum_{i=1}^{N} \exp(2m_{Y_i} + 2\sigma_{Y_i}^2) + \\ &\quad +2 \sum_{i=1}^{N-1} \sum_{j=i+1}^{N} \exp(m_{Y_i} + m_{Y_j}) \times \\ &\quad \exp\left[\frac{1}{2}(\sigma_{Y_i}^2 + \sigma_{Y_j}^2 + 2r_{ij}\sigma_{Y_i}\sigma_{Y_j})\right] = u_2. \end{aligned} \tag{3.14}$$

The left-hand side of (3.14) can be evaluated using the mean values m_{Y_i}, standard deviations σ_{Y_i} and correlation coefficient r_{ij}, and will be denoted by u_2.

Expressions (3.12) and (3.14) form a system of equations with unknowns m_Z and σ_Z. By solving this system of equations, and using $Z = \lambda X$, we finally obtain

$$m_X = (1/\lambda)\,(2\ln u_1 - \frac{1}{2}\ln u_2), \tag{3.15}$$

$$\sigma_X = (1/\lambda)\,\sqrt{\ln u_2 - 2\ln u_1}. \tag{3.16}$$

An important feature of Wilkinson's method is that the assumption of $\sum_i I_i$ being lognormally distributed is actually used in the computation of m_X and σ_X.

3.2.2 Schwartz and Yeh's Method

Schwartz and Yeh proposed a method based on the *exact* computation of the mean value m_X and standard deviation σ_X of the sum of $N = 2$ lognormal RVs. For $N > 2$, a recursive approach is used, approximating the sum of two lognormal RVs by another lognormal RV, and computing the mean and standard deviation of the sum.

Consider the sum of N lognormal RVs in (3.6), rewritten as

$$Z = \ln(e^{Y_1} + e^{Y_2} + \cdots e^{Y_N}). \tag{3.17}$$

Let Z_k denote $\ln(e^{Z_{k-1}} + e^{Y_k})$, where Z_{k-1} is *assumed* to be normally distributed. Schwartz and Yeh's method then computes the mean m_{Z_k} and standard deviation σ_{Z_k} of Z_k, for $k = 2, 3, \cdots, N$. Following notation used in [36], m_{Z_k} and σ_{Z_k}, for $k = 2, 3, \cdots, N$, are given by

$$\begin{aligned} m_{Z_k} &= m_{Z_{k-1}} + G_1(m_{w_k}, \sigma_{w_k}) && (3.18) \\ \sigma^2_{Z_k} &= \sigma^2_{Z_{k-1}} - G_1^2(m_{w_k}, \sigma_{w_k}) + G_2(m_{w_k}, \sigma_{w_k}) + \\ &\quad +2\,\frac{(r_{(Z_{k-1})(Y_k)}\sigma_{Y_k} - \sigma_{Z_{k-1}})\sigma_{Z_{k-1}}}{\sigma^2_{w_k}}\, G_3(m_{w_k}, \sigma_{w_k}), && (3.19) \end{aligned}$$

where m_{w_k} and σ_{w_k} are the mean and standard deviation of $w_k = Y_k - Z_{k-1}$. Since Y_k is normally distributed and Z_{k-1} is assumed to be normally distributed, w_k is also assumed to be a normal RV, with probability density function $p_{w_k}(w_k)$

$$p_{w_k}(w_k) = \frac{1}{\sqrt{2\pi}\sigma_{w_k}} \exp\left[-\frac{(w_k - m_{w_k})^2}{2\sigma^2_{w_k}}\right], \qquad (3.20)$$

where

$$\begin{aligned} m_{w_k} &= m_{Y_k} - m_{Z_{k-1}} && (3.21) \\ \sigma_{w_k} &= \sqrt{\sigma^2_{Y_k} + \sigma^2_{Z_{k-1}} - 2\, r_{(Z_{k-1})(Y_k)}\, \sigma_{Y_k}\, \sigma_{Z_{k-1}}}. && (3.22) \end{aligned}$$

The term $r_{(Z_{k-1})(Y_k)}$ in (3.19) and (3.22) is the correlation coefficient of Z_{k-1} and Y_k, given by [44]

$$r_{(Z_{k-1})(Y_k)} = \sigma_{Z_{k-2}}\,\frac{r_{(Z_{k-2})(Y_k)}}{\sigma_{Z_{k-1}}} + \frac{r_{(k-1)(k)}\sigma_{Y_{k-1}} - r_{(Z_{k-2})(Y_k)}\sigma_{Z_{k-2}}}{\sigma_{Z_{k-1}}\sigma^2_{w_{k-1}}}\, G_3(m_{w_{k-1}}, \sigma_{w_{k-1}}). \qquad (3.23)$$

The functions G_1, G_2 and G_3 in (3.18), (3.19) and (3.23) are given by

$$\begin{aligned} G_1(m_{w_k}, \sigma_{w_k}) &= E\{\ln(1 + e^{w_k})\} \\ &= \int_{-\infty}^{\infty} \ln(1 + e^{w_k})\, p_{w_k}(w_k)\, dw_k, && (3.24) \end{aligned}$$

$$\begin{aligned} G_2(m_{w_k}, \sigma_{w_k}) &= E\{\ln^2(1 + e^{w_k})\} \\ &= \int_{-\infty}^{\infty} \ln^2(1 + e^{w_k})\, p_{w_k}(w_k)\, dw_k, && (3.25) \end{aligned}$$

and

$$\begin{aligned} G_3(m_{w_k}, \sigma_{w_k}) &= E\{(w_k - m_{w_k})\ln(1 + e^{w_k})\} \\ &= \int_{-\infty}^{\infty} (w_k - m_{w_k})\ln(1 + e^{w_k})\, p_{w_k}(w_k)\, dw_k. && (3.26) \end{aligned}$$

The integrals in (3.24), (3.25) and (3.26) must be numerically evaluated. It should be noted that $Z_1 = Y_1$. Therefore, by recursively applying expressions (3.18) through (3.26), for $k = 2, 3, \cdots, N$, the mean and standard deviation of X are finally given by $m_X = \lambda m_{Z_N}$ and $\sigma_X = \lambda \sigma_{Z_N}$, respectively.

3.2.3 Discussion

Schwartz & Yeh's method directly computes the mean value m_X and standard deviation σ_X in dB of the sum of lognormal RVs, while Wilkinson's method obtains the moments of X by computing the first two moments of $I = 10^{X/10}$. Furthermore, Schwartz & Yeh's method computes the *exact* moments of X for $N = 2$ summands. For more than two summands, the method is recursively applied, *assuming* that the sum of two lognormal RVs is lognormally distributed. On the other hand, Wilkinson's method computes m_X and σ_X *assuming* that $I = \sum_i I_i$ is lognormally distributed. We will see subsequently that Schwartz & Yeh's method gives more exact results than Wilkinson's method, when estimating m_X and σ_X.

3.2.4 Monte Carlo Simulation

The accuracy analysis of Wilkinson's and Schwartz & Yeh's methods is carried out by comparing the mean values and standard deviations of the sum computed using these two methods, to the mean value m_{sim} and standard deviation σ_{sim} of the sum computed using extensive Monte Carlo simulation. The Monte Carlo simulation is based on generating K (where $K > 10000$) sets of samples (denoted by $(v_1^{(k)}\ v_2^{(k)}\ \cdots\ v_N^{(k)})$) of N lognormally distributed signals v_i (representing the interference signals I_i) with a specific range of means m_{X_i} and standard deviations σ_{X_i} in decibel units, and correlated with correlation coefficient r_{ij}. To generate the k-th set of samples $(v_1^{(k)}\ v_2^{(k)}\ \cdots\ v_N^{(k)})$, we first generate the vector $\mathbf{a}$,

$$\mathbf{a} = [a_1\ a_2\ \cdots\ a_N]^T, \tag{3.27}$$

where a_i, $1 \leq i \leq N$, are samples of N uncorrelated normal processes with the specific means m_{X_i} and standard deviations σ_{X_i}, and T indicates transpose operation on a vector. The vector $\mathbf{a}$ is then converted into vector $\mathbf{b} = [b_1\ b_2\ \cdots\ b_N]^T$, using [6]

$$\mathbf{b} = \mathbf{L}\mathbf{a}, \tag{3.28}$$

in order to induce the desired correlation among the samples. The matrix $\mathbf{L}$ is a lower triangular matrix, computed from Cholesky decomposition on the desired autocorrelation

matrix $\mathbf{R}$

$$\mathbf{R} = E\{\mathbf{b}\,\mathbf{b}^T\} = \mathbf{L}\,\mathbf{L}^H, \tag{3.29}$$

whose elements are given by

$$R_{ij} = \begin{cases} r_{ij} & \text{for } i \neq j \\ 1 & \text{for } i = j. \end{cases} \tag{3.30}$$

The variables b_i are then converted into the desired samples $v_i^{(k)}$, by using $v_i^{(k)} = 10^{b_i/10}$. The samples $v_i^{(k)}$ $(1 \leq i \leq N)$ are added to generate the k-th sample $p^{(k)}$ of the sum of N lognormally distributed processes. By repeating the entire procedure K times, we generate a collection of K samples $p^{(k)}$ $(1 \leq k \leq K)$. The samples $p^{(k)}$ are then converted into decibel units, and the mean value m_{sim} and standard deviation σ_{sim} of the collection are then determined.

Once m_{sim} and σ_{sim} are computed by simulation, and m_X and σ_X are computed using Schwartz & Yeh's and Wilkinson's methods, the absolute errors in the mean value and standard deviation for each method are determined as

$$\text{error in the mean} = |m_X - m_{sim}| \qquad \text{(in dB)}, \tag{3.31}$$

$$\text{error in the standard deviation} = |\sigma_X - \sigma_{sim}| \qquad \text{(in dB)}. \tag{3.32}$$

In the following, several cases of the sum of log-normal RVs are analyzed for uncorrelated and correlated signals, where the correlation coefficient between signals X_i and X_j is set to $r_{ij} = 0.7$, for the correlated case.

3.3 Comparison

3.3.1 Two summands with different mean values and standard deviations

Consider the sum of two lognormal RVs I_1 and I_2. The mean value and standard deviation of $X_1 = 10\log_{10} I_1$ are set to $m_{X_1} = 0$ dBm and $\sigma_{X_1} = 8$ dB, respectively, while the mean value and standard deviation of $X_2 = 10\log_{10} I_2$ are chosen such that $\Delta m = m_{X_2} - m_{X_1}$ and $\Delta\sigma = \sigma_{X_2} - \sigma_{X_1}$ are within the ranges

$$-40 \text{ dB} \leq \Delta m \leq 40 \text{ dB} \;\Rightarrow\; -40 \text{ dBm} \leq m_{X_2} \leq 40 \text{ dBm} \tag{3.33}$$

$$-4 \text{ dB} \leq \Delta\sigma \leq 4 \text{ dB} \;\Rightarrow\; 4 \text{ dB} \leq \sigma_{X_2} \leq 12 \text{ dB}. \tag{3.34}$$

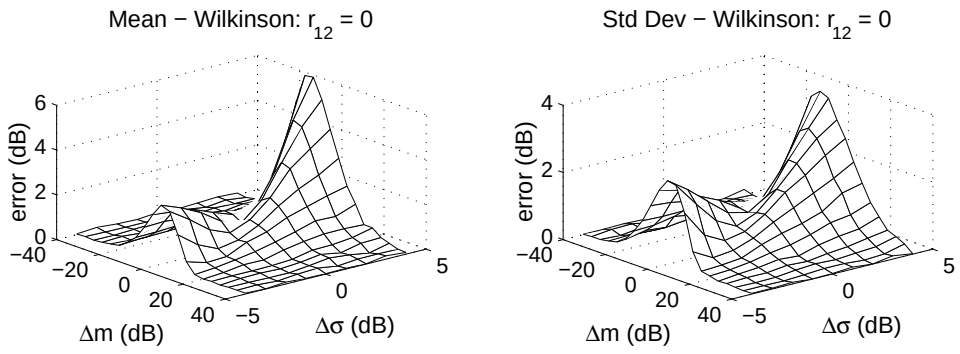

Figure 3.1: Absolute errors in the mean value and standard deviation of the sum of two uncorrelated lognormal signals, using Wilkinson's method.

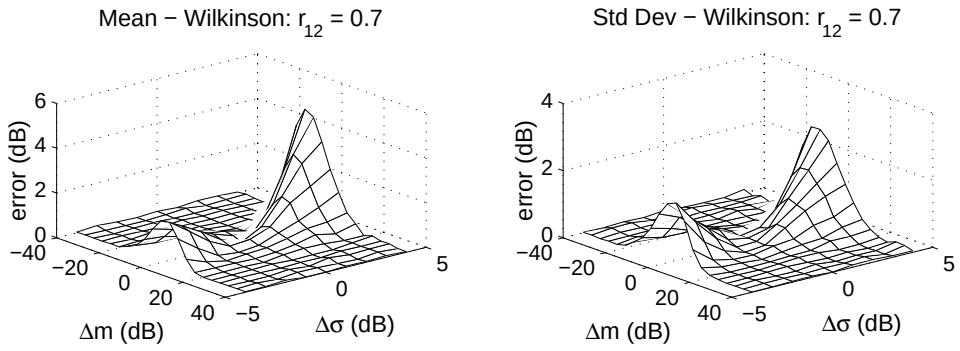

Figure 3.2: Absolute errors in the mean value and standard deviation of the sum of two correlated ($r_{12} = 0.7$) lognormal signals, using Wilkinson's method.

The errors in the mean and standard deviation for uncorrelated and correlated I_1 and I_2, using Wilkinson's method, are shown in Figure 3.1 and 3.2, respectively. For Wilkinson's method, when one of the summands is dominant ($|\Delta m| > 20$ dB), the errors in the mean and standard deviation are negligible. However, when the summands have about the same mean value and different standard deviations, the errors in the mean value and standard deviation of X are not negligible and can be as high as 6 dB and 4 dB, respectively, for uncorrelated summands. For correlated summands, the maximum errors in the mean and standard deviation drop to 4 dB and 2 dB, respectively. On the other hand, the errors for Schwartz & Yeh's method can be shown to be zero, for both correlated and uncorrelated summands, since this method computes the exact mean and standard deviation of X.

The higher accuracy of Schwartz & Yeh's method, compared with Wilkinson's method, is at the expense of higher complexity, as one can see from expressions presented in Section 3.2. However, Figures 3.1 and 3.2 show that, for some values of Δm and $\Delta\sigma$, Wilkinson's

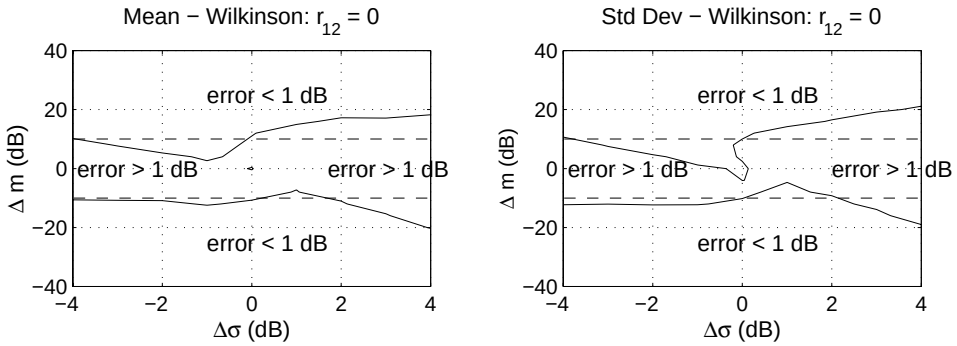

Figure 3.3: Regions on the plane $[\Delta\sigma \times \Delta m]$ where the errors in the mean value and standard deviation are less than 1 dB in Wilkinson's method - uncorrelated signals.

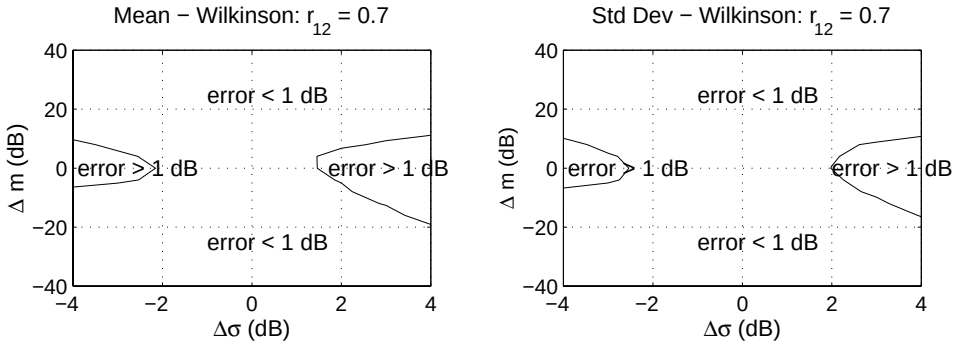

Figure 3.4: Regions on the plane $[\Delta\sigma \times \Delta m]$ where the errors in the mean value and standard deviation are less than 1 dB in Wilkinson's method - correlated signals ($r_{12} = 0.7$).

method presents accuracy that may be acceptable for some applications. Let us assume that the maximum tolerable error between the true values and the analytical approach is 1 dB, in both mean and standard deviation. Figures 3.3 and 3.4 show the regions on the plane $[\Delta\sigma \times \Delta m]$ where the errors using Wilkinson's method are less than 1 dB, for uncorrelated and correlated signals ($r_{12} = 0.7$), respectively. As a rule of thumb, if the difference between the mean values of two uncorrelated signals X_1 and X_2 is less than 10 dB, the errors in both mean value and standard deviation computed using Wilkinson's method are larger than 1 dB, regardless of the difference between the standard deviations. For correlated signals with correlation coefficient of 0.7, the errors in the mean value and standard deviation are larger than 1 dB if the difference between the mean values is less than 10 dB and the difference between the standard deviations is larger than 2 dB.

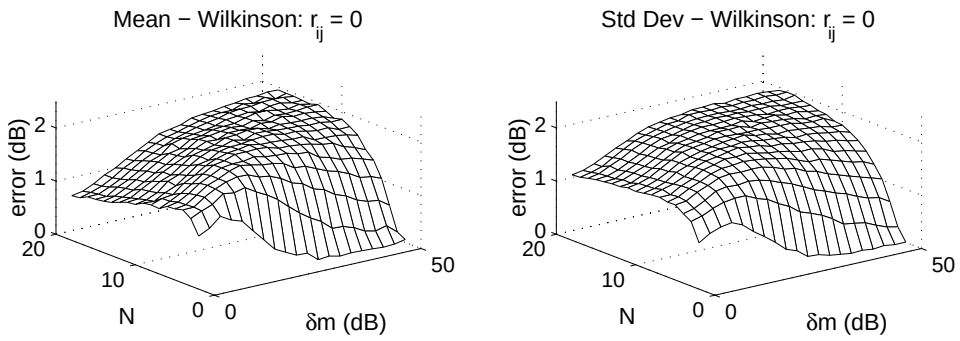

Figure 3.5: Absolute errors in the mean value and standard deviation of the sum of N uncorrelated lognormal signals with same standard deviation ($\sigma_{X_i} = 8$ dB) and different means, using Wilkinson's method.

3.3.2 N summands with different mean values and same standard deviation

Now consider the case of the sum of N ($2 \leq N \leq 18$) lognormal RVs with the same standard deviation $\sigma_{X_i} = 8$ dB, but different mean values. The mean values m_{X_i} of the N summands are equally spaced distributed over the interval from (0 dBm $- \delta m/2$) to (0 dBm $+ \delta m/2$), where δm is the *width* of the interval and is adjusted from 0 to 50 dB in our simulation. For example, for $N = 5$ signals and $\delta m = 20$ dB, the mean values are -10, -5, 0, 5 and 10 dBm.

Figure 3.5 shows that the errors in m_X and σ_X, computed using Wilkinson's method for uncorrelated summands, are non-zero over the *entire ranges* of δm and N considered. The manner in which the errors vary with δm depends on the number of summands N. For small N ($N < 8$), both errors tend to decrease as δm increases. This is due to the fact that, with few summands and large δm, the summand with the largest mean value dominates the sum and the other summands are negligible, reducing the errors. However, when the number of summands is large ($N > 10$), the errors in m_X and σ_X increase as δm increases. For large N, several summands will have large mean values, giving rise to the conclusion that the accuracy of Wilkinson's method degrades as the number of summands with about the same mean value increases. We see that the errors in the mean and standard deviation in Wilkinson's method are larger than 1 dB in almost all the ranges considered, except when the number of summands is small ($N < 3$) and $\delta m < 10$ dB.

For N correlated RVs, with correlation $r_{ij} = 0.7$, it can be shown that the errors in m_X and σ_X are almost invariant with N and δm, and are smaller than 0.3 dB.

Comparisons between our simulations and values of m_X and σ_X for Schwartz & Yeh's

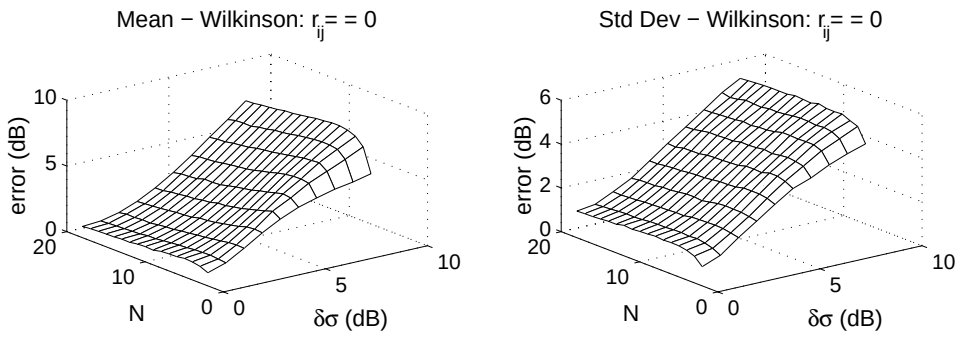

Figure 3.6: Absolute errors in the mean value and standard deviation of the sum of N uncorrelated lognormal signals with same mean ($m_{X_i} = 0$ dBm), and different standard deviations, using Wilkinson's method.

method demonstrate that errors are almost invariant with N and δm, and smaller than 0.5 dB, for both uncorrelated and correlated signals.

3.3.3 N summands with different standard deviations and same mean value

Consider now the case of the sum of N ($2 \leq N \leq 18$) lognormal RVs with the same mean value $m_{X_i} = 0$ dBm, but different standard deviations. The standard deviations σ_{X_i} of the N summands are equally spaced distributed over the interval from (8 dB $- \delta\sigma/2$) to (8 dB $+ \delta\sigma/2$), where $\delta\sigma$ can be adjusted from 0 to 8 dB.

The errors in the mean and standard deviation for Wilkinson's method, with respect to Monte Carlo simulation results, are presented in Figure 3.6, for uncorrelated signals, and Figure 3.7, for correlated signals, with correlation $r_{ij} = 0.7$. The results for Wilkinson's method agree with the well known results that the accuracy of Wilkinson's method degrades as the standard deviations of the individual signals increase [38].

Figure 3.6 also shows that, for uncorrelated signals, the errors are larger than 1 dB over the entire range analyzed. From the results in Figure 3.7, it can be shown that, for correlated signals, the errors in the mean and standard deviation may be acceptable (smaller than 1 dB) , if N and $\delta\sigma$ meet the following conditions

- ⋆ error in the mean < 1 dB if $\delta\sigma < 0.15N + 1.72$ (dB)
- ⋆ error in the standard deviation < 1 dB if $\delta\sigma < 0.14N + 2.33$ (dB)

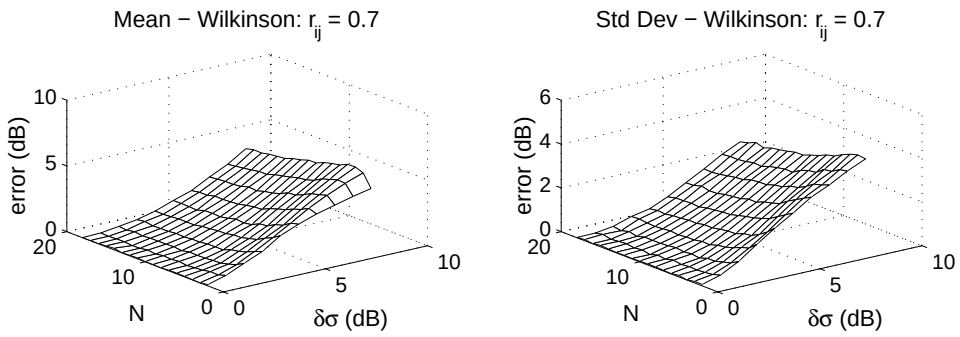

Figure 3.7: Absolute errors in the mean value and standard deviation of the sum of N correlated lognormal signals ($r_{ij} = 0.7$) with same mean ($m_{X_i} = 0$ dBm), and different standard deviations, using Wilkinson's method.

Our results also show that the errors in the mean and standard deviation in Schwartz & Yeh's method are virtually zero and invariant with the number of signals N and range $\delta\sigma$.

3.3.4 Summands with different mean values and standard deviations

Now consider the case of $N = 6$ summands, with different mean values and different standard deviations. The standard deviations of the summands are equally spaced distributed over the interval from (8 dB$-\delta\sigma/2$) to (8 dB$+\delta\sigma/2$), and $\delta\sigma$ can be adjusted from 0 to 8 dB. Likewise, the mean values are equally spaced distributed over the interval from (0 dBm $- \delta m/2$) to (0 dBm$+\delta m/2$), where δm can be adjusted from -75 to 75 dB. Note that we allow δm to be negative in order to analyze not only the effects of the spreads δm and $\delta\sigma$ on the accuracy of both methods, but also the effects of

- summands with small (large) mean values having small (large) standard deviations, which is obtained by using large $\delta\sigma$ and large positive δm,
- summands with small (large) mean values having large (small) standard deviations, which is obtained by using large $\delta\sigma$ and large negative δm.

Figure 3.8 shows the combinations of mean values and standard deviations of the individual signals on the plane $[\delta\sigma \times \delta m]$.

The errors for Wilkinson's method are shown in Figures 3.9 and 3.10, for uncorrelated and correlated signals ($r_{ij} = 0.7$), respectively, which are similar to the results presented in Section 3.3.1, for $N = 2$. The imprecision of the estimation of mean and standard

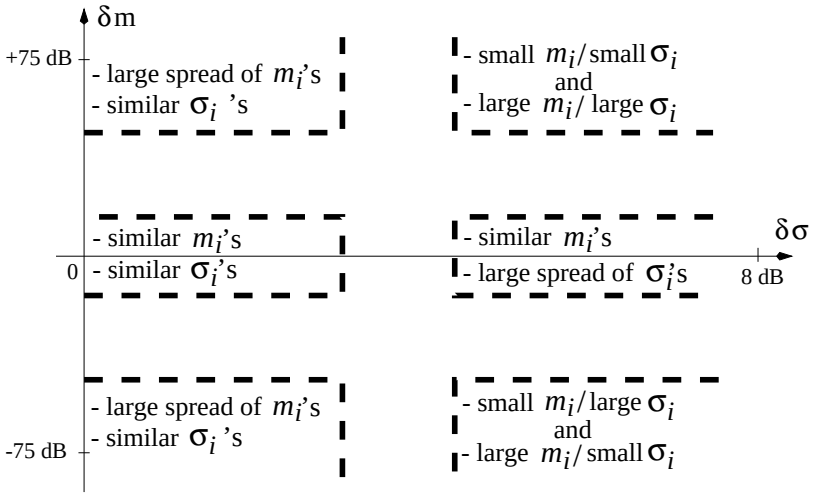

Figure 3.8: Combinations of mean values m_{X_i} and standard deviations σ_{X_i} of the summands.

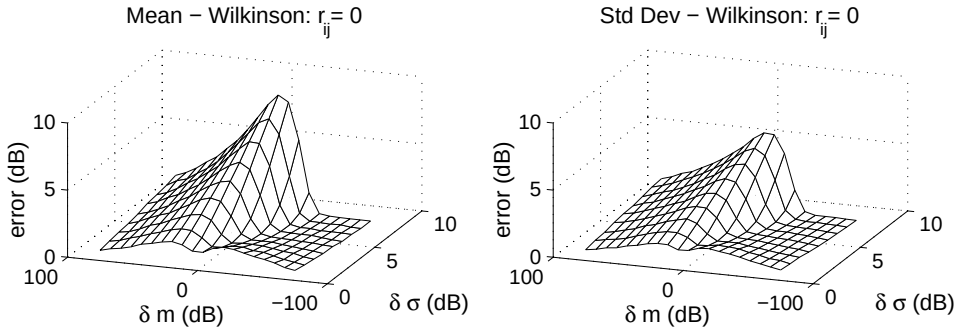

Figure 3.9: Absolute errors in the mean value and standard deviation of the sum of N uncorrelated lognormal signals with different means and different standard deviations, using Wilkinson's method.

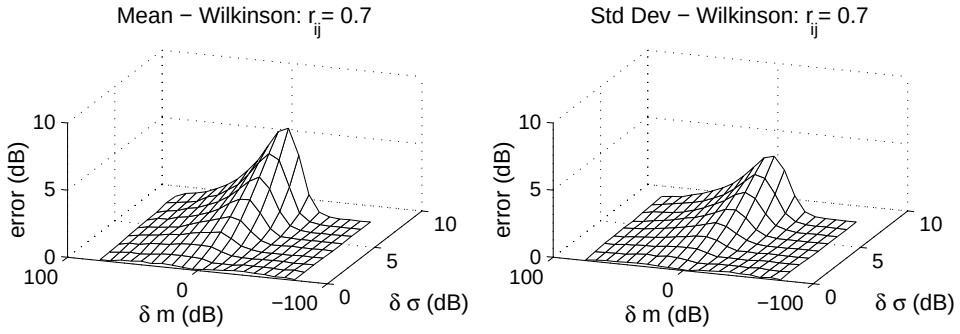

Figure 3.10: Absolute errors in the mean value and standard deviation of the sum of N correlated lognormal signals ($r_{ij} = 0.7$) with different means and different standard deviations, using Wilkinson's method.

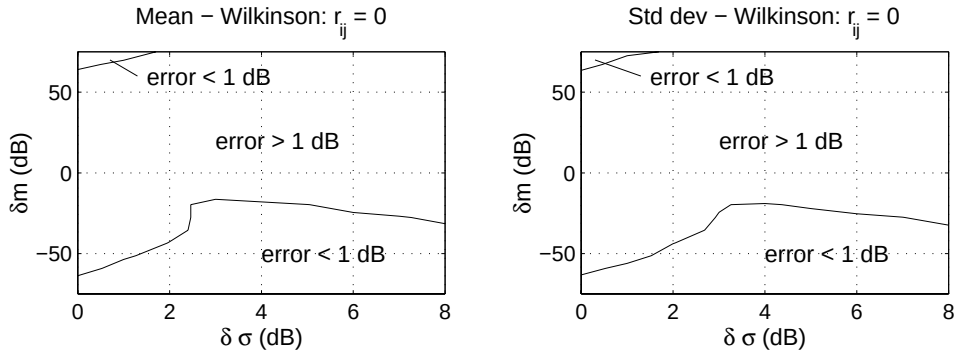

Figure 3.11: Regions on the plane $[\delta\sigma \times \delta m]$ where the errors in the mean value and standard deviation are less than 1 dB in Wilkinson's method - uncorrelated signals.

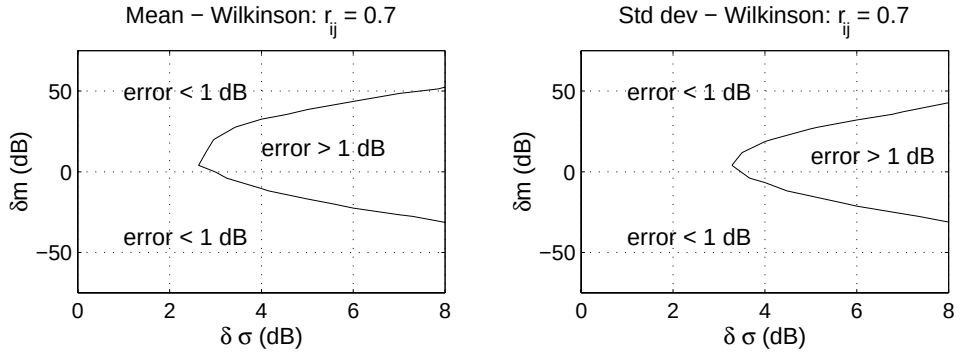

Figure 3.12: Regions on the plane $[\delta\sigma \times \delta m]$ where the errors in the mean value and standard deviation are less than 1 dB in Wilkinson's method - correlated signals.

deviation using Wilkinson's method increases as the spread of standard deviation of the summands increases (large $\delta\sigma$), and the spread of mean values decreases (small δm), for both uncorrelated and correlated signals. Figures 3.11 and 3.12 show the regions on the plane $[\delta\sigma \times \delta m]$ where the errors are smaller than 1 dB, for uncorrelated and correlated signals, respectively. For uncorrelated signals, the errors are only acceptable when signals with small (large) mean values have large (small) standard deviations. For correlated signals, the errors are *not* acceptable only when all signals have similar mean values and the spread of the standard deviations is large.

On the other hand, additional results show that the errors in both mean and standard deviation in Schwartz & Yeh's method are virtually zero, for both uncorrelated and correlated signals.

3.4 Conclusion

Schwartz & Yeh's and Wilkinson's methods are widely used for computing the moments of the total co-channel interference in wireless communications systems, modeled as the sum of lognormal distributed signals. These two methods have been extensively analyzed in previous studies under the assumption of having all the summands identically distributed. This assumption rarely holds in practical cases of emerging wireless communications systems, where interference signals coming from different physical environments may present different mean values and standard deviations in decibel units. To understand the conditions needed to accurately use both methods, we developed an extensive simulation to compare the performance of Schwartz & Yeh's and Wilkinson's methods for the general case, when the summands have different means and different standard deviations.

First, we considered the sum of two interference signals with different mean values and different standard deviations. As expected, the errors in the mean value and standard deviation in Schwartz & Yeh's method are zero, since this method computes the exact moments for the case of two summands. On the other hand, the accuracy of Wilkinson's method is poor when the standard deviations of the summands are different. The accuracy of Wilkinson's method is acceptable when the summands have about the same standard deviation.

We also analyzed cases of the sum of $N > 2$ signals. In all cases, Schwartz & Yeh's method presented excellent accuracy, for both uncorrelated and correlated signals. However, the accuracy of Wilkinson's method depends on the spread of the mean values and standard deviations of the individual signals in the sum. From the results presented in this work, we have shown quantitative results which highlight the fact that the accuracy of Wilkinson's method degrades as the spread of mean values of the summands decreases and as the spread of the standard deviations of the summands increases. It is also observed that the performance of Wilkinson's method degrades as the correlation of the signals in the summation decreases, and the number of summands increases. Such results may be useful in simulation and analysis of co-channel signals in emerging wireless communications systems.

Chapter 4

Narrowbeam Antennas and Fractional Loading Factor in Cellular Communication Systems

4.1 Introduction

The rapid growth in demand for cellular mobile communications and emerging fixed wireless access has created the need to increase system capacity through more efficient utilization of the frequency spectrum. One approach for achieving high spectral efficiency is to reduce the channel reuse distance by reducing the *cluster size* $N = M/N_c$ of a cellular system [1], where M is the total number of voice channels available in the spectrum allocation, and N_c is the number of channels per cell. For AMPS in North and South America, $M = 395$, N is typically 7 (7-cell reuse) and $N_c = 57$. Reduction in the cluster size leads to greater spectrum reuse, but increases co-channel interference, which reduces the link quality, thereby requiring the use of some co-channel interference control techniques at the base station or in the air interface.

Several techniques for controlling co-channel interference have been proposed in literature. Narrowbeam adaptive antennas ("smart antennas") at the base stations can significantly reduce co-channel interference by steering a high gain in the direction of the desired mobile stations and/or very low gains in the direction of the undesired co-channel mobile stations [15], [22], [27], [46]. Power control has also been considered to control co-channel interference, allowing cluster size reduction and capacity improvement [47]. Another technique that has

been proposed is based on a fractional cell loading factor [48], which reduces the probability that a given channel is in use in the co-channel cells which, consequently, reduces the total co-channel interference level for a particular channel.

In this chapter, we analyze, by means of extensive simulation, the combined application of narrowbeam adaptive antennas at the base stations and the fractional loading factor. The combined application of these two techniques was first analyzed by Frulluone *et al.* in [49], using an 8-element circular array at base stations in a GSM system. It was shown in [49] that the use of a specific adaptive antenna combined with the fractional loading factor allows cluster size reduction from $N = 12$ to 4. This reduction in cluster size, along with the higher trunking efficiency, leads to an increase of about 500% in system capacity. We extend and generalize the results of [49] by considering narrowbeam antennas with a wide range of beamwidths (BWs) and side lobe levels ($SLLs$) on both forward and reverse links. We determine, by simulation, the capacity improvement from cluster size reduction, with respect to a reference 7-cell reuse system ($N = 7$, 3 sectors per cell). As shown subsequently, the reduction of the loading factor leads to a reduction in the co-channel interference at the expense of an intrinsic capacity loss. Therefore, when using narrowbeam antennas combined with a fractional loading factor, we first explore controlling the co-channel interference by using narrowbeam antennas alone, with no reduction in channel loading in each cell. Then, as additional reduction in interference is needed to maintain a particular ratio of signal to co-channel interference (SIR), we reduce the cell loading factor. From the results of the extensive system simulations, we are able to observe how blocking probability and co-channel interference limit the resulting system capacity.

In the remainder of this chapter, Section 4.2 reviews how narrowbeam antennas and the fractional loading factor may be used for controlling co-channel interference. The limiting factors for capacity of a cellular system are also presented in Section 4.2.

In Section 4.3, the simulated macrocellular system is described, and Section 4.4 presents results along with an extensive analysis of capacity improvement that is achieved by combining narrowbeam antennas and the fractional loading factor. Finally, Section 4.5 summarizes the results of this chapter.

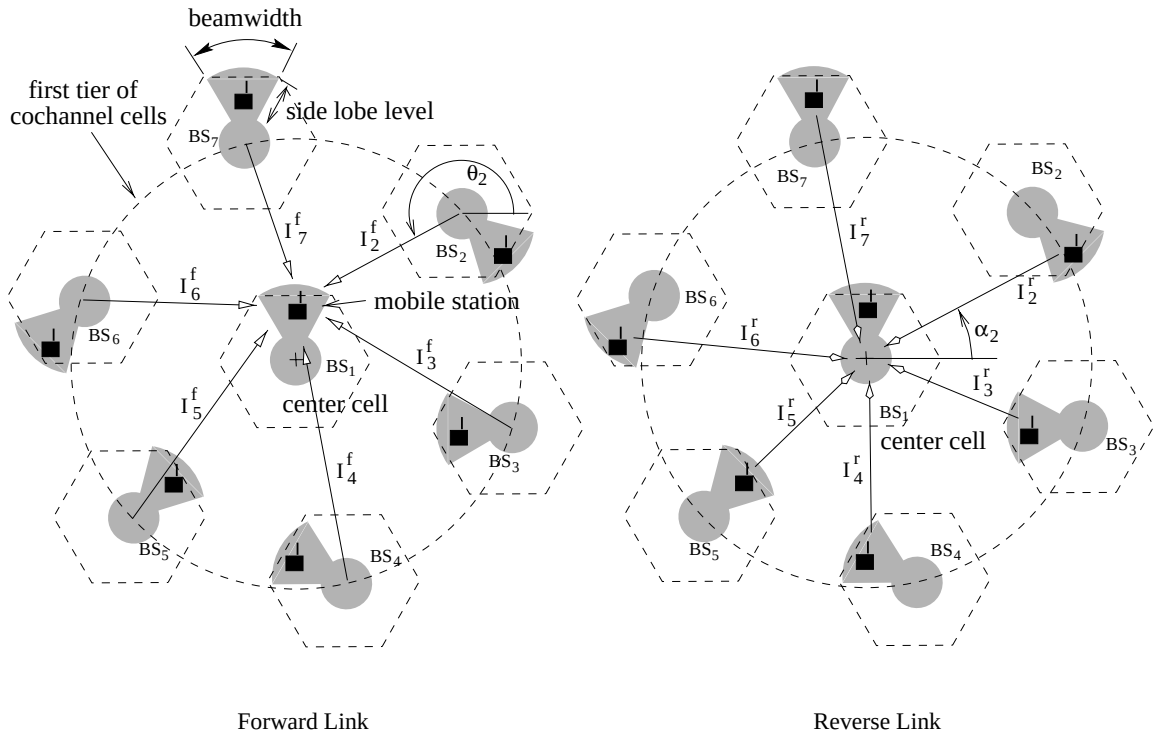

Figure 4.1: Narrowbeam antennas in cellular system: forward and reverse links.

4.2 Methods for Reducing Cochannel Interference

4.2.1 Narrowbeam Antennas

When adaptive narrowbeam antennas are used at base stations in both the forward and reverse links, beams are steered toward the desired in-cell users, as shown in Figure 4.1. In this figure, the first tier of co-channel cells is shown, which consists of six cells. Throughout this chapter, we consider only the first tier of co-channel cells, and more distant tiers of co-channel cells are not considered in the simulation. We show in Appendix A that using only the first tier of cells induces a worst-case error of less than 1.1 dB in the estimation of *SIR*, *regardless of the cluster size*, when 40 dB/decade of path loss is assumed, and a worst-case error of less than 2.3 dB for 30 dB/decade of path loss. It should be noted that the methodology presented here may be generalized for an arbitrary path loss value.

Assuming that all co-channel cells in the first tier are active, the total forward link interference power at the mobile at the center cell is:

$$I^f = I_2^f + \cdots + I_7^f, \tag{4.1}$$

where I_i^f is the interference power received from the i-th co-channel base station. Likewise for the reverse link, the total reverse link interference power received at the base station at the center cell is:

$$I^r = I_2^r + \cdots + I_7^r, \tag{4.2}$$

where I_i^r is the interference power received from the i-th co-channel mobile stations. We assume that the interference signals add incoherently, so that the powers can be summed[1]. The co-channel interference received at the mobile at the center cell, caused by a given co-channel base station, is attenuated by the antenna gain when the mobile is not within the main lobe of the antenna of that co-channel base station transmission. For example, in Figure 4.1, the co-channel interference signals from base stations 2, 4, 6 and 7 are attenuated due to the use of narrowbeam antennas. However, there is no reduction in the interference caused by base stations 3 and 5. The same principle is valid for the reverse link.

It is obvious that the extent of co-channel interference reduction depends on the beamwidth and the side lobe level of the base station antennas. If the antenna is implemented using an array of antennas, the BW and SLL will depend on the number of elements in the array. The first tradeoff presented in this chapter demonstrates how the reduction of interference (which is required in order to decrease cluster size and thus improve capacity) is related to the beam pattern and complexity of the base station antenna.

4.2.2 Fractional Loading Factor

The total co-channel interference at a given mobile or base station depends on the k co-channel cells that are using the same pair of forward and reverse channels (active cells) as the cell where the interference level is being measured. This number k is related to the loading factor p_{ch} of each cell, which defines the probability that a given channel is in use within a cell. Considering the first tier of co-channel cells, a given channel is in use in k out of six co-channel cells (interferers). The random variable k is binomially distributed and the probability of having n ($0 \leq n \leq 6$) interferers is, therefore,

$$P_n = \text{Prob}\{k = n\} = \begin{pmatrix} 6 \\ n \end{pmatrix} p_{ch}^n (1 - p_{ch})^{6-n}. \tag{4.3}$$

[1]This is a realistic assumption for wireless signals, since the phase shifts of the individual interference signals may be assumed to be independent and vary significantly due to scattering and travel distance.

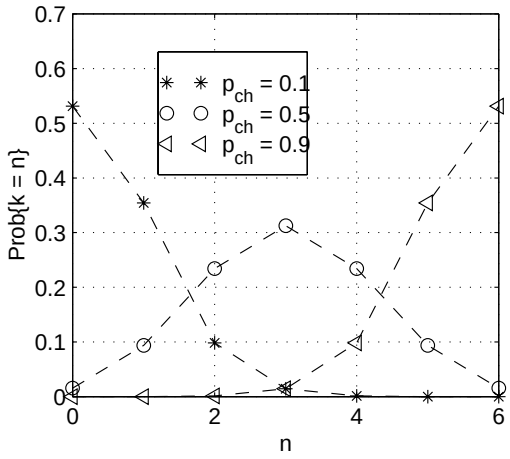

Figure 4.2: Probability that a given channel is in use in n co-channel cells.

The loading factor p_{ch} is a function of the offered traffic A (in Erlangs), blocking probability P_B, and number of channels N_c assigned to each cell (or sector) [22]:

$$p_{ch} = \frac{A(1 - P_B)}{N_c}. \tag{4.4}$$

Assuming that *blocked calls are cleared*, the quantities A, P_B and N_c are related to each other through the Erlang B formula [1],

$$P_B = \frac{\frac{A^{N_c}}{N_c!}}{\sum_{i=0}^{N_c} \frac{A^i}{i!}}. \tag{4.5}$$

Figure 4.2 shows P_n for several values of p_{ch}.

We see that, as the loading factor increases, the probability of having all six co-channel cells active also increases, which corresponds to a higher total co-channel interference level. Therefore, the number of interferers and, consequently, the total interference depend upon the loading factor.

Consider now a standard AMPS cellular system with 395 voice channels and a target blocking probability of 0.02. Table 4.1 shows the number of channels and traffic capacity per cell, as well as the corresponding loading factor for different cluster sizes. We see that p_{ch} increases as the cluster size decreases. This means that cluster size reduction has a twofold effect, as far as interference is concerned: (1) the interference increases, since co-channel cells are closer to each other and (2) due to the increase in the loading factor, the probability that co-channel cells are using the same channel increases (see Figure 4.2), which implies that

Table 4.1: Number of channels (N_c), traffic capacity (A) for a blocking probability of 0.02, and maximum loading factor (p_{ch}) for a system with 395 voice channels and different values of cluster sizes N. (*) Trunking loss is one limiting factor in overall capacity in cell.

cluster size N	channels per cell N_c	A (Erlangs)	p_{ch} (%)
7, 3-sector	3×18	$3 \times 11.5 = 34.5^*$	62.6
7, omni	56	45.9	80.2
4, omni	98	86	86.0
3, omni	131	118	88.4
1, omni	395	380	94.2

the total interference increases. It should be clear, then, that the loading factor p_{ch} plays an important role in the total system co-channel interference, which could enable a smaller reuse factor to be used.

The *Fractional Loading Factor* technique, introduced by Frullone *et al* [48], aims to reduce the co-channel interference level by reducing the loading factor. The reduction of the loading factor is achieved by hard limiting the number of channels that may be used simultaneously in a cell. However, the hard limit imposed on the instantaneous channel usage reduces the maximum possible carried traffic and thus the maximum capacity of each cell. Considering again a cellular system with $M = 395$ channels and a target blocking probability of 0.02, Figure 4.3 plots the loading factor versus the maximum number of channels (N_{max}) that may be used simultaneously, for cluster sizes $N = 1$, 3, 4 and 7, using (4.4). Note that in (4.4), A is the traffic carried by N_{max} trunked channels and is determined by (4.5).

While the use of a low loading factor reduces the total co-channel interference, it also reduces the system capacity, since only a fraction of the channels assigned to a cell are allowed to be used at the same time. This leads to the second tradeoff: the reduction in interference level (which is required for smaller reuse factor and thus capacity improvement) is related to the loading factor reduction and the corresponding capacity loss, and this relationship varies as a function of cell cluster size.

When the fractional loading factor technique is used, an appropriate *call admission control* (CAC) must be employed in order to keep the cell loading factor (or, equivalently, the number of channels in use in a cell) at the desired level [50]. In the chapter presented here, we implement CAC simply by adjusting the number of active cells, according to the desired

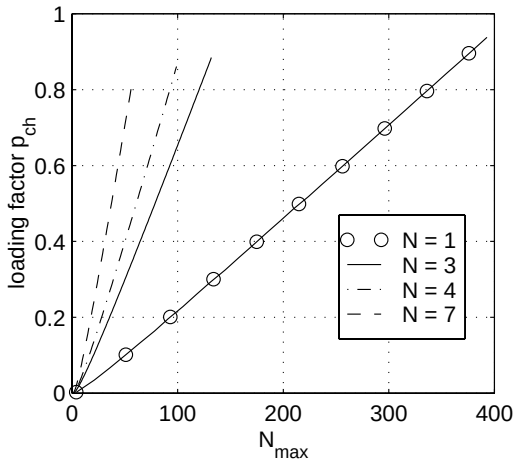

Figure 4.3: Loading factor vs. N_{max} (number of channels that can be in use simultaneously) for cluster sizes $N = 1$, 3, 4 and 7 for a blocking probability of 0.02.

loading factor p_{ch} and the probability P_n (equation (4.3)) of having n active cells.

We determine total system capacity by conducting a parametric study of the cellular system performance by systematically adjusting the specifications of the antennas at the base stations (in both the forward and reverse links), the fractional loading factor, and cluster size. For each combination of parameters, the system capacity is computed and compared to a reference cellular system (7-cell reuse, 3 sectors per cell). As shown in Section 4.4, we find that, by combining these techniques, low complexity narrowbeam antennas can be used, and that results are sometimes counter-intuitive.

4.2.3 Interference-Limited and Blocking-Limited Capacity

The fractional loading factor technique and narrowbeam antennas have some intrinsic characteristics that are now discussed. Suppose that, in order to increase the capacity of a cellular system, the cluster size is reduced, while employing narrowbeam antennas at the base stations and reducing the loading factor to control the co-channel interference. Two different cases for the resulting system capacity can occur:

- **Capacity is limited by blocking probability:** In this first case, the side lobe level and the beamwidth of the antennas are such that the total interference per user is smaller than a maximum level. Therefore, no loading factor reduction is needed and the traffic capacity per cell will, consequently, be limited by blocking probability.

- **Capacity is limited by co-channel interference:** In this case, suppose that the narrowbeam antennas do not sufficiently reduce the interference to or below the maximum tolerable level and a reduction in the loading factor is required in order to provide the needed additional interference reduction for sufficient average link performance. This means that each cell will be allowed to use only a portion of its channel set at the same time, thereby limiting the capacity in favor of co-channel interference mitigation.

To illustrate these two cases, consider a cellular system with 395 voice channels and a target blocking probability of 0.02. Considering the forward link, suppose that the signal-to-interference ratio (*SIR*) is required to be greater than 17 dB with a probability of 95% or higher in order to guarantee the *minimum acceptable system performance*. If cluster size $N = 3$ is employed, each cell is assigned $N_c = 131$ channels, corresponding to 118 Erlangs at 2% of blocking probability. Using expression (4.4), we see that the loading factor is 88.4%. Consider now that narrowbeam antennas are used at the base stations in order to meet or exceed the co-channel interference performance specification. If the narrowbeam antennas are able to guarantee $P[SIR > 17\text{dB}] \geq 95\%$, the resulting capacity per cell will be 118 Erlangs, which is limited by blocking probability. Suppose now that the narrowbeam antennas are *not* able to guarantee $P[SIR > 17\text{dB}] \geq 95\%$ and, therefore, an additional interference reduction is needed. Then, the loading factor must be reduced from 88.4% to some value p^*_{ch} in order to reduce the co-channel interference below the performance specification. In an actual system, the *SIR* or the corresponding frame error rate may be monitored for each user, and used for determination of p^*_{ch}. In this chapter, we determine the value of p^*_{ch} by simulation in several conditions, as described in Section 4.4.

Let us assume that, for the present example, p^*_{ch} is found to be equal to 60%. Using expression (4.4) again, with $p_{ch} = 60\%$, $P_B = 2\%$ and $N_c = 131$, we find that the traffic capacity per cell is only 80.2 Erlangs, and only 92 of the 131 channels may be used at any one time in order to provide 2% of blocking probability and 80.2 Erlangs. The control of the number of simultaneously active channels can be performed by an appropriate call admission control. The capacity in this case is limited by interference, rather than by blocking. An extensive discussion on this subject is found in reference [51].

4.3 Simulated System

The capacity of a cellular system employing narrowbeam antennas at the base stations on both links, fractional loading factor, and reduced cluster size is compared to a standard AMPS system defined in Section 4.3.3. The comparison is made under the condition that both the reference system and the system using narrowbeam antennas have the same system performance regarding SIR. We compute the probabilities P_{th}^f and P_{th}^r that the *SIRs* at the mobile (forward link) and at the base station (reverse link), respectively, exceed a given threshold SIR_0

$$P_{th}^f = P[SIR^r > SIR_0] \quad \text{and} \quad P_{th}^r = P[SIR^r > SIR_0]. \tag{4.6}$$

The probabilities P_{th}^f and P_{th}^r are usually referred to as system *reliability*.

We consider an Advanced Mobile Phone System (AMPS), where the base stations are placed at the center of the cells. To simplify the simulation, a flat-top radiation pattern [15] is used for the base station narrowbeam antennas, with beamwidth BW and side lobe level SLL as parameters, as shown in Figure 4.1. Several values of BW ($10^o, 30^o, 45^o, 60^o$ and 120^o) and SLL (-12 dB, -18 dB, -30 dB, -40 dB and $-\infty$ dB) are used in simulations. The maximum antenna gain within the main lobe is set to 0 dB, which is a valid simplification since *SIR*, and not absolute power levels, form the basis of the system performance specification, and all base stations and mobile stations are assumed to transmit with identical powers, respectively. We do not consider power control here, although power control will likely improve the system capacity even more, by reducing interference and increasing p_{ch}^*. The probabilities P_{th}^f and P_{th}^r are computed for the mobile and base station in the center cell (see Figure 4.1).

4.3.1 Channel Model

The propagation channel model considers path loss and shadowing with path loss exponent $\gamma = 4$ and a shadowing standard deviation of $\sigma = 6$ dB in both links. The desired signal power S and the individual co-channel interference signal powers I_i^f and I_i^r are, therefore, *local mean powers* and are lognormally distributed. Assuming that the interference signals add incoherently, the power of total interference signal at the mobile station at the center cell, I^f, is the sum of the signal powers received from all active co-channel base stations

$$I^f = \sum I_i^f. \tag{4.7}$$

Likewise, the power of total interference signal at the base station at the center cell, I^r, is

$$I^r = \sum I_i^r. \tag{4.8}$$

Both I^f and I^r are assumed to be lognormally distributed [38], as discussed below.

Only the first tier of co-channel cells is considered, regardless of cluster size N, which corresponds to a maximum of six interfering co-channel cells. It is assumed that the effects of further tiers of co-channel cells can be neglected. This assumption has been adopted in similar works [22, 28], and we show in Appendix A that the inaccuracy associated with this assumption is small for path loss exponents greater than 3. Considering area mean values, we show that the error when computing *SIR* (at a mobile near the cell boundary) induced by considering only the first tier is less than 1 dB for path loss $\gamma = 4$ and cluster sizes $N = 1$, 3, 4 and 7. We also consider in Appendix A the case with shadow fading, with standard deviation $\sigma = 6$ dB, and a reliability of 95%. We show in Appendix A that the error induced by considering only the first tier when estimating SIR_0, such that $P[SIR > SIR_0] = 95\%$, is smaller than 1.1 dB, for path loss $\gamma = 4$ and cluster sizes $N = 1$, 3, 4 and 7. The results are valid for both the forward and reverse links.

4.3.2 Computation of P_{th}^f and P_{th}^r

Both the forward and reverse link probabilities P_{th}^f and P_{th}^r are computed as described below. For the sake of clarity, the superscripts f and r are used only when necessary. Expressing the desired signal power S and the total interference power $I = \sum I_i$ in decibel units, $SIR = S - I$ is normally distributed. Therefore, denoting SIR by X, P_{th} is

$$P_{th} = \int_{SIR_0}^{+\infty} \frac{1}{\sqrt{2\pi}\sigma_X} \exp\left[\frac{(X - m_X)^2}{2\sigma_X^2}\right] dX, \tag{4.9}$$

where m_X and σ_X^2 are the mean value and variance of X, respectively, given by

$$m_X = m_S - m_I \quad \text{(in dBm)} \tag{4.10}$$

$$\sigma_X = \sqrt{\sigma_S^2 + \sigma_I^2} \quad \text{(in dB)}. \tag{4.11}$$

m_S and m_I are the mean values of S and I, respectively. Since S and I are local mean powers, m_S and m_I are usually referred to as *area mean powers*. σ_S and σ_I are the standard deviations of S and I, respectively.

For the forward link, the mean value of S is modeled as

$$m_S^f = P_{BS} - 10K\gamma \log d_D^f \quad \text{(dBm)}, \tag{4.12}$$

where P_{BS} is the base station transmitted power in dBm (assumed to be equal for all base stations) and d_D^f is the transmitter to receiver (T-R) separation. The constant K comprises all terms that do not change in the model. Likewise, the mean value of S for the reverse link is

$$m_S^r = P_{MS} - 10K\gamma \log d_D^r \quad \text{(in dB)}, \tag{4.13}$$

where P_{MS} is the mobile station transmitted power in dBm (assumed to be equal for all mobile stations) and d_D^r is the T-R separation. The mobile antennas on both links are assumed to be omnidirectional. Perfect knowledge about the position of the mobile is assumed, so that the serving base station beams are perfectly centered on the desired mobiles and the antenna gains on both links in the direction of the desired mobile are always equal to 0 dB (the maximum gain) and do not appear in expressions (4.12) and (4.13). The standard deviations of S on both links are equal to the shadowing standard deviation σ.

The computation of the mean and standard deviation of the total interference signal power (both links), m_I and σ_I, is more intricate. It can be shown [38] that the distribution of the sum of lognormal random variables can be approximated by a lognormal distribution, whose moments depend on the mean values and variances of the summands. Therefore, we assume in this chapter that $I^f = \sum I_i^f$ and $I^r = \sum I_i^r$ are lognormally distributed. Several techniques have been proposed for computing the mean and variance of the resulting lognormal distribution. In this chapter, we employ Schwartz and Yeh's method [38]. The mean values of the individual interferers, $m_{I,i}$, are modeled as m_S in (4.12), with appropriate modifications. For the forward link, we have:

$$m_{I,i}^f = P_{BS} + G_{BS_i}^f(\theta_i) - 10K\gamma \log d_{I,i}^f \quad \text{(dBm)}, \tag{4.14}$$

where $G_{BS_i}^f(\theta_i)$ is the antenna gain of the i-th base station in the direction θ_i toward the mobile in the center cell (see Figure 4.1) and $d_{I,i}^f$ is the corresponding T-R separation. For the reverse link,

$$m_{I,i}^r = P_{MS} + G_{BS_1}^r(\alpha_i) - 10K\gamma \log d_{I,i}^r \quad \text{(dBm)}, \tag{4.15}$$

where $G_{BS_1}^r(\alpha_i)$ is the antenna gain of the base station in the center cell in the direction α_i toward the mobile in the i-th co-channel cell (see Figure 4.1) and $d_{I,i}^r$ is the corresponding

T-R separation. The standard deviations $\sigma^f_{I,i}$ and $\sigma^r_{I,i}$ are equal to the shadowing standard deviation σ.

The number of individual interference signals, or in other words, the number of summands in $\sum I^f_i$ and $\sum I^r_i$, is equal to the number k of co-channel cells in the first tier that are using the same pair of forward/reverse channels as the center cell. As described in Section 4.2.2, k is a random variable varying from zero to six and binomially distributed with the probability of a given co-channel cell being active equalling the desired loading factor p_{ch}.

The system simulation is performed as follows. Mobiles are placed within the center cell and within k (out of six) co-channel cells, following a uniform distribution in each cell area. The number k is the outcome of a binomial random process with probability of k being equal to n ($0 \leq n \leq 6$) given by (4.3). The assumed loading factor p_{ch} is the same in all cells. These $1 + k$ mobiles define a *set of mobile positions*. Narrow beams are then steered toward each mobile by their serving base stations. The mean value of the desired and interference signal powers in both links are determined using (4.12) through (4.15). Schwartz & Yeh's method is then used to compute the mean values and standard deviations of the total interference signal powers in both links. Using (4.9), (4.10) and (4.11), the probabilities P^f_{th} and P^r_{th} for the threshold SIR_0 are then computed for that set of mobile positions. A Monte Carlo procedure is repeated for 5000 sets of mobile positions, so that 5000 values of P^f_{th} and P^r_{th} are generated for a specific set of system parameters $\{SLL, BW, p_{ch}, \text{and } N\}$. The area-averaged P^f_{th} and P^r_{th}, denoted by $\overline{P}^f_{th}$ and $\overline{P}^r_{th}$, respectively, are then computed by averaging P^f_{th} and P^r_{th}. This approach for computing $\overline{P}^f_{th}$ and $\overline{P}^r_{th}$ has been used in a similar work in [28].

4.3.3 Reference System

The reference cellular system employs cluster size $N = 7$, 3-sector antennas ($BW = 120^o$), with a SLL of -30 dB and 395 channels available per cluster (18 channels per sector). This corresponds to 34.5 Erlangs per cell at 2% of blocking probability and a loading factor $p_{ch} = 62.6\%$, and is typical for the AMPS cellular system. Following common practice for AMPS [1], [52], we assume that the minimum acceptable SIR_0 is 17 dB for both links. Simulation results have shown that, for the reference system, the area-averaged probabilities $\overline{P}[SIR > 17 \text{ dB}]$ on both links (denoted here as $\overline{P}^f_{th,ref}$ and $\overline{P}^r_{th,ref}$) are equal to 95%, which we deem to be the *minimum acceptable system performance* (regarding co-channel interference) and must be achieved when using other cluster sizes.

4.4 Simulation Results

We are interested in finding the maximum BW and most relaxed SLL (i.e. minimum array complexity), and maximum loading factor (minimum intrinsic capacity loss), when the cluster size is reduced from $N = 7$ (reference system) to $N = 4$, 3 and 1, while maintaining the same quality in both links, that is, $\overline{P}^f_{th} = \overline{P}^f_{th,ref}$ and $\overline{P}^r_{th} = \overline{P}^r_{th,ref}$. It should be noted that, in practical cases, different antenna configurations may be used in each link, but the loading factor is necessarily the same for both links.

Table 4.1 presents the number of channels assigned to each cell, the corresponding traffic capacity A in Erlangs, and the maximum loading factor p_{ch} (based on equation (4.4)) at 2% blocking probability ($P_B = 0.02$) for cluster sizes $N = 4$, 3 and 1. The capacities shown in Table 4.1 are limited by blocking probability.

As discussed before, controlling co-channel interference by using narrowbeam antennas does not intrinsically decrease system capacity. Therefore, after reducing the cluster size, we first try to reduce the co-channel interference below the maximum tolerable level using narrowbeam antennas alone, with no reduction in loading factor in each cell. If the narrowbeam antennas are unable to sufficiently reduce the co-channel interference, the loading factor must then be reduced. In the following we describe the procedure used to determine the capacity gain over the reference system for cluster size $N = 4$. The same procedure is used for cluster sizes $N = 1$ and 3.

There are two antenna parameters to be adjusted, namely SLL and BW. Figure 4.4 shows the forward and reverse link probabilities $\overline{P}[SIR > 17 \text{ dB}]$, for cluster size $N = 4$ and narrowbeam antennas at the base stations with different values of SLL and BW.

The loading factor was set to its maximum value ($p_{ch} = 86$ %). Note that for $SLL \leq -18$ dB and $BW \leq 20^o$, it is possible to obtain equal or better performance than the reference system on a SIR basis, while reducing the cluster size from 7 to 4. This provides a 150% capacity improvement (2.5 times) over the reference system, as shown in Table 4.1 (86 vs. 34.5 Erlangs). No significant improvement is obtained by using $SLL < -18$ dB for any BW in both links for $N = 4$.

The results in Figure 4.4 show that if we desire $N = 4$ and have antennas with $BW > 20^o$ and $SLL > -18$ dB, additional interference reduction is required in order to achieve the minimum acceptable performance. This means that we must reduce the loading factor to some value, denoted here by p^*_{ch}, to maintain the threshold of $\overline{P}[SIR > 17 \text{ dB}] = 95\%$. Since a small loading factor corresponds to reduced capacity, we need to find the highest value of

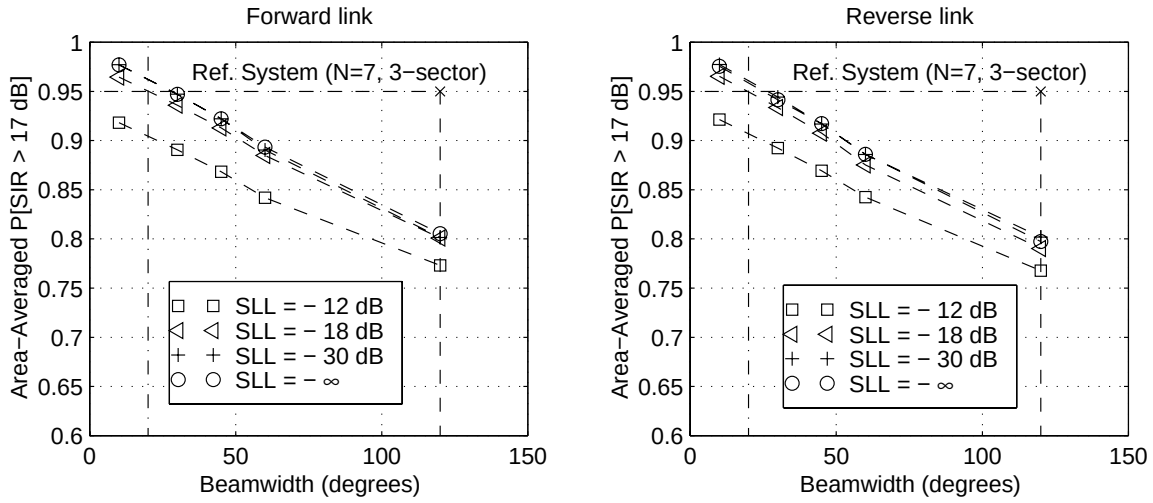

Figure 4.4: $\overline{P}[SIR > 17 \text{ dB}]$ for the forward and reverse links, $N = 4$ and several values of BW and SLL, with no reduction in loading factor.

p^*_{ch} possible.

The value of p^*_{ch} for a given BW and SLL is determined by interpolation, as follows. First, we determine, by simulation, the probability $\overline{P}[SIR > 17 \text{ dB}]$ using course values of p_{ch} (10%, 50% and 86%). Then, using a second order curve-fit interpolation, we compute the required value p^*_{ch} to achieve $\overline{P}[SIR > 17 \text{ dB}] = 95\%$. As an example of this procedure, Figure 4.5 shows the adjusted curve $\overline{P}[SIR > 17 \text{ dB}]$ vs. p_{ch} for cluster size $N = 4$, BW 45^o, $SLL = -18$ dB on the forward link.

From this plot, we can see that p^*_{ch} must be equal to 47% to maintain $\overline{P}[SIR > 17 \text{ dB}]$ $= 95\%$.

Figure 4.6 presents the resulting required loading factor p^*_{ch} for both links and several values of BW and SLL.

We see that both links require about the same loading factors for the same antenna configuration.

The maximum value of p^*_{ch} plotted in Figure 4.6 is 86%, which is the maximum loading factor for $N = 4$. When p^*_{ch} is equal to 86% in this figure, the corresponding values of SLL and BW are the side lobe level and beamwidth required so that no reduction in the loading factor is needed. When the required p^*_{ch} is equal to the maximum loading factor, the capacity is limited by blocking probability, instead of interference, as we shall see later.

So far we have computed the required loading factor that maintains $\overline{P}[SIR > 17dB] =$ 95% for several antenna configurations. However, as mentioned before, the drawback of

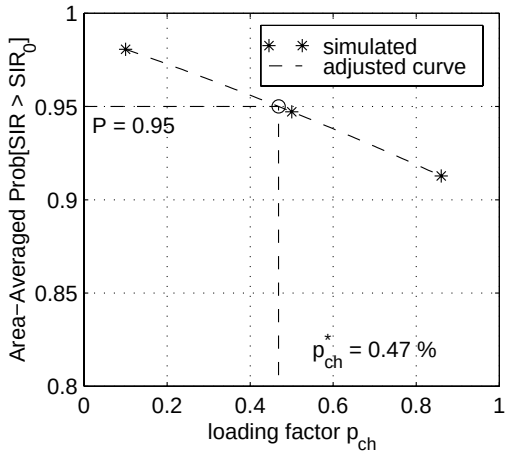

Figure 4.5: Computation of the required loading factor for $N = 4$, $SLL = -18$ dB, $BW = 45^o$ and forward link.

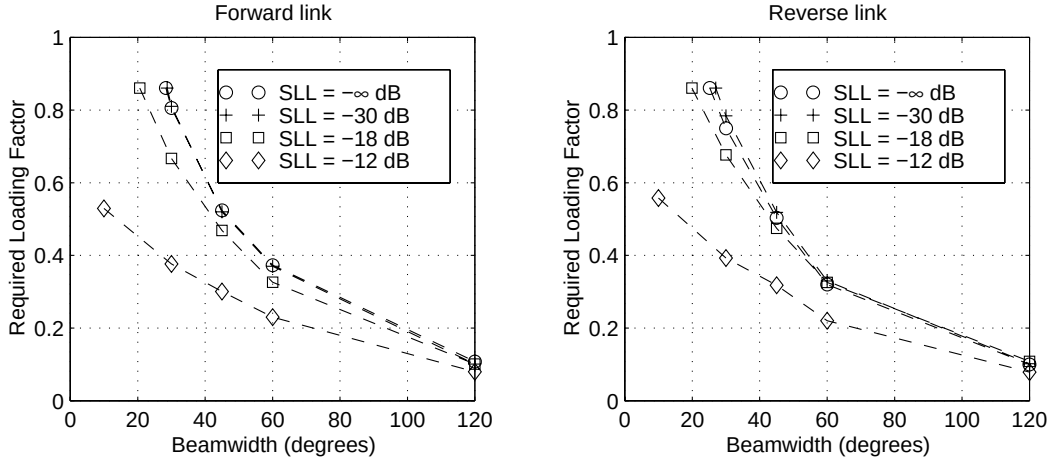

Figure 4.6: Required loading factor to achieve $\overline{P}[SIR > 17dB] = 95\%$ for $N = 4$.

reducing the loading factor is the intrinsic capacity loss. The resulting overall capacity must be analyzed at this point.

Using the required loading factor p^*_{ch} shown in Figure 4.6 and (4.4), we can compute the capacity per cell in Erlangs, A_N, for cluster size N and a given BW and SLL as

$$A_N = \frac{N_c\, p^*_{ch}}{1 - P_B}. \tag{4.16}$$

Note that N_c in this expression is equal to the total number of channels assigned to each cell (see Table 4.1) and $P_B = 0.02$. The capacity gain Ψ with respect to the reference system ($N = 7$, 3-sector cells) is then computed as

$$\Psi = \frac{A_N - A_{ref}}{A_{ref}} \times 100\%, \tag{4.17}$$

where A_{ref} is the capacity per cell of the reference system, 34.5 Erlangs.

The required loading factors p^*_{ch} and the resulting capacity gains Ψ with respect to the reference system, for the most significant cases for cluster sizes $N = 1$, 3 and 4, are presented in Table 4.2 and 4.3, respectively.

We see that, for the same antenna configuration and cluster size, both links present about the same capacity gains. For a given SLL and cluster size, the capacity gain increases as BW decreases, since a smaller reduction in the loading factor is needed to achieve the minimum acceptable system performance. The results in Table 4.3 can be classified into two scenarios, as discussed in Section 4.2.3. In the first scenario, which comprises the majority of the cases in Table 4.3, the narrowbeam antennas are unable to reduce the co-channel interference below the maximum tolerable level, and the loading factor needs to be reduced in order to achieve $\overline{P}[SIR > 17 \text{ dB}] = 95\%$. The capacity in this group is *limited by interference* [51]. Therefore, for a given BW and SLL, the *capacity gain decreases as cluster size decreases*, despite the fact that the number of channels per cell increases. This can be explained by noting that small cluster size leads to high co-channel interference, which requires a considerable reduction in the loading factor in order to achieve $\overline{P}[SIR > 17 \text{ dB}] = 95\%$. This reduction in the loading factor leads to capacity loss, that offsets the capacity gain achieved from the cluster size reduction.

In the second scenario, the narrowbeam antennas are able to reduce the co-channel interference below the maximum tolerable level and no loading factor reduction is required to achieve the minimum acceptable performance. Therefore *capacity is limited by blocking probability* [51]. For a given beamwidth and side lobe level, the *capacity gain increases*

Table 4.2: Loading factor required to achieve $\overline{P}[SIR > 17\ dB] = 95\%$, for cluster sizes $N = 1$, 3 and 4. † maximum loading factor.

Antenna Configuration		**Loading factor p^*_{ch} (%)**					
		Forward Link			**Reverse Link**		
SLL	**BW**	**N=1**	**N=3**	**N=4**	**N=1**	**N=3**	**N=4**
$-\infty$ dB	10^o	49.5	88.4 †	86.0 †	47.9	88.4 †	86.0 †
	30^o	13.7	59.3	80.5	11.8	52.8	75.0
	45^o	4.5	34.3	52.4	0	31.5	50.3
	60^o	0	20.5	37.3	0	19.0	32.0
-40 dB	10^o	49.3	88.4 †	86.0 †	47.7	88.4 †	86.0 †
	30^o	13.3	59.0	81.0	9.7	49.2	76.1
	45^o	2.9	34.0	52.0	0	34.8	54.1
	60^o	0	20.3	37.0	0	19.7	35.0
-30 dB	10^o	38.0	88.4 †	86.0 †	39.6	88.4 †	86.0 †
	30^o	7.8	50.7	81.1	7.0	54.9	78.4
	45^o	0	33.5	52.0	0	32.0	51.9
	60^o	0	20.3	37.1	0	19.3	33.0
-18 dB	10^o	0	72.6	86.0 †	0	76.4	86.0 †
	30^o	0	39.3	66.7	0	38.2	74.2
	45^o	0	27.1	46.9	0	28.1	50.2
	60^o	0	14.4	32.6	0	16.4	32.6
-12 dB	10^o	0	30.0	52.9	0	28.3	55.8
	30^o	0	17.7	37.6	0	18.1	39.3
	45^o	0	10.9	30.0	0	14.2	31.8
	60^o	0	8.1	23.4	0	7.8	22.0

Table 4.3: Capacity gains with respect to $N = 7$, 3-sector cells reference system: (†) capacity is limited by blocking probability rather than by interference; ($\star$) $\overline{P}[SIR > 17\ dB] = 95\%$ is achieved only if p^*_{ch} is zero, i.e. the system performance specification cannot be met.

Antenna Configuration		**Capacity Gain Ψ (%)**					
		Forward Link			**Reverse Link**		
SLL	**BW**	**N=1**	**N=3**	**N=4**	**N=1**	**N=3**	**N=4**
$-\infty$ dB	10^o	477	243†	150†	460	243†	150†
	30^o	60	130	134	37	105	120
	45^o	−48	33	52	($\star$)	22	46
	60^o	($\star$)	−20	8	($\star$)	−26	−6
−40 dB	10^o	477	243†	150†	460	243†	150†
	30^o	55	129	134	14	91	121
	45^o	−65	32	52	($\star$)	35	57
	60^o	($\star$)	−21	7	($\star$)	−24	2
−30 dB	10^o	344	243†	150†	363	243†	150†
	30^o	−9	97	135	−18	112	127
	45^o	($\star$)	30	51	($\star$)	24	50
	60^o	($\star$)	−21	7	($\star$)	−25	−5
−18 dB	10^o	($\star$)	182	150†	($\star$)	196	150†
	30^o	($\star$)	52	93	($\star$)	48	96
	45^o	($\star$)	5	36	($\star$)	9	38
	60^o	($\star$)	−44	−5	($\star$)	−36	−5
−12 dB	10^o	($\star$)	5	54	($\star$)	10	62
	30^o	($\star$)	−31	9	($\star$)	−30	14
	45^o	($\star$)	−58	−13	($\star$)	−45	−8
	60^o	($\star$)	−68	−33	($\star$)	−70	−36

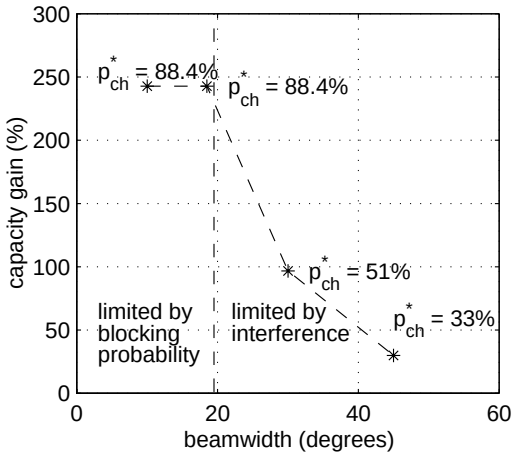

Figure 4.7: Forward link capacity gain for $N = 3$, $SLL = -30$ dB and several values of beamwidth.

as cluster size decreases, since the number of channels per cell increases. This scenario is indicated in Table 4.3 by (†).

As examples of these two distinct situations, consider the forward link case for cluster size $N = 3$, $SLL = -30$ dB. The simulations show that the maximum beamwidth required such that no reduction of loading factor occurs is 18^o. Figure 4.7 presents the graph of capacity gain versus beamwidth, showing the operating points where capacity is limited by blocking probability and by interference.

Points within the region where capacity is limited by interference represent the cases where the loading factor is smaller than the maximum loading factor for cluster size $N = 3$ (88.4%). In this region, capacity increases as beamwidth narrows, since the required loading factor increases. On the other hand, when the beamwidth is narrower than 18^o (operating points where capacity is limited by blocking probability), the loading factor is equal the maximum value and further reduction in the beamwidth does not lead to capacity improvement.

Analyzing the results presented above, we conclude that the fractional loading factor technique plays an important role in this combined technique. In most of the cases, narrowbeam antennas alone are not able to reduce the co-channel interference below the maximum tolerable level. By reducing the fractional loading factor, a less complex antenna (less restrictive side lobe level and beamwidth) can be used, providing substantial capacity gain. Also, when the fractional loading factor is introduced, the relationship between BW, SLL,

the cluster size, and the capacity gain may change unexpectedly. The commonly held belief that *the lower the base station SLL/narrower BW, the higher the system capacity* is not always valid. For example, from Table 4.3, we see that, for the forward link, the use of cluster size $N = 4$ with $SLL = -18$ dB and $BW = 30^o$ leads to a higher system capacity ($\Psi = 93\%$) than cluster size $N = 1$ with $SLL = -30$ dB and $BW = 30^o$ ($\Psi = -9\%$). The reason is that for $N = 1$ system, a greater reduction in the loading factor is required to meet the system performance specification, which induces system capacity loss.

4.5 Conclusions

Capacity improvement which comes about by reducing cluster size causes an increase in co-channel interference, which can then be controlled by the application of narrowbeam (smart) antennas combined with the fractional loading factor. The capacity gain, with respect to a reference system (cluster size $N = 7$, tri-sectorized cells), for a wide range of antenna parameters and fractional loading factors, was computed by extensive simulation. Results show that combinations of cluster size/antenna configuration/fractional loading factor can be divided into two scenarios: *blocking-limited capacity* and *interference-limited capacity*. For the first scenario, which implies the use of highly directional narrowbeam antennas, no loading factor reduction is required. On the other hand, when the antennas are unable to sufficiently reduce the interference, the loading factor must be reduced, reducing the system capacity, which implies the capacity is limited by interference.

Capacity gains as high as 477% above the reference system were observed, but at the expense of large *SLL* reduction and narrow beamwidth. Lower, but still considerable capacity gains can be obtained with less complex antennas. The simulation results show that, as expected, *BW* and *SLL* play an important role in the capacity gain. However, when the fractional loading factor was introduced, we showed that the relationship between antenna parameters, the cluster size and the capacity gain may change in a non-intuitive fashion.

An important conclusion from the results is the importance of the fractional loading factor. In most of the cases shown here, minimum acceptable system performance was achieved because of the *combined use* of narrowbeam smart antennas and fractional loading factor, allowing cluster size reduction. This means that low complexity antennas can be used and still provide system capacity gain, while decreasing cluster size. The results and methodology presented here may be used for cellular and fixed wireless system design.

Chapter 5

Power Control in Cellular Communication Systems

5.1 Introduction

Transmitted power in cellular radio systems is a scarce resource. From the **mobile station perspective**, the transmitted power level limits battery life, which can be prolonged by controlling the mobile transmitted power, while maintaining it at the minimum level required to achieve the desired link quality. When a mobile approaches its serving base station, the mobile transmitted power level can be reduced, since the received power at the base station increases [1]. From the point of view of battery life conservation, power control is particularly important on the reverse link (communication link from mobile to base station).

From the **cellular system perspective**, controlling the transmitted power level, on both forward and reverse links, eliminates unnecessary co-channel interference. Excessive transmitted power does not improve system performance, but adds to the co-channel interference in the system. The reduction in co-channel interference can be traded for capacity, since it allows more users to share the same channel. Power control as a method for increasing system capacity has been extensively studied for application in systems employing orthogonal multiple access techniques, such as FDMA and TDMA. As is well known, the capacity of such systems can be improved by reducing the cluster size, which, in turn, leads to undesired increased co-channel interference. Several authors have investigated the use of power control in TDMA and FDMA systems as a technique for increasing capacity by simultaneously controlling the co-channel interference and reducing cluster size. An extensive

discussion on this subject is presented in Chapter 6.

In this chapter, we study reverse link power control techniques applied to TDMA or FDMA systems. The same techniques can be used on the forward link (communication link from base station to mobile). The power control techniques studied in this chapter can be divided into two groups: In the first group, the power control is solely based on the level of the desired signal. The transmitter power is adjusted in order to compensate a fraction of the path gain of the received signal. Power control techniques based on the level of the desired signal, usually called *Signal-Level-Based Power Control techniques*, are intrinsically *distributed* techniques, since the adjustment of the power of a given link requires only the knowledge of its own path gain.

In the second group, the power control techniques are based on balancing the *SIR* in the co-channel links, that is, the *SIR* of all links using the same channel are equalized. Several techniques based on this approach are discussed in this chapter. Power control techniques in this group are usually called *Signal-to-Interference Balancing Ratio Techniques*, require the knowledge of path gains of all links using the same channel, being, therefore, *centralized*. However, distributed versions of such techniques have been proposed, as described in this chapter.

5.2 The Cellular System and the Propagation Channel Model

Consider a cellular radio system with cluster size N ($N = 1, 3, 4, 7, \cdots$). Assuming hexagonal shapes for the cells, the number of co-channel cells in the i-th tier is $6i$. Figure 5.1 shows a cellular system with cluster size $N = 4$ and the first tier of co-channel cells. We assume that base stations are located at the center of the cells and mobiles are connected to the nearest base stations. Thus, a given base station receives its desired signal from the mobile located in its cell, but also receives interference signals from all mobiles located in the other co-channel cells, as shown in Figure 5.1. The propagation channel model adopted in present chapter models the *local mean power* of the received signals. The propagation path gain G_{ij} between the mobile at the i-th cell (MS_i) and the BS at the j-th cell (BS_j) (see Figure 5.2) is given by:

$$G_{ij} = \frac{A_{ij}\, G_{t,ij}\, G_{r,ij}}{d_{ij}^{n}}, \tag{5.1}$$

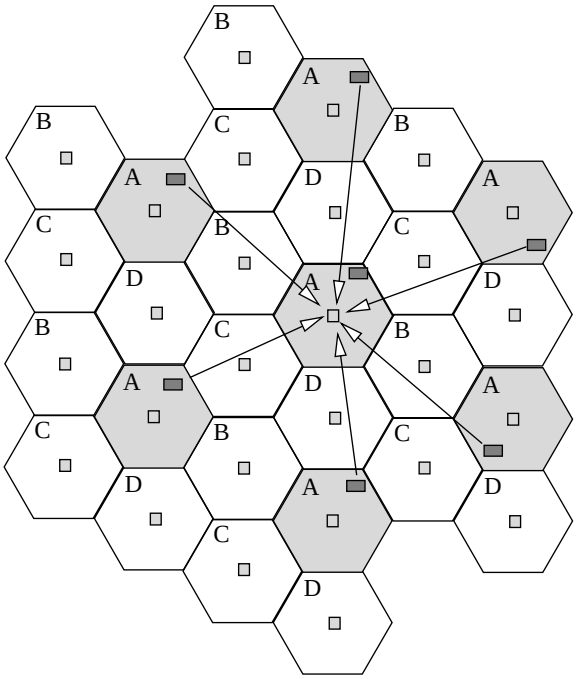

Figure 5.1: Cellular system with cluster size $N = 4$ and first tier of co-channel cells.

where A_{ij} models the power variation due to shadowing caused by obstruction in large objects, d_{ij} is the transmitter to receiver (T-R) distance and n is the path loss exponent. $G_{t,ij}$ and $G_{r,ij}$ are the antenna gains at the mobile and base station, respectively, in the direction of propagation, as shown in Figure 5.2. The variable A_{ij} is assumed to be log-normally distributed, such that $A_{ij,dB} = 10 \log_{10} A_{ij}$, in dB, is normally distributed with zero mean and standard deviation σ_{ij} dB. The power received by the i-th base station from the mobile at the j-th cell is, therefore, $P_j G_{ij}$, where P_j is the power transmitted by the mobile.

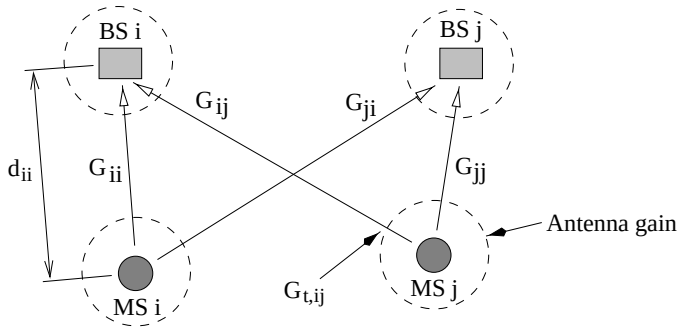

Figure 5.2: Radio Propagation Model

The total interference power received by base station BS_i is modeled as the sum of the signal powers received from all interfering co-channel mobiles. We assume that the interference signals add incoherently, so that the powers can be summed. This is a realistic assumption for wireless communication, since the phase shifts of the individual interference signals may be assumed to be independent and vary significantly due to scattering.

The Signal-to-Interference Ratio (*SIR*) Γ_i at the i-th base station is the ratio of the power received from the desired mobile, $G_{ii}P_i$, to the power of the total interference:

$$\Gamma_i = \frac{G_{ii}P_i}{\sum\limits_{\substack{j=1 \\ j\neq i}}^{M} G_{ij}P_j}, \tag{5.2}$$

where M is the number of co-channel cells.

Dividing both the denominator and numerator of the right-hand side of equation (5.2) by G_{ii}, we have:

$$\Gamma_i = \frac{P_i}{\sum\limits_{\substack{j=1 \\ j\neq i}}^{M} \frac{G_{ij}}{G_{ii}}P_j} = \frac{P_i}{\sum\limits_{j=1}^{M} Z_{ij}P_j - P_i}, \tag{5.3}$$

where

$$Z_{ij} = \frac{G_{ij}}{G_{ii}}. \tag{5.4}$$

G_{ij} and Z_{ij} define the $(M \times M)$ matrices *link gain* $\mathbf{G}$ and *normalized link gain* $\mathbf{Z}$ [47]

$$\mathbf{G} = [G_{ij}]_{i,j=1,\cdots,M} \quad \text{and} \quad \mathbf{Z} = [Z_{ij}]_{i,j=1,\cdots,M}. \tag{5.5}$$

Next section introduces the power control techniques studied in this chapter.

5.3 Power Control Techniques

According to (5.2), the *SIR* at any given base station depends on the path gains of all co-channel links. In order to control the *SIR* of any link, an ideal power control technique requires the use of a *central controller*, connected to all cells, as shown in Figure 5.3. The path gains G_{ij} and the current transmitter powers P_i of all links are reported to the central controller, that properly adjusts P_i. In this case, power control is classified as *centralized* and the transmitter power of any given mobile is a function of the link gain matrix $\mathbf{G}$ and the power vector $\mathbf{P} = [P_1\ P_2 \cdots P_M]^T$:

$$P_i = f(\mathbf{G}, \mathbf{P}). \tag{5.6}$$

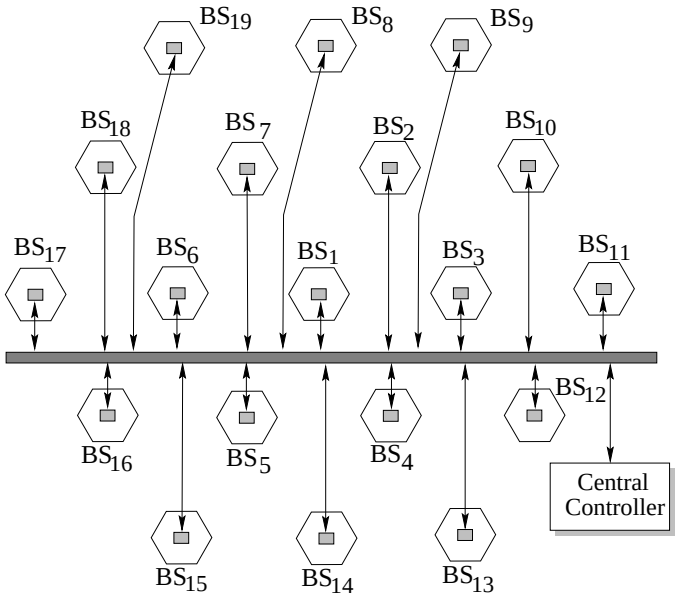

Figure 5.3: Centralized Power Control

However, the use of a central controller sometimes is not feasible, especially in large cellular systems, since it requires additional infrastructure and communication links between the base stations and the central controller. In these cases, a *distributed* power control is more suitable, where the control is based on *local* information, as shown in Figure 5.4. Therefore, the adjustment of P_i is based on the link gain between MS_i and its serving base station, BS_i, and the *SIR* at BS_i: , and:

$$P_i = f(G_{ii}, \Gamma_i). \tag{5.7}$$

The function $f(.)$ in both centralized and distributed cases is chosen such that a cost function is minimized. In the following, we discuss two approaches for selecting the function $f(.)$. The first approach is intrinsically distributed and the transmitter power is adjusted based on the level of the desired signal, aiming to minimize the variance of *SIR*. In the second approach, the objective is to balance the *SIR* of all co-channel links and both centralized and distributed techniques are presented.

5.3.1 Minimum-Variance Signal-Level-Based Power Control

The Signal-Level-Based approach is based on adjusting the transmitter power P_i according to the path gain of the corresponding link, G_{ii}, being, therefore, a distributed approach.

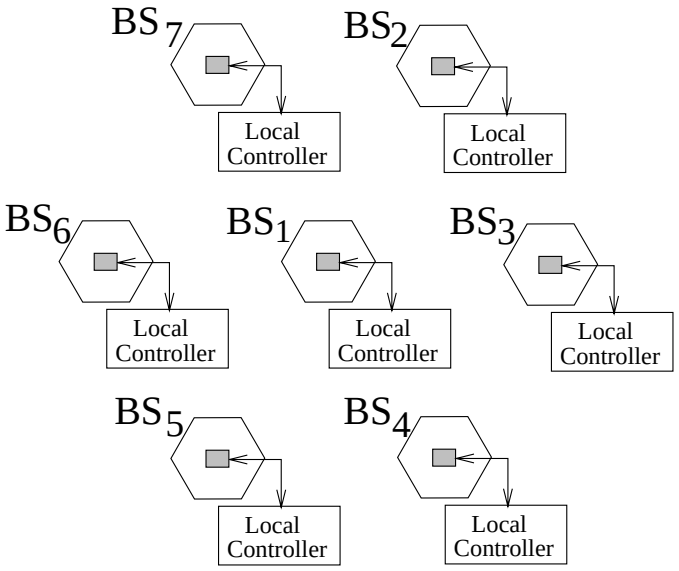

Figure 5.4: Local Power Control

Using dB values, we have

$$P_{i,dB} = f(G_{ii,dB}), \tag{5.8}$$

where

$$P_{i,dB} = 10\log_{10} P_i \quad \text{and} \quad G_{ii,dB} = 10\log_{10} G_{ii}. \tag{5.9}$$

We have seen that the *SIR* at the i-th base station is

$$\Gamma_i = \frac{G_{ii}P_i}{I_T}, \tag{5.10}$$

where I_T is the total interference, given by:

$$I_T = \sum_{j\neq i}^{M} G_{ij}P_j. \tag{5.11}$$

I_T is the sum of log-normally distributed random variables ($G_{ij}P_j$) and is usually approximated by another log-normal random variable, as discussed in Chapter 3. Therefore, the *SIR* in dB at the i-th base station is modeled as a normal random variable and is given by:

$$\begin{aligned}\Gamma_{i,dB} &= P_{i,dB} + G_{ii,dB} - 10\log_{10}\left(\sum_{j\neq i} 10^{\frac{P_{j,dB}+G_{ij,dB}}{10}}\right) \\ &= f(G_{ii,dB}) + G_{ii,dB} - 10\log_{10}\left(\sum_{j\neq i} 10^{\frac{f(G_{jj,dB})+G_{ij,dB}}{10}}\right).\end{aligned} \tag{5.12}$$

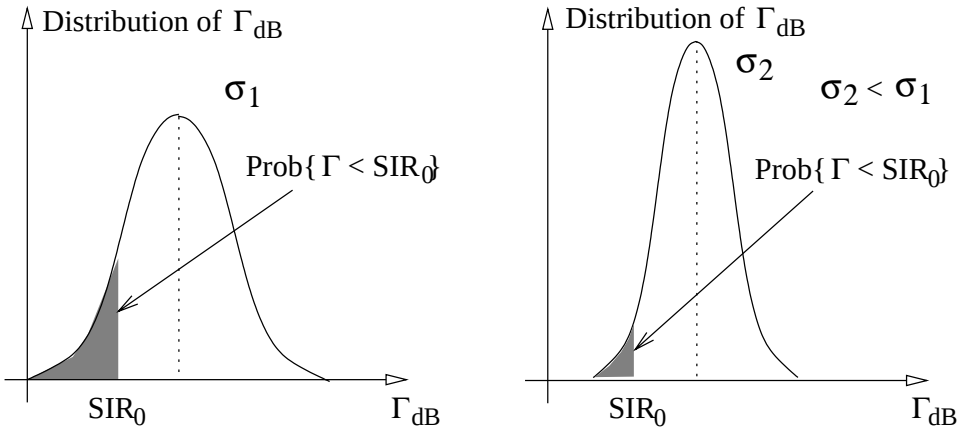

Figure 5.5: Reduction in the standard deviation of Γ_{dB} leads to a reduction in the outage probability.

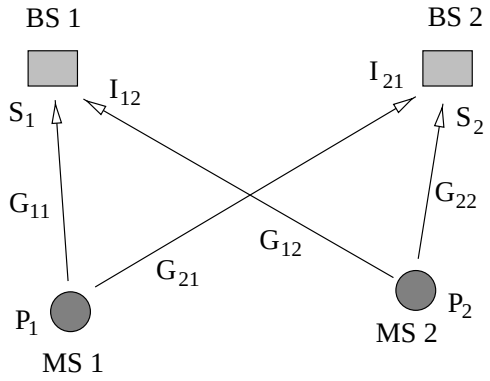

Figure 5.6: Model with two co-channel cells.

In cellular communications, the quality of a communication link is usually measured by the outage probability, defined as the probability that the *SIR* in that link is below a minimum tolerable level SIR_0:

$$Prob\{outage\} = Prob\{\Gamma_{i,dB} < SIR_0\}. \tag{5.13}$$

Assuming that the *mean value of* $\Gamma_{i,dB}$ *remains fixed*, a reduction in the variance of $\Gamma_{i,dB}$ will correspond to a system performance improvement, since the outage probability reduces (see Figure 5.5).

Therefore, the function $f(.)$ in (5.8) must be selected such that the variance of $\Gamma_{i,dB}$ is minimized. We will determine the function $f(.)$ for the case of only two co-channel cells, as depicted in Figure 5.6, and assume that the result can be extended to the general case with more than two co-channel cells.

Using variational analysis, Whitehead showed in [53] that, for the case of only two co-channel cells, the function $f(.)$ that minimizes the standard deviation of $\Gamma_{i,dB}$ is linear

$$P_{i,dB} = f(G_{ii,dB}) = \alpha\, G_{ii,dB} + \beta. \tag{5.14}$$

Next, we determine the constant α in (5.14). β is an arbitrary constant.

The *SIR* $\Gamma_{i,dB}$, in dB, at base station BS_1 is:

$$\Gamma_{1,dB} = S_{1,dB} - I_{12,dB}, \tag{5.15}$$

where $S_{1,dB}$ is the desired signal and $I_{12,dB}$ is the interference caused by mobile MS_2

$$S_{1,dB} = (\alpha+1)G_{11,dB} + \beta \tag{5.16}$$

$$I_{12,dB} = \alpha G_{22,dB} + \beta + G_{12,dB}. \tag{5.17}$$

The variance of $\Gamma_{1,dB}$, denoted by $\sigma^2_{\Gamma_{1,dB}}$ is

$$\sigma^2_{\Gamma_{1,dB}} = \sigma^2_{S_1} + \sigma^2_{I_{12}}. \tag{5.18}$$

The variances $\sigma^2_{S_1}$ and $\sigma^2_{I_{12}}$ can be determined using expressions (5.16) and (5.17), assuming that G_{ij} and G_{kl} are independent for $ij \neq kl$. Therefore, we have

$$\sigma^2_{S_1} = (\alpha+1)^2\sigma^2_{G_{11}} \tag{5.19}$$

$$\sigma^2_{I_{12}} = \alpha^2\sigma^2_{G_{22}} + \sigma^2_{G_{12}}, \tag{5.20}$$

where $\sigma_{G_{ij}}$ is the standard deviation of $G_{ij,dB}$. Note that, $\sigma_{G_{ij}}$ is *not* equal to the shadowing standard deviation associated with the path gain G_{ij} (denoted by σ_{ij}). The path gain $G_{ij,dB}$ can be split into two terms:

$$G_{ij,dB} = \underbrace{A_{ij,dB}}_{\text{shadowing attenuation}} + \underbrace{X_{ij,dB}}_{\text{large scale path loss}} \tag{5.21}$$

where

$$A_{ij,dB} = 10\log_{10} A_{ij}, \tag{5.22}$$

and

$$X_{ij,dB} = 10\log_{10}\frac{G_{t,ij}G_{r,ij}}{d^n_{ij}}. \tag{5.23}$$

The large scale path loss, $X_{ij,dB}$, is also a random variable, due to the spatial distribution of the mobile. Therefore, $\sigma_{G_{ij}}$ also includes the variation of $X_{ij,dB}$.

Substituing expressions (5.19) and (5.20) into (5.18), we finally get

$$\sigma^2_{\Gamma_{i,dB}} = \sigma^2_{G_{12}} + (1 + 2\alpha + 2\alpha^2)\sigma^2_{G_{11}}. \tag{5.24}$$

Note that we have assumed that $\sigma_{G_{11}} = \sigma_{G_{22}}$. The variance $\sigma^2_{\Gamma_{1,dB}}$ reaches its minimum value at $\alpha = -1/2$. Therefore, the signal-level-based power control technique, that minimizes the variance of *SIR*, adjusts the transmitter power level $P_{i,dB}$ by compensating half of the path gain $G_{ii,dB}$ [53]

$$P_{i,dB} = -\frac{1}{2}\, G_{ii,dB} + \beta, \tag{5.25}$$

where β is an arbitrary constant.

It is worth noting that the power control in (5.25) ($\alpha = -1/2$) minimizes the outage probability when the mean value of $\Gamma_{i,dB}$ remains constant with α, which is the case for two co-channel cells.

Constant Received Power

The Signal-Level-Based approach can also be used to adjust the transmitter power $P_{i,dB}$ such that the received power at the base station is kept constant. In this case, the path gain $G_{ii,dB}$ is fully compensated, which corresponds to setting the coefficient α to -1, or

$$P_{i,dB} = -\, G_{ii,dB} + \beta, \tag{5.26}$$

CDMA cellular systems employ power control techniques based on the *Constant Received Power* approach, since, in such systems, the primary objective of a power control technique is to equalize the power levels received by the base station from all users.

5.3.2 Signal-to-Interference Ratio Balancing

In the Signal-to-Interference Ratio Balancing approach, the primarily goal is to equalize, or *balance*, the signal-to-interference ratio of all links using the same channel [47]. Both centralized and distributed techniques can be designed based on this approach, as described below.

Centralized Algorithm

In Section 5.2, we have seen that the *SIR* in the i-th link is

$$\Gamma_i = \frac{P_i}{\sum\limits_{j\neq i}^{M} \frac{G_{ij}}{G_{ii}} P_j} = \frac{P_i}{\sum\limits_{j=1}^{M} Z_{ij}P_j - P_i} \quad \text{for } \; i = 1, 2, \cdots, M. \tag{5.27}$$

Since the *SIR* at any given link depends on the path gains and transmitter powers of all co-channel links, the *SIR*s Γ_i and Γ_j are related to each other. In this context, the *SIR* level γ is said to be *achievable* if there exists a set of powers $P_i \geq 0$, such that [47]

$$\Gamma_i \geq \gamma \quad \text{for all links.} \tag{5.28}$$

Given a matrix $\mathbf{Z} = [Z_{ij}]_{i,j=1,\cdots,M}$, we want to determine the *maximum* achievable γ and the corresponding powers P_i. In other words, we want to determine the powers P_i that maximize the minimum *SIR* among all links. Let Γ_{min} denote the minimum *SIR* among all links:

$$\Gamma_{min} = \min\{\Gamma_i\}_{i=1,\cdots,M}. \tag{5.29}$$

Using (5.27), we have

$$\frac{P_i}{\sum\limits_{j=1}^{M} Z_{ij}P_j - P_i} \geq \Gamma_{min} \;\text{ for }\; i = 1, 2, \cdots, M \tag{5.30}$$

or, in matrix form

$$\frac{1 + \Gamma_{min}}{\Gamma_{min}}\, \mathbf{P} \geq \mathbf{ZP}, \tag{5.31}$$

where, as already defined, $\mathbf{P} = [P_1\ P_2\ \cdots\ P_M]^T$. Therefore, we want to determine the vector $\mathbf{P} > \mathbf{0}$ that satisfies (5.31) and maximize Γ_{min}.

In order to solve this problem, we need to use the following theorem due to Perron, Frobenius and Wielandt [54].

Theorem 5.1 *Let* $\mathbf{H}$ *be a* $(M \times M)$ *non negative irreducible matrix, with eigenvalues* $\lambda_1, \lambda_2, \cdots, \lambda_M$. *Then:*

(a) $\mathbf{H}$ *has one real positive eigenvalue* $\lambda^* = \max\{|\lambda_i|\}_{i=1,\cdots,M}$.

(b) The eigenvector $\mathbf{V}^*$ *associated with* λ^* *is positive, that is, all components of* $\mathbf{V}^*$ *have the same sign.*

(c) The minimum real value λ, *such that the inequality*

$$\lambda \mathbf{V} \geq \mathbf{HV} \tag{5.32}$$

has solution for $\mathbf{V} \geq 0$, *is* $\lambda = \lambda^*$.

(d) The maximum real value λ, such that the inequality

$$\lambda \mathbf{V} \leq \mathbf{H}\mathbf{V} \tag{5.33}$$

has solution for $\mathbf{V} \geq 0$, is $\lambda = \lambda^*$. □

In order to apply Theorem 5.1 in our problem, let us rewrite (5.31) as

$$\lambda \mathbf{P} \geq \mathbf{Z}\mathbf{P}, \tag{5.34}$$

where

$$\lambda = \frac{1 + \Gamma_{min}}{\Gamma_{min}} \quad \text{or} \quad \Gamma_{min} = \frac{1}{\lambda - 1}. \tag{5.35}$$

From (5.35) we see that Γ_{min} is maximum when λ is minimum. Based on Theorem 5.1, the minimum λ that satisfies (5.34) for $\mathbf{P} \geq 0$ is equal to the largest eigenvalue of $\mathbf{Z}$, λ^*. Also, the vector $\mathbf{P}$ that maximizes Γ_{min} is equal to the eigenvector corresponding to λ^*. Therefore, given a matrix $\mathbf{Z}$, the maximum achievable *SIR* is

$$\gamma^* = \frac{1}{\lambda^* - 1}, \tag{5.36}$$

where λ^* is the largest eigenvalue of $\mathbf{Z}$, and the power vector $\mathbf{P}^*$ achieving this maximum is the eigenvector associated with λ^*.

From Theorem 5.1, we see that λ^* and its corresponding eigenvector also provide the solution for

$$\lambda \mathbf{P} \leq \mathbf{Z}\mathbf{P}, \tag{5.37}$$

for $\mathbf{P} \geq 0$. Let Γ_{max} be the maximum *SIR* among all links. Using (5.27), we have

$$\frac{P_i}{\sum\limits_{j=1}^{M} Z_{ij} P_j - P_i} \leq \Gamma_{max} \quad \text{for} \quad i = 1, 2, \cdots, M \tag{5.38}$$

or, in matrix form

$$\frac{1 + \Gamma_{max}}{\Gamma_{max}} \mathbf{P} \leq \mathbf{Z}\mathbf{P}. \tag{5.39}$$

Therefore, if $\mathbf{P}$ is equal to the eigenvector corresponding to λ^*, we have

$$\frac{1 + \Gamma_{max}}{\Gamma_{max}} = \lambda^* \quad \text{or} \quad \Gamma_{max} = \frac{1}{\lambda^* - 1}. \tag{5.40}$$

We conclude that, by choosing $\mathbf{P}$ equal to the eigenvector associated with the largest eigenvalue of $\mathbf{Z}$, the minimum *SIR* is maximized and all *SIR*s are *balanced*, that is

$$\Gamma_i = \frac{1}{\lambda^* - 1} \quad \text{for} \quad i = 1, 2, \cdots, M. \tag{5.41}$$

Therefore, the Centralized *SIR* Balancing Power Control is summarized as follows [47]:

1) Given the normalized link gain matrix $\mathbf{Z}$, compute the maximum eigenvalue of $\mathbf{Z}$, λ^*, and the corresponding eigenvector, $\mathbf{V}^*$.

2) Set the power $\mathbf{P}$ equals the eigenvector $\mathbf{V}^*$. The *SIR* of all links will be equal to $\Gamma_i = \gamma^* = 1/(\lambda^* - 1)$.

However, there is no guarantee that γ^* is higher than a minimum acceptable SIR_0. For the case when the balanced γ^* is smaller than SIR_0, Zander proposed a technique for increasing γ^*, based on removing cells from the set of co-channel cells, as presented in the next section.

Centralized Algorithm with Cell Removal

Consider the set $\mathcal{S}_M$ of M *active* co-channel links (all using the same channel), with the maximum achievable *SIR* denoted by γ^*. Suppose that γ^* is smaller than a desired threshold SIR_0. From the discussion presented above, we know that it is not possible to have *all* links in the set $\mathcal{S}_M$ with *SIR* larger than γ^*. However, if some links are turned off, the maximum achievable *SIR* of the remaining links will increase and the threshold SIR_0 may be achieved.

The *cell removal* strategy is based on constructing smaller and smaller *balanced* systems by *removing* links from the set of co-channel cells [47]. The *optimum* procedure is to find the largest submatrix $\mathbf{Z}$' (minimum number of cells removed) for which the balanced *SIR* γ^* is higher than or equal to the desired threshold SIR_0. Starting from the original matrix $\mathbf{Z}$, links are removed one by one, computing the resulting balanced γ^*. If the desired SIR_0 is not achieved, we then try removing all combinations of two links and so on. This procedure is straightforward, but tedious, specially for a large number of co-channel links M. Zander has proposed a simple procedure called *Stepwise Removal Algorithm* (SRA). In this procedure, the links are removed one after other, until the balanced γ^* of the remaining links is higher than or equal to the required SIR_0. The procedure is summarized as follows:

1) Starting from the original matrix $\mathbf{Z}$ (all links are active), compute the balanced γ^* using the largest eigenvalue λ^* of $\mathbf{Z}$. If $\gamma^* \geq SIR_0$, the power vector $\mathbf{P}$ is given by the eigenvector corresponding to λ^*.

2) If $\gamma^* < SIR_0$, form the sub matrix $\mathbf{Z}$' by removing the link k for which the sum

$$\sum_{i=1}^{M} Z_{ki} + \sum_{i=1}^{M} Z_{ik} \tag{5.42}$$

is maximum.

3) Compute the balanced γ^* corresponding to $\mathbf{Z}$'. If $\gamma^* \geq SIR_0$, the power vector $\mathbf{P}$ is given by the eigenvector corresponding to the maximum eigenvalue λ^* of $\mathbf{Z}$'. If $\gamma^* < SIR_0$, repeat step 2), removing another link.

Although the cell removal strategy may appear to be a drastic way to improve system performance and a contradictory way to achieve high system capacity, we should note that those links where the threshold SIR_0 could not be achieved (*bad links*) are useless and the corresponding calls would be probably dropped or handed off to other channels. With bad links present in the set of co-channel links, the *SIR* balancing strategy may be disastrous to *all* links, since the *SIR* of all links may be dropped below the required SIR_0. Cell removal is actually performed by handing off calls to other channels.

Distributed Algorithms

The main drawback of both centralized algorithms presented in the previous sections is that measurements of the path gains of all co-channel links in the system need to be reported to a central controller, that adjusts the power levels of each link. In other words, the centralized algorithm adjusts the transmitter power level, based on *all* current power levels and *SIR*s.

In a distributed algorithm, the adjustment of the transmitter power of a given link is instead based only on the current *SIR* and transmitter power

$$P_i^{(k)} = g\left(P_i^{(k-1)}, \Gamma_i^{(k-1)}\right), \tag{5.43}$$

where $P_i^{(k)}$ and $\Gamma_i^{(k)}$ are the transmitter power and *SIR* in the i-th link at the k-th time instant, and $g(.)$ is the function that maps $P_i^{(k-1)}$ and $\Gamma_i^{(k-1)}$ into $P_i^{(k)}$. Note that the quantities used in the power adjustment, namely $P_i^{(k-1)}$ and $\Gamma_i^{(k-1)}$, can be measured at the i-th mobile and its serving base station, respectively. Zander [55] and Grandhi [56] proposed *distributed algorithms*, based on *SIR* balancing, as described in the following.

- **Distributed Balancing Algorithm (DBA) [55]**

In the Distributed Balancing Algorithm, proposed by Zander, the transmitter power level of the i-th mobile at the k-th time instant is adjusted using the expression:

$$P_i^{(k)} = \kappa \, P_i^{(k-1)} \left(1 + \frac{1}{\Gamma_i^{(k-1)}}\right), \tag{5.44}$$

where κ is some positive constant. In matrix form, this algorithm can be expressed as:

$$\mathbf{P}^{(k)} = \kappa\, \mathbf{Z}\, \mathbf{P}^{(k-1)}, \tag{5.45}$$

where

$$\mathbf{P}^{(k)} = [P_1^{(k)}\ P_2^{(k)}\ \cdots\ P_M^{(k)}]. \tag{5.46}$$

The algorithm is initialized with an arbitrary positive vector $\mathbf{P}^{(0)}$.

It has been shown in [55] that this scheme converges to the optimum solution, that is:

$$\lim_{k\to\infty} \Gamma_i^{(k)} = \gamma^* = \frac{1}{\lambda^* - 1} \tag{5.47}$$

and

$$\lim_{k\to\infty} \mathbf{P}^{(k)} = \mathbf{P}^* = \mathbf{V}^* \tag{5.48}$$

where λ^* is the largest eigenvalue of $\mathbf{Z}$ and $\mathbf{V}^*$ is the eigenvector corresponding to λ^*.

Since all terms in (5.44) are positive, the transmitter powers in the DBA scheme are all increasing, unless we select κ at the time instant k as [55]:

$$\kappa = \kappa^{(k)} = \frac{1}{|\mathbf{P}^{(k)}|}. \tag{5.49}$$

However, this selection of κ is not possible in a completely distributed system.

- **Distributed Power Control (DPC) [56]**

Grandhi *et al.* proposed an alternative scheme, where the power adjustments at the k-th time instant is:

$$P_i^{(k)} = \zeta\, \frac{P_i^{(k-1)}}{\Gamma_i^{(k-1)}}, \tag{5.50}$$

where ζ is some positive constant. In matrix form, this algorithm is:

$$\mathbf{P}^{(k)} = \zeta\, \mathbf{B}\, \mathbf{P}^{(k-1)}, \tag{5.51}$$

where $\mathbf{B} = [B_{ij}]$ and

$$B_{ij} = \begin{cases} Z_{ij} & \text{for } i \neq j \\ 0 & \text{for } i = j. \end{cases} \tag{5.52}$$

Note that $\mathbf{Z} = \mathbf{B} + \mathbf{I}$, where $\mathbf{I}$ is the identity matrix. It has been shown that the DPC scheme also converges to the optimum solution, that is, (5.47) and (5.48) also hold for the DPC scheme.

As for the case of the DBA scheme, we need to choose the coefficient ζ in order to ensure a constant power level. A possible choice is [56]:

$$\zeta = \zeta^{(k)} = \frac{1}{\max(\mathbf{P}^{(k)})}, \tag{5.53}$$

which would require some communication among the base stations.

Distributed Balancing Algorithm with Cell Removal

The DBA and DPC schemes presented above are basically distributed algorithms based on the *SIR* balancing approach. As for the case of the centralized algorithm, the maximum achievable *SIR* in the distributed algorithms, γ^*, may be smaller than the required threshold SIR_0. Zander proposed a distributed algorithm where the cell removal strategy is employed [55]. The algorithm basically combines the DBA scheme with the cell removal strategy. The algorithm is summarized below:

1) With $\mathbf{P}^{(0)} = 1$, determine and store the vector $\mathbf{\Gamma}^{(0)}$; If $\Gamma_i^{(0)} > SIR_0$ for all i, stop algorithm; Otherwise,

(2) Apply the distributed balancing algorithm for at most L iterations. If $\Gamma_i^{(k)} > SIR_0$ for all i and any $k \leq L$, stop algorithm; otherwise,

(3) Remove the cell l that has the smallest initial *SIR* ($\Gamma_l^{(0)} = \min_i \Gamma_i^{(0)}$). Go to step 1).

A critical parameter in this algorithm is the maximum number of iterations in the distributed balancing algorithm, before a cell is removed (L). We have seen in Section 5.3.2 that, in the DBA scheme, $\Gamma_i^{(k)}$ approaches the maximum achievable γ^*. Therefore, if $\gamma^* > SIR_0$, we should keep applying DBA, without removing any cell, since, eventually, all $\Gamma_i^{(k)}$ will approach γ^*. In this case, L should be large enough to guarantee the convergence. On the other hand, if $\gamma^* < SIR_0$, we should remove a cell as quickly as possible, that is, L should be short. Therefore, large L is required in order to guarantee the convergence of the algorithm when $\gamma^* > SIR_0$. On the other hand, small L is better when $\gamma^* < SIR_0$, so that we quickly remove cells. However, in the DBA scheme, we do not have prior knowledge of γ^* and the selection of L must be a tradeoff between the benefits of using large L (convergence is guaranteed, when $\gamma^* > SIR_0$) and small L (cells are quickly removed, when $\gamma^* < SIR_0$).

5.4 Autonomous *SINR* Balancing Algorithm

In this section, we present another power control algorithm based on the SIR balancing approach. This particular algorithm is employed in the simulation analysis presented in Chapters 8, 9 and 10 of this dissertation. Since in the analysis presented in those chapters we take into consideration thermal noise, and following the original description of the algorithm in [57], we present the Autonomous *SINR* Balancing Algorithm assuming that thermal noise is *not* negligible. Therefore, we redefine the signal-to-interference (plus noise) $\Gamma_i(t)$ at the i-th base station (or mobile), at time t, as

$$\Gamma_i(t) = \frac{G_{ii}P_i(t)}{\sum\limits_{j\neq i}^{M} G_{ij}P_j(t) + N_i}, \tag{5.54}$$

where N_i is the thermal noise power at the receiver and the other variables were already defined. In the Autonomous *SINR* Balancing Algorithm, the i-th base station (or user) drives its $SINR$ ($\Gamma_i(t)$) toward a target $SINR$ (Γ_T), by an amount proportional to the offset between Γ_T and Γ_i. This dynamic can be expressed as [57]:

$$\frac{d}{dt}\Gamma_i(t) = -\rho[\Gamma_i(t) - \Gamma_T], \tag{5.55}$$

where ρ is the positive proportionality constant. In a distributed implementation, the i-th base station (or user) can control only its own transmitter power level $P_i(t)$, but not the transmitter power levels $P_j(t)$ of the other base stations (or users). Therefore, we assume that all power levels $P_j(t)$, $j \neq i$ in (5.54) do not change, and (5.55) is rewritten as

$$\left[\frac{G_{ii}}{\sum\limits_{j\neq i}^{M} G_{ij}P_j(t) + N_i}\right] \frac{d}{dt}P_i(t) = -\rho[\Gamma_i(t) - \Gamma_T], \tag{5.56}$$

Rearranging the terms in (5.56) we obtain

$$\frac{d}{dt}P_i(t) = -\rho\left\{P_i(t) - \frac{\Gamma_T}{G_{ii}}\left(\sum_{j\neq i}^{M} G_{ij}P_j(t) + N_i\right)\right\}. \tag{5.57}$$

Using the matrix notation introduced in Section 5.2, we can write equation (5.57) as

$$\frac{d}{dt}\mathbf{P}(t) = -\rho\left[\Gamma_T\mathbf{Z} + \mathbf{I}\right]\mathbf{P}(t) + \rho\mathbf{N} \tag{5.58}$$

where $\mathbf{N}$ is a vector composed by all terms N_i. From equation (5.58), we can write the difference equation,

$$\mathbf{P}^{(k+1)} - \mathbf{P}^{(k)} = -\rho \left[\Gamma_T \mathbf{Z} + \mathbf{I}\right] \mathbf{P}^{(k)} + \rho \mathbf{N} \tag{5.59}$$

or, for the i-th link [58],

$$P_i^{(k+1)} - P_i^{(k)} = -\left(1-\rho\right) P^{(k)} \left[1 + \frac{\rho \Gamma_T}{(1-\rho)\Gamma_i^{(k)}}\right], \tag{5.60}$$

where $P_i^{(k)}$ and $\Gamma_i^{(k)}$ are the transmitter power level and $SINR$ at the i-th link and at the k-th iteration, respectively. It should be noted that, when the i-th base station (or user) adjusts its transmitter power using (5.60), $SINR$ at all other co-channel links will change. Consequently, the transmitter power levels of other co-channel links are also adjusted, characterizing a recursive process. It is shown in [57] that the fastest convergence rate is achieved with $\rho = 1$, such that (5.60) becomes

$$P_i^{(k+1)} = P_i^{(k)} \frac{\Gamma_T}{\Gamma_i^{(k)}}. \tag{5.61}$$

Therefore, the autonomous $SINR$ balancing power control algorithm is based on adjusting the transmitter power to the value needed to achieve the desired target $SINR$.

5.5 Conclusion

In this chapter, we have presented several techniques for power control, applied to TDMA or FDMA cellular radio communications. Power control techniques have been proposed mainly for battery conservation and link quality improvement by reducing the co-channel interference level. The link quality improvement that results from the use of power control may be traded for capacity improvement. The reduction of the co-channel interference level due to the use of power control may allow reduction in cluster size or channel reuse distance, increasing the system capacity.

The power control techniques studied in this chapter can be divided into two groups: In the first group, the power control is based on the level of the desired signal. The transmitter power is adjusted in order to compensate a fraction of the path gain of the received signal. When *half* the dB value of the path gain is compensated, the outage probability is reduced. When the path gain is *fully* compensated, the received power is kept constant. Power control techniques based on the level of the desired signal are intrinsically distributed techniques,

since the adjustment of the power of a given link requires only knowledge of its own path gain.

In the second group, the power control techniques are based on balancing the *SIR* of the co-channel links, that is, the power control technique aims to equalize the *SIR* of all links using the same channel. Based on the knowledge of path gains of all links, the transmitter powers are adjusted so that all links have the same *SIR*. However, the resulting *SIR* may happen to be lower than a desired threshold. In order to maximize the resulting *SIR*, a technique based on switching off links with poor link quality, called the *cell removal strategy*, has been proposed in literature and reviewed in this chapter. Switching off links is apparently a drastic measure, but we should keep in mind that links with low *SIR* only add to interference in the system and the calls in those links would be eventually handed off to other channels. The *SIR* balancing approach is intrinsically a centralized approach, since it requires path gain of all links to be reported to some central controller. In order to avoid the use of a central controller, distributed version of *SIR* balancing (with and without cell removal) have been proposed in literature and discussed in this chapter.

The power control techniques presented in this chapter, especially the distributed techniques, are very suitable for combined use with channel allocation techniques and adaptive antennas, as we will see in Chapter 6.

Chapter 6

Resource Allocation in Cellular Communication Systems

6.1 Introduction

The rapid growth in the demand for cellular mobile communications has motivated the study of more efficient methods and strategies for resource allocation. An efficient resource allocation strategy guarantees the quality of service of all ongoing calls, while efficiently using the radio resources. Basically, two resources are involved in the maintenance of a call in cellular communications [59]:

- **Communication channels:** a pair of channels that provide the communication link on both forward (base station to mobile) and reverse (mobile to base station) links, between a mobile and its serving base station.
- **Transmitter power:** In cellular systems, many mobiles share the same communication channel and transmission from one mobile causes interference to the others. Therefore, transmitter power must be appropriately assigned both to provide mobiles an acceptable connection and to minimize the interference caused by each mobile to the others.

Channel allocation and power allocation are usually studied and implemented independently, even though they are closely related to each other through the basic trade-off in cellular communication: *capacity versus link quality*. The *cell clustering* is an example of this trade-off: the geographic area where cellular communication service is to be provided is split into

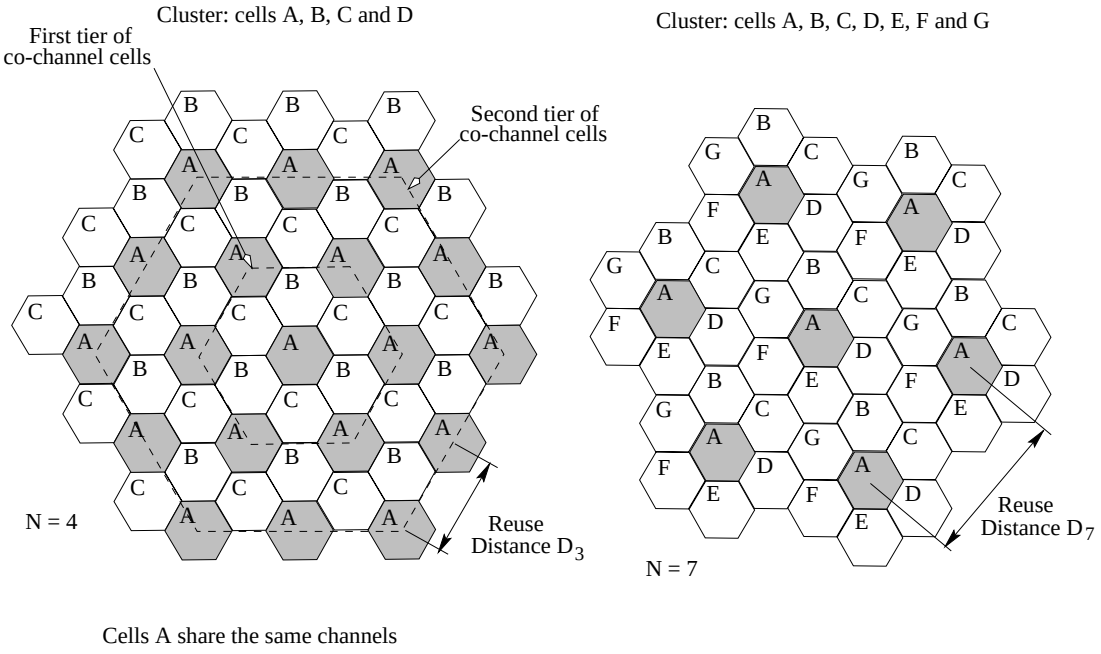

Figure 6.1: Cell clustering in cellular communication systems.

cells, which are grouped into *cluster* of N cells (see Figure 6.1). The total available spectrum for the geographic service is then assigned to each cluster, so that cells in the same cluster do not share any communication channel [1]. If M channels are available for the service area, each cell is assigned M/N channels. As the clusters are replicated, the reuse of channels leads to *tiers* of co-channel cells and *co-channel interference*, and the level of interference is directly related to the cluster size N. The minimum distance between the center of two co-channel cells is called the *reuse distance* D_N, which, for cells with hexagonal shapes, is

$$D_N = \sqrt{3N}R, \tag{6.1}$$

where R is the radius of the cell. Therefore, small cluster size leads to high capacity at the expense of low transmission quality, due to the increased co-channel interference (small D), while high transmission quality (low co-channel interference) can be achieved by using a large cluster size or reuse distance.

The basic problem of resource allocation can be stated as follows: given a set $\mathbf{S_C}$ of C communication channels

$$\mathbf{S_C} = \{c_1\ c_2\ \cdots\ c_C\}, \tag{6.2}$$

a set $\mathbf{S_M}$ of M mobiles requiring a radio connection to the cellular system,

$$\mathbf{S_M} = \{m_1\ m_2\ \cdots\ m_M\}, \tag{6.3}$$

and, finally, a set $\mathbf{S_B}$ of B base stations

$$\mathbf{S_B} = \{b_1\ b_2\ \cdots\ b_B\}, \tag{6.4}$$

allocate a communication channel from the set $\mathbf{S_C}$ and appropriate transmission power levels to each radio link between a mobile from the set $\mathbf{S_M}$ and its serving base station. Usually, the number C of channels is limited, limiting the number of mobiles that are going to be able to establish a radio link with a base station. Additionally, another constraint is the co-channel interference level required to guarantee an acceptable link quality. Therefore, the two major constraints in any resource allocation is the limited number of channels and the required Signal-to-Interference Ratio (SIR). By efficiently allocating channel and transmitter power, system capacity improvement can be achieved, which means more calls carried at the same time by the system, while maintaining an acceptable link quality. It should be noted that the capacity improvement achieved by a particular allocation technique is sometimes measured by the reduction in the probability that a new call is blocked (blocking probability P_b). The reduction in the blocking probability means that more call can be admitted in the system, before the blocking probability reaches a maximum acceptable level.

As mentioned earlier, channel and power allocation techniques have been extensively studied, but in most of the studies, they have been considered separately. Only in the last few years have some studies been carried out on joint channel and power allocation. A short description of the basic ideas of power and channel allocation techniques and a literature review on these topics are presented in the remainder of the chapter.

6.2 Power Control

In the early days of cellular systems, power control techniques were primarily designed for *battery life conservation* and *link quality*, while maintaining the transmitter power at the minimum level required to achieve the desired link quality. When a mobile approaches its serving base station, the mobile transmitted power level can be reduced, since the received power at the base station increases [1]. From the point of view of battery life conservation, power control is particularly important on the reverse link (communication link from mobile to base station).

A change in the paradigm regarding the purpose of power control has appeared in literature in the past few years. This change in paradigm is necessary when one realizes that

the transmitter power is, in fact, a resource that should be appropriately assigned. Excessive transmitted power only adds to the interference with users sharing the same channel. Controlling the transmitted power level, on both forward and reverse links, eliminates unnecessary co-channel interference, and the resulting reduction in co-channel interference can be traded for capacity, since it allows more users to share the same channel. The relationship between system capacity and transmitted power is clear in CDMA systems, whose capacity is limited by the co-channel interference [1].

This new paradigm has motivated the study of new power control techniques for systems employing orthogonal multiple access techniques, such as FDMA and TDMA. As is well known, the capacity of such systems can be improved by reducing the cluster size, which, in turn, leads to undesired increased co-channel interference. Several authors have investigated the use of power control on both forward and reverse links in TDMA and FDMA systems as a technique for increasing capacity by simultaneously controlling the co-channel interference and reducing cluster size.

When no power control technique is employed, the signal-to-interference ratios measured at mobiles using a particular channel have a large variance, due to path loss and shadow fading. Some links will have a *SIR* which is larger than a minimum required SIR_0, while others will present a link quality below the minimum acceptable level. The links in which *SIR* is below SIR_0 will likely be dropped, reducing the overall system capacity. Zander has shown [47] that the maximum number of links, in which *SIR* is larger than SIR_0, is achieved by adjusting their transmitter power in order to balance the *SIR* of the *links that can be supported*. The rest of the links must be handed off to another channel. As a result of the *SIR* balancing, the variance of the *SIR* measured at the links using the same channel is ideally reduced to zero, as shown in Figure 6.2.

An important aspect of power control is how these techniques are implemented. As discussed in Chapter 5, power control techniques can be classified or *centralized* and *distributed*. Centralized power control techniques require information about *all* links, such as path gains, power settings, etc., and involve additional infrastructure and a central controller. On the other hand, distributed techniques are based on *local* information only, being, therefore, of special interest, since they do not require exchange of information among the different base stations and a central controller. Results presented in literature have shown that, as expected, centralized techniques present better results if compared with distributed techniques, at the expense of higher complexity and infrastructure requirements. The better

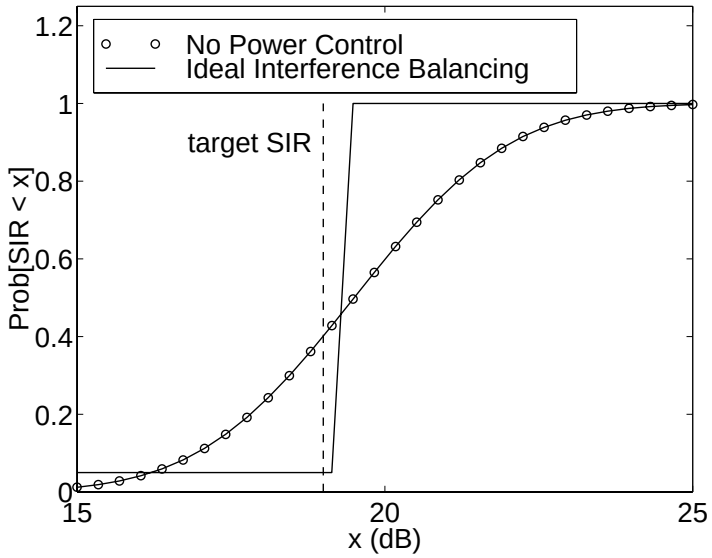

Figure 6.2: Probability that $SIR < X$.

performance of centralized techniques is due to fact that the decisions on power settings are based on a global information about the whole system in terms of co-channel interference.

Power control techniques will be briefly discussed in the following and an extensive discussion on this subject is presented in Chapter 5.

6.2.1 Power Control as a Technique for Controlling Co-channel Interference

Two approaches for controlling the transmission power of both links have been proposed in the literature. In the first approach, usually known as *Interference Balancing Power Control*, the transmission power levels are adjusted aiming to balance the *SIR* in all links using the same channel, that is, the *SIR* of all links using the same channel are equalized. However, depending on the propagation conditions and the number of co-channel users, the maximum achievable balanced *SIR* may be lower than the minimum required SIR_0 for acceptable performance. In this case, some co-channel links must be switched off in order to increase the maximum achievable balanced *SIR*. Finding the optimum set of links to be turned off is a very difficult problem and some heuristic approaches have been proposed. Zander [47, 55] has proposed a power control technique based on interference balancing, which is reviewed in Chapter 5. When the balanced *SIR* is lower than the minimum required SIR_0, co-channel

links are stepwise turned off, until the remaining links achieve the minimum acceptable SIR_0. Capacity gains of three times, for a distributed version of this technique, and four times, for a centralized version, with respect to a reference system using cluster size $N = 7$, have been reported.

In the second approach, usually known as *Signal-Level-Based Power Control* and also reviewed in Chapter 5, the transmission power levels are adjusted aiming to compensate a fraction of the signal path gain, which consists of the path loss and shadowing. It can be shown [53], that the policy that minimize the variance of *SIR* consists of compensating half of the path gain in dB.

In Chapter 5, interference balancing techniques, proposed by Zander [47, 55] and Grandhi *et. al* [56], and Signal-Level-Based techniques, proposed by Whitehead [53], will be reviewed in details, with simulation results.

6.3 Channel Allocation

Channel allocation techniques have been extensively investigated for application in cellular communication systems. Several techniques have been proposed and an extensive survey of most of these techniques can be found in [60]. The basic problem involving channel allocation consists of allocating a channel from the set $\mathbf{S_C}$ to each radio link connecting a mobile from the set $\mathbf{S_M}$ to a base station from the set $\mathbf{S_B}$. The ideal allocation technique is the one that minimizes the number of required channels to serve all mobiles by reusing channels more efficiently, while meeting some requirements in terms of link and service quality. Several techniques can be designed for this allocation process, depending on the constraints that need to be observed and information available to perform this task. The allocation techniques can be classified into *Fixed Channel Allocation* (FCA), *Dynamic Channel Allocation* (DCA) and *Hybrid Channel Allocation* (HCA).

In FCA techniques, a fixed number of channels are assigned to the base station of each cell, following some reuse pattern and desired link quality. A mobile requesting a channel can be allocated only a channel from the channel set assigned to its serving base station. FCA techniques are very simple, but since the number of channel in each cell is fixed, they can not adapt to traffic changes. It is well known that the number of users in a particular region of a geographic service area changes throughout the day. For example, during business hours, more calls are made in the downtown region of a city than in the residential region. On

the other hand, after business hours, more calls are placed in the residential region. Some variations of FCA schemes have been proposed to cope with traffic changes, such as **channel borrowing** and **directed retry** [2]. In the channel borrowing technique, channels assigned to a base station can be borrowed by a neighboring base station if necessary. In the directed retry, if a base station does not have an available channel to service a call from a mobile station, the mobile station tries to acquire a channel from a neighboring base station that provides a satisfactory link quality.

In DCA techniques, any channel can, in principle, be assigned to the base station of any cell, as long as some requirements are met. The core idea behind all DCA techniques is to assign a call the channel that minimizes a given cost function. Several cost functions have been proposed and the most common parameters involved in these functions include the blocking probability, the reuse distance of the selected channel, propagation measurements, average blocking probability of the system, channel occupancy, etc. [60]. Since the number of assigned channels to a given cell is flexible, DCA techniques provide the system with some flexibility to cope with time varying traffic, explained earlier. It has been shown that FCA techniques perform better than DCA techniques under high traffic load, However, under low load, DCA outperforms FCA [60]. Of particular interest are the DCA techniques based on co-channel interference, which will be discussed in Section 6.3.1.

HCA techniques combine some features of both FCA and DCA techniques. In this class of algorithms, part of the set of channels available for the system is used for fixed allocation, while the rest of the channels are dynamically allocated, following some criteria. HCA techniques have proven to give better results than both FCA and DCA over a wide range of traffic load.

As mentioned before, different channel allocation techniques can be designed based on different constraints and requirements. Based on the trade-off between capacity and link quality, it is clear that the co-channel interference plays an important role in the channel allocation process. Also, co-channel interference is of special interest in this work since it is the common physical bond between channel allocation, transmission power allocation and adaptive antennas. In the following, we briefly discuss channel allocation from the point of view of co-channel interference.

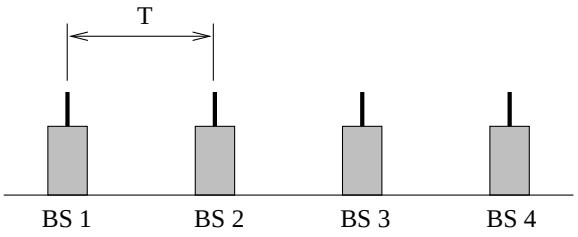

Figure 6.3: One-dimension cellular system with 4 cells

6.3.1 Dynamic Channel Allocation and Co-channel Interference

As mentioned earlier, a fundamental trade-off in a cellular system involves capacity and transmission quality. Channel allocation is a very important component in this fundamental trade-off and can lead to capacity and link quality improvements. In this context, the *adaptability to interference* [61, 62] is an important feature of dynamic channel allocation techniques and will be discussed next.

For most of the dynamic channel allocation techniques, the transmission quality in terms of co-channel interference is assured by means of an a-priori planning process, based on the *compatibility matrix* $\mathbf{G}$. Two cell are said to be *compatible* if the same channel can be used simultaneously in both cells. The compatibility matrix is usually defined as [63]:

$$\mathbf{C} = [c_{ij}]_{i,j=1,\cdots,K} \tag{6.5}$$

where K is the number of cells in the system. The elements c_{ij} defines the compatibility between the i-th and j-th cells:

$$c_{ij} = \begin{cases} 0 & \text{if cells } i\text{-th and } j\text{-th are compatible} \\ 1 & \text{if cells } i\text{-th and } j\text{-th are not compatible} \end{cases} \tag{6.6}$$

As an example, consider an one-dimensional cellular system with 4 cells (such as along a highway), as shown in Figure 6.3, where T is the distance between adjacent base stations. Assuming that the minimum distance between two compatible base stations is $D = 2T$, the compatibility matrix for the system in Figure 6.3 is:

$$\mathbf{C} = \begin{bmatrix} 1 & 1 & 0 & 0 \\ 1 & 1 & 1 & 0 \\ 0 & 1 & 1 & 1 \\ 0 & 0 & 1 & 1 \end{bmatrix}. \tag{6.7}$$

Therefore, based on the compatibility matrix, a channel in use in BS 2 can be used simultaneously in BS 4, but not in BS 1 or BS 3. Note the **C** is based on worst case assumptions (regarding the interference level) about the mobile location within the cell and propagation conditions. Allocation techniques that are based on the compatibility matrix are said to be *traffic adaptive* [61]. The assumptions adopted in the compatibility matrix, regarding co-channel interference, require the use of a large *margin* in the minimum acceptable signal-to-interference ratio in order to cope with the variations in the desired received and interference signals on both links. Those signal variations are basically due to:

- **propagation conditions:** due to shadow fading, the desired received signal may experience a strong fade,
- **user mobility:** when the mobile approaches the cell boundary, the co-channel interference at the mobile increases,
- **traffic load:** if more users share the same channel, co-channel interference in the system increases.

The use of a fading margin decreases the probability that the received signal is below a threshold. Due to the variations in the *SIR*, many calls will have *SIR* higher than the required level SIR_0. The excess *SIR* corresponds to *unused capacity*, since calls with high *SIR* could use a smaller cluster size or lower transmitted power [62]. Therefore, the required large margin in the *SIR* when using the compatibility matrix causes a considerable waste in capacity [64].

Reuse partitioning is one example of techniques that exploit the unused capacity [65]. The basic idea behind reuse partitioning is the use of two or more cluster sizes in the same geographic area. Small cluster sizes are used for mobiles located closer to their BSs, since they receive strong desired signal levels and, therefore, are able to tolerate high co-channel interference. On the other hand, large cluster sizes are used for mobiles located near the cell boundaries, since the received desired signals are weaker. One way to implement reuse partitioning is by dividing the cells in inner and outer regions, as shown in Figure 6.4. The inner regions can be considered as a cellular system where a small cluster size can be used, while the outer regions must use a larger cluster size. It should be noted that the reuse partitioning technique can be viewed as an improved version of the FCA technique, suffering from some problems typically found in FCA techniques, such as lack of ability to deal with traffic changes.

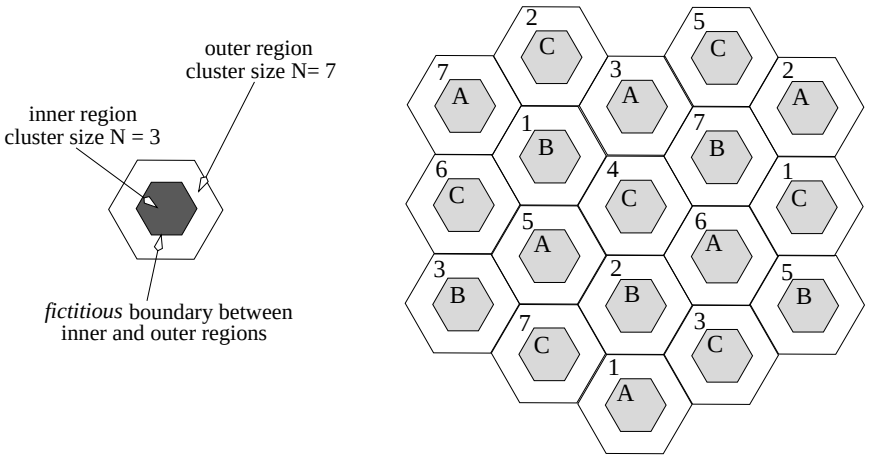

Figure 6.4: Reuse partitioning: inner regions (cells A, B and C) use cluster size $N = 3$, while outer regions (cells 1 through 7) use cluster size $N = 7$.

As mentioned before, the compatibility matrix is based on worst case assumptions regarding the co-channel interference, which depends on traffic load, propagation conditions and user mobility. For example, it is assumed that the mobiles are located near the cell boundary, where the *SIR* is usually low. Additionally, in order to cope with shadowing fading, a large margin is added to the minimum required SIR_0. Consider now that, instead of assuming these worst case conditions, the compatibility matrix is based on actual or more realistic co-channel interference conditions. Therefore, lower minimum required SIR_0 and link margin could be used, reducing the waste of capacity and yielding a more accurate compatibility matrix $\mathbf{C}$. As a consequence, channels could be packed closer, resulting in a capacity gain. For these reasons, dynamic channel allocation techniques based on signal strength and *SIR* measurements have attracted a lot of attention in the past few years.

Several dynamic channel allocation techniques based on signal strength measurement and *SIR* information have been proposed [60] and those using a distributed approach are of particular interested. In an distributed allocation technique, the received signal or the *SIR* at the mobile is measured or predicted at the beginning of the call and a channel is selected to serve the call as long as the *SIR* on the selected channel is above a threshold. However, the *SIR* will likely vary as the mobile moves or the propagation conditions change and call will have to be handed off to another channel in the the same cell or sector (*intra-cell handoff*), in order to keep the *SIR* above the threshold SIR_0. Another issue related to SIR-based DCA is that the allocation of a given channel to a new call may degrade the *SIR* in ongoing calls using the same channel, causing service *interruption*. When a service interruption occurs,

an intra-cell handoff is required in order to maintain a high link quality. If no channel is available for the handoff, the call is terminated, resulting in a *deadlock*.

Deadlock and interruption in some distributed channel allocation schemes were investigated by Serizawa and Goodman in [66]. Two algorithms for channel allocation were considered, the *Sequential Channel Search* (SCS) and the *Maximum SIR* (MSIR). In the SCS algorithm, the channels available for the entire cellular system are ordered in an arbitrary, but fixed, sequence. When a new call arrives at the base station, an idle channel is searched following the channel ordering. The first channel found in which both the forward and reverse *SIR*s are above a threshold is selected to serve the new call or the handoff request. In the MSIR algorithm, the channel with the maximum *SIR* is selected. Simulation results show that the SCS algorithm is more vulnerable to interruptions than the MSIR algorithm. In other words, the allocation of a channel to a new call using the SCS technique will likely cause interruptions in ongoing calls. This can be explained as follows. Since SCS always searches for channels in the same order, the channel reuse distance (the smaller distance between cells using the same channel) decreases. Therefore, the SCS algorithm tends to allocate highly loaded channels to new calls. On the other hand, MSIR attempts to allocate lightly loaded channels (high *SIR*). When the blocking probability is examined, simulation results show that SCS outperforms MSIR. Therefore, it was observed that, in distributed channel allocation, there is a trade-off between avoiding call blocking and avoiding call interruption.

In order to avoid interruption and deadlock, a *channel segregation* technique was proposed [67, 68], where the allocation is based on a preferable channel list, adaptively created. The preferable channel lists are independently formed in each cell by ordering the channel according to their *probability of selectability* $P(i)$. When a new call arrives at the system, the serving base station tunes a radio port at the channel with the highest probability of selectability and measures the received power of that channel (this operation is usually called *sensing the channel*). If the received power is below a certain threshold, the channel is assumed to be idle (i.e. it is not in use in the surrounding cells) and is selected to service the new call. Simultaneously, the probability of selectability of the selected channel, $P(i)$, is increased, using the expression

$$P(i) = \frac{P(i)N(i) + 1}{N(i) + 1} \quad \text{and} \quad N(i) = N(i) + 1, \tag{6.8}$$

where $N(i)$ is the number of times channel i is accessed. On the other hand, if the received power is above the threshold, the channel is assumed to be in use in the surrounding cells.

Its probability $P(i)$ is then decreased using the expression

$$P(i) = \frac{P(i)N(i)}{N(i)+1} \text{ and } N(i) = N(i)+1, \tag{6.9}$$

and the next channel on the list is sensed. This technique presents several advantages, such as adaptation to traffic and interference, reduced blocking probability compared with FCA and other DCA schemes, reduced number of intra-cell handoffs and no communication among the base station is required. [60].

6.4 Combined Techniques

We have seen in the previous sections that co-channel interference plays a very important role in the system capacity and link quality of a wireless system. Also, we have seen how channel allocation can use co-channel interference information to allocate channels more efficiently and increase system capacity. In Chapter 5, we have shown that power control can be used to reduce co-channel interference. Therefore, it seems clear that the combination of power control and channel allocation techniques may result in additional capacity improvement, if compared with the capacity gains achieved when both techniques are used independently. Additionally, since adaptive antennas can be used to control the co-channel interference, as we have seen in Chapter 2, we can expect that the combination of power control, channel allocation and adaptive antennas will result in a considerable capacity gain. In the following, we present some works found in literature where the combination of these three techniques was studied.

6.4.1 Power Control and Channel Allocation

The combined use of power control and dynamic channel allocation has been investigated in the past few years, showing promising results in terms of capacity improvement. Percia and De Marca presented in [69] a performance analysis of the *channel segregation* technique combined with two power control techniques: the *Distributed Balancing Algorithm* (DBA), proposed by Zander [55], and *distributed power control* (DPC), proposed by Grandhi *et. al* [56]. Both techniques are reviewed in Chapter 5. The combined procedure is rather simple and is summarized as follows. The mobile and base station power levels of all links using a given channel are continuously updated using the interference balancing algorithm. When a call request is received, the serving base station selects a given channel c, according to

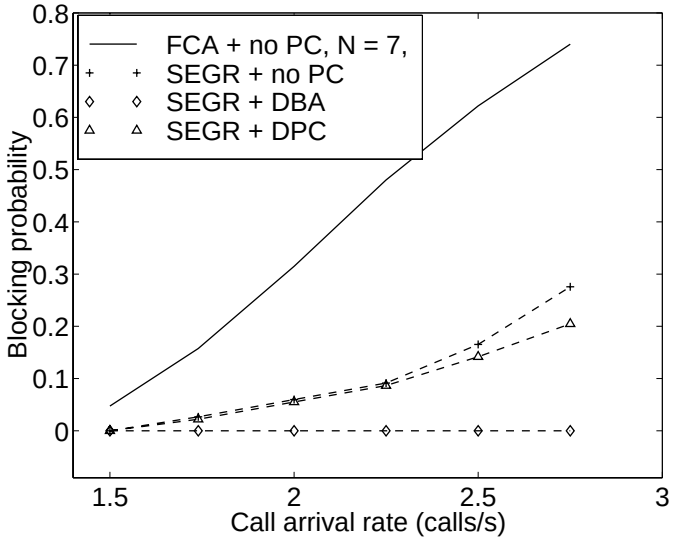

Figure 6.5: Blocking probability of a cellular system with 49 cells and 147 channels: SEGR - Channel Segregation Technique; DBA - Distributed Balancing Algorithm; DPC Distributed Power Control.

the channel segregation technique. If the *SIR* of any ongoing call using the channel c falls below a threshold after the new call is assigned channel c, the serving base station tries to reassign the new call another channel. If the reassignment is not possible, the new call is lost due to excessive interference. A cellular system was simulated, using 49 cells, 147 channels available for the whole system and propagation model assuming deterministic path loss only (no shadowing was simulated). Mean duration of calls was equal to 3 minutes and call arrival rate varied from 1.5 to 3 calls per second. Figure 6.5 shows the blocking probability for the system using channel segregation scheme combined with both power control techniques. Results for FCA using cluster size $N = 7$ without power control and channel segregation without power control are also presented.

Simulation results have shown that the combination of power control with channel segregation provides additional capacity gain when compared with the gain achieved by using channel segregation alone. For example, at a blocking probability of 10%, the carried traffic using channel segregation *without power control* increased 40% with respect to the carried traffic using FCA. When *power control* is combined with channel segregation, the increase in the carried traffic was 43%, for the DPC scheme. For the DBA scheme, the blocking probability was almost zero at the traffic levels simulated.

However, simulation results have also shown that the inclusion of power control increases

the probability of handoff failure. Channel segregation alone does decrease the probability of handoff failure if compared with to FCA scheme, but when the balancing power control is included, this probability increases. It is claimed that power adjustments tend to produce more handoff requests from mobiles that do not achieve the minimum required SIR_0. The overall conclusion of this study is that, by combining channel segregation and balancing power control, some aspects of the system performance improve, such as blocking probability. However, other aspects degrade, such as handoff failure. It should be noted that in the combined approach proposed in [69], the selection of the channel to serve the new call is performed solely by the segregation channel algorithm, that is, the power control technique does not take part in the channel selection process.

The benefits of combining power control with channel allocation was also investigated for a line-of-sight microcell environment by Valenzuela in [70]. A single street with equidistant base stations spaced 500 feet apart was assumed. The DCA used was based on the *SIR*s at both forward and reverse links. When a new call arrives, the serving base station selects a channel in which both the forward and reverse link *SIR*s are above a threshold. The power control technique studied in [70] attempts to equalize the received power levels at the base stations, by adjusting the transmitted power. The performance of this system was analyzed by simulation and, for comparison, a FCA scheme was also simulated, using reuse distance $D = 2$, that is, the same channel can be used in every other cell. Simulation results showed that power control is more beneficial for dynamic channel allocation than for fixed allocation. This benefit is due to the reduction the interference level. In fixed allocation, this reduction may not be enough to allow the use of the next smaller cluster size or reuse distance. On the other hand, in systems using dynamic channel allocation any *SIR* reduction is used and converted into a smaller blocking probability. For example, Table 6.1 shows the number of channels required by a FCA scheme to carry the same traffic as a DCA scheme with and without power control. In the channel model used here, the received power varies as the inverse-square of the T-R distance (path loss $n = 2$).

Foschini and Miljanic [71] investigated a local autonomous dynamic channel allocation technique including power control, where the selection of the channel to serve a new call is assisted by the power control algorithm. The power control algorithm adjusts the transmission power of the mobile, up to an upper limit P_{max}, attempting to keep the *SIR* as close as possible to the desired level SIR_0. If the desired SIR_0 is not achievable by controlling the transmitter power, the mobile will naturally drive its transmission power to the upper

Table 6.1: Number of required channels by a FCA system to carry the same traffic as a DCA scheme at a blocking probability of 1% [70]

DCA	**FCA**
10 channels, without power control	12 channels
10 channels, with power control	16 channels

limit P_{max}. Therefore, a power transmission equal to the upper limit P_{max} is an indication that the mobile is suffering from excessive interference and an intra-cell handoff must be performed. This power adjustment is used for both new calls and ongoing calls. When a new call arrives, a free channel is probed by looking at its required transmitter power. If P_{max} is required, another free channel is probed, until a channel with required transmission power less than P_{max} is found. If no channel is found, the new call is blocked. For ongoing calls, whenever P_{max} is requested, an intra-cell handoff is requested. If no channel is available for the handoff, the call which is dropped. The performance of this algorithm was analyzed by simulation, by evaluating the probability of an unsuccessful call. A call is considered *successful* if it is accepted for service and served until completed. Therefore, a call dropped due to increased co-channel interference caused by a new call is considered an unsuccessful call. The simulation results showed that a local autonomous dynamic channel allocation technique does not trigger catastrophic events (call interruptions and deadlocks). However, for the dynamic channel allocation technique studied, most of the unsuccessful call were inadvertently dropped call due to increased co-channel interference caused by a new call. Channel allocation algorithms that cause ongoing calls to be dropped are called *aggressive*.

The results from [71] have shown that an important issue related to dynamic channel allocation is the ongoing dropped calls caused by new calls. When a channel is assigned to a new call, the link quality of ongoing calls using that channel may degrade due to the presence of the new call, requiring an intra-cell handoff. If the handoff is not possible, the deteriorated one or more of the ongoing call are dropped. Dropping of ongoing calls caused by new calls can happen very often in distributed schemes, where little (if any) information about ongoing calls is used in the channel selection process for new calls. Therefore, the cost of a call admission must be evaluated in order to reduce the link quality degradation of ongoing calls. Additionally, a power control technique can be used to reduce the interference caused by the new call. In [72] and [62], DCA techniques were combined with power control,

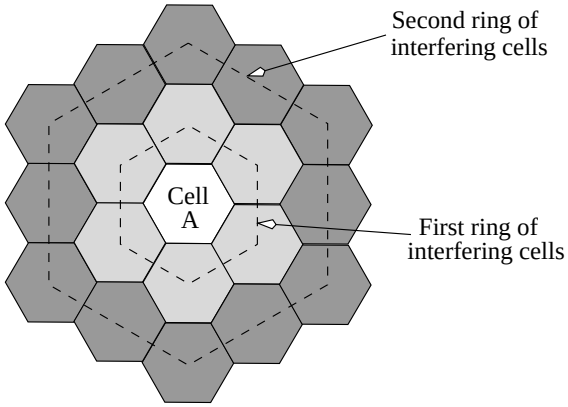

Figure 6.6: Rings of interfering cells.

taking into account the cost of call admission.

In [72], Ni proposed a distributed channel allocation technique combined with power control where a cost function, associated with each free channel in the serving cell, is used to select the lowest cost channel to be allocated to the new call. The cost function is based on the tier of the co-channel cell that is using a given candidate channel. For example, if a candidate channel is in use in a cell in the first tier, a high cost value is attributed to that channel. For channels in use by a cell in the second tier, a lower cost value is attributed to it. Channels with lower cost have higher priority for allocation. Once the highest priority channel is found, its *SIR* is measured and power control is applied in order to adjust its *SIR* to a predefined value. If its *SIR* cannot be adjusted, the next channel in the priority list is tested. The search is limited to four channels. Simulation results show that this combined algorithm presents lower blocking probability than a FCA scheme using cluster size $N = 3$. More importantly, the intra-cell handoff rate, defined as the ratio of the number of requests of intra-cell handoff to the number of admitted calls, is about 40%. That is, each new call causes only 0.4 intracell handoff requests. For comparison, for the local autonomous dynamic channel allocation technique proposed by Foschini and Miljanic in [71], the intra-cell handoff rate was about 700%.

In [62], Whitehead examined two DCA algorithms, called *timid* and *polite*, combined with Minimum-Variance Signal-Level-Based Power Control and Distributed Balancing Power Control, studied in Chapter 5. The DCA algorithms studied in [62] are based on *ring of interfering cells*. Consider Figure 6.6. Assuming hexagonal shapes for the cells and that a particular channel can be reused in every cell, the first ring of interfering cells of cell A consists of the six surrounding cells. The timid DCA technique [73] allocates a channel to

a new call if the *SIR*s on both forward and reverse links exceed an admission threshold *and* none of the cells in the first ring of interfering cells is using that channel. Therefore, new calls do not deliberately perturb ongoing calls. A base station can check whether a particular channel is in use or not in the surrounding cells by measuring the received power of that channel.

The polite algorithm allocates a channel to a new call even if that channel is in use in one of the cells in the first ring. Because of the increased interference caused by the new call, ongoing calls using that channel may need to be reassigned.

Note that, even though these algorithms try to be *timid* or *polite*, they sometimes are *aggressive* [73]. That is because the measurement of the received power of the candidate channel may not indicate interference caused *to* ongoing calls. Sometimes the admission of a new call may cause several ongoing calls to be dropped.

When several channels satisfy the required conditions to be allocated to a new call (as described above), a *channel selection policy* must be used. Four policies were studied: (a) *random*: channels are searched in a random order and the first one found is assigned; (b) *lowest*: the lowest-numbered channel is assigned; (c) *priceisright*: the channel with the lowest *SIR* is assigned and (d) *bestquality*: the channel with the highest *SIR* is assigned. The performance of all combinations of DCA algorithm and power control techniques were simulated in a system with 18 channels at different traffic loads. For comparison purpose, a FCA system with cluster size $N = 3$ was also simulated. Simulation results, in terms of carried traffic for a given blocking probability, showed that the combinations using Distributed Balancing Power Control outperformed the other combinations using Signal-Level-Based Power Control. Also, for the same power control technique, the polite DCA presented better performance than the timid DCA, which can be explained by the fact that the former technique accepts a new call, even when reassignment of ongoing calls is required. When the selection policies are compared, the *lowest* strategy provides the highest capacity, followed by *priceisright*, *random* and *bestquality*. As expected, *priceisright* required the highest number of reassignments per call (about one reassignment per call), while the others required less than 0.2 reassignment per calls. The poor performance of the *priceisright* policy can be explained by the fact that calls that are assigned channels with low *SIR* are likely to request an intra-cell handoff.

Another important issue related to DCA schemes is their performance under imbalance of load among the cells. This is especially important in microcell systems, where the load among the cells may vary considerably due to their small sizes. Also, load imbalance is a

Table 6.2: Blocking probabilities P_b for FCA and DCA at 26 Erlangs per base station and different load imbalances [74]

	FCA	**FCA**
load imbalance 15%	$P_b = 8.5\%$	$P_b = 2\%$
load imbalance 30%	$P_b = 21\%$	$P_b = 7.5\%$

typical situation when there is a highway passing through some cells, creating a strip of high traffic load. Argyropoulos *et al.* [74] studied the performance of combined distributed DCA and power control under imbalance of traffic load conditions. The DCA scheme used is based on selecting the channel with the least interference among all channels. When a new call enters the system, the interference levels at the co-channel mobiles increase. If the *SIR* at any mobile drops below a threshold SIR_0, its power is momentarily increased and a channel with less interference is searched to serve that call (intracell handoff). If no channel is found, the higher power level is maintained, increasing the overall interference level and forcing other co-channel mobiles to increase their power as well. If the *SIR* at any time drops below a threshold SIR_D ($SIR_D < SIR_0$), for 3 seconds, the call is dropped. The performance of this combined DCA and power control technique was compared with the performance of a FCA scheme, using cluster size $N = 7$, combined with the same power control technique. The analysis was carried out by simulating a service area consisting of 64 cells. The imbalance of load was simulated by uniformly distributing a percentage (15% and 30%) of the aggregate incoming traffic in a strip crossing several cells. The rest of the incoming traffic was uniformly distributed over the whole service area. Simulation results have shown that this DCA algorithm outperforms FCA in terms of blocking probability. Table 6.2 shows the blocking probability for both FCA and DCA techniques at load imbalances of 15% and 30%.

The better performance achieved by DCA is explained by the fact that the blocking probability in the system using FCA is dominated by the heavily loaded cells, which have a hard limited number of channels. On the other hand, there is no hard limit on the number of channels that can be used in a cell in a DCA scheme. Therefore, the blocking probability of the system using DCA is dominated by the blocking probability of the cells surrounding the heavily loaded cells. Another important result is that the difference between the blocking probabilities of the two schemes increases as the load imbalance increases (from

15% to 30%), showing that DCA schemes reallocate resource in order to accommodate traffic imbalance. Simulations have also shown that the average mobile transmission power in the system employing DCA is higher than in the system using FCA. The higher power in DCA is due to the fact that the effects of high-load cells is spread over surrounding cells, while in FCA the effects are confined to the high-load cells. A consequence of the high average transmission power in DCA is a high handoff request rate. It was suggested that the use of a more appropriate power control technique could control this high handoff request rate.

6.4.2 Power Control and Adaptive Antennas

It is well known that base station adaptive antennas are able to control the co-channel interference level by placing nulls in the directions of the interference sources and high gain towards the desired signal, as shown in Chapter 2.

On the other hand, as we have already seen, the *SIR* can be maximized by controlling the transmission power. As an example, the interference balancing technique, proposed by Zander [47, 55] and discussed in Chapter 5, can be used for this purpose.

Rashid-Farrokhi *et al.* [75] combined Zander's power control technique with base station adaptive antennas in the forward link of a CDMA system, showing promising results in terms of capacity improvement. The algorithm is distributed and uses only local interference information. The algorithm consists of two basic steps, repeated in an iterative mode: first, the radiation pattern or, equivalently, the weight vectors of the adaptive antenna array at the base stations are computed such that the *SIR*s are minimized. Using the computed radiation patterns of the antenna arrays, the base station transmission power levels are updated using the Distributed Balancing Algorithm (DBA). The performance of this combined technique was evaluated by simulation in a CDMA system with 36 base stations and cluster size $N = 1$. The propagation channel model included only path loss, with path loss exponent $n = 4$. The minimum acceptable signal-to-interference-plus-noise ratio (*SINR*) was -14 dB. The capacity of the system was defined as the maximum number of users that achieve $SINR \geq -14$ dB. Table 6.3 shows the system capacity for different configurations. We see that the use of 4-element arrays at the base stations increases system capacity in 200% (three times) compared to the configuration with omnidirectional base station antennas. However, we note that power control leads to a capacity improvement even greater.

Table 6.3: Capacity of a CDMA system in terms of number of users for different system configurations.

System	**Number of users**
fixed power & omnidirectional antennas	30
fixed power & adaptive antennas (4-element array)	90
power control & omnidirectional antennas	660
power control & adaptive antennas (4-element array)	2800

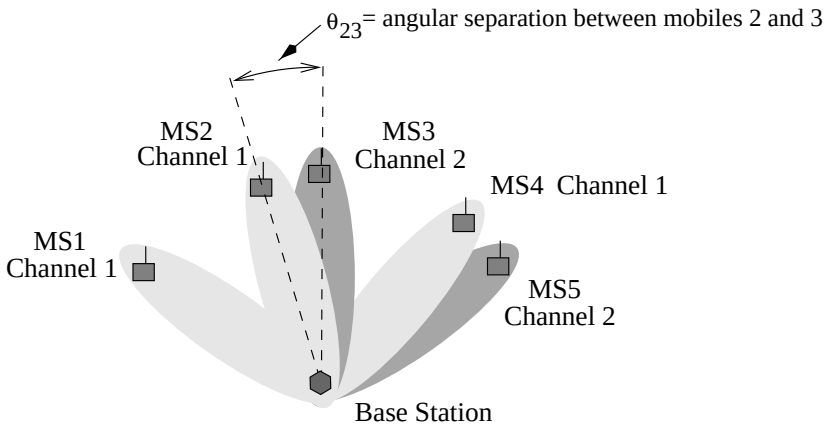

Figure 6.7: SDMA approach: channels are reused within the cell.

6.4.3 DCA and Adaptive Antennas in SDMA systems

Adaptive antennas at the base station have been studied as a technique to increase coverage range and improve capacity. Coverage range is increased by steering high antenna gains towards the desired mobiles. Capacity improvement can be achieved by two different approaches. In the first approach, base station adaptive antennas are used to reduce the co-channel interference by steering nulls towards the co-channel mobile stations. The resulting co-channel interference reduction allows cluster size reduction, improving the system capacity. An example of this approach was extensive studied in Chapter 4. In the second approach, base station adaptive antennas are used to allow channel reuse within the cell, by filtering out co-channel users in the spatial domain. Systems employing the second approach are usually referred to as *Spatial Division Multiple Access* (SDMA) systems and an example is depicted in Figure 6.7. High gain beams are steered towards the mobiles and, depending on some factors, channels can be reused within the cell, as is discussed subsequently.

In the SDMA approach, the capacity improvement depends on the ability of the system

to allocate the same channel to several in-cell users. Three major factors determine this ability [76]:

(1) channel propagation parameters,

(2) antenna parameters - beamwidth and side lobe level,

(3) spatial distribution of the user.

These factors will determine whether a channel can be shared among in-cell users. In the following we discuss two basic requirements that must be met by two in-cell users so that they can share the same channel.

The first requirement that must be met is that the angular separation φ between the co-channel mobiles must be larger than a minimum threshold φ_{min}, which can be derived from the propagation channel model used and the antenna parameters. This basic requirement is imposed in order to guarantee that a signal from a co-channel in-cell user does not lie within the beam steered towards another co-channel user.

In order to derive φ_{min}, we need to assume a propagation channel model. It is usually assumed in wireless communications that a signal transmitted by a mobile station arrives at the base station antenna through reflections from large objects, diffraction of the electromagnetic waves around objects, and signal scattering. It is also assumed that the scatterers surrounding the mobile station are about the same height, or are higher than, the mobile. Considering a *macrocell environment*, the base station is typically deployed higher than the surrounding scatterers. Therefore, the received signals at the base station antenna result mainly from the scattering process in the vicinity of the mobile station, as shown in Figure 6.8 [6], and the angle of arrival (AOA) of the signals impinging upon the base station antenna are distributed over an angular spread α. On the other hand, in the microcell environment, some scatterers may be as high as the base station antennas, implying that the angular spread α of the AOA of the received signals at the base station is larger than in the microcell case. Several models for the distribution of the AOA have been proposed and an extensive literature search can be found in [6]. In this chapter we will adopt the model where the scatterers are assumed to be uniformly distributed over a circle of radius R. If the T-R distance is d, the angular spread α seen by a base station receiver is:

$$\alpha = 2\sin^{-1}\left(\frac{R}{d}\right). \tag{6.10}$$

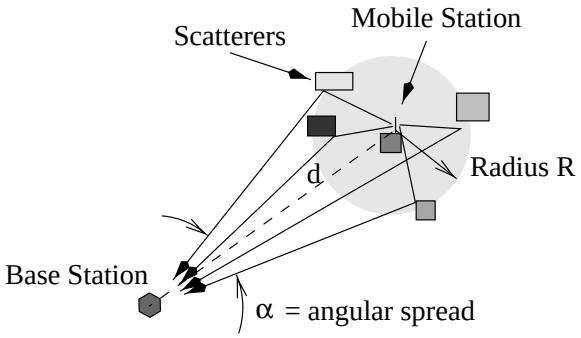

Figure 6.8: Scattering process in a macrocell environment.

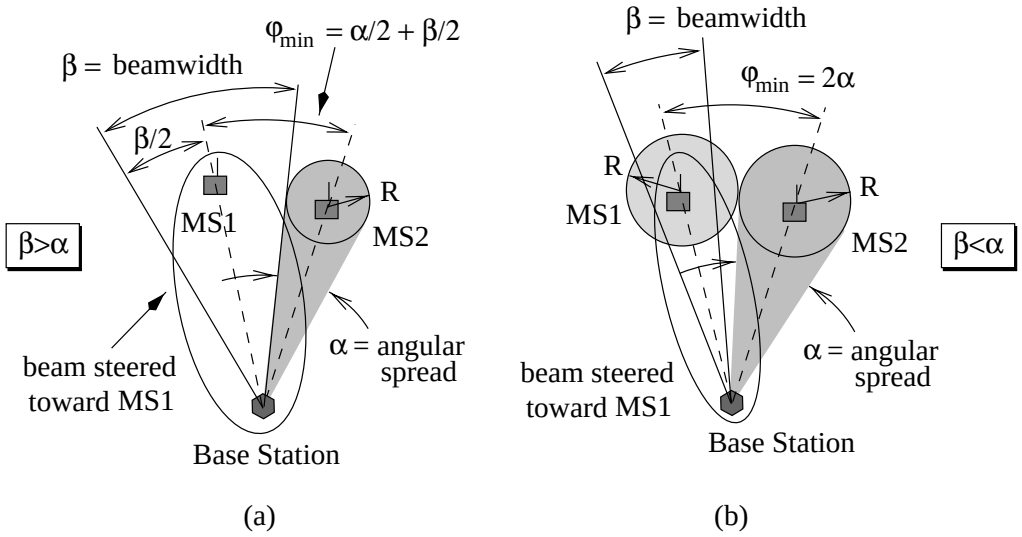

Figure 6.9: Minimum angular separation φ_{min}.

The angular spread α is, therefore, a channel propagation parameter that should be taken into account when deciding whether a channel can be shared between two in-cell mobiles. Figure 6.9 depicts a typical situation, from which the minimum angular separation φ_{min} can be derived. Let us assume that the beam steered toward the mobile MS1 has a beamwidth of β degrees. We assume that signals impinging upon the base station antenna outside the beamwidth β will be sufficiently attenuated by the antenna. We will show later that there is a limit on this attenuation, which will result in the second requirement. If the angular spread of the mobile station is $\alpha < \beta$, we see in Figure 6.9 (a) that the minimum angular separation φ_{min} is equal to $\alpha/2 + \beta/2$. On the other hand, if the angular spread α is larger than the beamwidth β, the minimum angular separation will be determined only by the angular spread, as shown in Figure 6.9 (b) and is equal to α. Therefore, in general, the

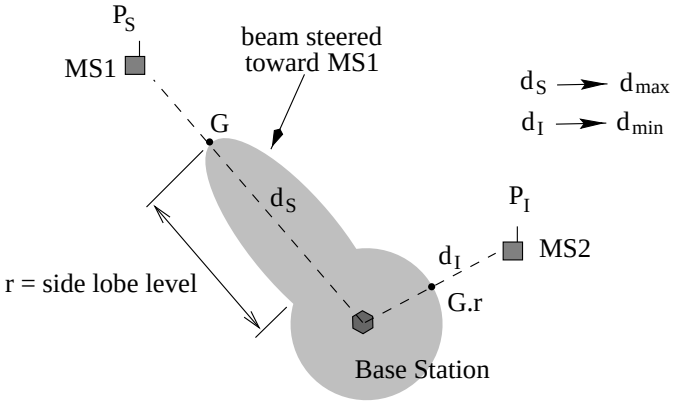

Figure 6.10: SDMA approach - two in-cell co-channel users.

minimum angular separation between two in-cell co-channel users is [76]:

$$\varphi_{min} = \frac{\alpha}{2} + \frac{\min(\alpha, \beta)}{2}. \tag{6.11}$$

It was assumed above that if an in-cell co-channel user is not within the main lobe of the radiation pattern, its signal will be sufficiently attenuated by the antenna. However, due to the array limitations, there is a limit on the attenuation of the in-cell co-channel signals. For example, the side lobe level (SLL) and the depth of nulls of the radiation pattern depend on the number of elements in the array. If an in-cell co-channel mobile is too close to the serving base station, the side lobe level or the depth of the null steered toward that co-channel user may be insufficient to guarantee a required SIR_0. Therefore, there is a limit, denoted by d_{min}, on how close to the base station an in-cell co-channel user can be. On the other hand, if the desired user is too far from its serving base station, the antenna gain may be insufficient to guarantee the required SIR_0 and an upper limit, denoted by d_{max}, should be imposed on the distance between an user and its base station. As we will see, the ratio of d_{min} and d_{max} consists the second requirement that must be met by potential in-cell users. The limits d_{min} and d_{max} can be alleviated by using a power control technique.

Consider two in-cell co-channel users as shown in Figure 6.10. Assume that a beam is steered toward the mobile MS1 (desired user) and the mobile MS2 (interfering mobile) is not within that beam. In order to determine the received power levels S and I from the desired and interfering mobiles, respectively, we will assume a channel model that consists of path loss only, with path loss exponent γ. S and I are, therefore, given by:

$$S = P_D \; K \; G \; d_D^{-\gamma}, \tag{6.12}$$

$$I = P_I \; K \; G \; r \; d_I^{-\gamma}, \tag{6.13}$$

where P_D and P_I are the transmitter power levels and d_D and d_I are the T-R distances. The maximum gain within the main beam is G (actual value, not dB), while the side lobe level is r ($r < 1$), which, for simplicity, is assumed to be constant. The constant K comprises all terms of the channel that do not change in this derivation. Let us suppose that the minimum acceptable signal-to-interference ratio is SIR_0. Therefore, we want:

$$\frac{S}{I} \geq SIR_0. \tag{6.14}$$

As discussed above, for a given propagation channel and array antenna, there will be an upper limit for d_D (d_{max}) and lower limit for d_I (d_{min}), such that the threshold SIR_0 can be achieved. Following the approach used by Gerlich in [76], these limits can be determined by substituting expressions (6.12) and (6.13) into (6.14):

$$\frac{S}{I} = \frac{P_D \; d_{max}^{-\gamma}}{P_I \; r \; d_{min}^{-\gamma}} = \frac{P_D}{r \; P_I} \left(\frac{d_{min}}{d_{max}}\right)^{\gamma} \geq SIR_0, \tag{6.15}$$

Finally, the lower limit on the ratio d_{min}/d_{max} is:

$$\frac{d_{min}}{d_{max}} \geq \left(\frac{r \; P_I \; SIR_0}{P_D}\right)^{1/\gamma}. \tag{6.16}$$

As an example, assume that the $P_D = P_I$ with no power control, $\gamma = 3.0$, $SIR_0 = 10$ and the side lobe level of the array is $SLL = -23$ dB ($r = 0.005$). Using expression (6.16), we find that:

$$\frac{d_{min}}{d_{max}} \geq 0.37 \quad \text{or} \quad d_{min} \geq 0.37 \; d_{max}. \tag{6.17}$$

This means that, in order to guarantee $S/I \geq 10$ dB, the minimum T-R distance of an interfering co-channel user is 37% of the T-R distance of the user where the SIR is measured, as depicted in Figure 6.11.

On the other hand, if the array side lobe level is increased to $SLL = -7$ dB ($r = 0.2$), we find that the minimum T-R distance d_{min} is *larger* than the maximum T-R distance d_{max} ($d_{min} \geq 1.26 \; d_{max}$) and, therefore, the system is not feasible.

Expressions (6.11) and (6.16) represent the two basic requirements that must be met by two in-cell users so that they can share the same channel. Summarizing:

- the angular separation φ between two in-cell co-channel users must be:

$$\varphi \geq \frac{\alpha}{2} + \frac{\min(\alpha, \beta)}{2}, \tag{6.18}$$

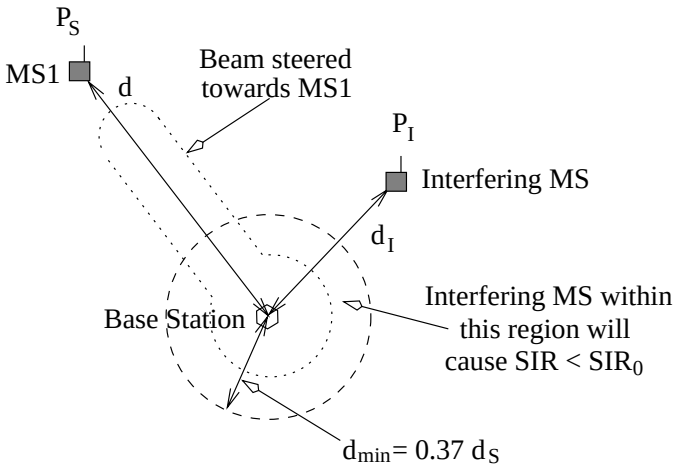

Figure 6.11: T-R distances to guarantee $SIR \geq SIR_0$.

- the ratio of the minimum and maximum T-R distances of in-cell co-channel users must be:

$$\frac{d_{min}}{d_{max}} \geq \left(\frac{r \; P_I \; SIR_0}{P_D} \right)^{1/\gamma}. \tag{6.19}$$

Several studies have been carried out on channel allocation strategies for SDMA systems. In [77] three strategies for allocating channels to incoming calls are proposed. An incoming call can be either a new call or a call requesting a channel reassignment. A channel reassignment is requested when the angular separation between two co-channel mobiles drops below a threshold. In the simplest algorithm, denoted here by A_1, the channel is selected randomly among the channels that satisfy the requirement for the minimum angular separation among co-channel users. This criteria is sufficient in a scenario where the mobiles are static. However, future channel reassignments due to mobile movement are not taken into account when the channel is selected using algorithm A_1. In this context, channel reassignments may not be completely avoided, but we can try to maximize the time interval between two subsequent channel reassignments. In the second algorithm, A_2, the channel to be assigned to the incoming call is chosen such that the angular separation among the co-channel users is maximized. This criteria will increase the time interval between two subsequent channel reassignments. However, A_2 does not exploit information about the topology of the service area and mobile movement. A third algorithm, A_3, is then proposed, where the topology of the area and movement of the mobiles are taken into account. According to A_3, two mobiles on the same road, but moving in opposite directions, would not be assigned the same channel, since a channel reassignment is likely to be necessary. All three algorithms require

the measurement of the direction of arrival (DOA) associated with each mobile. In addition, algorithm A_3 requires the estimation of the direction of movement of the mobiles. The performance of all three algorithm is analyzed by simulation, using three different scenarios, representing a rural area, an urban area and a residential area. The simulation results show that the use of mobile spatial distribution information when assigning channels improves the performance in terms of capacity or assignment success rate, at the expense of complexity. Therefore, the best performance is achieved by A_3, followed by A_2 and A_1.

In the DCA algorithms proposed in [77], the channel assignment is based on the assumption that two users separated by a minimum angle and sharing the same channel have their *SIR*s above a threshold SIR_0. In [78], Chen *et al* proposed an algorithm for channel allocation using adaptive antennas assuming a more realistic situation. Actual base station antenna arrays with M elements are simulated, which attempt to null out in-cell cochannel users. The DCA algorithm used in [78] is based on reuse partitioning, using a predefined sequence of channels to search for a channel to be assigned to a new call or a handoff request. All the base stations search for channels using the same predefined sequence of channels. When a new call arrives or a handoff is requested, the serving base station assigns the channel that meets the following requirements: *(a) no more than* $M-1$ *in-cell users can be using that channel*; *(b) the SIR at the new mobile is above a threshold* SIR_0. The first requirement is based on the assumption that a M-element array can steer up to $M-1$ nulls. Therefore, assuming that the positions of the in-cell users are known by the base station, a null can be steered towards each in-cell co-channel user. However, it is not guaranteed that all nulls will have the desired attenuation and that the *SIR* at the new mobile will be higher than the threshold SIR_0. In order to guarantee the minimum acceptable *SIR* at the new user, requirement *(b)* must be satisfied. Channels already in use in the cell are candidate channels to serve an incoming call. In doing so, channel reuse within the cell is allowed, reducing the average reuse distance and increasing the capacity of the system. The performance of the proposed technique was analyzed by simulation using a 3-element array in a cellular systems with 37 cells. It was observed a capacity improvement of 170% over a system using omnidirectional antennas at the base stations and reuse partitioning for channel allocation.

In the studies presented in [77] and [78], the channel allocation schemes rely on some technique to estimate the angles of arrival and departure (AOA and AOD) of the signals associated with the co-channel users. Therefore, the performance of the allocation technique and, consequently, the overall system capacity, will be dependent on the accuracy of the

technique used for estimating AOAs and AODs. In order to avoid the use of any technique for directly estimating AOA and AOD, Ohgane *et al* proposed a channel allocation technique combined with adaptive array for SDMA based on the *spatial correlation coefficient* [79]. The spatial correlation coefficient ρ between two signals impinging upon an array is defined as the inner product of the array response vectors associated with each signal [80]. The absolute value of ρ ($|\rho| \leq 1$) is a measure of the angular separation of the mobiles. In [79], it is shown that, for two mobiles transmitting in the same channel, the signal-to-interference ratio (*SIR*) and, consequently, the bit error rate (*BER*) of the array output signal corresponding to each mobile depend on the spatial correlation coefficient. Based on the relationship between *BER* and the spatial correlation, a maximum value of ρ, denoted by ρ_M, such that two mobiles can share the same channel is derived. The proposed channel allocation technique uses a 2-element linear array and channels are allowed to be shared between two in-cell mobiles. According to the proposed technique, when a new call arrives, the serving base station attempts to allocate a channel that is not in use in the cell. If no idle channel is available, channels in use in one in-cell call are then examined. The serving base station selects the first channel found in which the spatial correlation between the ongoing call and the new call is less than ρ_M. The performance of such channel allocation technique was analyzed by simulating a system with one cell and 10 channels. Results show that the resulting blocking probability corresponds to the blocking probability of a system using 18 channels and no channel reuse allowed within the cell. Therefore, the proposed channel allocation technique was almost successful in allocating every channel to two in-cell mobiles.

DCA schemes combined with fixed base station narrowbeam antennas in a SDMA scenario were studied in [81]. Each base station is located in the center of the cell and equipped with a 24-beam switched beam antenna. Each beam has a beamwidth of 15 degrees. When a new call or a handoff request arrives, the beam that provides the best communication link between the serving base station and the mobile is selected. Perfect knowledge about the mobiles positions is assumed. Once a beam is selected, the base station searches for a channel following some DCA strategy. Two DCA schemes are tested. In the first scheme, called *Even Channel Load Algorithm* (ECL), each base station creates a list with all channels available for the system, with channels ordered in a *descending* order of *channel usage* in that base station. Channel usage of a given channel is defined here as the number of calls assigned to that channel. When a call arrives, the serving base station searches for a channel, using its list, and selects the first channel in which both the forward and reverse links *SIR* are above a

threshold SIR_0. In the second scheme, called *Concentrated Channel Load Algorithm* (CCL), the list created by each base station orders the channels in an *ascending* order of channel usage. The selected channel in CCL is the first one in which both the forward and reverse links *SIR* are above the threshold. The ECL algorithm aims to uniformly distribute the calls over all channels, while the CCL algorithm attempts to minimize the number of channels required to serve all calls. Note that, in both algorithms, all channels available for the system are searched, since channel reuse within the cell is allowed. The performance of both DCA schemes is analyzed by simulation and compared with a reference system using FCA, cluster size $N = 7$ and tri-sectorized cells. Power control based on constant received power is used in the reverse link. Both uniform and non-uniform distribution of users are analyzed, in order to evaluate the degradation of the SDMA scheme due to the distribution of the users. Assuming that 100 channels are available for the entire system and an uniform distribution of users, simulation results showed that both DCA algorithms provided capacity gains of 77 times, with respect to the capacity of the reference system. The capacity gains dropped to 35 times the capacity of the reference system, for the ECL algorithm, and 40 times, for the CCL algorithm, when the distribution of users was non-uniform. Even though mobility was not simulated, the simulation results presented in [81] show the potential capacity gain achieved by combining adaptive antennas and DCA techniques.

6.5 Conclusion

We have presented in this chapter a discussion on resource allocation in cellular systems. Channel and transmitter power allocation strategies were presented, along with an extensive literature review. Also, the use of base station adaptive antennas is discussed in the context of resource allocation.

Traditionally, we consider the frequency spectrum to be the resource which must be optimally allocated in a cellular system, wih a goal of high capacity while maintaining an adequate link quality. However, we have seen that transmitter power must be considered as another resource to be appropriately allocated in order to increase system capacity. Although we can also consider the serving base station (the base station that should be linked to a mobile to serve a call) as a third resource to be allocated, we leave this issue for future discussion. From the discussion presented here and the results from recent work, it is clear that good results can be obtained when channel and power allocation techniques are

combined.

The use of base station adaptive antennas is a very efficient way for controlling the co-channel interference and, consequently, increasing the system capacity. Therefore, it is also clear that the combination of adaptive antennas with power and channel allocation can result in capacity and link quality improvement, as some recent works have already shown.

The discussion and the literature review presented in this chapter will substantiate the proposal for the future work.

Chapter 7

Simulation of Cellular Networks

7.1 Introduction

In the remaining chapters of this dissertation, we analyze the performance of the combined application of channel allocation algorithms, adaptive antennas and power control in macrocell cellular communication. The analysis presented in Chapters 8 through 10 relies on the simulation approach, which includes user mobility and call processing. The simulation approach is required in this analysis since analytical models for the interrelationship among the parameters involved in the resource allocation processes are very difficult to be found.

In the present chapter, we describe the main features of the simulation program developed for this analysis. Several different scenarios are studied in Chapters 8 through 10 and particular features of cellular systems used in each scenario are described in the respective chapter.

7.2 Cellular Network

7.2.1 Toroidal Universe of Cells

An important issue when simulating a cellular network is the size of the network in terms of number of cells. The simulated network must be large enough to replicate the behavior of a real cellular system regarding especially the co-cochannel interference. The average level of interference must be uniform over all cells. When a finite bounded area is used to simulate the coverage area of a cellular network, the average interference measured at center

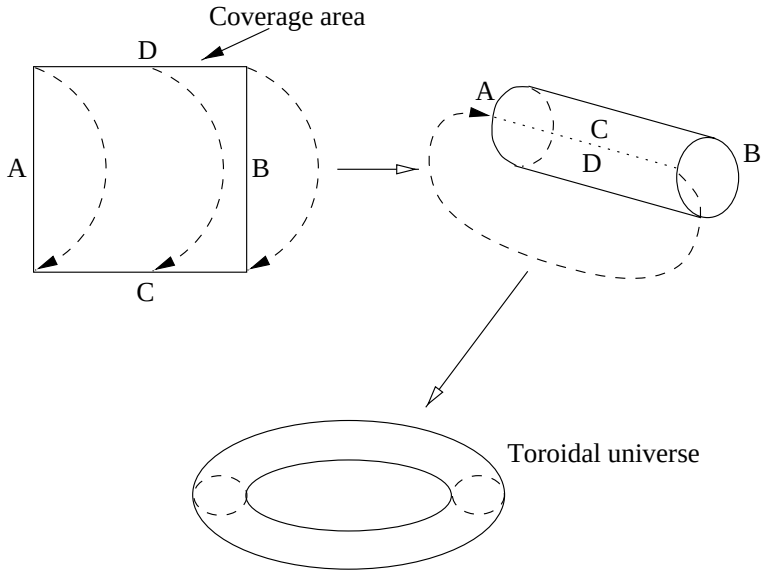

Figure 7.1: Coverage area simulated using the toroidal universe approach.

cells is higher than at cells close to the boundaries of the coverage area. Different levels of interference may affect the simulation results. A technique for minimizing the effects of different levels of average interference is to simulate a coverage area with a larger number of cells, but collect the performance parameters only at central cells. This solution is not efficient, since all the cells must be simulated anyway, but only central cells are effectively used. Additionally, large number of cells means long simulation time, which, of course, is not desired.

Another technique for simulating cellular networks is based on the *toroidal universe of cell* [58]. In this technique, the borders of the simulated coverage area are connected to each other in such way to form a *toroidal*, as shown in Figure 7.1. By using the toroidal universe approach, we *artificially* replicate the original coverage area around itself, as shown in Figure 7.2. As a result, a mobile M located at any point of the original coverage area "sees" all the cells (of the original coverage area) as if the mobile was located at the central area of the original coverage area (see Figure 7.2). Another characteristic of the toroidal universe of cells is that mobiles leaving the coverage area reappear in the other side of the coverage area, as shown in Figure 7.3 . Therefore, calls are not lost because mobiles "left" the coverage area.

Note that, even when the toroidal universe technique is employed, the number of simulated cells must be sufficiently large in order to guarantee an appropriate representation of

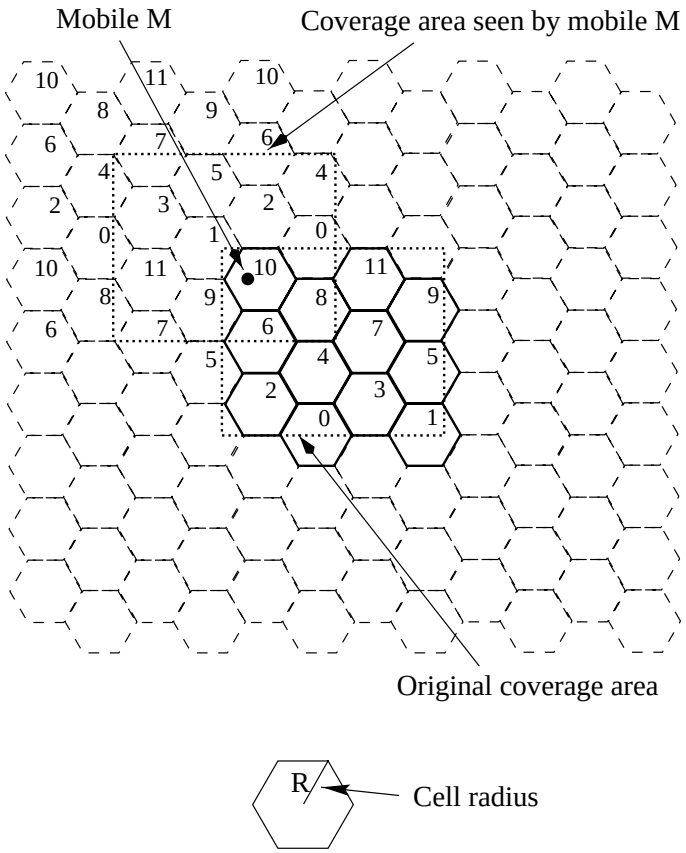

Figure 7.2: Toroidal universe with hexagonal cells.

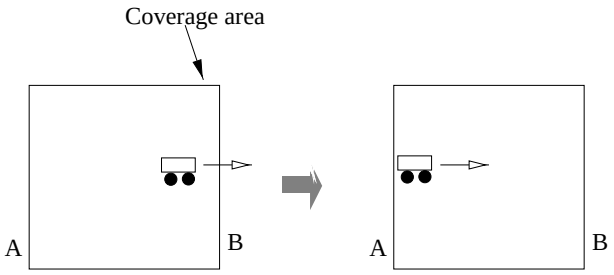

Figure 7.3: In the toroidal universe, a mobile leaving the coverage area reappears in the other side.

Table 7.1: Number of cells in the network for each cluster size N.

Cluster size N	Number of cells in the network
1	80
3	90
4	80
7	84

a real cellular network in terms of co-channel interference. In the analysis presented in this dissertation, a network with around 80 hexagonal cells with radius $R = 3000$ m (see Figure 7.2) is simulated. The exact number of cells in the system depends on the cluster size N employed, as shown Table 7.1. The different numbers of cells in the network is due to the fact that, the original coverage area has to have an integer number of *clusters*. Base stations are located at the center of each cell.

7.2.2 Mobility Models

The mobility model used in the simulations is based on the *random walk* approach. Mobiles move at speed v in segments of straight lines in the direction δ with respect to a given reference. The location of each mobile is updated every $T_{loc} = 1$ second. A change in the direction of movement occurs every $T_{dir} = 10$ seconds. The new direction δ_t is a random variable that follows a cosine-shaped distribution function with mean value equal to the current direction of movement δ_{t-1} (see Figure 7.4):

$$f_\delta(\delta_t) = \begin{cases} K_\delta \cos(\delta_t - \delta_{t-1}) & \text{for } \delta_{t-1} - \pi \leq \delta_t \leq \delta_{t-1} + \pi \\ 0 & \text{otherwise,} \end{cases} \tag{7.1}$$

where K_δ is used to obtain $\int_{-\infty}^{-\infty} f_\delta(\delta) d\delta = 1$.

The speed v is kept constant over the entire duration of the call and is assigned to the mobile at the beginning of the call. The value of v depends on the class of users that the mobile belongs. Two classes of users are simulated: Pedestrians and vehicular:

- Pedestrian: the speed v is a random variable that follows a cosine-shaped probability density function, as in Figure 7.4, over the interval from 0 to 5 km/h;

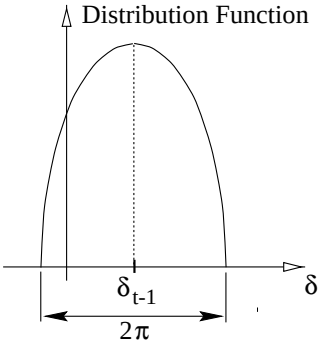

Figure 7.4: Distribuiton function of the direction of movement δ.

Table 7.2: User profiles used in the simulation.

Profile	**Composition**
Hybrid I	80% pedestrian + 20% vehicular
Hybrid II	20% pedestrian + 80% vehicular

- Vehicular: the speed v is a random variable that follows a cosine-shaped probability density function over the interval from 0 to 60 km/h;

These two classes of users are combined to create two user profiles regarding user mobility, as shown in Table 7.2. Hybrid I is a predominantly pedestrian, while Hybrid II is predominantly vehicular.

7.3 Logical Layer

The simulated cellular network employs orthogonal multiple access technique, that is, different traffic channels do not interfere with each other[1]. Therefore, it is supposed that a mobile using channel CH_i experiences interference (downlink) only from base stations using channel CH_i. Examples of orthogonal multiple access techniques are Time Division Multiple Access (TDMA) and Frequency Division Multiple Access (FDMA) [1] In TDMA systems, a traffic channel is defined as a time-slot, while in FDMA systems a traffic channel is a RF (radio frequency) channel.

[1]In system employing orthogonal multiple access, different channels may interfere with each other due to *adjacent channel interference*. However, careful RF filtering and channel assignment can minimize adjacent channel interference [1]

The entire coverage area is allocated N_C pairs (downlink and uplink) of orthogonal traffic channels. If fixed channel allocation (FCA) is employed, the entire set of N_C pairs of channels is allocated to each cluster and, therefore, each cell is allocated N_C/N pairs of channels, where N is the cluster size.

If dynamic channel allocation (DCA) is used, all N_C pairs of channels are available for each cell. We suppose that in both FCA and DCA cases, base stations have enough radio equipment to use any channel. Therefore, calls are not blocked due to lack of radio equipment.

Each base station is allocated a different pair of control channels (uplink and downlink) and mobiles are able to tune to any control channel. Control channels are used to initiate a call. Also, mobiles periodically listen to control channels of all base stations in order to check whether a intercell handoff (see Section 7.5) is required or not. Control channels are always transmitted using omnidirectional antennas and at fixed transmitter power. During a call, traffic channels may be used to transmit control information between base station and mobile. For example, during intercell and intracell (channel reassignment) handoff processing, control information is exchanged between base station and mobile through the traffic channel currently allocated to the call.

7.4 Physical Layer

7.4.1 Propagation Channel Model

In the simulation analysis presented in this dissertation, we assume the macrocell propagation environment, as discussed in Chapter 2. The propagation channel model consists of distance-dependent path loss and log-normal shadowing with standard deviation σ dB. The local mean power P_R received at a given location from a single transmitter is [1]

$$P_R = \frac{P_T \, G_T \, G_R \, L}{d^\gamma}, \tag{7.2}$$

where P_T is the transmitter power in watt, d is the transmitter-receiver separation distance and L is a log-normal random variable that models the shadowing fading. The terms G_T and G_R are the receiver and transmitter antenna gains in linear scale, in the direction of propagation. Depending on the link analyzed (uplink or downlink), G_T and G_R can be either base station antenna gain or mobile antenna gain. We assume that mobiles are equipped

with omnidirectional antennas (antenna gain is equal to 0 dB). Base station antennas are described subsequently. When P_R is expressed in decibel units, we have:

$$P_{R,dB} = P_{T,dB} + G_{T,dB} + G_{R,dB} - 10\gamma \log_{10} d + \chi \quad \text{(dB)}, \tag{7.3}$$

where the variables are the same as in (7.2), but in decibel units. Note that, now the term $\chi = 10 \log_{10} L$ is a Gaussian random variable with zero mean and standard deviation σ dB.

The local mean power of the composition of signals received from several transmitters is assumed to be the sum of the individual local mean powers. For example, the local mean power of the total interference received at a given location is [1]

$$I_T = \sum_{i=1}^{N_I} \frac{P_{T,i}\, G_{T,i}\, G_{R,i}\, L_i}{d_i^{\gamma}}, \tag{7.4}$$

where $P_{T,i}$ is the transmitter power of the i-th interfering transmitter, $G_{T,i}$ is the transmitter antenna gains towards the receiver, $G_{R,i}$ is the receiver antenna gain in the direction of propagation, and d_i is the transmitter-receiver separation distance for the i-th interfering transmitter. The term L_i models the log-normal shadowing fading with respect to the i-th interfering transmitter.

The channel allocation and power control algorithms analyzed in this dissertation are based on measurements of signal-to-interference-plus-noise ratio ($SINR$) Γ

$$\Gamma = \frac{S}{I_T + N_0}, \tag{7.5}$$

where S is the local mean power of the desired received signal, I_T is the local mean power of the total interference, and N_0 is the thermal noise power at the receiver. We assume that the exact values of Γ are available at base stations and mobiles, being computed in the simulation by using expressions (7.2) and (7.4). Methods for estimating Γ are discussed in Appendix B. The thermal noise N_0 is adjusted such that the signal-to-noise ratio at the cell boundary is 40 dB, in order to guarantee that the performance and capacity of the system are limited by interference, and not by thermal noise.

The transmitter power levels can be either fixed or controlled. Several power control algorithms are discussed in chapter 5. The algorithm analyzed in the simulations is based on the *Autonomous SINR Balancing Power Control* technique (see Section 5.4), that attempts to balance the $SINR$ of all links transmitting on the same channel. The power levels are updated every $T_{PC} = 0.25$ seconds using:

$$P_{T,i}^{(k)} = \Gamma_T \, \frac{P_{T,i}^{(k-1)}}{\Gamma_i^{(k-1)}}, \tag{7.6}$$

where $P_{T,i}^{(k-1)}$ and $\Gamma_i^{(k-1)}$ are the transmitter power and $SINR$ of the i-th link at instant $t = kT_{PC}$, and Γ_T is the target $SINR$. Practical implementation issues of this power control technique are discussed in Chapter 8.

Note that the propagation channel model adopted in the simulations includes only line-of-sight propagation. Strictly speaking, since we will analyze the performance of adaptive base station antennas, some sort of spatial information about the propagation channel would be required. However, it is well known that, in macrocell propagation environment, the angle spread of the angle of arrival of multipath components at the base station is small [6] (angle spread = $2^o \sim 6^o$), which, combined with the relatively broad beamwidth of the adaptive antenna to be used in the simulation analysis (45^o and 60^o), causes negligible effects on the performance of the cellular system.

A spatial propagation channel model is, in fact, used in Chapter 10, when we analyze the performance of SDMA systems. The spatial channel model used is described in that chapter.

Distance Correlated Shadowing

Shadowing fading is caused by obstruction of signal due to large objects, like buildings, hills, etc, which implies that the shadowing fading term χ in (7.3) observed at locations close to each other present some level of correlation. Therefore, the model used to generate χ must include some form of spatial correlation. In this work, we use the method for generating samples of correlated shadowing fading presented in [82], which will be described here with the help of Figure 7.5. The coverage area is divided into square grids and the intersections of the grid are denoted *grid points*. Each grid point is associated with a sample of uncorrelated shadowing fading with respect to a reference point. For example, the samples of shadowing fading at grid points I, II, III and IV are χ_I, χ_{II}, χ_{III} and χ_{IV}, respectively. The grid points in the simulation correspond to the locations, in the real system, where samples of shadowing fading are uncorrelated with each other. The smallest distance between two grid points is called *decorrelation distance* d_{dec}. The shadowing fading at locations between grid points are, therefore, correlated with the shadowing fading samples associated with the closest grid points. For example, in the Figure 7.5, the shadowing fading at location P, denoted by χ_P, is correlated with the shadowing fading samples χ_I, χ_{II}, χ_{III} and χ_{IV}. The value of χ_P can be computed by interpolation. In this dissertation, linear interpolation is used, and χ_P is given by:

$$\chi_P = [\chi_I\ (1 - X) + \chi_{II}\ X]\ (1 - Y) + [\chi_{III}\ (1 - X) + \chi_{IV}\ X]\ Y, \tag{7.7}$$

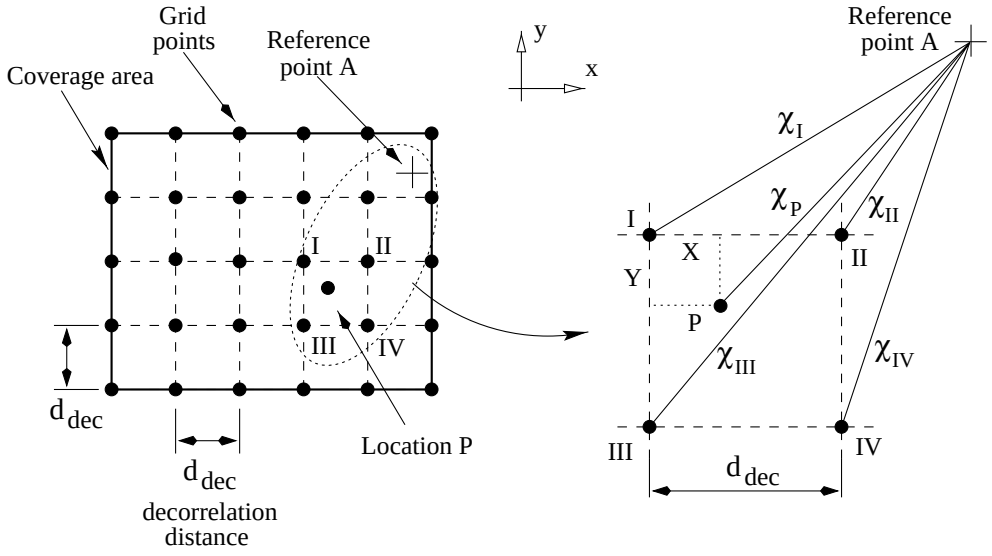

Figure 7.5: Model for computing samples of shadowing fading correlated with distance.

where X and Y are the distances in the x-axis and y-axis directions between location P and grid point I. Distances X and Y are normalized by the decorrelation distance d_{dec}. It is shown in [83] that the samples of shadowing computed by interpolation have smaller standard deviation than the standard deviation of the samples at the grid points. In order to correct the value of the standard deviation, the samples of correlated shadowing are corrected using the expression

$$\chi'_P = \frac{\chi_P}{\sqrt{(1-2X+2X^2)(1-2Y+2Y^2)}}. \tag{7.8}$$

Note that, for each reference point, a set of samples of uncorrelated shadowing fading associated with grid points is required. Reference points are the base station locations, while locations where we are interested in computing the correlated shadowing, like location P in Figure 7.5, are the mobile station locations. Therefore, each base station has its own set of samples of uncorrelated shadowing fading. For urban environments, d_{dec} is in the order of tens of meters [58]. In this dissertation, we use $d_{dec} = 50$ m. Also, following common practice, we assume that shadowing fading on the uplink and downlink are identical [58].

Figure 7.6 shows the autocorrelation function computed from samples generated by the method just described with $d_{dec} = 50$ m and shadowing standard deviation $\sigma = 8$ dB. And for illustration purpose, Figure 7.7 shows an example of samples of shadowing with respect to an arbitrary base station for $d_{dec} = 50$ m and shadowing standard deviation $\sigma = 8$ dB.

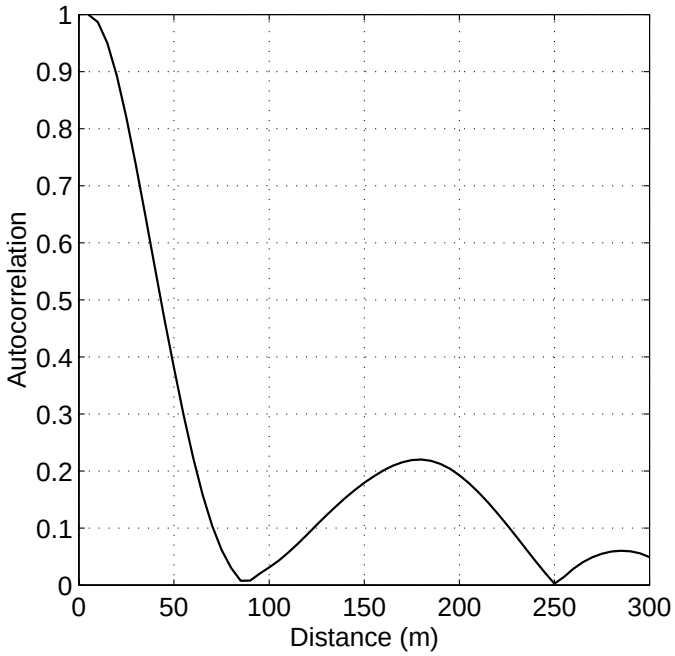

Figure 7.6: Autocorrelation function of samples of shadowing fading for $d_{dec} = 50$ m and shadowing standard deviation $\sigma = 8$ dB.

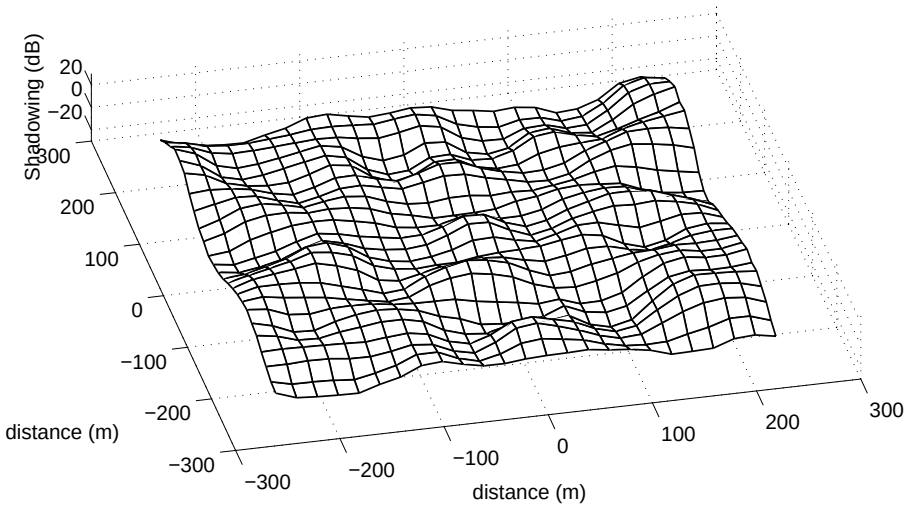

Figure 7.7: Samples of shadowing fading for $d_{dec} = 50$ m and shadowing standard deviation $\sigma = 8$ dB.

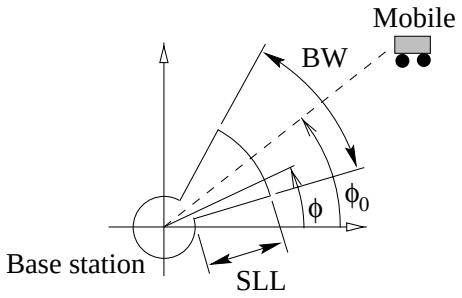

Figure 7.8: Radiation pattern of an adaptive antenna sterred toward ϕ_0.

7.4.2 Base Stations Antennas

Base stations can be equipped with omnidirectional antennas, adaptive antennas or sector antennas, depending on the case studied.

For the case of adaptive antennas, the radiation pattern of the antennas are simulated using the stepped function, described as (see Figure 7.8):

$$G(\phi)_{dB} = \begin{cases} 0 & \text{for } -BW/2 \leq \phi - \phi_0 \leq BW/2 \\ SLL & \text{otherwise,} \end{cases} \tag{7.9}$$

where $G(\phi)_{dB}$ is the antenna gain in decibel units in the direction ϕ, BW is the beamwidth and SLL is the average side lobe level in dB. The angle ϕ_0 is the direction towards the desired mobile. Several values of BW and SLL are used in the simulation. It is supposed that base stations are able to perfectly track the location of mobiles connected to them, such that the main beam of the radiation pattern is always steered towards the desired mobile. It is also supposed that base stations are able to form one beam for each desired mobile, with no limitation on the number of beams. This model for radiation pattern has been used in other similar studies [85, 86], with the advantage that the results of the system performance analysis will not be dependent on a particular beamforming algorithm or array geometry.

For the case of sector antennas, we use the same model described in (7.9), for $BW = 120^o$ (three sectors per cell) and $SLL = -12$ dB. This value of SLL is based on radiation patterns of commercially available antennas.

Uplink and downlink radiation patterns are assumed to be identical in all cases studied. Note that, since shadowing fading is also assumed to identical on both links, the uplink and downlink *path gains*

$$\frac{G_T^{up}\, G_R^{up}\, L^{up}}{d^\gamma} \quad \text{and} \quad \frac{G_T^{down}\, G_R^{down}\, L^{down}}{d^\gamma} \tag{7.10}$$

are consequently identical.

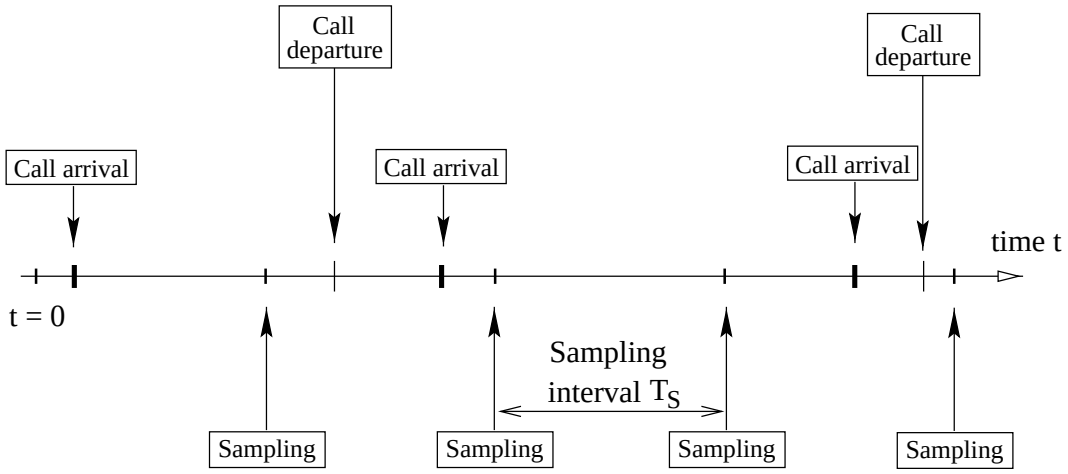

Figure 7.9: Events in the simulation: call arrivals and call departure occur at any time, while sampling occurs at periodic interval.

7.5 Simulation of Channel Management

7.5.1 Events in the Simulation

The simulation process consists of three main events: *Call Arrival*, *Call Departure*, and *Sampling the Status of the System*. These three events are controlled in the simulation program using the *Event Scheduling Technique* [87]. An event is a change in the state of the system. For example, when a call arrives at the system and a channel is assigned to that call, this assignment will change the interference level experience by ongoing co-channel calls. Events are previously scheduled in time, and the next event to occur is the most imminent one. Call arrivals and call departures may occur at any time, while the system status is sampled at periodic time intervals T_S, as shown in Figure 7.9.

Call arrivals and call departures are random processes. The interval τ between two consecutive call arrivals follows an exponential distribution:

$$p_\tau(\tau) = \lambda\, e^{-\lambda\tau}, \tag{7.11}$$

where λ is the average number of call arrivals per unit time (calls per unit time). The duration s of the calls is also random variable following exponential distribution:

$$p_s(s) = \mu\, e^{-\mu s}, \tag{7.12}$$

where $1/\mu = H$ is the average call duration (units of time).

The *offered traffic* A, in Erlangs, generated by a population of users is defined as

$$A = \lambda\, H. \tag{7.13}$$

Assuming that (i) blocked calls are cleared, (ii) call arrivals are memoryless, (iii) the number of users is infinite, the probability P_B that a call is blocked is given by the *Erlang B* formula as [1]

$$P_B = \frac{A^C/C!}{\sum_{k=0}^{C} A^k/k!} \tag{7.14}$$

In this dissertation, we assume that the average call duration H is 100 seconds, and we adjust λ in order to obtain a desired offered traffic A *per cell*. For example, if there are 80 base stations in the system and a traffic of 40 Erlangs per cell is desired, the average number of call arrivals at the entire system per unit time is

$$40 \text{ Erlangs per cell} \times 80 \text{ cells} = \lambda \times H \Rightarrow \lambda = 32 \text{ call arrivals per second.} \tag{7.15}$$

In order to study the steady state performance of the simulated system, we should start collecting date after the number of active users exceeds 90% of the steady state value, which is given by [84]

$$N_{users,ss} = \eta N_{cells} N_{ch} \tag{7.16}$$

where η is the loading factor of the system, defined in Chapter 4, N_{cells} is the number of cells in the system and N_{ch} is the number of channels per cell. In our simulations, we start collecting data after discarding the first $3 \times N_{users,ss}$ calls and collected the data in three independent simulation runs, with $N_{users,ss}$ calls each.

Next, we describe the steps performed when each event occurs.

7.5.2 Call Arrival Processing

When a call arrives at the system, the mobile originating the call selects the serving base station by measuring the power of the signals received from each base station on the control channels, and selecting the base station with the strongest signal. Note that, the serving base station is not always the closest base station, due to shadowing fading. Control channel is used to determine the serving base station since it is not power controlled and is transmitted using omnidirectional antennas.

Next, the serving base station, together with the mobile station, selects a channel to be allocated to the new call, using the appropriate channel allocation algorithm. The channel allocation algorithms analyzed in this dissertation are described in Chapters 8 - 10, when the respective simulation results are presented. All channel allocation algorithms require the estimation of $SINR$ on candidate channels. As already mentioned, in this dissertation we assume that exact $SINR$s are available at base stations and mobiles. The computation of $SINR$ in the simulation is based on the propagation channel model described in Section 7.4.1 and antenna radiation patterns described in Section 7.4.2.

Common to all channel allocation algorithms analyzed in Chapters 8 - 10 is the fact that the admission of calls to the system is controlled in order to maintain the link quality above a minimum acceptable level. A call is admitted only if it is possible to find a channel that meets the condition $\Gamma > \Gamma_{adm,new}$ on both links. This call admission control may be explicit, as in fixed channel allocation, or implicit, as in dynamic channel allocation. Call admission control is discussed in Section 8.3.1.

If no channel at the serving base station satisfies the requirements imposed by the channel allocation algorithm in use, the call is blocked. Note that, when channel allocation fails at the serving base station, no attempt is made to set up a link through another base station (for example, the one with the second strongest control channel signal).

After processing a call arrival, the next call arrival is scheduled, independently whether the call arrival just processed was blocked or admitted. If the call is admitted to the system, its departure time is scheduled

7.5.3 Call Departure Processing

At the end of a call, the assigned channel is released and returned to the pool of idle channels of the serving base station.

7.5.4 Sampling the Status of the System

The purpose of sampling the system status is to check whether one of the following actions is requested by any ongoing call:

- *Intercell handoff* (or simply 'handoff'): if there is a base station with stronger control channel signal received at the mobile than the signal from the serving base station, an intercell handoff is required. In order to avoid the so called "ping-pong effect"

(consecutive handoffs between two base stations), the signal from the candidate base station must be H_{HO} dB above the signal from the serving base station. Handoffs are mainly caused by user mobility, but may be also caused by propagation effects, such as shadowing fading. Handoff is necessary to allow users to move throughout the entire coverage area, without having their calls dropped.

In the analysis presented in the subsequent chapters, the performance of this intercell handoff algorithm (measured by, for example, the number of intercell handoffs per call) is not taken into consideration when analyzing the performance of the cellular system.

- *Channel reassignment* (or intracell handoff): when the link quality, measured in terms of signal to interference plus noise ratio on the assigned channel (both links) drops below a threshold $\Gamma_{th,re}$, channel reassignment is requested. Note that, in this case, the serving base station is still the best base station. Low link quality (or high co-channel interference level) can be caused by:
  - admission of a call on the same channel (new call, intercell or intracell handed off calls);
  - in systems employing base station adaptive antennas, user mobility may lead to situations where the serving base station antenna is no longer able to reduce the interference from a particular co-channel mobile on the reverse link. The same situation may occur on the forward link.
  - propagation effects: even though the serving base station is still the best base station, its signal on either link may suffer from strong shadowing fading at a particular location;

  Channel reassignments are important to keep the link quality and, therefore, the service quality above a given minimum acceptable level.

  Call admission control is also used to readmit intercell and intracell handoff calls. A call is readmitted only if it is possible to find a channel that meets the condition $\Gamma > \Gamma_{adm,re}$ on both links. However, readmission of an ongoing call is preferred to the admission of a new call. Handoff call is an ongoing call in need of a new channel due to the poor link quality on its assigned channel. If the readmission of a handoff call is not completed, the call may be dropped. And, from users' point of view, call dropping is more annoying than new call blocking. Therefore, the (re)admission threshold $\Gamma_{adm,re}$

is set smaller than the admission threshold $\Gamma_{adm,new}$ for new calls. Also, by setting $\Gamma_{adm,re} < \Gamma_{adm,new}$, the disturbance caused by admission of new calls on ongoing co-channel calls is reduced.

Steps performed during sampling

At every sampling event $t = k\,T_S$, where T_S is the sampling interval, the following steps are performed for each mobile:

1. The received power level of the control channel of all base stations are measured at the mobile. If the signal from the current serving base station is not the strongest one, an intercell handoff to the base station with the strongest signal (candidate BS) is requested. As mentioned before, a handoff is request only if the signal from the strongest base station is H_{HO} dB above the signal from the serving BS.

   If the candidate BS does not have any idle channel, the uplink and downlink $SINR$ on the currently allocated channels are measured. If $SINR$ on either link is below the threshold Γ_{min} for more than T_{drop} consecutive seconds (that is, it is not possible to complete handofff during T_{drop} consecutive seconds) the call is dropped.

2. If intercell handoff is not required, the uplink and downlink $SINR$s on the current channels are measured by the serving base station and mobile, respectively.

   If $SINR$ on either link is below the threshold $\Gamma_{th,re}$, channel reassignment is requested. Then, the serving base station, together with the mobile, tries to assign a new channel to that call, using the same algorithm used to allocate channels to new calls. If no channel is found, the current channel remains allocated to the call. However, if $SINR$ on either link is below the threshold SIR_{min} for more than T_{drop} consecutive seconds, the call is dropped.

In our implementation, the sampling interval is set to $T_S = 1$ second and the threshold values used in each algorithm are described in Chapters 8, 9 and 10, when the results are presented. Table 7.3 lists the common simulation parameters used in those chapters.

7.6 Conclusion

In this chapter we presented details of the cellular network simulated in the subsequent chapters. The models used in the physical layer, such as propagation channel model, shadowing

Table 7.3: Simulation parameters.

Parameter	**Value**
Number of base stations	around 80
Cell radius R	3000 m
SNR at cell boundary	40 dB
Path loss exponent γ	3.5
Shadowing standard deviation σ	8 dB
Decorrelation Distance d_{de}	50 m
Handoff hysteresis H_{HO}	4 dB
Sampling interval T_S	1 second
Power control update interval T_{PC}	0.25 seconds
Time interval before call is dropped due to low $SINR$ T_{drop}	5.0 seconds
Mean call holding time H	100 seconds

fading generator, antenna radiation pattern model, user mobility, were described. Also, models used in the logical layer and details of the call processing were presented. The simulation structure described in this chapter is used in all analyses presented in the subsequent chapters, except for some particular details, which are presented in the respective chapter.

Chapter 8

Capacity Improvement Using Adaptive Antennas and Reduced Cluster Size

8.1 Introduction

In this chapter we analyze the performance of a cellular system using fixed channel allocation (FCA) and base station adaptive antennas. In system using FCA, capacity improvement is achieved by reducing cluster size, which increases the number of channels allocated to each cell. However, when cluster size is reduced, link quality degrades due to higher co-channel interference levels. In this chapter, we use adaptive antennas at the base stations to mitigate the increased interference. The analysis is carried out using simulation of a cellular network, as described in Chapter 7. Several aspects of the cellular system are analyzed, including carried traffic, outage probability, number of channel reassignment requests. We also analyze the capacity gain and performance improvement when uplink and downlink power control is used. Simulation results show that the use of power control allows less complex adaptive antennas to be used to achieve a given capacity improvement.

We start this chapter by discussing how the performance analysis will be carried out. Next, we present the simulation results for fixed transmitter power and controlled transmitter power.

8.2 Reference System

In cellular systems employing fixed channel allocation, the carried traffic per cell is hard limited by the number of channels allocated to each cell, which, in turn, depends on the number of channels available for the entire system and the cluster size used in the system. However, in some situations, co-channel interference may be too high such that capacity becomes limited by interference, as discussed in Chapter 4. Therefore, when we reduce the cluster size from, say, $N = 7$ to $N = 4$, aiming to increase system capacity, and use some technique for controlling the increased co-channel interference, the expected (desired) results are twofold: (1) We expect the performance, in terms of outage probability, dropping probability, number of channel reassignment requests, of the system using reduced cluster size to be similar to the performance of the system with larger cluster size (reference system); (2) We also expect the system using reduced cluster size to use the available channels efficiently. In other words, we expect system capacity to be limited by blocking probability. The analysis presented in this chapter will focus on these two aspects above. Next, we define the reference system of our analysis.

The reference system employs the commonly used cluster size $N = 7$, with sectorized cells with three sectors of 120^o. The cellular network consists of 84 cells (12 clusters) with cell radius 3000 m. The number of duplex traffic channels available for the entire cellular network is $N_C = 400$ channels, such that each sector is allocated 19 channels. Fixed transmitter power is assumed, with base stations (BSs) transmitting at $P_{BS} = 10W$ and mobiles (MSs) transmitting at $P_{MS} = 0.6W$. In this chapter, we use user profile Hybrid I (see Table 7.2), which is predominantly pedestrian. The channel management used in the reference system follows the same strategy used in similar studies described in [74, 91]. When a call arrives at the system, the originating MS determines the serving BS by selecting the BS with the strongest control channel signal. The serving BS then passes to the mobile a list of idle channels with uplink signal-to-interference-plus-noise ratio ($SINR$) Γ larger than $\Gamma_{adm,new}$, assuming that the mobile transmits at power level P_{MS}. The mobile finally selects the first channel found, among the channels on the list, that satisfies $\Gamma > \Gamma_{adm,new}$ on the downlink. Note that this channel management requires that MS and BS measure $SINR$ on traffic channels. Appendix B describes how $SINR$ can be measured. The channel management used in the reference systems also allows channel reassignment when $SINR$ on either link drops below threshold $\Gamma_{th,re}$, as discussed in Chapter 7. Table 8.1 shows the threshold values used in the reference system, which are usually employed in similar studies [74, 91].

Table 8.1: Thresholds used in the reference cellular system: Cluster size $N = 7$, 3 sectors per cell.

Parameter	**Value**
Admission $SINR$ for new calls ($\Gamma_{adm,new}$)	19 dB
Admission $SINR$ for reassigned calls ($\Gamma_{adm,re}$)	17 dB
Threshold $SINR$ for channel reassignment ($\Gamma_{th,re}$)	15 dB
Threshold $SINR$ for call dropping (Γ_{drop})	14 dB

Figure 8.1 (a) shows the blocking and dropping probability for the reference system. Note that the blocking probability is slightly higher than the probability computed using the Erlang B formula (for 19 channels per sector). The reason is that some calls are blocked due to lack of channel with enough link quality.

Blocking and dropping probabilities are important performance parameters from users' point of view. However, other performance parameters are also important from system perspective. For example, the *outage probability*, defined as the probability that $SINR$ is below a given threshold Γ_0, is a measure of the quality of the communication link. The threshold Γ_0 is the minimum acceptable level of $SINR$ for reliable system operation. In the analysis presented in this chapter, we assume $\Gamma_0 = 17$ dB, which is the commonly accepted value in systems based on IS-136 [51]. Since the uplink and downlink outage probabilities may be different, we here refer to "outage probability" of the system as the largest one between the uplink and downlink outage probabilities:

$$\text{Outage Probability} = \max\Big(Pr\{\Gamma^{up} < \Gamma_0\}, Pr\{\Gamma^{down} < \Gamma_0\} \Big). \tag{8.1}$$

The outage probability depends on the traffic load, which, in turn, determines the blocking probability of the system. Let us assume a target blocking probability 2%, which corresponds to a traffic load of 35.5 Erlangs per cell in the reference system. The simulated outage probability at this traffic load in the reference system is 2.4%.

Another important performance parameter from system perspective is the number of channel reassignment requests per call. The number of reassignment requests depends on the carried traffic, blocking and dropping probabilities, user mobility, among other parameters. Figure 8.1 (b) shows the channel reassignment request rate (requests per call) and completed reassignments per call for our reference system. Note that not all channel reassignment requests result in *completed* channel reassignment, due to lack of idle channels or acceptable

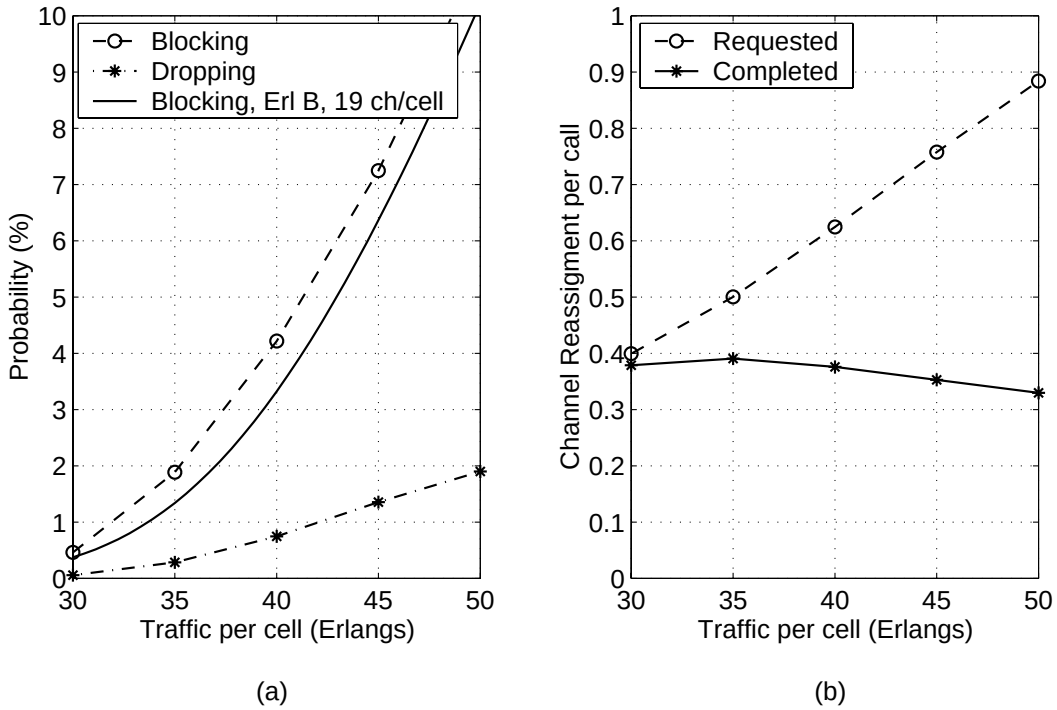

Figure 8.1: Reference system: (a) Blocking and dropping probabilities, and (b) channel reassignment rate for FCA, cluster size $N = 7$, 3-sector cells and 19 channels per cell.

channels to be assigned. A channel reassignment that is not completed may result in call dropping. From the users perspective, the percentage of *completed* channel reassignments is more important than the number of *requested* channel reassignments. However, from the system perspective, the number of channel reassignment requests per call is probably more important, since it represents the load on control channels. Throughout this dissertation, we will use the channel reassignment request rate, rather than completed channel reassignment rate, as a performance parameter.

Table 8.2 summarizes the performance of the cellular system using cluster size $N = 7$ and 3-sector, at a blocking probability of 2%.

Next, we present a preliminary discussion on the performance of systems using reduced cluster size.

8.3 Preliminary Discussion

Before analyzing the performance of systems using adaptive antennas, let us first analyze some effects of reducing cluster size from $N = 7$ to, say, $N = 4$. Let us initially suppose that

Table 8.2: Performance of a cellular system using cluster size $N = 7$ and 3-sector, at a blocking probability of 2%

Blocking probability	2%
Carried traffic load	35.5 Erlangs per cell
Dropping probability	0.33 %
Outage probability at $\Gamma_0 = 17$ dB	2.4%
Channel reassignment request per call	0.51
Channel reassignment rate per call	0.39

Table 8.3: Blocking probability composition for cluster size $N = 4$ with sectorized antennas at 70 Erlangs per cell.

Cause	**Blocking**
No idle channel	0.44 %
High interference	3.53 %
Overall	3.97 %

the base stations are still equipped with sectorized antennas (3 sectors), such that $N_C = 100$ channels are allocated to each cell, or 33 per sector. Therefore, using the Erlang B formula, we would expect a carried traffic of 73.9 Erlangs per cell at a blocking probability of 2%. On the other hand, since co-channel cells are closer to each other, co-channel interference for cluster size $N = 4$ is much higher than for cluster size $N = 7$. The higher interference will prevent idle channels from having acceptable link quality. As a direct consequence, blocking probability will be dominated by blocking due to low link quality of idle channels. For example, Table 8.3 shows how the overall blocking probability is composed for cluster size $N = 4$ with sectorized antennas. Therefore, it is clear that capacity in a cellular system using cluster size $N = 4$ and sectorized cells is limited by interference. Another consequence of high interference is the larger number of channel reassignment requests, which increases the control traffic load of the system.

Base station adaptive antennas were shown in Chapter 4 to be an effective technique for reducing co-channel interference. However, we also showed in Chapter 4 that a call admission control technique must be combined with base station adaptive antennas in order to guarantee the desired outage probability. In this dissertation, we use a simple admission control also used in reference system. However, when adaptive antennas are used, admission

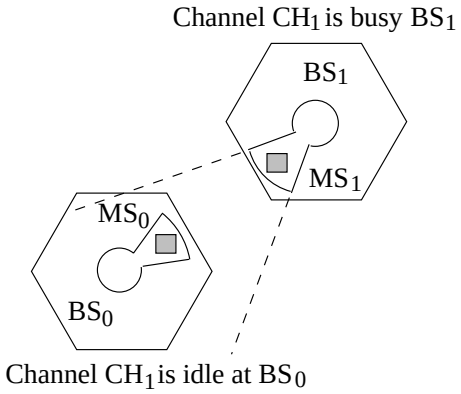

Figure 8.2: Typical situation where CH_1 cannot be allocated to mobile MS_0, even though channel CH_1 is idle at BS_0.

control and channel reassignment are even more important, as discussed subsequently.

8.3.1 The Importance of Call Admission Control and Channel Reassignment

When adaptive antennas are employed at base stations, it is well known that the average co-channel interference experienced by a given mobile (or base station) reduces. Let us consider a typical situation when a call arrives at a system using adaptive antennas. As already noted, regardless of the type of base station antenna used, it not guaranteed that all idle channels at the serving base station will experience low interference. Propagation effects, variation of traffic, location of mobiles may lead to unfavorable situations regarding interference on a specific channel. When adaptive antennas are used, these negative effects may be emphasized, which increase the importance of call admission control and channel reassignment.

For example, suppose that a given mobile MS_0 originates a new call at base station BS_0, and that channel CH_1 is idle at that base station. In principle, channel CH_1 might be allocated to the new call. Let us also suppose that channel CH_1 is in use at the neighbor base station BS_1, and (unluckily) its main beam is steered towards mobile MS_0, as depicted in Figure 8.2. Therefore, it is very unlikely that channel CH_1 will be allocated to mobile MS_0. The situation depicted in Figure 8.2 can happen during a call, due to user mobility. In that case, a channel reassignment would be required and performed as described in Chapter 7.

Table 8.4: Thresholds used in the cellular systems using adaptive antennas.

Parameter	**Value**
Admission $SINR$ for new calls ($\Gamma_{adm,new}$)	21 dB
Admission $SINR$ for reassigned calls ($\Gamma_{adm,re}$)	19 dB
Threshold $SINR$ for channel reassignment ($\Gamma_{th,re}$)	17 dB
Threshold $SINR$ for call dropping (Γ_{drop})	14 dB
Threshold $SINR$ for computing outage probability (Γ_0)	17 dB

The thresholds $\Gamma_{adm,new}$, $\Gamma_{adm,re}$, $\Gamma_{th,re}$ and Γ_{drop} affect the performance of the system. In this chapter, the thresholds used in the systems using adaptive antennas were selected such that the performance, in terms of link quality, is similar to the performance of the reference system. The reason to use this approach is that, the primarily result from the analysis presented in this chapter is how efficiently different adaptive antennas, combined with other techniques, mitigate co-channel interference such that interference does not limit capacity. Therefore, comparison will be primarily made among the systems using adaptive antennas. Table 8.4 shows the threshold values used in the systems using adaptive antennas.

We analyze in this chapter the performance of cellular systems employing cluster sizes $N = 3$ and $N = 4$ and adaptive antennas with beamwidth $BW = 45^o$ and a range of side lobe levels: $SLL = -12$ dB, -18 dB and -40 dB. The side lobe level is a measure of the capability of the antenna to mitigate undesired signals impinging on the antenna. This capability may be limited by the number of array elements or by the use of low performance beamforming algorithms. Since, we are not interested in the performance of a cellular system when a particular antenna array and beamforming technique are employed, we represent the capability of adaptive antennas to mitigate co-channel interference by simulating different side lobe levels.

Next we present the simulation results, considering first a system with fixed transmitter power, and later the case with power control on both links.

8.4 Fixed Transmitter Power

Figures 8.3 and 8.4 show the blocking and dropping probabilities when adaptive antennas are used with cluster sizes 3 and 4, and without power control. As expected, as the side lobe level decreases, the blocking and dropping probabilities decrease. Low side lobe level

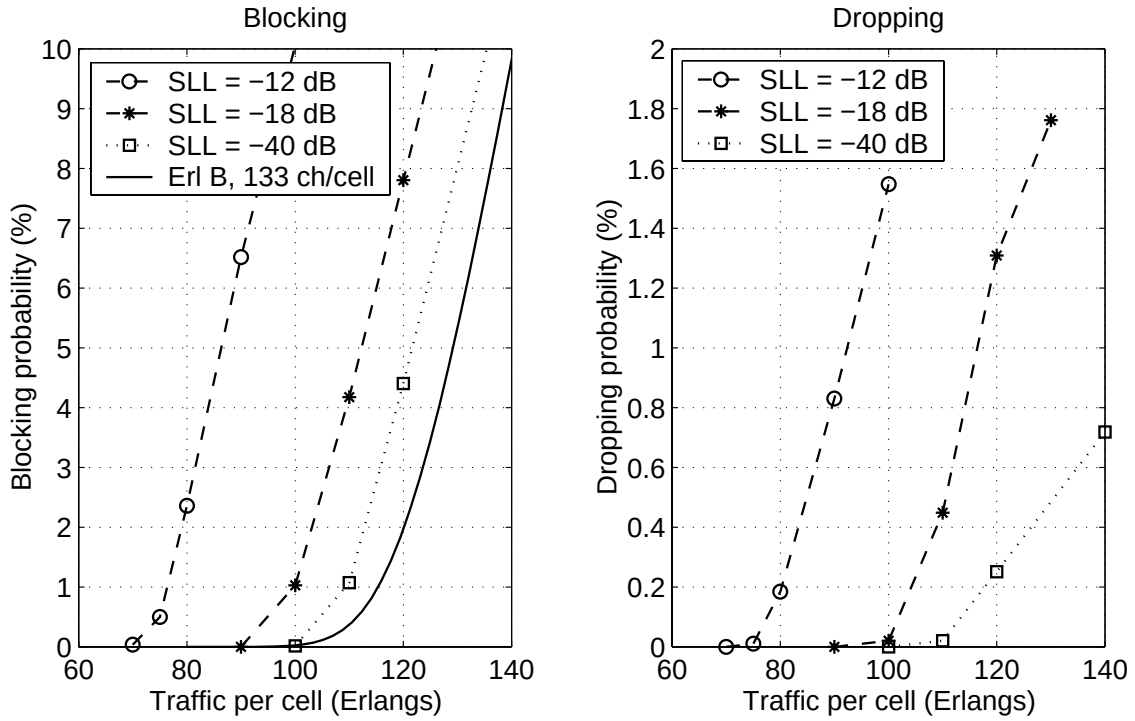

Figure 8.3: Blocking and dropping probabilities for cluster size $N = 3$, $BW = 45^o$ and several values of side lobe level.

reduces the overall co-channel interference in the system, such that more channesl from the pool of idle channels will meet the admission threshold $\Gamma_{adm,new}$.

We also plotted in Figures 8.3 and 8.4 the blocking probabilities given by the Erlang B formula for cluster size $N = 3$ (133 channels per cell) and cluster size $N = 4$ (100 channels per cell), which correspond to the maximum carried traffic for each cluster size. Note that, the blocking probability computed using the Erlang B formula considers only blocked calls due to lack of channels (the effects of interference are not taken into account). We see that, even with a side lobe level of -40 dB and $BW = 45^o$, the maximum carried traffic for both cluster sizes is not achieved. We discuss this result later in this section.

Assuming that the target blocking probability of the cellular system is 2%, we present in Tables 8.5 and 8.6 the maximum carried traffic, dropping probability, channel reassignment request rate and outage probability at $\Gamma_0 = 17$ dB, for cluster sizes $N = 3$ and 4. These tables give the performance of each configuration at their "operating point". We can see the effects of reducing the side lobe level: Interference reduction is transformed into higher carried traffic as more channels will meet the condition $\Gamma > \Gamma_{adm,new}$ upon call arrival. Note that, as side lobe level decreases, the number of channel reassignment requests decreases,

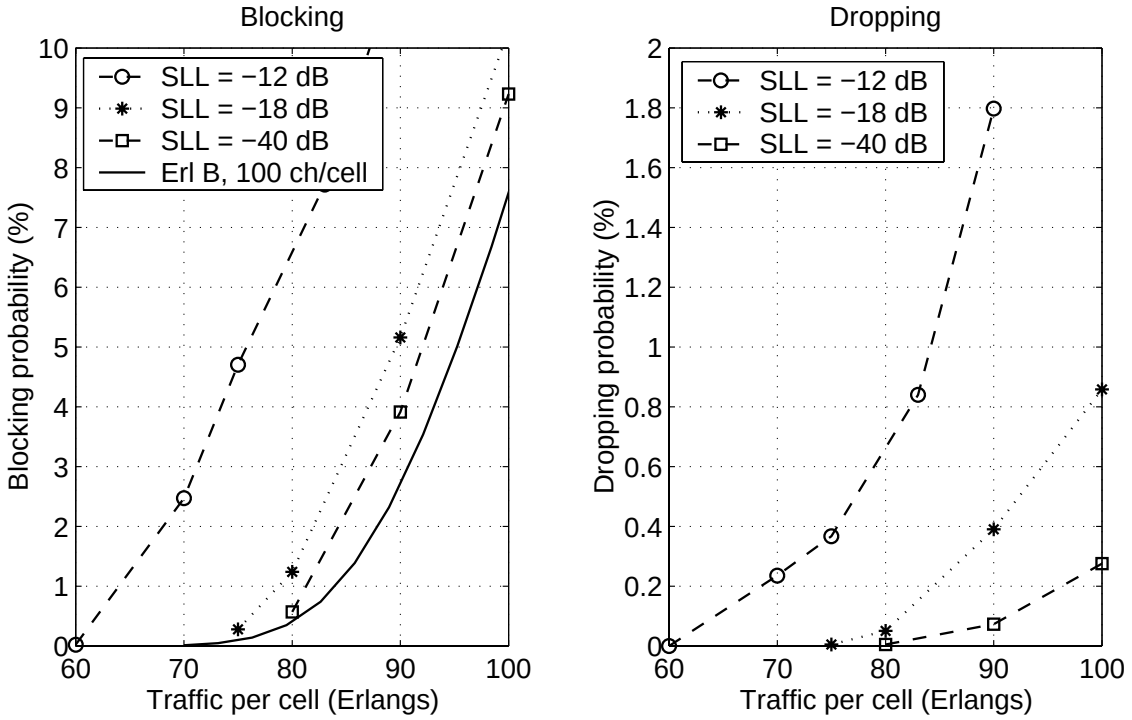

Figure 8.4: Blocking and dropping probabilities for cluster size $N = 4$, $BW = 45^o$ and several values of side lobe level.

Table 8.5: System performance at blocking probability 2% for cluster size $N = 3$ and several values of side lobe level (133 channels per cell).

SLL (dB)	Carried Traffic Erlangs/cell	Dropping Prob. (%)	Reassign. Requests per call	Outage Prob. (%)
-12	79	0.18	2.0	2.0
-18	103	0.10	1.7	1.7
-40	112	0.07	1.4	1.3
$N = 7$, 3-sectors	35.5	0.33	0.51	2.4
Erl B, 133 ch	120.1	-	-	-

Table 8.6: System performance at blocking probability 2% for cluster size $N = 4$ and several values of side lobe level (100 channels per cell).

SLL (dB)	Carried Traffic Erlangs/cell	Dropping Prob. (%)	Reassign. Requests per call	Outage Prob. (%)
-12	68	0.18	1.7	1.6
-18	82	0.12	1.3	1.2
-40	84	0.03	1.0	0.8
$N = 7$, 3-sectors	35.5	0.33	0.51	2.4
Erl B, 100 ch	87.9	-	-	-

even though traffic increases. One would expect that number to increase, since there are more users sharing the same channel (higher traffic). However, the admission control mechanism prevents channels with low link quality from being allocated to a call.

For comparison purpose, we replicate in Tables 8.5 and 8.6 the results for the reference system. We see that the number of reassignment requests increases with adaptive antennas and reduced cluster size, which can be explained by the combined effect between user mobility and spatial filtering, as discussed in Section 8.3.1. The higher number of reassignments can be considered the price to be paid for the higher carried traffic.

Let us now analyze how efficiently each configuration (cluster size/antenna parameters) uses all the installed capacity, in terms of carried traffic. The maximum carried traffic is given by the Erlang B formula. Figure 8.5 shows the percentage of the maximum carried traffic per cell, at blocking probability 2%, that is carried per cell, for different cluster sizes and side lobe levels. It is clear in Figure 8.5 that, even with a side lobe level of -40 dB, capacity is still limited by co-channel interference. The reason is that a beamwidth of 45^o is broad enough to illuminate a large area of co-channel cells. Another reason is related to the random characteristics of mobile locations and propagation effects.

8.5 Controlled Transmitter Power

As discussed in Chapter 5, power control can be used to increase capacity in cellular systems, as it optimizes the usage of the resource "transmitter power". By optimizing the transmitter power, the overall co-channel interference measured on a particular channel is reduced. We are here interested in analyzing the benefits of combining adaptive antennas with power

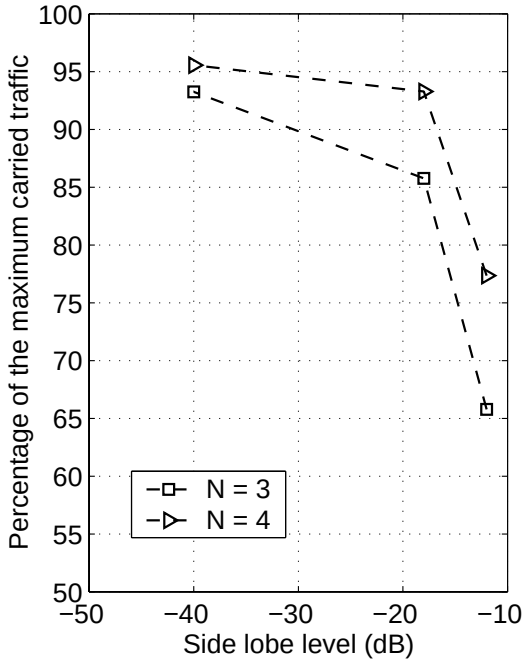

Figure 8.5: Percentage of the maximum carried traffic, at blocking probability 2%, for different configurations, for $BW = 45^o$.

control in systems using FCA. The additional co-channel interference reduction provided by power control may allow the use of a less complex adaptive antenna (for example, broader beamwidth or smaller side lobe level reduction) to achieve a given performance or system capacity.

In this section, we will consider the *SINR Balancing Power Control* technique, that attempts to balance the $SINR$ of all links transmitting on the same channel, as described in Chapter 5. The power update for the i-th link is given by:

$$P_{T,i}^{(k)} = \Gamma_T \, \frac{P_{T,i}^{(k-1)}}{\Gamma_i^{(k-1)}}, \tag{8.2}$$

where $P_{T,i}^{(k-1)}$ and $\Gamma_i^{(k-1)}$ are the transmitter power and $SINR$ at instant k. The target $SINR$, Γ_T, must be higher than the minimum acceptable $SINR$, which in our simulation is set to $\Gamma_0 = 17$ dB. However, excessively high Γ_T decreases carried traffic, as it happens without power control. On the other hand, as discussed in [58], some protection margin above Γ_0 is desirable in mobility conditions. Due to variations of propagation path losses caused by mobility, $SINR$ fluctuates, Now, if we set $\Gamma_T = \Gamma_0$, link quality will degrade due to user mobility. Therefore, in the analysis presented in this chapter, we set $\Gamma_T = 21$ dB.

Practical implementation of this technique involves some issues to be analyzed here. First, the application of expression (8.2) implies that an accurate estimate of the current $SINR$ is available. In the analysis presented in this dissertation, as already pointed out, we assume that the exact $SINR$s on both links are available.

A second issue that needs to be analyzed regards how the power level of the transmitter is adjusted. Ideally, the power level adjustment is continuous, that is, $P_{T,i}^{(k)}$ can assume any value. However, in practical situations, the transmitter power levels are discretized and can assume only certain values. On top of that, we may be limit to adjust the power levels in a step-by-step fashion. For example, if the transmitter power level can only assume the values 0 dBm, -3 dBm, -6 dBm and -9 dBm, the power of the transmitter cannot jump from 0 dBm to -6 dBm. Another important issue regards the fact that, due to practical reasons, the output power level of a transmitter is upper and lower limited. Before analyzing the performance of a cellular system using power control and adaptive antennas, let us analyze the effects of discretization described above on the performance of power control.

8.5.1 Effects of Discretization of Power Control

Consider the case where the base stations of the cellular system are equipped with adaptive antennas with beamwidth $BW = 45^o$ and side lobe level $SLL = -6$ dB. We chose a larger side lobe level than the one used in the previous analysis, so that the power control technique faces an unfavorable situation regarding interference. We are going to analyze three implementation approaches for adjusting the power level in the $SINR$ Balancing power control:

- *Continuous Power Control*: transmitter power level $P_{T,i}$ can assume any value, but is limited to $P_{min} \leq P_{T,i} \leq P_{max}$,
- *Discrete Power Control*: the power levels are discretized and the difference between two consecutive values is Δ_P; also, the maximum and minimum power levels are limited to P_{max} and P_{min}, respectively,
- *Step-by-step Power Control*: the power levels are discretized and the difference between two consecutive values is Δ_P, as in the previous case, but the transmitter power increment or decrement at each iteration is limited to Δ_P.

Table 8.7 presents the power control parameters used in the simulation. The approaches

Table 8.7: Power Control Parameter used in the simulation for both links.

	Downlink	Uplink
P_{max}	10 dBW	-2.2 dBW
P_{min}	-20 dBW	-32.2 dBW
Δ_P	3 dB	3 dB

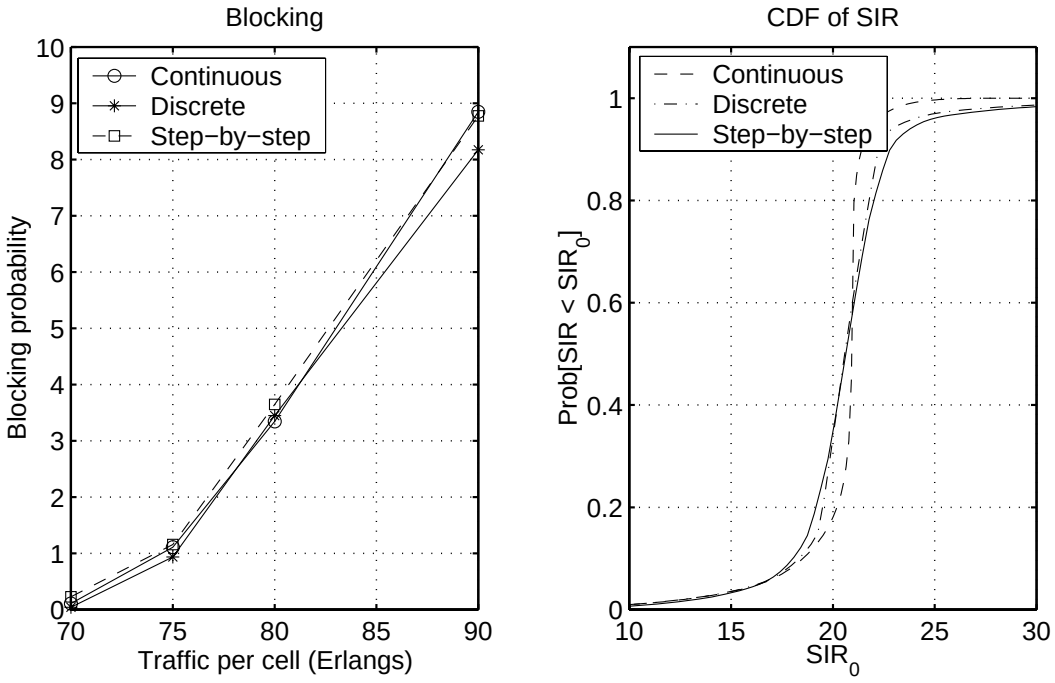

Figure 8.6: Performance of different implementation approaches of power control for cluster size $N = 4$, $BW = 45^o$ and $SLL = -6$ dB: (a) blocking probability; (b) CDF of downlink $SINR$ at 80 Erlang per cell.

for adjusting the transmitter power described above and the parameters in Table 8.7 are often found in practice [92, 93].

Figure 8.6 shows the blocking probability and the cumulative distribution function (CDF) of the downlink $SINR$ for all three approaches of power control. We see that discretization of the transmitter power causes little degradation, if any, on the performance of the system. Even though the variance of $SINR$ is higher for the discrete and step-by-step approaches, the outage probability at $\Gamma_0 = 17$ dB of all three approaches are about the same. The channel reassignment request rates for each approach are found to be about the same.

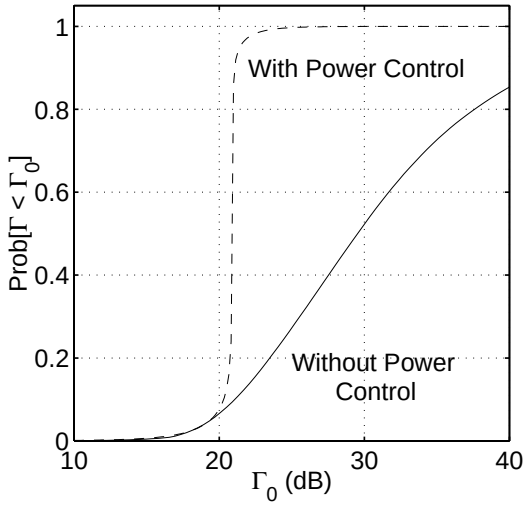

Figure 8.7: Cumulative distribution function of the uplink $SINR$ with and without power control for $N = 4$, $BW = 45^o$, $SLL = -40$ dB and carried traffic 80 Erlangs/cell.

We conclude that the effects of discretization for $\Delta_P = 3$ dB is very small, as also noted in [90]. In the rest of this dissertation, we will use the continuous approach.

8.5.2 Perfomance of Cellular System using Power Control and Adaptive Antennas

Before analyzing the effects of power control on the performance of cellular systems, let us see how power control changes the distribution of $SINR$. Figure 8.7 shows for illustration purpose the cumulative distribution function of the uplink $SINR$ with and without power control for the case $N = 4$, $BW = 45^o$ and $SLL = -40$ dB. We see that without power control, most of the links (around 98%) have $SINR$ higher than $\Gamma_0 = 17$ dB. High $SINR$ means that excessive and unnecessary transmitter power, that only adds to the co-channel interference in the system. On the other hand, when power control is used, most of the links (around 80%) have $SINR$ around $\Gamma_T = 21$ dB, which reduces the interference level in the system.

Figures 8.8 and 8.9 show the blocking and dropping probabilities for cluster sizes $N = 3$ and 4, with power control. The curves of blocking probability vs. carried traffic per cell are closer to the Erlang B curve with power control, indicating that the resources of the cellular system are more efficiently used. In other words, capacity is becoming limited by blocking probability, instead of by interference. A comparison between the performance of systems

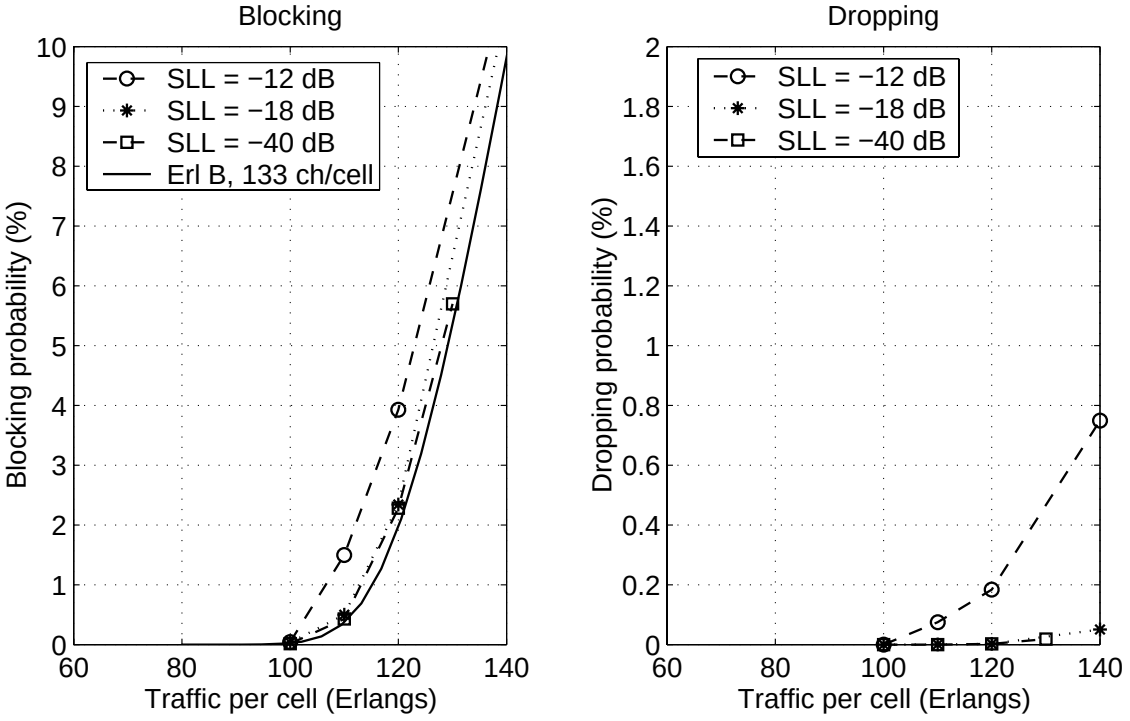

Figure 8.8: Blocking and dropping probabilities for cluster size $N = 3$, $BW = 45^o$, with power control and several values of side lobe level.

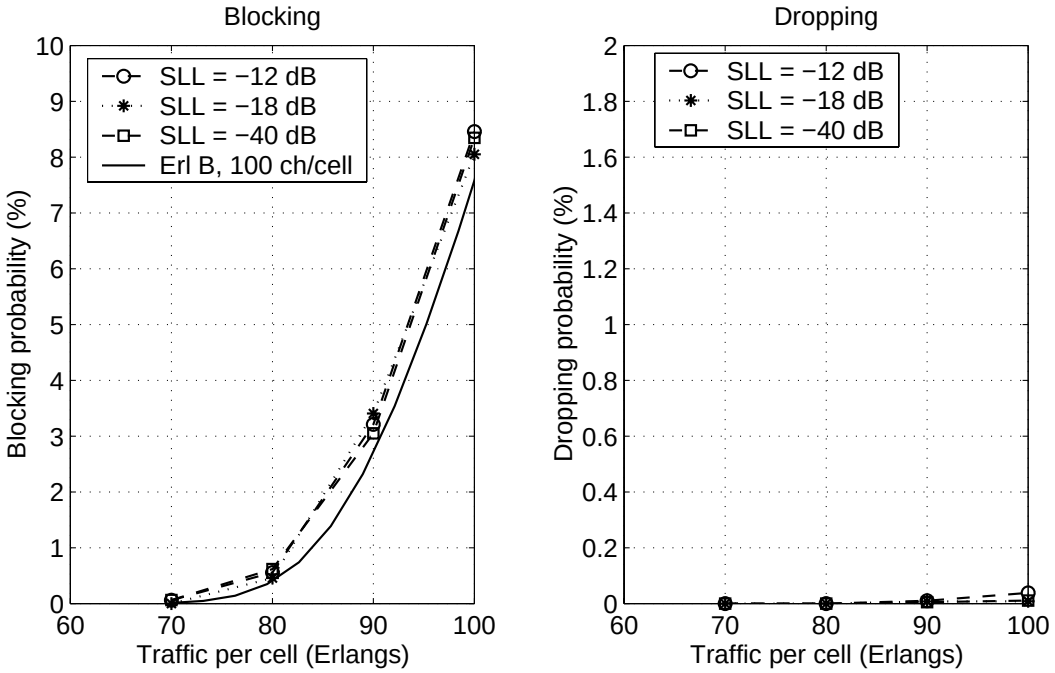

Figure 8.9: Blocking and dropping probabilities for cluster size $N = 4$, $BW = 45^o$, with power control and and several values of side lobe level.

Table 8.8: System performance at blocking probability 2% for cluster size $N = 3$, with power control and several values of side lobe level (133 channels per cell).

SLL (dB)	Carried Traffic Erlangs/cell	Dropping Prob. (%)	Reassign. Requests per call	Outage Prob. (%)
-12	112	0.10	3.10	3.5
-18	118	0.01	1.02	2.2
-40	118	0.01	0.49	2.2
Erlang B	120.1	-	-	-

Table 8.9: System performance at blocking probability 2% for cluster size $N = 4$, with power control and several values of side lobe level (100 channels per cell).

SLL (dB)	Carried Traffic Erlangs/cell	Dropping Prob. (%)	Reassign. Requests per call	Outage Prob. (%)
-12	86	0.01	1.21	2.5
-18	86	0.01	0.40	1.5
-40	86	0.01	0.21	1.5
Erlang B	87.9	-	-	-

with and without power control is presented later in this chapter. First, let us determine the *operating point* of each configuration when power control is used. Tables 8.8 and 8.9 show the carried traffic per cell, dropping probability, number of reassignment requests per call and outage probability at $\Gamma_0 = 17$ dB, when each configuration using power control experiences a blocking probability of 2%. A quick analysis of the carried traffic shown in these tables confirms that the capacity of a cellular system using power control and base station adaptive antennas approaches the maximum capacity carried by the set of channels allocated to each cell (given by the Erlang B formula), or, in other words, co-channel interference is more effectively controlled when power control is used. Figure 8.10 shows the percentage of the maximum carried traffic per cell, at blocking 2%, achieved by using different side lobe levels and cluster sizes with power control. As before, the maximum carried traffic is computed using the Erlang B formula.

Next, we compare the performance with and without power control in order to evaluate the importance of power control.

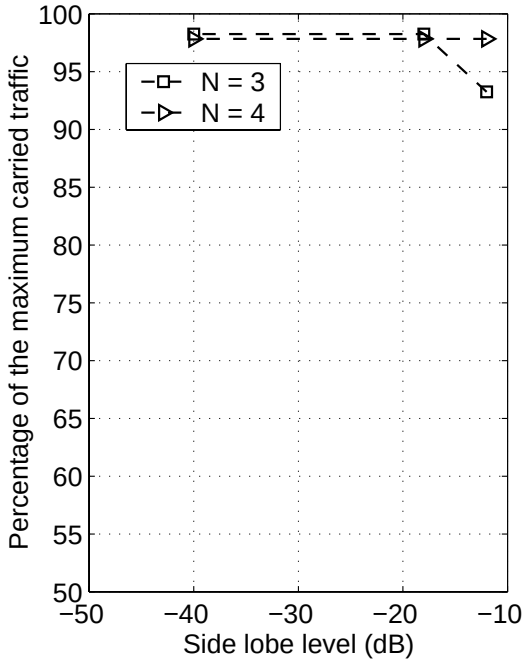

Figure 8.10: Percentage of the maximum carried traffic, at blocking 2%, achieved for different side lobe levels and cluster sizes, with power control and $BW = 45^o$.

8.6 Comparison Between the Performances with and without Power Control

The benefits of using power control can be observed by comparing Figures 8.5 and 8.10. For example, for beamwidth 45^o and side lobe level $SLL = -12$ dB, the use of power control increases the carried traffic from 66% to 92% of the maximum capacity. The difference between these two percentages decreases as side lobe level decreases, since the adaptive antenna will play a more important role in the reduction of co-channel interference.

As briefly mentioned before, as co-channel interference is efficiently controlled by using adaptive antennas and power control, system capacity becomes limited by blocking due to lack of idle channels. To corroborate that statement, Table 8.10 shows the probabilities that a call is blocked due to high interference and due to lack of idle channels, for the case of cluster size $N = 4$, beamwidth $BW = 45^o$ and side lobe level $SLL = -12$ dB. The results for controlled transmitter power and fixed transmitter power cases are shown. For the specific configuration shown in Table 8.10, co-channel interference is the cause of almost all blocked calls when power control is not used. On the other hand, if power control is used, this

Table 8.10: Blocking probabilities due to lack of channel and high interference for cluster size $N = 4$, $BW = 45^o$ and $SLL = -12$ dB. The respective percentages of overall blocking probability are indicated in parentheses.

	without power control	with power control
Blocking due to lack of channels (%)	0.015 (0.01%)	2.74 (85.4%)
Blocking due to high interference (%)	11.53 (99.9%)	0.47 (14.6%)
Overall blocking probability (%)	11.55 (100%)	3.21 (100%)

Table 8.11: Capacity improvement, at blocking probability 2%, achieved by using power control with respect to the case without power control.

	Capacity improvement	
$SLL(dB)$	$N = 3$	$N = 4$
-12	39.2%	26.5%
-18	14.6%	4.9%
-40	5.3%	2.4%

percentage drops to 14.6%.

Let us now turn our attention to the practical benefits of using power control. Comparing the carried traffic per cell at a blocking probability of 2% given in Tables 8.5, 8.6, 8.8 and 8.9, we can estimate the capacity improvement achieved by using power control and adaptive antennas with respect to the case without power control. Table 8.11 summarizes the results. We can see that the importance of power control decreases as cluster size increases or side lobe level decreases. The reason is that, by increasing cluster size or decreasing side lobe level, co-channel interference reduces, reducing the need for an additional co-channel interference control technique, such as power control.

Another way to analyze the capacity improvement when power control is combined with adaptive antennas is to estimate the reduction of the complexity of the antenna (in terms of beamwidth and side lobe level) allowed by the use of power control. In our case, we will define the complexity of the adaptive antennas in terms of the average side lobe level. Large side lobe level reduction requires a large number of array elements and more sophisticate beamforming algorithms. Using again the results from Tables 8.5, 8.6, 8.8 and 8.9, we conclude that, for example, for cluster size $N = 3$, the carried traffic achieved with side lobe level $SLL = -40$ dB without power control is also achieved with a side lobe level slightly

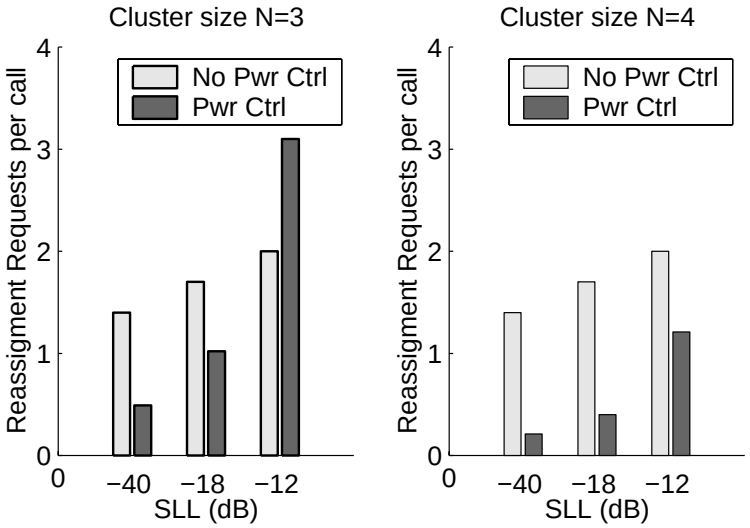

Figure 8.11: Number of channel reassignment requests at blocking probability 2%, for different cluster sizes and side lobe levels.

higher than −18 dB. In other words, since the side lobe level depends on the number of elements in the array antenna, fewer arrays elements are required in the antenna if power control is used.

We have seen so far the benefits of using power control. However, it should be noted that the use of power control may increase the number of channel reassignment requests per call, as the price to be paid for the capacity improvement achieved. The effects of power control on the number of channel reassignment requests depends on the importance of power control in the process of reducing capacity. Figure 8.11 compares the numbers of reassignment requests for different side lobe levels at blocking probability 2% (from Tables 8.8 and 8.9). When power control effectively increases capacity, as for cluster size $N = 3$ and $SLL = -12$ dB, the use of power control also increases the number of channel reassignment. In this case, even with power control, capacity is still limited by interference. Even though more channels are available for assignment, a new call admitted to the system disturbs several ongoing calls on the same channel. Therefore, capacity improvement is at the expense of more channel reassignment requests.

On the other hand, in the cases where interference is already small without power control, and capacity is mainly limited by blocking (for example, for cluster size $N = 4$), the use of power control does not significantly increase capacity, but does reduce even further interference, reducing the number of channel reassignment.

We have seen in this section how base station adaptive antennas and power control can improve capacity in cellular systems using fixed channel allocation. The importance of power control in this combined technique depends on how much interference is still limiting capacity, after adaptive antennas is employed. The capacity of the systems analyzed in this chapter is hard limited by the number of channels allocated to each cell. Therefore, after certain point, reduction of co-channel interference does not improve capacity. In the next chapter, we analyze the situation when all channels available for entire the system can be used in any cell.

8.7 Conclusion

In this chapter, we analyzed the performance of a cellular network employing base station adaptive antennas and reduced cluster size. The effects of adaptive antennas on the capacity and system performance were analyzed by using several different configurations of adaptive antennas, with different average side lobe levels. The maximum capacity available per cell (carried traffic) in systems using fixed channel allocation is hard limited by the number of channels allocated to each cell. However, when the cluster size is small and no appropriate interference control technique is employed, carried traffic is mainly limited by interference, and not by blocking probability, indicating that the cellular system is not efficient regarding the use of the available resources.

Simulation results presented in this chapter showed that, adaptive antennas do improve capacity by reducing interference. However, simulation results also showed that, for fixed transmitter power, small side lobe levels (high complexity antennas) may be required in order to achieve the maximum capacity available. For example, for beamwidth $BW = 45^o$ and cluster size $N = 3$, a side lobe level of -40 dB is required to achieve 93% of the available capacity (given by Erlang B formula).

When transmitter power control on both links is used, the additional interference reduction provided by power control may be enough to allow that all channels allocated to each cell be efficiently used (i.e. maximum capacity is achieved), even with adaptive antennas with large side lobe level (low complexity). Using the example of $BW = 45^o$ with cluster size $N = 3$, simulation results showed that, with power control, a side lobe level of -12 dB is enough to achieve 93% of the available capacity. However, the higher capacity achieved with power control, in this case, is at the expense of a larger number of channel reassignment

requests. If, on the other hand, a smaller side lobe level is used, power control not only increases capacity, but also reduces the number of channel reassignment requests.

Chapter 9

Capacity Improvement by Combining DCA and Adaptive Antennas

9.1 Introduction

Dynamic channel allocation algorithms have been vastly studied in cellular communication systems, as shown in the literature review presented in Chapter 6. In the present chapter, we analyze the benefits of combining adaptive antennas, dynamic channel allocation and power control. When dynamic channel allocation is used, any channel available for the entire system can be used by any base station. Clearly, some technique must be employed for selecting the appropriate channel to be allocated to a given call. We will focus our attention on dynamic channel allocation algorithms based on interference, namely Least Interference Algorithm (LIA) and Autonomous Reuse Partitioning (ARP). The performance of channel allocation algorithms based on interference depends on the level of interference experienced by the channels. By combining channel allocation with interference reduction techniques, such as adaptive antennas and power control, one expects to improve the performance of such algorithms. Dynamic channel allocation algorithms transform the reduced interference into higher carried traffic. This chapter aims to analyze how efficiently LIA and ARP convert the reduction of interference, provided by adaptive antennas and power control, into higher carried traffic and higher system performance.

We start this chapter by describing LIA and ARP algorithms and specific details of the simulated system used in this chapter. Subsequently, we present the simulation results for fixed and controlled transmitter power.

9.2 Dynamic Channel Allocation Algorithms

9.2.1 Least Interference Algorithm

The Least Interference Algorithm (LIA) assigns the least interfered channel, among the idle channels at the base station [88]. When a mobile originates a new call and requests a channel, the serving base station (the one with the strongest control channel signal received at the originating mobile) compiles a list with idle channels that meets the condition $\Gamma^{up} > \Gamma_{adm,new}$, where Γ^{up} is the uplink $SINR$. The list is then sent to the mobile, that selects the channel with the highest downlink $SINR$ (Γ^{down}), among those channels that meet the condition $\Gamma^{down} > \Gamma_{adm,new}$. If no channel is found, the call is blocked. The same approach is used for intercell handoff calls and channel reassignment, but using threshold $\Gamma_{adm,re}$, instead of $\Gamma_{adm,new}$.

LIA maximizes the distance between base stations reusing the same channel, reducing the spectral efficiency of the system, and, consequently, the maximum carried traffic. However, since channels with low interference are allocated to incoming calls, ongoing co-channel calls suffer from small disturbance caused by incoming calls, resulting in a small channel reassignment request rate and outage probability.

9.2.2 Autonomous Reuse Partitioning Algorithm

Autonomous Reuse Partitioning (ARP), is based on sensing (measuring $SINR$) channels following an order that is common throughout all cells [89]. The first channel that presents interference levels below a given threshold on both links is assigned. When a call arrives at the system, the serving base station compiles a list with idle channels that satisfy the condition $\Gamma^{up} > \Gamma_{adm,new}$ and sends that list to the mobile. The mobile then measures the downlink $SINR$ on the channels on the list, following a common order used by all mobiles, and selects the first channel found that meets the condition $\Gamma^{down} > \Gamma_{adm,new}$. The same approach is used for handoff calls and channel reassignment, but using threshold $\Gamma_{adm,re}$, instead of $\Gamma_{adm,new}$. A consequence of this allocation strategy is that channels sensed first are reused more often in the system and, therefore, experience larger interference. Since the level of interference on those channels is high, only mobiles with strong desired signals can use those channels. Mobiles with strong signals usually are those close to their serving base stations. On the other hand, channels that are sensed later are used fewer times in the

Table 9.1: Thresholds used in the simulated system.

Parameter	**Value**
Admission $SINR$ for new calls ($\Gamma_{adm,new}$)	21 dB
Admission $SINR$ for reassigned calls ($\Gamma_{adm,re}$)	19 dB
Threshold $SINR$ for channel reassignment (Γ_{re})	17 dB
Threshold $SINR$ for call dropping (Γ_{drop})	14 dB

system and experience smaller interference, being allocated to mobiles with weak signals, which, usually, are located far from their serving base stations.

Therefore, ARP algorithm creates concentric rings (partitions) whiten the cell, such that channels allocated to mobiles located in the inner rings have smaller reuse distance than channels allocated to mobiles located in the outer rings. Therefore the name *reuse partitioning*, which is is achieved autonomously.

Channel Allocation and Admission Control

The admission control discussed in Chapter 8 is also implemented in this chapter. As already discussed, the threshold values $\Gamma_{adm,new}$ and $\Gamma_{adm,re}$ are adjusted such that the readmission of handed off calls and completion of channel reassignments are preferred to the admission of new calls. The thresholds used in this chapters are presented in Table 9.1 and follow the values used in chapter 8 for adaptive antennas. chapter. The effects of the values of the thresholds on the system performance are discussed later in this chapter.

9.3 Simulated System

The cellular network simulated follows the specifications described in Chapter 7. The number of cells in the systems is 80, and $N_C = 400$ pairs of channels are available for the entire systems. It is supposed that all base stations have enough radio equipment to use any channel. The adaptive antennas have beamwidth $BW = 45^o$ and a range of side lobe level: $SLL = -12$ dB, -18 dB and -40 dB. As before, we assume that base stations are able to perfectly track their mobiles, such that the main beam of the adaptive antennas are steered towards the desired mobiles. In this chapter, we use user profile Hybrid I (see Table 7.2), which is predominantly pedestrian.

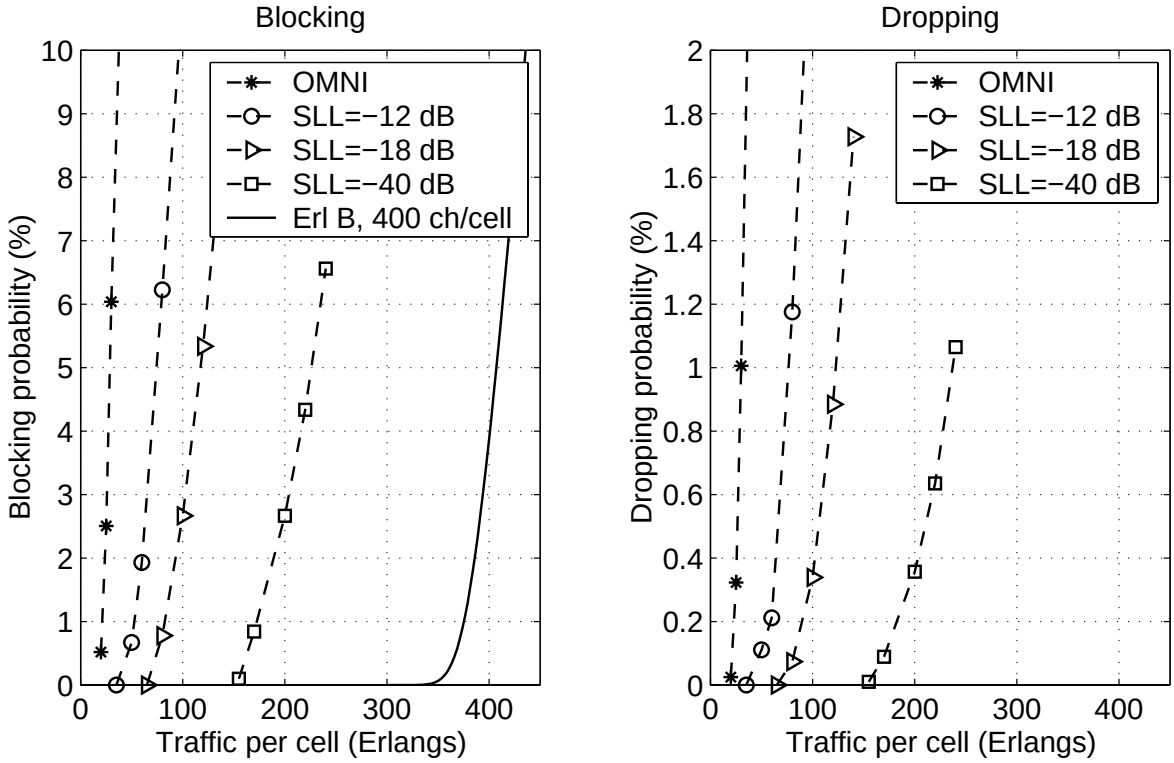

Figure 9.1: Blocking and dropping probabilities for algorithm LIA, $BW = 45^o$, without power control, and for several values of side lobe level.

In the subsequent sections, we analyze the performance of the simulated cellular network when dynamic channel allocation is combined with base station adaptive antennas with fixed and controlled transmitter power.

9.4 Fixed Transmitter Power

Consider a cellular system with fixed transmitter power and employing dynamic channel allocation (LIA or ARP). We are interested in the capacity improvement achieved by combining the algorithms LIA and ARP with adaptive antennas, with respect to the capacity achieved with omnidirectional antennas.

Figures 9.1 and 9.2 show the blocking and dropping probabilities of the cellular system using dynamic channel allocation algorithms LIA or ARP. The results for both omnidirectional and adaptive antennas are shown in the same figures for comparison. As expected, the use of adaptive antennas results in carried traffic increase, due to interference reduction.

Let us assume again that the target blocking probability is 2%, and determine the carried

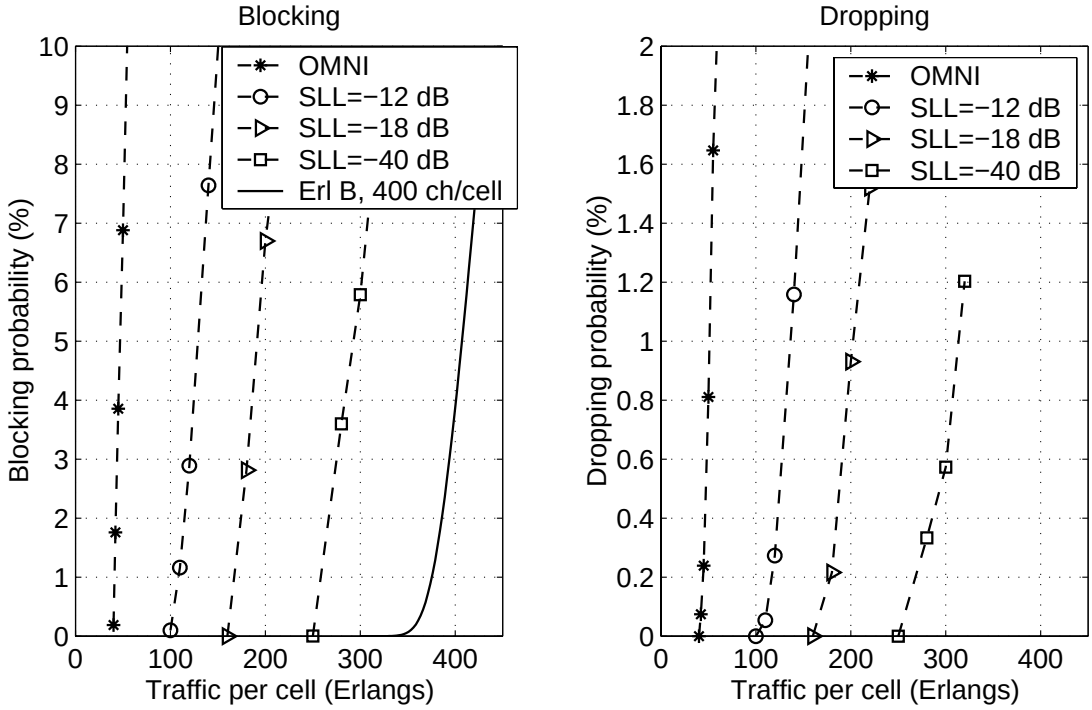

Figure 9.2: Blocking probability for algorithm ARP, $BW = 45^o$, without power control, and for several values of side lobe level.

traffic and other performance parameters at the target blocking. Tables 9.2 and 9.3 present the carried traffic per cell, along with dropping probability, number of channel reassignment requests per call and outage probability at $\Gamma_0 = 17$ dB for both allocation algorithms and different antenna side lobe levels.

Capacity improvement with respect to the omnidirectional antenna case

We compute the capacity gain in terms of carried traffic at blocking 2%, for each antenna configuration, with respect to the omnidirectional case, using

$$\text{Capacity gain } (\%) = 100 \times \left(\frac{A_{AA} - A_{omni}}{A_{omni}} \right), \tag{9.1}$$

where A_{omni} and A_{AA} are the carried traffic loads at blocking 2% with omnidirectional and adaptive antennas, respectively. The results for several side lobe level values, for both LIA and ARP are presented in Figure 9.3. We see that, for moderate co-channel interference reduction, that is, for $SLL = -12$ dB and -18 dB, both LIA and ARP transform the interference reduction into higher carried traffic with about the same efficiency. However,

Table 9.2: System performance at blocking probability 2% for algorithm LIA, without power control and several values of side lobe level.

SLL (dB)	Carried Traffic Erlangs/cell	Dropping Prob. (%)	Reassign. Requests per call	Outage Prob. (%)
Omni	23.7	0.24	1.06	1.0
-12	60.3	0.23	1.02	1.0
-18	92.9	0.24	1.09	1.1
-40	189.0	0.26	1.35	1.2
Erlang B	385.9	-	-	-

Table 9.3: System performance at blocking probability 2% for algorithm ARP, without power control and several values of side lobe level.

SLL (dB)	Carried Traffic Erlangs/cell	Dropping Prob. (%)	Reassign. Requests per call	Outage Prob. (%)
Omni	42.3	0.09	3.11	2.78
-12	114.8	0.16	2.98	2.7
-18	174.2	0.16	3.01	2.6
-40	266.7	0.18	2.70	2.1
Erlang B	385.9	-	-	-

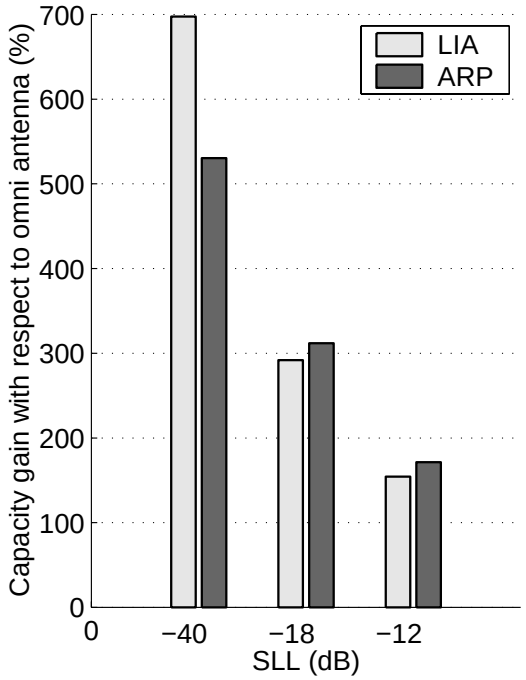

Figure 9.3: Capacity gain in terms of carried traffic at $P_B = 2\%$ for LIA and ARP and several side lobe level values. The gain is computed with respect to the omnidirectional antenna case.

for large reduction in the interference ($SLL = -40$ dB), LIA uses the interference reduction more efficiently than ARP.

The way both algorithms transform interference reduction into more carried traffic can be explained as follows. As we have seen, LIA selects the channel experiencing the lowest interference level. This policy tends to increase the reuse distance. With omnidirectional antennas, the isolation between co-channel base stations is provided by path loss attenuation only. Therefore, the minimum reuse distance, and, consequently, the capacity, is determined by the propagation environment[1] (path loss attenuation). When an additional isolation between co-channel cells is provided by using adaptive antennas, channels can be reused more often throughout the system (smaller reuse distance), increasing the carried traffic per cell.

ARP algorithm, on the other hand, is based on creating zones within the cell, where channels used in different zones have different reuse distances. In order to understand how the rings are created, consider a hypothetical "ideal" reuse partitioning, where all users using the same channel have the same path loss to their serving base stations [58]. Therefore, mobiles

[1]The admission thresholds also affect system capacity, as discussed in Section 9.5.

located at distance, say, d_0 from their serving base stations are ideally assigned the same channel (ignoring shadowing and Rayleigh fading). The smaller d_0, the smaller the reuse distance, since the signals from the mobiles are stronger. This arrangement autonomously creates rings within each cell, and each ring has its own reuse distance. Inner rings have smaller reuse distances than outer rings . In systems using omnidirectional antennas, the reuse distances depend on the propagation environment, since propagation losses are the only means to isolate co-channel cells. When additional interference isolation is provided by using adaptive antennas, the reuse distances of all rings shorten, increasing capacity. However, after a given value of interference reduction (or side lobe level), the reuse distances cannot be reduced further, limiting the capacity improvement.

It should be noted that, without power control, ARP still provides higher capacity than LIA for all values of SLL tested, as shown in Tables 9.2 and 9.3. The reason is that the structured reuse pattern created by ARP uses the channels more efficiently throughout the system. Therefore, systems using LIA have "more room" for improvement (in terms of carried traffic), than systems using ARP.

From Tables 9.2 and 9.3, we see that for both algorithms the use of adaptive antennas does not change significantly the number of channel reassignment requests per call and outage probability. It should be emphasized that Tables 9.2 and 9.3 give the performance parameters at the "operating points" of each configuration, that is, when blocking probability is 2%. Therefore, the values of dropping probability, channel reassignment rate and outage probability for each configuration (algorithm and side lobe level) are measured at different traffic loads. The reason for comparing different configurations at their corresponding operating points, as already discussed, is that those are the points at which each configuration is supposed to operate. For example, a cellular system using omnidirectional antennas and LIA algorithm can carry a traffic of 23.7 Erlangs per cell at a blocking probability of 2%. When adaptive antennas with $BW = 45^o$ and $SLL = -12$ dB are used at the base stations, the system can carry 60.3 Erlangs per cell at blocking 2%, and we expect to operate the system at this level of traffic load, and not at 23.7 Erlangs per cell, in order to increase profits.

Next, we analyze the effects of power control on the performance of both allocation algorithms combined with adaptive antennas.

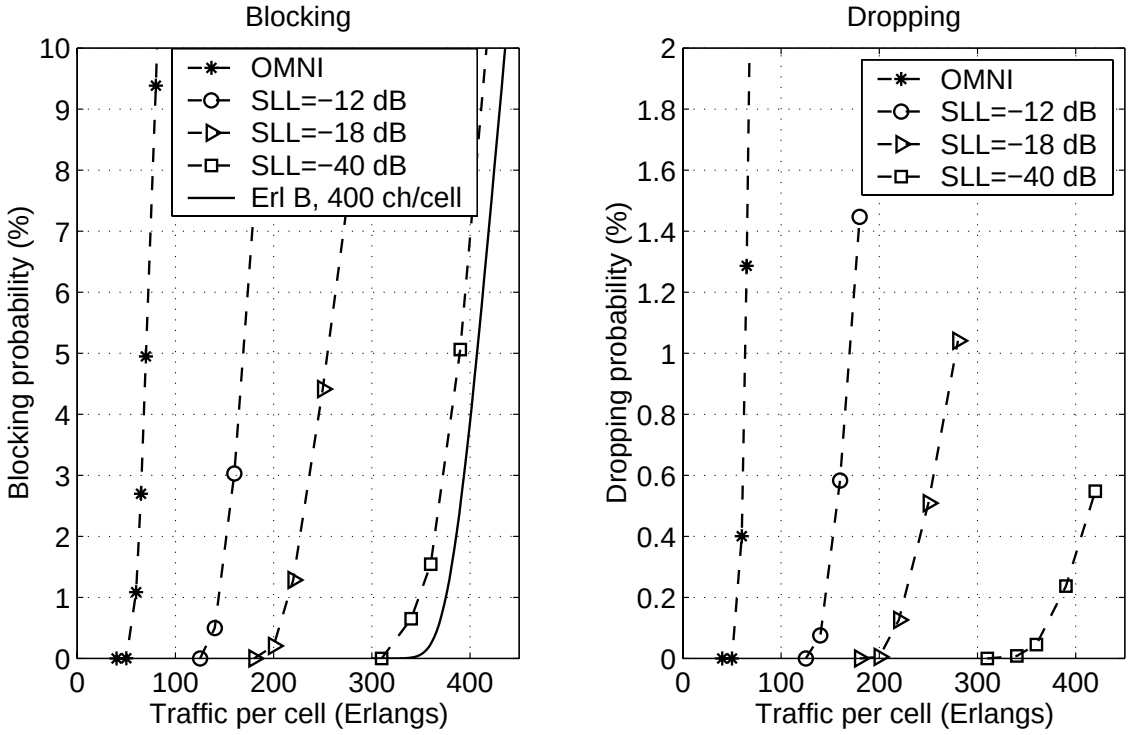

Figure 9.4: Blocking probability for algorithm LIA, $BW = 45^o$, with power control and several values of side lobe level.

9.5 Controlled Transmitter Power

We use the $SINR$ balancing power control technique, describe in Section 5.4, with continuous power adjustment and parameters described in Table 8.7. The target $SINR$ is set to $\Gamma_T = 21$ dB. Figures 9.4 and 9.5 show the blocking and dropping probabilities of LIA and ARP combined with adaptive antennas and power control. The power control technique employed is $SINR$ balancing (see Section 5.4) with continuous power level adjustment and $\Gamma_T = 21$ dB. The benefits of using power control, regarding the maximum carried traffic, can be observed in Figures Figures 9.4 and 9.5, by noting that the curves of blocking probability moved towards the Erlang B curve. Tables 9.4 and 9.5 summarize the performance of each antenna configuration and channel allocation algorithm at blocking probability 2%.

Before analyzing the capacity improvement achieved by using power control, let us analyze another important effect of the use of power control. Comparing the performance of systems using fixed and controlled transmitter power, we see that power control *increases* the number of channel reassignment requests per call, not only in systems using adaptive antennas, but also in systems using omnidirectional antennas. The increase in the number

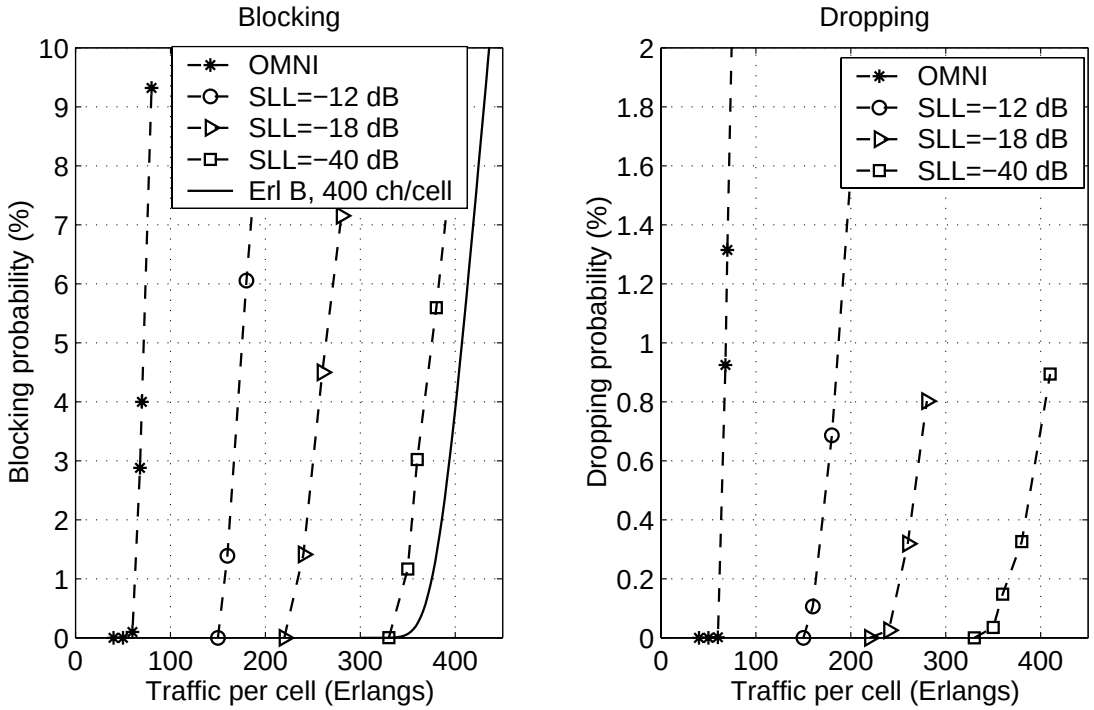

Figure 9.5: Blocking probability for algorithm ARP, $BW = 45^o$, with power control and several values of side lobe level.

Table 9.4: System performance at blocking probability 2% for algorithm LIA, with power control and several values of side lobe level.

SLL (dB)	Carried Traffic Erlangs/cell	Dropping Prob. (%)	Reassign. Requests per call	Outage Prob. (%)
Omni	62.8	0.90	17.2	20.3
-12	151.8	0.38	4.6	5.1
-18	226.8	0.21	2.8	3.1
-40	363.8	0.07	2.3	4.2
Erlang B	385.9	-	-	-

Table 9.5: System performance at blocking probability 2% for algorithm ARP, with power control and several values of side lobe level.

SLL (dB)	Carried Traffic Erlangs/cell	Dropping Prob. (%)	Reassign. Requests per call	Outage Prob. (%)
Omni	65.6	0.63	10.9	15.3
-12	162.6	0.18	5.2	5.2
-18	244.0	0.08	4.0	3.9
-40	354.5	0.06	4.7	5.4
Erlang B	385.9	-	-	-

of channel reassignments is due to the fact that, when power control is combined with dynamic channel allocation algorithms, calls are more densely packed (small reuse distances are possible due to reduced interference level) [74]. As a consequence, when a call arrives at the system and is allocated a channel, ongoing calls using that channel will suffer from stronger disturbance caused by the admission of that new call. And that disturbance may lead to channel reassignment requests. The disturbance depends on how densely packed the calls using the channel are.

It should be emphasized that the admission $SINR$ thresholds ($\Gamma_{adm,new}$ and $\Gamma_{adm,re}$) also play an important role in the context of combining power control with dynamic channel allocation. High levels of admission $SINR$ prevent some channels from being allocated, due to their poor link quality. However, when high levels of admission thresholds are used, the admission of a new call causes little disturbance on ongoing calls, reducing the number of channel reassignment requests. As a negative side effect of high admission $SINR$, few channels will meet the condition $\Gamma > \Gamma_{adm}$, and carried traffic will decrease.

Therefore, the threshold values $\Gamma_{adm,re}$ and $\Gamma_{adm,new}$ (and consequently the target Γ_T) are critical, since they control the trade off between capacity and number of channel reassignment requests. The values used in this chapter (see Table 9.1) are appropriated when adaptive antennas are used, since the increase in the number of channel reassignment requests caused by power control is not so drastic, as shown in Table 9.6. However, for the case of omnidirectional antennas, these values of threshold cause a severe increase in the number of channel reassignment requests when power control is used. To illustrate how the thresholds affect the performance of the system, additional simulation results show that for $\Gamma_{adm,new} = 23$ dB, $\Gamma_{adm,re} = 21$ dB and $\Gamma_T = 23$ dB, the number of channel reassignment

Table 9.6: Number of channel reassignment requests per call at blocking probability 2%.

	Without Power control		**With Power control**	
	LIA	ARP	LIA	ARP
OMNI	1.06	3.10	17.2	10.9
$SLL = -12$ dB	1.02	2.98	4.60	5.17
$SLL = -18$ dB	1.09	3.01	2.80	4.04
$SLL = -40$ dB	1.35	3.11	2.27	4.70

requests drops to 4.4 per call for ARP with omnidirectional antennas and power control. However, as a negative effect, capacity also drops, from 65.6 to 53 Erlangs per cell. The following comparison analysis between systems using omnidirectional antennas and adaptive antennas is carried out under the assumption that all systems use the same threshold values. In doing so, we can evaluate the effects of the use of adaptive antennas not only on carried traffic, but also on other performance parameters, such as the number of channel reassignment requests.

Capacity improvement with respect to the omnidirectional antenna case

The capacity gains achieved by each configuration of adaptive antennas, with respect to the omnidirectional case, at blocking probability 2%, are shown in Figure 9.6. A comparison between Figure 9.6 and Figure 9.3 reveals that the capacity gains achieved by using a particular adaptive antenna configuration, with or without power control, with respect to the omnidirectional case, are about the same. The reason is that systems using omnidirectional antennas also benefits from the use of power control.

Capacity improvement with respect to the fixed transmitter power case

A quick comparison of the values of carried traffic for fixed and controlled transmitter power shows the importance of power control in high capacity systems. As already point out, by balancing the $SINR$ of all links sharing the same channel, we make room for other links to use that channel. However, the capacity gain achieved by using power control depends on the technique used for allocating channels. The capacity gains achieved by using power

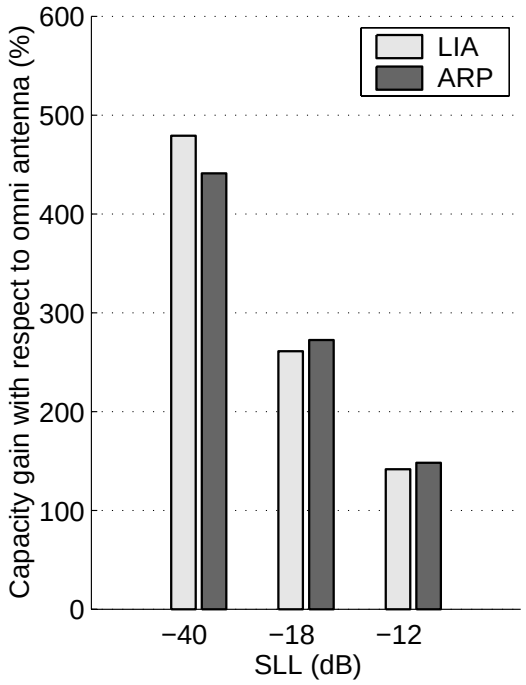

Figure 9.6: Capacity gain in terms of carried traffic at $P_B = 2\%$ for LIA and ARP and several side lobe level values. The gain is computed with respect to the omnidirectional antenna case.

control with different antenna configurations and allocation techniques are computed as:

$$\text{Capacity gain due to power control } (\%) = 100 \times \left(\frac{A_{PC} - A_{fixed\,power}}{A_{fixed\,power}} \right), \qquad (9.2)$$

where $A_{fixed\,power}$ and A_{PC} are the traffic loads carried at blocking 2% for fixed and controlled transmitter power, respectively. Using expression (9.2), the resulting capacity gains for each antenna configuration and channel allocation algorithm are shown in Figure 9.7. The results show that LIA uses more efficiently the interference reduction achieved by using power control. The reason is that, with power control, the transmitter power levels are adjusted according to the interference level on the channel, altering (decreasing) the correlation between received power and transmitter-to-receiver (T-R) separation distance. The correlation between received power and T-R separation distance is a key factor in the operation of ARP, since the algorithm creates concentric rings within the cells. When this correlation is weaken due to the use of power control, the process of creating rings with distinct reuse distances degenerates, reducing the advantage of using power control. Note that, with power control, the carried traffic loads for both allocation algorithms are close to each other, for all side lobe levels considered.

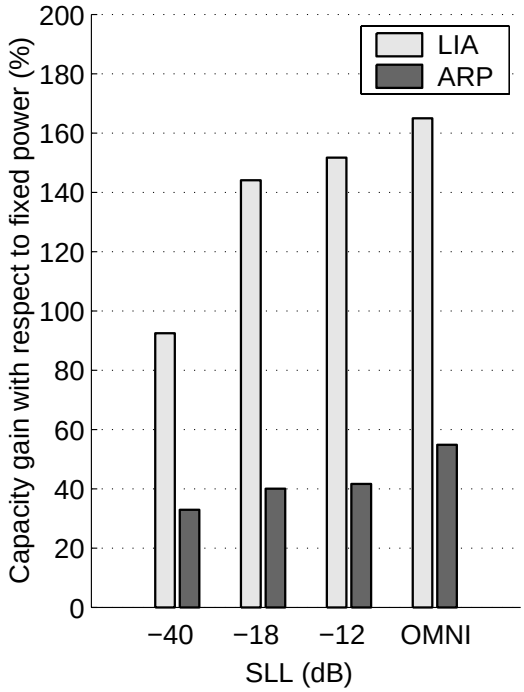

Figure 9.7: Capacity gain in terms of carried traffic at $P_B = 2\%$ achieved by using power control, with respect to fixed power case.

An interesting result from Figure 9.7 is that capacity gain achieved by using power control decreases as side lobe level descreases. The reason is that, with low side lobe level, interference is already low, and the use of power control does not add much to the process of reducing interference. And, as results have shown, capacity improvement is proportional to the reduction of interference.

Another important result is that, with large side lobe level reduction, both algorithms combined with power control are able to use almost all channels within every cell.

9.6 Conclusion

We analyzed in this chapter the performance of cellular systems using adaptive antennas, dynamic channel allocation and power control. The role of adaptive antennas and power control is to reduce co-channel interference, allowing channels to be reused more often throughout the entire system. Dynamic channel allocation algorithms attempt to organize the channel reuse.

Two allocation algorithms, LIA and ARP, with different allocation strategy were analyzed. While ARP attempts to create a structured channel reuse pattern, LIA allocates channels trying to minimize co-channel interference.

For fixed transmitter power, LIA and ARP transform the reduced co-channel interference provided by the use of adaptive antennas into higher carried traffic with similar efficiency. However, ARP provides a higher carried traffic per cell than LIA, due to the structured reuse pattern created by ARP. Simulation results also showed that, even with small side lobe level, neither algorithm was able to use all channels within every cell.

For the case of controlled transmitter power combined with adaptive antennas and dynamic channel allocation, results showed that LIA uses more efficiently the additional interference reduction achieved by using power control. Due to the fact that transmitter power is now controlled, ARP is not able to create an efficient channel reuse pattern. With small side lobe level, both algorithms were able to use almost all channels within every cell.

Chapter 10

Spatial Division Multiple Access

10.1 Introduction

As discussed in Chapter 2, the spatial filtering capability of adaptive antennas can be used to allow several users to share the same channel within the same cell, using the so called *Spatial Division Multiple Access Technique* (SDMA). It is well known that the channel allocation strategy used in SDMA systems plays an important role in the performance of such systems. In this chapter, we analyze the performance of SDMA cellular systems using several different channel allocation algorithms in different scenarios regarding user mobility. Also, just as done in the previous chapters for non-SDMA systems (where channel reuse within the cells is not allowed), we also analyze the performance of the cellular system with fixed and controlled transmitter power.

10.2 Allocation Algorithms

The use of an appropriate channel allocation strategy is of fundamental importance in SDMA systems, in order to efficiently exploit the potential capacity improvement provided by spatial filtering. Several studies have been carried out to analyze the potential capacity improvement achieved by using SDMA systems [94, 95, 96, 97, 98]. In this chapter, we present the analysis of some representative allocation algorithms for SDMA systems. Some of the algorithms analyzed are specially designed for SDMA systems, while others do not explicitly exploit the SDMA mechanism.

Four channel allocation algorithms are analyzed: *Concentrated Channel Load Algorithm*

(CCL), *Equal Channel Load Algorithm* (ECL), *Autonomous Reuse Partitioning Algorithm* (ARP), and *Least Interference Algorithm* (LIA). CCL and ECL represent two basic approaches for assigning channels in SDMA systems, since they explicitly exploit the fact that channels can be reused within cells. On the other hand, ARP and LIA do not make any *explicit* attempt to reuse channels within cells. These four algorithms are described in the following.

10.2.1 Concentrated Channel Load Algorithm (CCL)

CCL attempts to maximize the usage of channels within cells, while maintaining the quality of service (in terms of $SINR$) above a given minimum level [95]. When a call arrives at the system (new call, intracell or intercell handed off calls), the algorithm allocates the channel with the largest number of in-cell co-channel users at that moment at the serving base station. The allocated channel, however, needs to meet the condition $\Gamma > \Gamma_{adm,new}$ on both uplink and downlink. This approach is sometimes called *first duplicate* [94]. Since the algorithm tries to reuse channels within cells as much as possible, one may expect high level of co-channel interference, and, consequently, a large number of channel reassignment requests.

10.2.2 Equal Channel Load Algorithm (ECL)

With ECL, the serving base station allocates the channel least used within the cell, among all channels satisfying the condition $\Gamma > \Gamma_{adm,new}$ on both links [95]. This allocation strategy attempts to uniformly distribute the traffic in the cell among all channels. Since this algorithm tries to use all idle channels before reusing a channel within the cell, we expect a low level of interference. ECL algorithm is sometimes called *Duplicate at Last* [94].

10.2.3 Autonomous Partitioning Reuse Algorithm (ARP)

ARP algorithm has already been analyzed in Chapter 9, but for non-SDMA systems. For SDMA systems, ARP still senses the channels in a common sequence to all cells, and allocates the first channel that satisfies the condition $\Gamma > \Gamma_{adm}$ on both links. Differently from the ARP algorithm used in Chapter 9 for non-SDMA systems, in SDMA systems all channels are sensed, including busy channels. As in non-SDMA systems, ARP in SDMA systems

tries to create a structured reuse pattern, by creating concentric rings within the cells, with different reuse distances.

10.2.4 Least Interfered Algorithm (LIA)

LIA selects the channel with the least interference among the channels that meet the condition $\Gamma > \Gamma_{adm,new}$ on both links. LIA was also analyzed in non-SDMA systems in Chapter 9. In its SDMA version, all channels are sensed, including busy channels. LIA *tends* to select idle channels before selecting a channel already in use in the cell. Since LIA attempts to minimize the interference on all channels, the resultant number of channel assignment requests is expected to be low.

As in the previous chapters, the same allocation strategy is used for new calls, handoff calls or channel reassignment, except that, for handoff calls and channel reassignment, the admission threshold is $\Gamma_{adm,re}$.

10.2.5 General Comments and Implementation Issues

Simulation results, to be presented in this chapter, show that not all idle channels at a given cell have $SINR$ higher than the $SINR$ of channels already being used within that cell. The location of mobile, propagation conditions and the effects of spatial filtering may lead to the situation where a channel already in use within the cell is preferred to an idle channel. This situation occurs with all four algorithms studied in this chapter.

All algorithms in this chapter require the estimation of $SINR$ on both links. As in the previous chapters, we will assume that the exact values of $SINR$ on both links are available. We summarize in the following the basic operations to allocate a channel, which are common to all algorithms:

1. When a call arrives at the system (new, intracell or intercell handed off calls), the serving base station compiles a list of all channels (busy and idle) that satisfy the condition $\Gamma^{up} > \Gamma_{adm,new}$ (or $\Gamma_{adm,re}$), where Γ^{up} is the uplink $SINR$; the list is sent to the mobile;

2. The mobile then measures the downlink Γ^{down} on the channels on the list and, using the particular approach of each algorithm, selects a channel that meets the condition $\Gamma^{down} > \Gamma_{adm,new}$ (or $\Gamma_{adm,re}$).

Table 10.1: User profiles used in the simulation.

Profile	**Composition**
Hybrid I	80% pedestrian + 20% vehicular
Hybrid II	20% pedestrian + 80% vehicular

Table 10.2: Thresholds used in the simulation of SDMA system.

Parameter	**Value**
Admission $SINR$ for new calls ($\Gamma_{adm,new}$)	21 dB
Admission $SINR$ for reassigned calls ($\Gamma_{adm,re}$)	19 dB
Threshold $SINR$ for channel reassignment ($\Gamma_{th,re}$)	14 dB
Threshold $SINR$ for call dropping (Γ_{drop})	12 dB

3. If no channel meets both conditions $\Gamma^{down} > \Gamma_{adm,new}$ and $\Gamma^{up} > \Gamma_{adm,new}$ (or $\Gamma_{adm,re}$), the call is blocked, for the case of a *new* call. For the case of handoff calls or channel reassignment, the next steps follow the procedure described in Chapter 7.

10.3 Simulated System

The simulated system follows the specifications described in Chapter 7, except for some differences discussed in this section.

- All base stations are equipped with adaptive antennas with beamwidth 45^o and side lobe level -30 dB. The base stations are supposed to perfectly track their mobiles.

- The performance of SDMA systems are known to be very sensitive to user mobility. Therefore, the allocation algorithms will be analyzed using two different user profiles regarding mobility, as described in Table 10.1. Hybrid I is predominantly pedestrian, while Hybrid II is predominantly vehicular.

- The number of traffic channels available for the entire system is only 63 in order to reduce the simulation time.

- Table 10.2 shows the threshold values used in the simulated system. Note that the thresholds for reassignment trigger $\Gamma_{th,re}$ and call dropping Γ_{drop} are lower than the

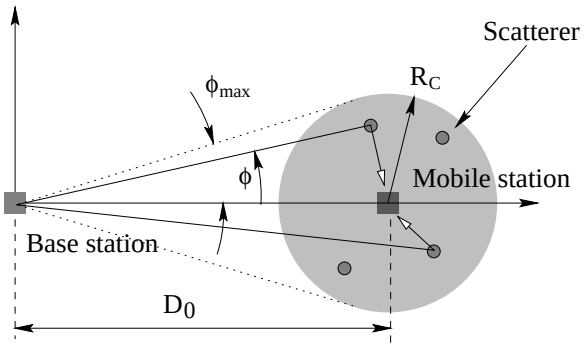

Figure 10.1: Illustration of the Geometrically Based Single Bounce Circular Model.

corresponding values used in the simulation of non-SDMA systems in Chapters 9 and 8. The use of lower values actually increases the level of interference in the system (mobiles with low quality calls are allowed to stay connected to the system longer). The higher interference level, in turn, creates more adverse conditions of operation for the algorithms, emphasizing the performance differences between the algorithms.

- The propagation channel model used includes distance-dependent path loss, log-normal shadowing, as in Chapter 9. Additionally, transmission through multipath components is modeled, in order to include some sort of spatial information in the propagation model. The Macrocell Geometrically Based Single Bounce Circular Model, discussed in Chapter 2 is used to generate the multipath components and their angles of arrival, as shown in Figure 10.1 The radius of scatterers R_c usually ranges from 30 to 200 m [6], and in this simulation is set to $R_c = 100$ m. Two multipath components plus the line-of-sight component are simulated. All components have the same path loss and shadowing fading. It is assumed that multipath components arrive at the receiver antenna with *no time delay* with respect to the line-of-sight component. In real systems, multipath components would arrive with different time delays, leading to small scale fading. In this simulation study, we do not intend to analyze the effects of small scale fading on the performance of the allocation algorithms. The spatial channel model is used here only to take into consideration the dispersion of angle of arrival of the multipath components. The uplink and downlink channel models are assumed to be identical.

  The line-of-sight and multipath components are generated as follows:

  – Every time a mobile moves to a new location, two scatterers are placed within

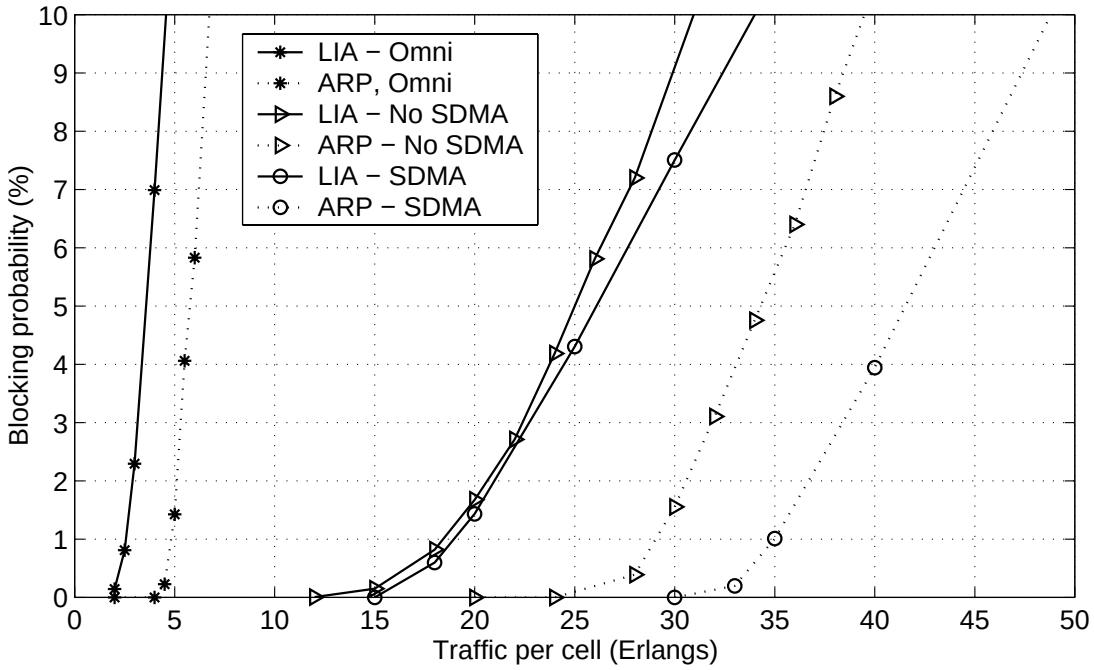

Figure 10.2: Blocking probability for LIA (solid curves) and ARP (dotted curves) with different base station antennas and operation modes, and without power control. User profile: Hybrid I.

the scatterer circle centered at the mobile location. The location of the scatterers follows an uniform distribution over the circle area.

– The angles of arrival and departure of the multipath components, with respect to the line-of-sight component, are computed using the geometry of the model.

All the other features of the simulated system are identical to those presented in Chapter 7. In the subsequent sections we analyze the performance of all four algorithms.

10.4 Fixed Transmitter Power

In this section, we consider a SDMA system with fixed transmitter power. Let us first compare the performance of LIA and ARP in different situations regarding how spatial filtering is employed. Figure 10.2 shows the blocking probabilities for LIA and ARP for (*i*) omnidirectional base station antennas, (*ii*) adaptive base station antennas, in non-SDMA mode and (*iii*) adaptive base station antennas, in SDMA mode. The capacity improvement achieved by using LIA or ARP algorithms with base station adaptive antenna, with respect

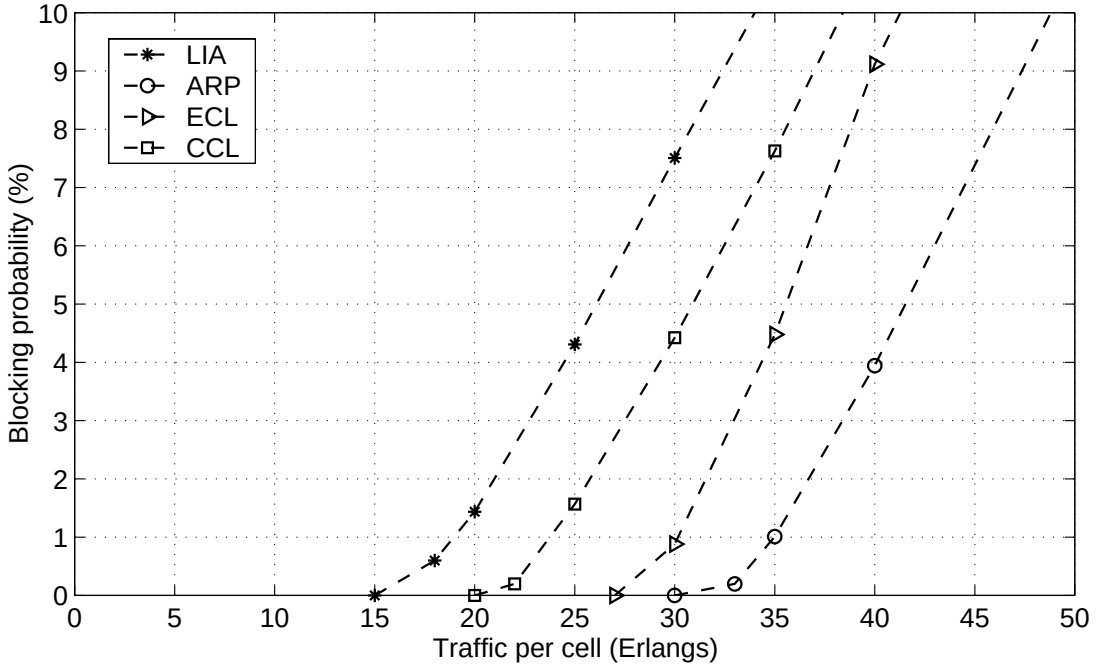

Figure 10.3: Blocking probability for different allocation algorithms and without power control in SDMA mode. User profile: Hybrid I.

to the case with omnidirectional antenna, is evident in this figure and has been analyzed in Chapter 9. The interesting result from this figure is that LIA does not use efficiently the permission to reuse channels within cells. A small capacity improvement is achieved only at high blocking probabilities, when the base stations start reusing channels within cells.

On the other hand, ARP seems to effectively use the permission to reuse channel within cells, resulting in a carried traffic gain of 20% at blocking probability 2%, with respect to the non-SDMA mode.

Figure 10.3 shows the blocking probabilities for LIA, ARP, ECL and CCL algorithms in SDMA mode. In order to compare the performance of each algorithm, let us assume that the target blocking probability is 2%. Table 10.3 shows the carried traffic per cell, dropping probability, channel reassignment request rate and outage probability (at $\Gamma_0 = 17$ dB), at blocking probability 2%, for all algorithms, including no SDMA cases.

When SDMA is used with ARP and LIA, the capacity gain with respect to the respective cases with omnidirectional antennas is about 7 times for both algorithms. However, as already noted, LIA and ARP in SDMA mode do not provide considerable capacity improvement with respect to the capacity for non-SDMA mode. Still, ARP in SDMA mode achieves

Table 10.3: System performance at blocking probability 2% for several allocation algorithms and without power control; outage probability computed at $\Gamma_0 = 17$ dB.

Allocation Algorithm	Carried Traffic Erlangs/cell	Dropping Prob. (%)	Reassign. Requests per call	Outage Prob. (%)
LIA, Omni	2.9	0.14	0.37	1.8
ARP, Omni	5.1	0.22	1.15	5.4
LIA, No SDMA	20.6	0.24	0.49	2.7
ARP, No SDMA	30.6	0.18	1.07	5.8
LIA, SDMA	21.0	0.28	0.47	2.3
ARP, SDMA	36.7	0.20	1.27	6.5
ECL, SDMA	31.6	0.23	1.10	4.8
CCL, SDMA	25.8	0.50	1.75	9.1

the highest carried traffic among all algorithms.

Surprisingly, CCL provides the second lowest carried traffic per cell among the algorithms in SDMA systems, despite the fact that CCL attempts to maximize the reuse of channels within the cells. This result can be explained by analyzing the distribution of channel usage (or load) among all channels for each algorithm. Figure 10.4 plots the distribution of the average number of users on the same channel within the cell, at traffic 40 Erlangs per cell. The left end of axis x corresponds to the most used channels, while the right end corresponds to the least used channels. Note the axis x of the plot in Figure 10.4 does not correspond to channel index. The most used channels at different base stations may be different from each other. Note, from Figure 10.4, that each base station uses only portion of the set of available channels. For example, base stations in the system using CCL algorithm use only half of the available channels (approximately 30 channels, out of 63). Comparing the curves for CCL and ECL algorithms, we see that, in fact, CCL algorithm reuses channels more often within cells than ECL. However, CCL uses fewer channels than ECL. The reason is that, when a channel is reused several times within a given cell, the interference on that channel becomes excessively high, preventing the surrounding cells from using that particular channel due to high interference. As a consequence, several idle channels at base stations cannot be allocated to any call, and calls are blocked even when there are idle channels at the serving base station. To illustrate the situation just described, Figure 10.5 shows a snapshot of channel usage at two neighboring base stations at a traffic of 40 Erlangs per cell. We see that some channels are reused as many as six times within one cell and not used at all in

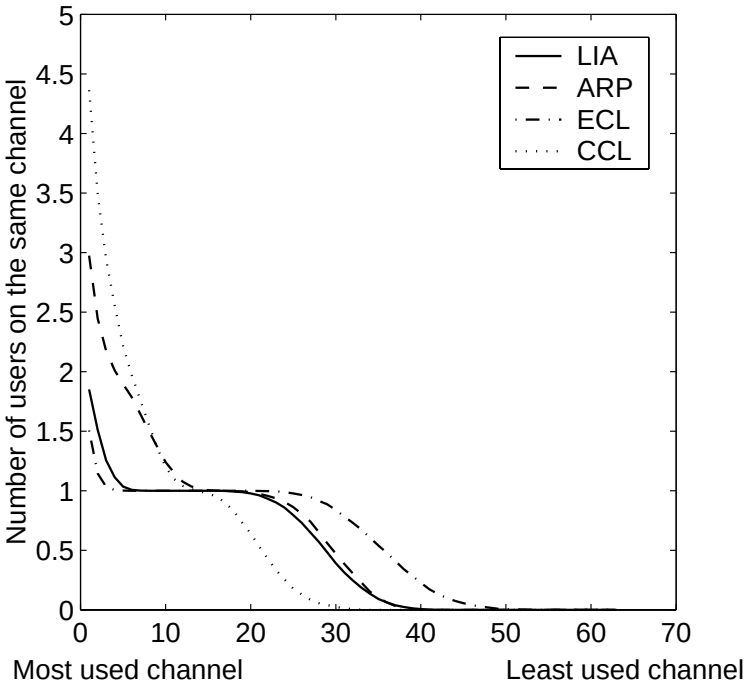

Figure 10.4: Distribution of the average number of users on the same channel at traffic load of 40 Erlangs per cell, for several allocation algorithms in SDMA systems. Without power control and user profile Hybrid I.

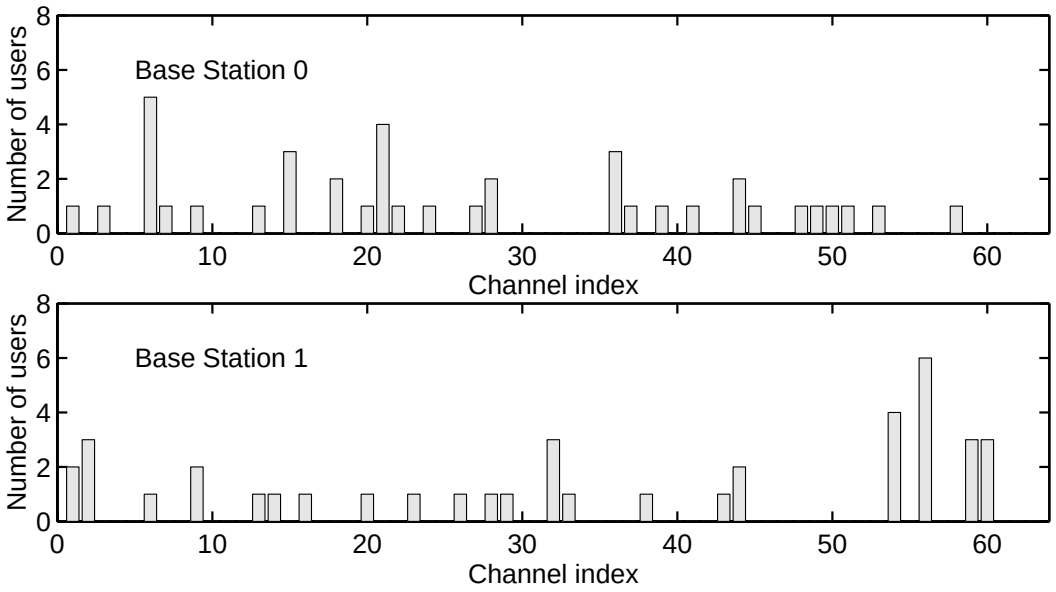

Figure 10.5: Number of users on each channel for algorithm CCL: traffic load of 40 Erlangs per cell, without power control: 80% of pedestrians and 20% of vehicles.

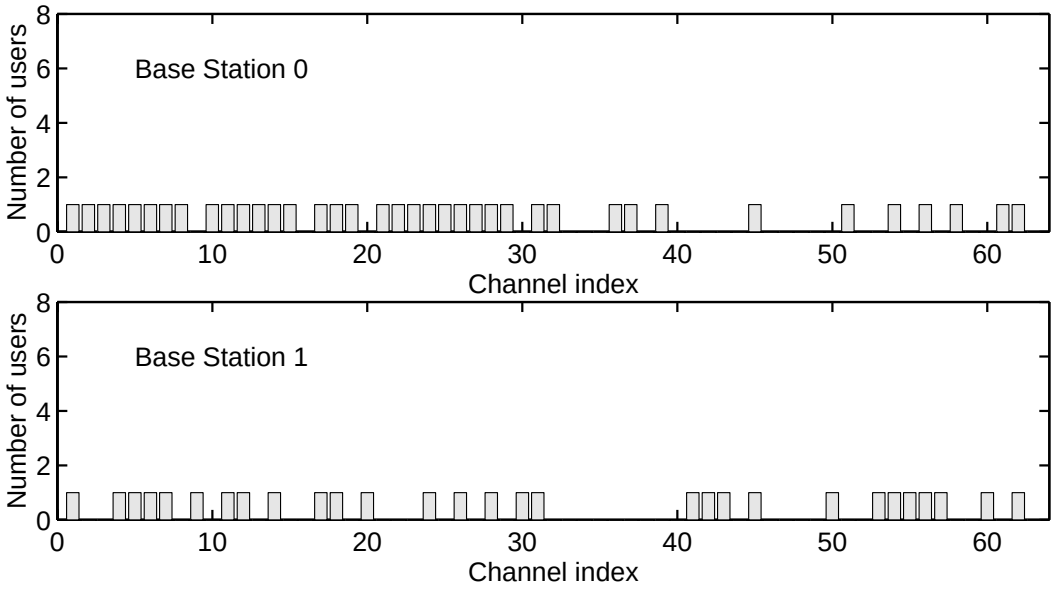

Figure 10.6: Number of users on each channel for algorithm ECL: traffic load of 40 Erlangs per cell, without power control: 80% of pedestrians and 20% of vehicles.

the other cell.

For comparison purpose, Figure 10.6 shows the channel usage at two base stations for ECL algorithm and traffic 40 Erlangs per cell. At the particular moment shown in Figure 10.6, no channel is reused within the cells, which emphasizes the strategy of ECL, which is "duplicate last."

It should be noted that unavailability of channels, even though idle, due to high interference also occurs in non-SDMA systems, using dynamic channel allocation. In fact, high interference on some channels is what limits capacity in systems employing dynamic channel allocation. Not all channels can be used by a particular base station, due to high interference level. In SDMA systems, if channel allocation is not appropriated performed, this situation is more pronounced due to the fact that a channel can be reused several times within cells.

Note from Figure 10.4 that, when ARP is used, base stations reuse some channels as many as three times within the cells, while with CCL, some channels are reused up to 4.5 times. However, the maximum carried traffic with ARP is higher than that when CCL is used. The reason for the performance difference between ARP and CCL is that, as already noticed in Chapter 9, ARP creates a structured channel reuse pattern among the cells, reducing the overall interference level. On the other hand, CCL algorithm just selects the most used channels, which, in fact, increases the level of interference on those channels. This strategy

causes CCL to have a poor performance in all aspects: high channel reassignment request rate, outage probability and dropping probability. Therefore, in SDMA environment, the allocation strategy used in ARP is more convenient than that used in CCL.

Figure 10.4 also explains the low performance of LIA algorithm in SDMA systems. Few channels are reused within cells, since LIA tries to minimize interference on all channels.

The results and analysis presented above show that allocation algorithms for SDMA systems must use appropriately the information about the interference level on the channels. The results of CCL algorithm emphasizes that the lack of structured channel reuse pattern leads to inefficient algorithms and poor performance.

Versions of the algorithms CCL and ECL, called *first duplicate* (FD) and *duplicate at last* (DL), respectively, have been analyzed in [94] using a theoretical approach in a simple scenario. FD algorithm attempts to allocate channels that are already in use within the cell. If it is not possible to reuse any channel, an idle channel is allocated. DL algorithm tries to allocate an idle channel before reusing a channel already in use. Expressions for blocking probability for both algorithms are derived in [94] for the case of two channels. A key element in the expressions is the probability P_S that a channel can be reused within the cell. When FD and DL are compared assuming the same probability P_S, the system using FD algorithm carries higher traffic than the system using DL algorithm, as shown in [94]. However, the probability P_S is a function of the interference level on the channels, and P_S for FD algorithm tends to be lower than for DL algorithm. Therefore, the FD algorithm should be compared to DL algorithm assuming a lower P_S for the former. When the appropriate values of P_S are used for each algorithm, it is expected, based on the analysis presented here, that DL algorithm outperforms FD algorithm.

Performance degradation due to user mobility

Let us now analyze the degradation of the performance of the algorithms LIA, ARP, CCL and ECL due to user mobility. Table 10.4 shows the carried traffic at blocking probability 2% for user profiles Hybrid I (20% vehicular) and Hybrid II (80% vehicular), for LIA, ARP, CCL and ECL. The carried traffic degradation due to higher user mobility level is less than 11%, as shown in Table 10.4.

However, strong effects of user mobility are observed on other performance parameters. A fair analysis of the effects of mobility on the performance is carried out by assuming the same traffic load for both user profiles. Table 10.5 shows the blocking probability (P_B),

Table 10.4: Carried traffic per cell and traffic degradation for each algorithm without power control, at blocking probability 2%, under different user profiles and without power control: Hybrid I - 20% vehicular; Hybrid II - 80% vehicular.

	Carried traffic per cell (Erl/cell)		
Algorithm	**Hybrid I**	**Hybrid II**	**Degradation (%)**
LIA	21.0	20.8	1.0
ARP	36.7	32.7	10.9
ECL	31.6	28.9	8.5
CCL	25.8	24.0	7.0

Table 10.5: Comparison of system performance under two user profiles: P_B = blocking probability, P_D = dropping probability, R_{re} = channel reassignment request rate and P_{out} = outage probability at $\Gamma_0 = 17$ dB - without power control.

		User Profile							
		Hybrid I				**Hybrid II**			
Algorithm	Traffic Erl/cell	P_B (%)	P_D (%)	R_{re}	P_{out} (%)	P_B (%)	P_D (%)	R_{re}	P_{out} (%)
LIA	21.0	2.00	0.28	0.47	2.3	2.10	0.28	1.45	4.3
ARP	36.7	2.00	0.20	1.27	6.5	4.92	1.07	4.18	12.0
ECL	31.6	2.00	0.23	1.10	4.8	2.82	0.70	3.39	9.3
CCL	25.8	2.00	0.50	1.75	9.1	3.45	0.75	4.23	13.1

dropping probability (P_D), channel reassignment request rate (R_{re}) and outage probability at $\Gamma_0 = 17$ dB (P_{out}) for all algorithms under different user profiles, but the same traffic load. The traffic load used for each algorithm is the one that results in 2% of blocking probability for user profile Hybrid I (predominantly pedestrian). Of particular interest in this table is the effect of mobility on the number of channel reassignment requests. Figure 10.7 shows the increase in the number of reassignments in percentage due to higher mobility level (from user profile Hybrid I to Hybrid II). Channel reassignments are requested whenever $SINR$ on either uplink or downlink drops below threshold $\Gamma_{th,re}$. When SDMA is used, low $SINR$ can be caused by interference from other cells, like in non-SDMA systems, and, additionally, by in-cell interference. In-cell interference is generated through two mechanisms. In order to understand them, suppose that two mobiles A and B are sharing the same channel, as depicted in Figure 10.8. The first mechanism that causes $SINR$ degradation occurs when the

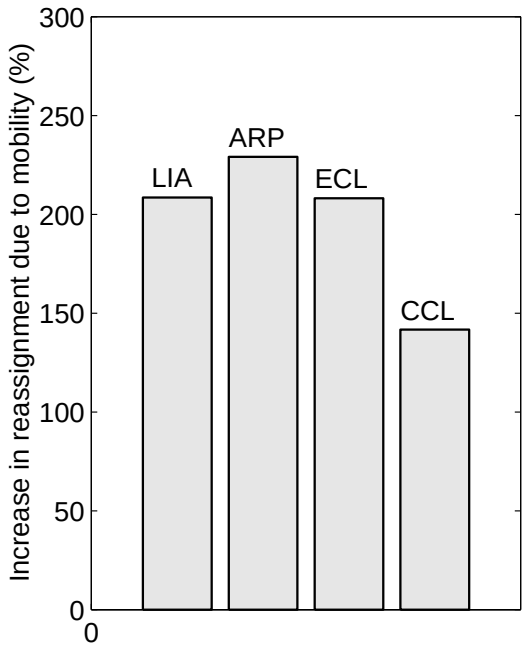

Figure 10.7: Performance degradation due to mobility: increase in the channel reassignment request rate when 80% of users are vehicular (profile Hybrid I) with respect to the case when only 20% of users are vehicular (profile Hybrid I) - no power control.

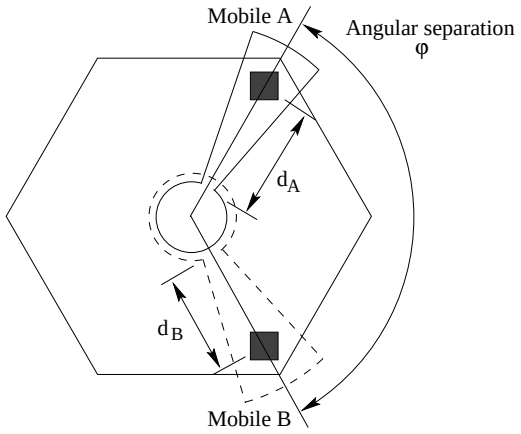

Figure 10.8: Two in-cell users sharing the same channel.

mobiles get too close to each other (small angular separation φ), such that the antenna beams "collide" and spatial filtering is no longer possible. The second mechanism regards the T-R separation distances d_A and d_B. If the ratio d_A/d_B is too large or too small, the attenuation provided by the side lobe of the antenna will not be enough to guarantee the desired $SINR$. Ideally, in fixed transmitted power systems, the ratio d_A/d_B of all in-cell mobiles sharing the same channel should be close to one. These two mechanisms are discussed in Chapter 6. Therefore, all in all, in SDMA systems there are three mechanisms that cause channel reassignment: (i) interference from other cells, (ii) beam collision and (iii) too large or too small ratio d_A/d_B. Note that, even though CLL is the less sensitive algorithm to mobility, its channel reassignment rates are the highest ones for both users profiles. The reason is that, by maximizing the channel reuse within the cell, the effects of mechanisms (ii) and (iii) are emphasized.

Table 10.5 also shows that outage probability follows the same trend observed in the channel reassignment rate, that is, there is a considerable increase in the interference level as the mobility level increases.

At this point we can analyze the overall performance of the algorithms using Table 10.3. Among all four algorithms, ARP is the one that provides the highest carried traffic for both user profiles, while LIA provides the smallest carried traffic. When we compare the reassignment rate, we see that there is a strong correlation between carried traffic and channel reassignment request rate and outage probability: High carried traffic is at the expense of a large number of channel reassignments in order to keep the link quality at a acceptable level. The reason is that high capacity is achieved by packing closer calls, that is, reusing channels more often, which increases interference level and reassignment requests. However, as the results for CCL algorithm show, high interference does not mean that high capacity has been achieved.

10.5 Controlled Transmitter Power

Let us now add power control in the system and analyze which algorithm benefits most from the interference reduction provided by power control. We use the $SINR$ balancing power control technique, describe in Section 5.4, with continuous power adjustment and parameters described in Table 8.7. The target $SINR$ is set to $\Gamma_T = 21$ dB.

Just as done for the case of no power control, let us compare the performance of LIA and

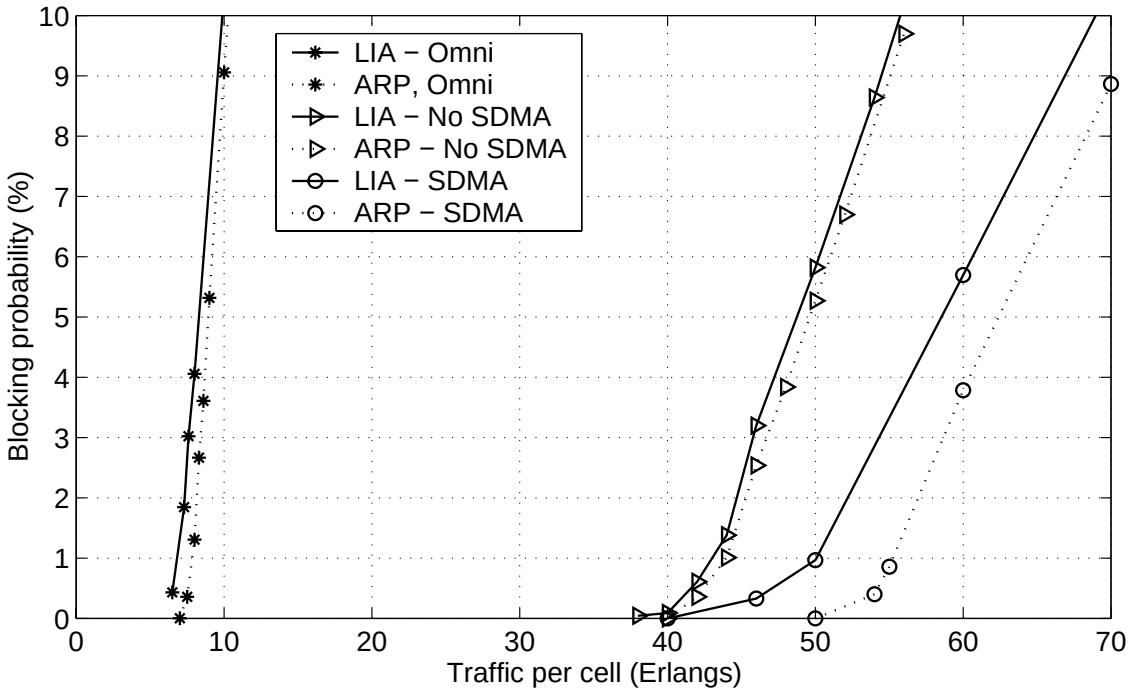

Figure 10.9: Blocking probability for LIA (solid curves) and ARP (dotted curves) with different base station antennas and operation modes, with power control. User profile: Hybrid I.

ARP with power control for different scenarios, regarding how spatial filtering is employed. Figure 10.9 shows the blocking probabilities for LIA and ARP with power control for (*i*) omnidirectional base station antennas, (*ii*) adaptive base station antennas, in non-SDMA mode and (*iii*) adaptive base station antennas in SDMA mode. The population of users consists of 80% of pedestrians

Unlike for the fixed transmitter power case, LIA does use the permission to reuse channels within cells when transmitter power is controlled. With power control, co-channel interference is reduced, allowing more channels to be reused among cells and, additionally, several channels are reused within cells.

Figure 10.10 shows the blocking probabilities for LIA, ARP, ECL and CCL algorithms in SDMA mode. As done before, we present in Table 10.6 the performance of all algorithms at blocking probability 2%. A comparison between the blocking probabilities with and without power control (see Figure 10.3) clearly shows the capacity improvement achieved by using power control. Even though ARP still provides the highest carried traffic, other algorithms use the interference reduction provided by the use of power control more efficiently than

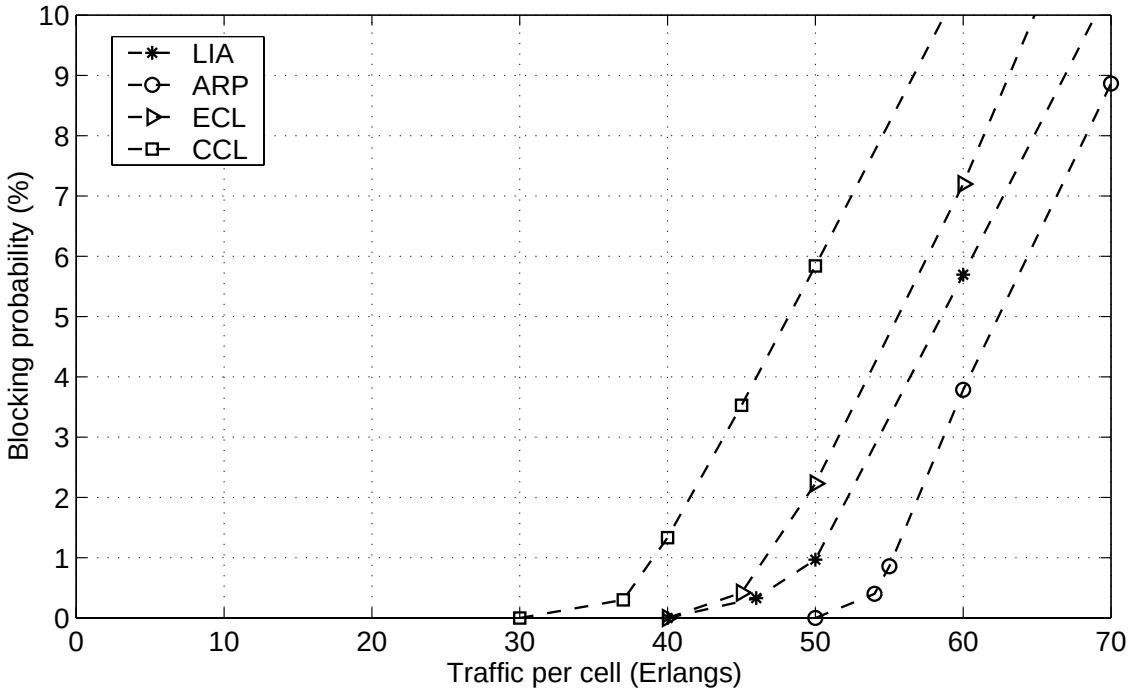

Figure 10.10: Blocking probability for different allocation algorithms and with power control in SDMA mode. User profile: Hybrid I.

Table 10.6: System performance at blocking probability 2% for several allocation strategies and with power control and user profile Hybrid I; outage probability computed at $\Gamma = 17$ dB.

Allocation Algorithm	Carried Traffic Erlangs/cell	Dropping Prob. (%)	Reassign. Requests per call	Outage Prob. (%)
LIA, Omni	7.30	0.21	3.30	10.0
ARP, Omni	8.20	0.24	3.80	11.5
LIA, No SDMA	44.7	0.06	0.80	3.1
ARP, No SDMA	45.3	0.07	1.35	5.8
LIA, SDMA	52.2	0.12	0.88	3.5
ARP, SDMA	56.9	0.10	1.54	6.7
ECL, SDMA	49.4	0.17	1.36	5.4
CCL, SDMA	41.5	0.25	1.24	5.0

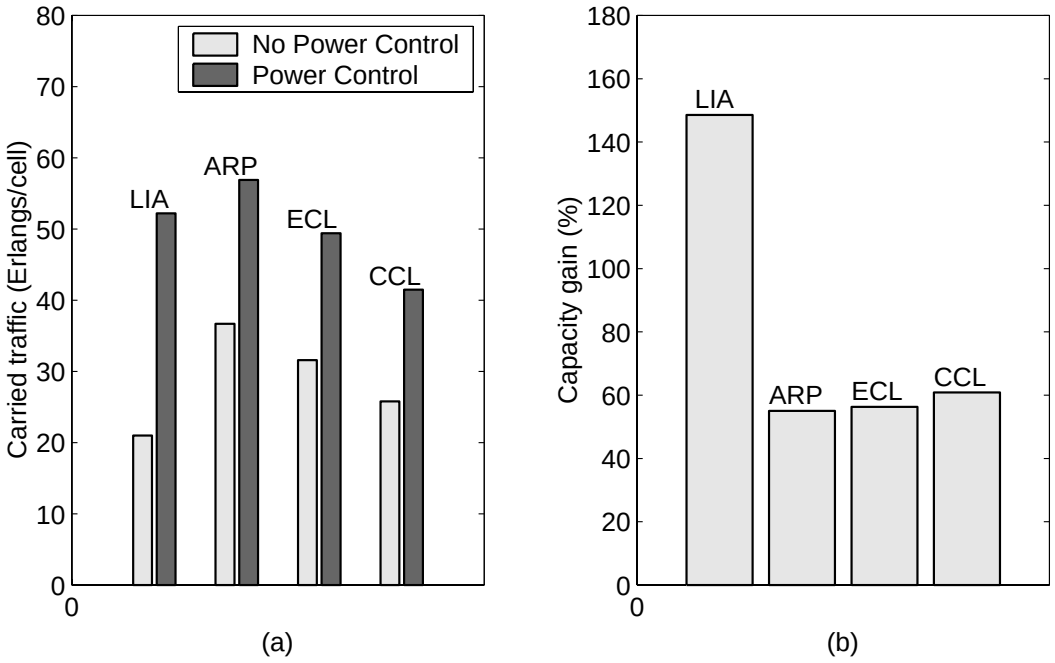

Figure 10.11: Capacity improvement by using power control for user profile Hybrid I: (a) carried traffic per cell at blocking probability 2%, (b) capacity gain due to the use of power control.

ARP. Figure 10.11 (a) shows the carried traffic for each algorithm with and without power control, at $P_B = 2\%$, while Figure 10.11 (b) shows the carried traffic improvement achieved by using power control, with respect to the case without power control. We see that LIA is the algorithm that uses the benefits of power control more efficiently.

The higher capacity achieved with power control is due to two distinct mechanisms: (1) power control leads to smaller reuse distance, as observed in non-SDMA systems in Chapters 8 and 9, and (2) power control allows more in-cell users to share the same channel. The effects of these two mechanisms can observed in Figure 10.12, which shows the distribution of the average number of users on the same channel at a traffic load of 60 Erlangs per cell and with power control. Comparing this figure with the corresponding figure for the case of without power control (Figure 10.4), we see that, for ARP, LIA and ECL, power control increases the number of channels effectively used in the cells. In addition, again for ARP, LIA and ECL, power control allows more channels to be reused within the cells. On the other hand, power control affects the performance of CCL differently. With power control, CLL reuses more channels within the cells, compared to the case without power control. However, fewer channels are used by each cell, due to the increased level of interference caused by the

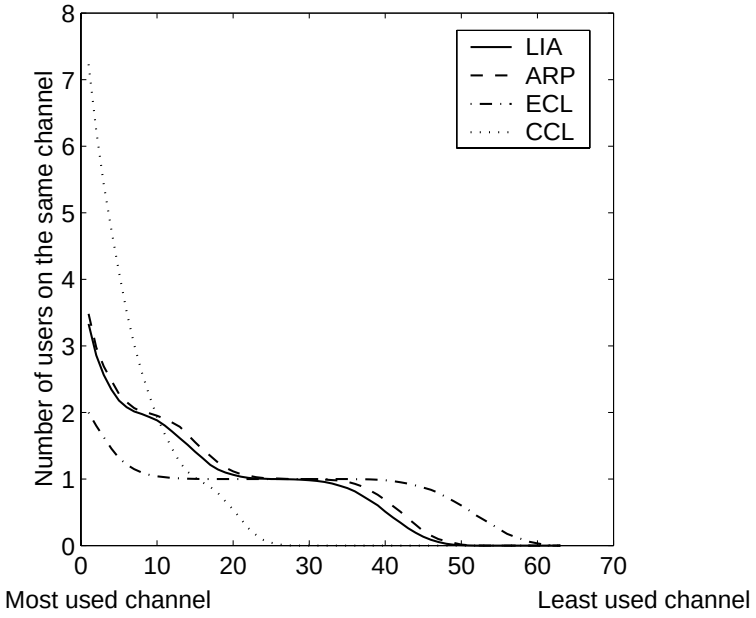

Figure 10.12: Distribution of the average number of users on the same channel at traffic load of 60 Erlangs per cell, for several allocation strategies, with power control and user profile Hybrid I.

large number of users sharing the same channel.

As a negative effect, the use of power control tends to increase the number of channel reassignment requests per call and outage probability. This side effect of power control was discussed in Chapter 9. With power control, calls are packed closer, decreasing the reuse distance. Therefore, any disturbance due to mobility, call arrival and propagation effects, can degrade the link quality, which may lead to channel reassignments.

Let us now analyze the effects of mobility on the performance when power control is used. Table 10.7 compares the carried traffic at 2% of blocking probability for the case with power control for both user profiles. As we have observed for the case of without power control, mobility causes little degradation on the carried traffic.

However, the "immunity" of carried traffic to mobility is at the expense of strong negative effects on other performance parameters. As we have done for the case of no power control, let us compare the performance of all algorithms for both user profiles, when the algorithms operate at the same traffic level. Table 8.8 shows the blocking probability (P_B), dropping probability (P_D), channel reassignment request rate (R_{re}) and outage probability at $\Gamma_0 = 17$ dB (P_{out}) for all algorithms. The traffic load used for each algorithm is the one that results in a blocking probability of 2% for user profile Hybrid I (predominantly pedestrian). Comparing

Table 10.7: Carried traffic per cell and traffic degradation for each algorithm with power control, at blocking probability 2%, under different user profiles and without power control: Hybrid I - 20% vehicular; Hybrid II - 80% vehicular.

	Carried traffic per cell (Erl/cell)		
Algorithm	**Hybrid I**	**Hybrid II**	**Degradation (%)**
LIA	52.2	50.8	2.7
ARP	56.9	55.7	2.1
ECL	49.4	46.9	5.1
CCL	41.5	40.4	2.7

Table 10.8: Comparison of system performance with power control under two user profiles: P_B = blocking probability, P_D = dropping probability, R_{re} = channel reassignment request and P_{out} = outage probability at $\Gamma_0 = 17$ dB.

		User Profile							
		Hybrid I				**Hybrid II**			
Alg	Traffic Erl/cell	P_B (%)	P_D (%)	R_{re}	P_{out} (%)	P_B (%)	P_D (%)	R_{re}	P_{out} (%)
LIA	52.2	2.0	0.12	0.9	3.5	2.7	0.33	3.0	4.3
ARP	56.9	2.0	0.10	1.5	6.7	2.5	0.11	4.8	12.0
ECL	49.4	2.0	0.17	1.4	5.4	3.0	0.27	4.1	9.3
CCL	40.5	2.0	0.25	1.2	5.0	2.3	0.23	3.4	13.1

the values in Table 8.8 for different user profiles, we see that, although blocking and dropping probability are not seriously affected by a higher level of mobility, the number of channel reassignment requests increases considerably. The reason why higher level of user mobility leads to more channel reassignment requests was explained before, for the case of without power control.

10.6 Conclusion

We have analyzed in this chapter the performance of several algorithms in SDMA systems. Two of the algorithms, namely ECL and CCL, explicitly attempt to benefit from the fact that, in SDMA, channels can be reused within cells. While CCL tries to reuse channels within cells as much as possible, ECL tries to uniform the load of traffic over all channels available in the cell. The other two algorithms, LIA and ARP, are not particularly designed for SDMA systems. LIA attempts to minimize the interference level on all channels, while ARP tries to create a structured channel reuse pattern throughout the entire coverage area.

Simulation results have shown that, with fixed transmitter power, the strategy used in LIA does not give good results in terms of carried traffic in SDMA systems. Channels already in use will have higher interference level than idle channels, and channel reuse within the cell will happen very seldom with LIA. When power control is used, the reduced interference allows channels to be reused more often not only among cells, but also within cells.

On the other hand, ARP with fixed transmitter power seems to use the permission to reuse channel within the cells. The channel reuse pattern, among the cells and within the cells is organized in a such structured way that leads to the highest carried traffic among all algorithms studied in this chapter.

Simulation results also showed that the strategy of maximizing the number of channels that are reused within the cells does not lead to high capacity. It actually leads to high levels of interference, which limits capacity.

We also analyzed the performance degradation due to user mobility. Results have shown that, while carried traffic is not severely affected by higher level of user mobility, other performance parameters, such as number of channel reassignment requests and outage probability, are strongly affected.

Chapter 11

Summary and Future Work

This dissertation has presented an analysis of resource allocation algorithms combined with adaptive antennas. In this chapter, we summarize the results and present some suggestions for future related work.

11.1 Summary of Contributions and Conclusions

In Chapter 4, we analyzed the capacity improvement achieved by reducing cluster size and controlling the increased co-channel interference by using narrowbeam antennas combined with the fractional loading factor. Capacity gains as high as 477% with respect to the reference system (cluster size $N = 7$, tri-sectorized cells) were observed, but at the expense of large antenna side lobe level reduction and narrow beamwidth. The simulation results show that, as expected, beamwidth and side lobe level play an important role in the capacity gain. However, when the fractional loading factor was introduced, we showed that the relationship between antenna parameters, the cluster size and the capacity gain may change in a non-intuitive fashion. An important conclusion from the results is the importance of the fractional loading factor. In most of the cases shown here, minimum acceptable system performance was achieved because of the *combined use* of narrowbeam smart antennas and fractional loading factor, allowing cluster size reduction. This means that low complexity antennas can be used and still provide system capacity gain, while decreasing cluster size.

In Chapter 8, we also analyzed the capacity improvement achieved by reducing cluster size and controlling the increased co-channel interference. In this chapter, however, user mobility, handoff and channel reassignment were considered, and adaptive antennas were

combined with power control. Simulation results showed that, for fixed transmitter power, large side lobe level reduction (high complexity antennas) is required to achieve the maximum capacity available (given by the number of channels allocated to each cell). For example, for beamwidth $BW = 45^o$ and cluster size $N = 3$, a side lobe level of -40 dB is required to achieve 93% of the maximum available capacity. However, when power control is used, the additional interference reduction provided by power control may be enough to achieve the maximum available capacity, even with small side lobe reduction (low complexity). For example, for $BW = 45^o$ and $N = 3$, a side lobe level of -12 dB is enough to achieve 93% of the available capacity. Simulation results also showed that the higher capacity achieved with power control may be at the expense of a larger number of channel reassignment requests.

In Chapter 9, we analyzed the combined application of adaptive antennas, dynamic channel allocation and power control in cellular systems. Two allocation algorithms were analyzed, namely LIA and ARP. For fixed transmitter power, LIA and ARP transform the reduced co-channel interference provided by the use of adaptive antennas into higher carried traffic with similar efficiency. However, ARP provides a higher carried traffic per cell than LIA, due to the structured reuse pattern created by ARP. When adaptive antennas, dynamic channel allocation and power control are combined, results showed that LIA uses more efficiently the additional interference reduction achieved by using power control. Due to the fact that transmitter power is now controlled, ARP is not able to create an efficient channel reuse pattern. With small side lobe level, both algorithm were able to reuse almost all channels available for the entire system among all cells.

Finally, the performance of several allocation algorithms in SDMA systems were analyzed in chapter 10. Two of the algorithms, ECL and CCL, explicitly attempt to benefit from the fact that, in SDMA, channels can be reused within the cells. Algorithms ECL and CCL are often analyzed for application in SDMA systems. The other two algorithms, LIA and ARP, are not particularly designed for SDMA systems. However, ARP is the most efficient algorithm among all algorithm studied, while CCL is the worst algorithm regarding not only carried traffic, but the number of reassignment requests. Simulation results show that *too timid* algorithms (LIA) or *too aggressive* algorithms (CCL) are not efficient in the SDMA environment. Timid algorithms do not use the permission to reuse channels within the cells, while aggressive algorithms overuse channels within the cells, increasing co-channel interference.

The analysis presented in this dissertation showed not only the benefits of combining

adaptive antennas, power control and dynamic channel allocation in terms of capacity improvement, but also the effects on other performance parameters. We showed that high capacity can be achieved by combining resource allocation techniques and adaptive antennas while maintaining a minimum acceptable link quality, but at the expense of the degradation of some other performance parameters (for example, a large number of channel reassignment requests, which increases the load on the control channel). The well known trade-off between capacity and link quality in cellular systems has now other components playing important roles.

A new accuracy analysis of Schwartz & Yeh and Fenton-Wilkinson's methods for computing the mean and standard deviation of the sum of lognormal random variables is presented in Chapter 3. Unlike previous works, we compared the accuracy of both methods when *the mean values and standard deviations of the summands are different*. We found that the accuracy of Fenton-Wilkinson's method is more sensitive to the difference between the standard deviations and means of the summands, than Schwartz & Yeh's method.

11.2 Future Work

- Throughout this dissertation, the radiation pattern of adaptive antennas were simulated using the average side lobe level and main beam with constant gain. Also, the channel model did not included multipath propagation. The next step in this research would be to analyze the performance of some representative beamforming techniques in the context studied in this dissertation, and include spatial information in the propagation channel model.

- In Chapters 8, 9 and 10, we simulated a cellular system with N_C traffic channels in circuit-switched mode. With the growing demand for data services, such as broadband multimedia services, video conferencing, and Internet access, the analysis of the combined application of adaptive antennas, power control and dynamic channel allocation in *packet-switched* systems becomes very important.

- The simulated cellular system used in Chapter 8, 9 and 10 assumed that the exact values of $SINR$ required for channel allocation were available at both base station and the mobile. When $SINR$ is estimated using, for example, the techniques listed in Appendix B, estimation errors may affect system performance.

- The dynamic channel allocation algorithms studied in Chapter 10, for SDMA systems, did not use any angle of arrival information in the process of allocating a channel. Angle of arrival information and mobile's direction of movement may be used to improve the performance of allocation algorithms and reduce channel reassignment rate.

- The effects of non-uniform user distribution on the performance of cellular systems using adaptive antennas, especially SDMA systems, must be investigated.

- In the work presented in Chapter 4, we implemented call admission control simply by adjusting the number of active cells, according to the desired loading factor p_{ch} and probability P_n of having n active cells. This implementation is valid in the context of the work presented in Chapter 4, since a statistical analysis of the performance of a cellular system is performed.

  On the other hand, call admission control was implemented in the systems simulated in Chapters 8, 9 and 10 by using admission threshold ($\Gamma_{adm,new}$ and $\Gamma_{adm,re}$)

  Another implementation of call admission control that can be analyzed is based on hard limiting the number of channels that can be simultaneously in use within a cell. If the number of channels in use at the serving base exceeds a given limit, calls are blocked.

11.3 Publications

- P. Cardieri, T.S. Rappaport, "Combined Effects of Narrowbeam Antennas and Fractional Loading Factor in Forward Link Cellular Communication Systems", *49th IEEE Vehicular Technology Conference*, May 1999.

- P. Cardieri, T.S. Rappaport, "Statistics of The Sum of Lognormal Variables in Wireless Communications", *50th IEEE Vehicular Technology Conference*, pp. 1823-1827, May 2000.

- P. Cardieri, T.S. Rappaport, "Statistics Analysis of Co-channel Interference in Wireless Communications Systems", accepted for publication in *Wireless Communications and Mobile Computing Journal*, published by John Wiley & Sons, Inc..

- P. Cardieri, T.S. Rappaport, "Application of Narrowbeam Antennas and Fractional Loading Factor in Cellular Communication Systems," accepted for publication in *IEEE Transactions on Vehicular Technology*.

- R. Ertel, P. Cardieri, K.W. Sowerby, T.S. Rappaport, J.H. Reed, "Overview of Spatial Channel Models for Antenna Array Communication System", *IEEE Personal Communications Magazine*, pp. 10-22, February 1998

Appendix A

Interference from Co-channel Tiers

Consider the forward link of a cellular systems with cluster size N, T tiers of co-channel cells and cell radius R. Assuming hexagonal shapes for the cells, the i-th tier of co-channel cells has $6i$ cells. A mobile station located at the cell boundary, as shown in Figure A.1, experiences worst case co-channel interference. Assuming that all base stations are equipped with omnidirectional antennas and transmit the same power $P = 1$, the total area mean co-channel interference, I_T, at a mobile located at the cell boundary is

$$I_T = \underbrace{\frac{1}{d_{1,1}^{\gamma}} + \cdots + \frac{1}{d_{1,6}^{\gamma}}}_{\textit{from the 1st tier}} + \underbrace{\frac{1}{d_{2,1}^{\gamma}} + \cdots + \frac{1}{d_{2,12}^{\gamma}}}_{\textit{from the 2nd tier}} + \cdots \underbrace{\frac{1}{d_{T,1}^{\gamma}} + \cdots + \frac{1}{d_{T,6T}^{\gamma}}}_{\textit{from the } T\textit{-th tier}}, \tag{A.1}$$

where γ is the path loss exponent and $d_{i,k}$ is the transmitter to receiver distance between the k-th base station in the i-th tier, where k assumes the values $k = 1, 2, \cdots, 6i$. Since the base stations in the first tier are closer to the mobile at the cell boundary than the other base stations, we use the exact distances $d_{1,k}$ in (A.1) for the base station in the first tier. For more distant tiers, we approximate all distances between the base station in a given tier i and the mobile as $d_{i,k} = \overline{d}_i = (d_{i,max} + d_{i,min})/2$, for all k, where $d_{i,max} = i\sqrt{(3N)}R$ and $d_{min} = i\,3NR/2$ are the maximum and minimum distances, as shown in Figure A.1. Thus

$$\overline{d}_i = i\left(\frac{\sqrt{3}+2}{4}\right)\sqrt{3N}\,R = i\,\overline{D} \tag{A.2}$$

Let I_1 denote the total area mean co-channel interference received from the base stations in the *first* tier:

$$I_1 = \frac{1}{d_{1,1}^{\gamma}} + \cdots + \frac{1}{d_{1,6}^{\gamma}}, \tag{A.3}$$

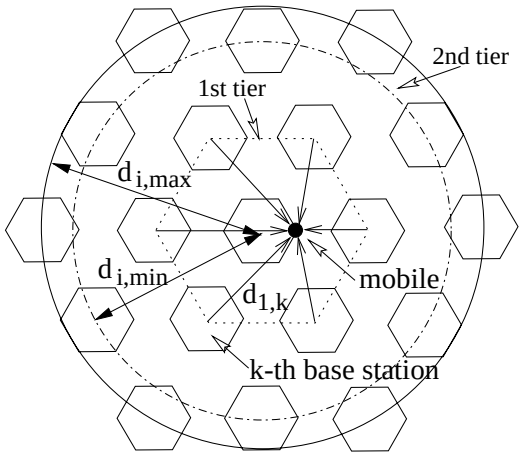

Figure A.1: Co-channel cells in the forward link cellular system: $d_{i,k}$ is the transmitter to receiver distance between the k-th co-channel base station ($k = 1, 2, \cdots, 6i$) in tier i, and the mobile.

Also, let I_{2+} denote the total mean co-channel interference *from tier 2, 3, $\cdots$, T*, using the approximation in (A.2)

$$\begin{aligned} I_{2+} &= \frac{12}{(2\,\overline{D})^\gamma} + \frac{18}{(3\,\overline{D})^\gamma} + \cdots + \frac{6T}{(T\,\overline{D})^\gamma} \\ &= \frac{6}{\overline{D}^\gamma}\left(\sum_{t=1}^{T} \frac{1}{t^{\gamma-1}} - 1\right). \end{aligned} \tag{A.4}$$

Thus

$$I_T = I_1 + \frac{6}{\overline{D}^\gamma}\left(\sum_{t=1}^{T} \frac{1}{t^{\gamma-1}} - 1\right). \tag{A.5}$$

The fraction of total co-channel interference, I_T, that corresponds to the interference from the first tier is given by the ratio $\epsilon = I_1/I_T$. Table A.1 presents the computed values of ratio ϵ, for cluster sizes $N = 1$, 3, 4 and 7, and path loss exponents $\gamma = 3$, 4 and 5, when T tends to infinite. Note that the sum in (A.5) *does not* converge when T tends to infinite, for a path loss exponent of 2. This means that the fraction of total interference that corresponds to the interference from the first tier goes to zero, when free space propagation ($\gamma = 2$) is assumed. We see from Table A.1 that, for path exponent $\gamma = 4$, the area mean interference from the first tier accounts for at least 82% of total interference. Denote SIR_T as *SIR* computed using the total interference I_T, and denote SIR_1 as *SIR* computed using the interference from the first tier I_1. Using dB units, we have:

$$\begin{aligned} SIR_1 &= 10\log\left(\frac{S}{I_1}\right) \\ &= SIR_T - 10\log(\epsilon), \end{aligned} \tag{A.6}$$

Table A.1: Ratio of the interference (ϵ) from the base stations in the first tier (I_1) to the total interference (I_T), for cluster sizes $N = 1$, 3, 4 and 7, and path loss exponents $\gamma = 3$, 4 and 5.

	$\epsilon = I_1/I_T$ (%)			
γ	$N = 1$	$N = 3$	$N = 4$	$N = 7$
3	72.0	62.3	60.4	58.4
4	92.4	85.8	84.0	82.0
5	98.0	94.7	93.5	92.1

where $S = 1/R^\gamma$ is the desired area mean signal received at the mobile. Therefore, the error caused by considering only the first tier when computing the area mean *SIR* is less than 1 dB ($10 \log 0.82 \approx -0.9$ dB), for path loss $\gamma = 4$ and cluster sizes $N = 1$, 3, 4 and 7.

Consider now that shadowing fading is taken into account in the computation of *SIR*, and the mobile is uniformly distributed over the cell area. The forward link area averaged *SIR* at the mobile is computed by simulation, assuming a cellular system with a large number of tiers with omnidirectional base stations. We assume 15 tiers, which corresponds to 720 co-channel cells. Path loss $\gamma = 4$ and shadowing standard deviation $\sigma = 6$ dB are assumed. Figure A.2(a) and (b) compare the probabilities $P[SIR > SIR_0]$ when *all 15 tiers* are considered and when *only the first tier* is considered, for cluster size $N = 1$, 3, 4 and 7. We see that the error induced by considering only the first tier is small. Assuming that we are interested in a reliability of 95%, we computed the required values of SIR_0 such that $P[SIR > SIR_0] = 95\%$, for the cases with 15 tiers (denoted by $SIR_0^{(15)}$) and only one tier (denoted by $SIR_0^{(1)}$). Figure A.2(c) shows that the difference $\Delta SIR_0 = SIR_0^{(1)} - SIR_0^{(15)}$ is smaller than 1.1 dB for cluster sizes $N = 1$, 3, 4 and 7. Using the same approach used for the forward link, it can be shown that the results presented in this appendix are valid for the reverse link.

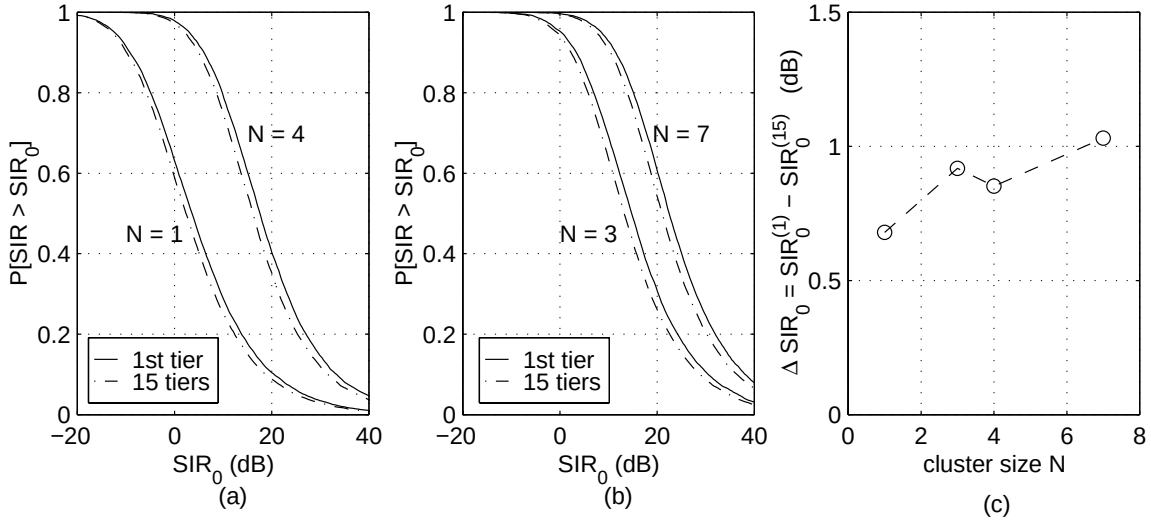

Figure A.2: Forward link $P[SIR > SIR_0]$ computed using 15 tiers and only the first tier, with path loss exponent $\gamma = 4$, shadowing standard deviation $\sigma = 6$ dB and omnidirectional base station antennas: (a) cluster sizes $N = 1$ and 4; (b) cluster sizes $N = 3$ and 7; (c) Difference $\Delta SIR_0 = SIR_0^{(1)} - SIR_0^{(15)}$ between the required values of SIR_0 such that $P[SIR > SIR_0] = 95\%$, for the cases with only one tier and all 15 tiers.

Appendix B

Signal-to-Interference Ratio Measurement

Signal-to-interference-plus-noise ratio ($SINR$) is very often used as a measure of link quality in channel allocation, channel reassignment, handoff and power control algorithms. Estimation of $SINR$ are, therefore, required in several different situations regarding the status of the channel to be measured. For example, during allocation of a channel to a new call, $SINR$ must be estimated on channels that are not allocated to the mobile originating the call. On the other hand, in order to check whether channel reassignment is needed or not, $SINR$ must be measured on the channel currently in use. Therefore, the situations where $SINR$ needs to be estimated can be grouped as follows:

- MS and BS are requested to measure $SINR$ on their allocated channels,
- MS and BS are requested to measure $SINR$ on channels different from their allocated channels.

Even though in this dissertation we assume that the exact values of uplink and downlink $SINR$s are available whenever they are needed, we briefly discuss in this appendix how $SINR$s can be estimated in these two classes of situations.

MS and BS are requested to measure $SINR$ on their allocated channels

In order to check whether channel reassignment is necessary or not, MS and BS need to measure $SINR$ on the channels currently allocated to them.

Since BS and MS are connected to each other through traffic channels (downlink and uplink), direct measurement of *SINR* is not possible. The reason is that, when the power level on the traffic channel is measured, the BS (or MS) is actually measuring $S+I+N$, where S the desired signal power, I is the total interference, and N is the thermal noise power. For high values of *SINR*, we can approximate $S \approx S + I + N$. However, this approximation is not always appropriate, since the estimation of *SINR* is more important when *SINR* is low (i.e. when channel reassignment is needed). Also, we still need to estimate $I + N$ to be able to compute *SINR*. In order to overcome this problem, several approaches have been proposed:

- Signal processing on the received training sequence: This technique is appropriate for TDMA systems. The frames of TDMA cellular systems, such as IS-54 and GSM, contain known training sequences that can be used for SINR estimation [100, 101].
- Estimate *SINR* based on eye-opening and error rate measurements [102].

MS and BS are requested to measure $SINR$ on channels different from their allocated channels

This case occurs during channel allocation to new calls, when MS and BS are connected with each other through control channel, and $SINR$ must be measured on candidate traffic channels. Another typical situation occurs during intercell or intracell handoffs, when now BS and MS are connected through a traffic channel and $SINR$ must be measured on other traffic channels. The measurement of $SINR$ on downlink and uplink can be performed as follows:

- **Downlink link:** The MS measures the received power level of the total interference I plus noise on each candidate channel, and reports the measurements to the BS through the control channel or the currently allocated traffic channel. The desired received power S from the serving BS must be indirectly estimated: the MS measures the received power level on the control channel or currently allocated traffic channel, and reports the result to the BS. Since the BS transmitter power is known at the BS, the path loss between the BS and MS on the forward link can be estimated. Based on the path loss, the desired received power at the MS on the traffic channels can be estimated. Note that, when the measurement is made on the control channel, we assume that the propagation channels on the traffic and control channels are similar.

- **Reverse link:** The BS measures the received power level on each idle channel (total interference I). Note that the desired MS is not transmitting on the traffic channel to be measured and, therefore, the power level I measured by the base station corresponds to interference plus noise. To estimate the desired signal S on a particular traffic channel, the BS can measure the received power from the MS on the control channel or traffic channel used by the MS. Again, assuming that the propagation channels on traffic and control channels are similar, we can estimate the received power on any traffic channel based on the measurement on a particular control channel.

Bibliography

[1] T.S. Rappaport, *Wireless Communications - Principles and Practice*, New Jersey, NJ, Prentice Hall, 1996.

[2] Yacoub, M.D., *Foundations of Mobile Radio Engineering*, CRC Press, Boca Raton, 1993.

[3] R.H. Clarke, "A Statistical Theory of Mobile-Radio Reception", *The Bell Systems Technical Journal*, Vol. 47, pp. 957-1000, 1968.

[4] Lee, W.C.Y, *Mobile Communication Engineering*, McGraw-Hill, 1998.

[5] H.G. Booker, J.A. Ratcliff, D.H. Shinn, "Diffraction from an irregular Screen with applications to ionosphere problems", *IEEE Trans. Royal Society* (London), vol. 262, sec. A, 1950, p. 579.

[6] R. Ertel, P. Cardieri, K.W. Sowerby, T.S. Rappaport, J.H. Reed, "Overview of Spatial Channel Models for Antenna Array Communication System", *IEEE Personal Communications Magazine*, pp. 10-22, February 1998

[7] Lee, W.C.Y., "Effects on Correlation Between Two Mobile Radio Base-Station Antennas", *IEEE Trans. on Communications*, COM-21, pp. 1214-1224, November 1973.

[8] Jakes, W.C., *Microwave Mobile Communications*, Wiley-Interscience, 1974.

[9] Lee, W.C.Y., "Mobile Radio Signal Correlation Versus Antenna Height and Spacing", *IEEE Trans. on Vehicular Technology*, VT-25, pp.290-292, August 1977.

[10] Kalkan, M., Clarke, R.H., "Prediction of the Space-Frequency Correlation Function for Base Station Diversity Reception", *IEEE Transactions on Vehicular Technology*, vol. 46, pp. 176-184, February 1997.

[11] Turkmani, A.M.D., Arowojolu, A.A., Jefford, P.A., Kellett, C.J., "An Experimental Evaluation of the Performance of Two-Branch Space and Polarization Diversity Schemes at 1800 MHz", *IEEE Transactions on Vehicular Technology*, vol. 44, pp. 318-326, May 1995.

[12] Schwartz, M., Bennet, W.R., Seymour, S., *Communications Systems and Techniques*, McGraw-Hill, New York, 1966.

[13] Papoulis, A., *Probability, Random Variables and Stochastic Processes* 2nd edition, McGraw-Hill, 1984.

[14] L.C. Godara, "Application of Antenna Arrays to Mobile Communications, Part II: Beam-forming and Direction-of-Arrivel Considerations", *Proceedings of the IEEE*, Vol. 85, No. 8, pp. 1195-1245, August 1997.

[15] J.C. Liberti Jr., T.S. Rappaport, *Smart Antennas for Wireless Communications*, Prentice Hall PTR, Upper Saddle River, NJ, 1998.

[16] J. Litva, T.K-Y Lo, *Digital Beamforming in Wireless Communications*, Norwood, Artech House, 1996.

[17] J. Butler, R. Lowe, "Beamforming Matrix Simplifies Design of Electronically Scanned Antennas", *Electronic Design*, April 1961.

[18] M. J. Gans, "A Power Spectral Theory of Propagation in the Mobile Radio Environment", *IEEE Trans. Vehicular Techology*, vol. VT-21, pp. 27-38, February 1972.

[19] F. Adachi et al., "Crosscorrelation Between the Envelopes of 900 MHz Signals Received at a Mobile Radio Base Station Site", *IEE Proceedings.*, vol. 133, Pt. F, no. 6, pp. 506-12, October 1986.

[20] P. Petrus, J.H. Reed, *Novel Adaptive Array Algorithm and Their Impact on Cellular System Capacity*, Ph.D. Dissertation, Virginia Polytechnic Institute and State University, March 1997.

[21] A.R. Lopez, "Performance Predictions for Cellular Switched-Beam Intelligent Antenna System", *IEEE Communications Magazine*, pp. 152-154, October 1996.

[22] S.C. Swales, M.A. Beach, D.J. Edwards, J.P. McGeehan, "The Performance Enhancement of Multibeam Adaptive Base-Station Antennas for Cellular Land Mobile Radio Systems", *IEEE Trans. on Vehicular Technology*, Vol. VT-39, No. 1, pp. 56-67, February 1990.

[23] P. Zetterberg, B. Ottersten, "The Spectrum Efficiency of a Base Station Antenna Array System for Spatially Selective Transmission", *IEEE Trans. on Vehicular Technology*, Vol. VT-44, No. 3, pp. 651-660, August 1995.

[24] J.C. Liberti Jr., T.S. Rappaport, "Analysis of CDMA Cellular Radio Systems Employing Adaptive Antennas in Multipath Environments", *IEEE Vehicular Technology Conference*, pp. 1076-1080, 1996.

[25] J.H. Winters, J. Salz, R.D. Gitlin, "The impact of Antenna Diversity on the Capacity of Wireless Communication Systems", *IEEE Transactions on Communications*, Vol. 42, No. 2/3/4, pp. 1740-1751, February/March/April 1994.

[26] B. Hagerman, S. Mazur, "Adaptive antennas in IS-136", *IEEE Vehicular Technology Conference*, pp. 2282-2286, 1998.

[27] P. Petrus, R.B. Ertel, J.H. reed, "Capacity Enhancement Using Adaptive Array in an AMPS System", *IEEE Trans. on Vehicular Technology*, Vol. 47, No. 3, pp. 717-727, August 1998.

[28] Ho, M-J., Stüber, G.L., Austin, M.D., "Performance of Switched-Beam Smart Antennas for Cellular Radio Systems", *IEEE Trans. on Vehicular Technology*, Vol. 47, No. 1, pp. 10-19, February 1998

[29] R. French, "The Effect of Fading and Shadowing on Channel reuse in Mobile Radio," *IEEE Trans. on Vehicular Technology*, Vol. 28, No. 4, pp. 171-181, August 1979.

[30] D.C. Cox, "Co-channel Interference Considerations in Frequency Reuse Small Coverage Area Radio Systems," *IEEE Trans. on Communications*, Vol. 30, pp. 135-142, January 1982.

[31] R. Muammar and S.C. Gupta, "Cochannel Interference in High Capacity Mobile Radio Systems," *IEEE Trans. on Communications*, Vol. 30, pp. 1973-1982, August 1982.

[32] M-S Alouini and A.J. Goldsmith, "Area Spectral Efficiency of Cellular Mobile Radio Systems," *IEEE Trans. on Vehicular Technology*, Vol. 48, No. 4, pp. 1047-1066, July 1999.

[33] G.L. Stüber, *Principle of Mobile Communication*, Kluwer, 1996.

[34] D.C. Cox, R. Morris, A. Norris, "800 MHz Attenuation Measured in and around Suburban Houses," *AT&T Bell Laboratories Technical Journal*, Vol. 673, No. 6, July-August 1984.

[35] H. Hashemi, "The Indoor Radio Propagation Channel," *Proceedings of the IEEE*, Vol. 81, No. 7, pp. 943-968, July 1993.

[36] Abu-Dayya, A.A., Beaulieu, N.C., "Outage Probabilities in the Presence of Correlated Log-normal Interferers", *IEEE Trans. on Vehicular Technology*, pages 164-173, vol. 43, No. 1, February 1994.

[37] C-L Ho, "Calculating the Mean and Variance of Power Sums with Two Log-Normal Components," *IEEE Trans. on Vehicular Technology*, Vol. 44, No. 4, pp. 756-762, November 1995.

[38] S.C. Schwartz, Y.S. Yeh, "On the distribution function and moments of power sums with log-normal interferers", *Bell System Technical Journal*, vol. 61, pp. 1441-1462, September 1982.

[39] S. Y. Seidel, T.S. Rappaport, "914 MHz Path Loss Prediction Models for Indoor Wireless Communications in Multifloored Buildings", *IEEE Trans. on Antennas and Propagation*, Vol. 40, No. 2, pp. 207-217, February 1992.

[40] K.S. Butterworth, K.W. Sowerby, A.G. Williamson, "Base Station Placement For Inbuilding Mobile Communication Systems to Yield High Capacity and Efficiency," accepted for publication in *IEEE Trans. Communications*.

[41] P. Cardieri, T.S. Rappaport, "Statistics of The Sum of Lognormal Variables in Wireless Communications", *50th IEEE Vehicular Technology Conference*, pp. 1823-1827, May 2000.

[42] P. Cardieri, T.S. Rappaport, "Statistics Analysis of Co-channel Interference in Wireless Communications Systems", accepted for publication in *Wireless Communications and Mobile Computing Journal*, published by John Wiley & Sons, Inc..

[43] P. Cardieri, T.S. Rappaport, "Combined Effects of Narrowbeam Antennas and Fractional Loading Factor in Forward Link Cellular Communication Systems", *49th IEEE Vehicular Technology Conference*, May 1999.

[44] A. Safak, "Statistical Analysis of the Power Sum of Multiple Correlated Log-Normal Components", *IEEE Trans. on Vehicular Technology*, pages 58-61, vol. 42, No. 1, February 1993.

[45] R.B. Ertel, J.H. Reed, "Generation of two equal power correlated Rayleigh fading envelopes" *IEEE Communications Letters*, Vol. 2, No. 10, pp. 276-278, October 1998.

[46] A.F. Naguib, A.Paulraj, T. Kailath, "Capacity Improvement with Base-Station Antenna Arrays in Cellular CDMA" *IEEE Trans. on Vehicular Technology*, vol.VT-43, No. 3, pp. 691-698. August 1994.

[47] J. Zander, "Performance of Optimum Transmitter Power Control in Cellular Radio Systems", *IEEE Trans. on Vehicular Technology*, vol.VT-41, No. 1, pp. 57-62, February 1992.

[48] M. Frullone, C. Passerini, P. Grazioso, G. Riva, "Advanced Frequency Planning Criteria for Second Generation Cellular Radio Systems", *ICT 96*, Istambul, April 1996.

[49] M. Frullone, C. Passerini, P. Grazioso, G. Riva, "Usage of Adaptive Arrays to Solve Resource Planning Problems", *46th IEEE Vehicular Technology Conference*, pp. 527-530, 1999.

[50] M. Frullone, G. Riva, Paolo Grazioso, G. Falciasecca, "Advanced Planning Criteria for Cellular Systems", *IEEE Personal Communications*, pp. 10-15, December 1996.

[51] Jovanović, V.M., Gazzola, J., "Capacity of Present Narrowband Cellular Systems: Interference-Limited or Blocking-Limited", *IEEE Personal Communications*, pp. 42-51, December 1997.

[52] V.H. MacDonald, "The Cellular concept", *Bell System Technical Journal*, vol. 58, pp. 15-41, January 1979.

[53] J.F. Whitehead, "Signal-Level-Based Dynamic Power Control for Co-channel Interference Management", *IEEE Vehicular Technology Conference*, p. 499-502, 1993.

[54] F.R. Gantmacher, *The Theory of Matrices*, New York: Chelsea, 1974.

[55] J. Zander, "Distributed Co-channel Interference Control in Cellular Radio Systems", *IEEE Transactions on Vehicular Technology*, Vol. 41, No. 3, pp. 305-311, August 1992.

[56] S.A. Grandhi, R. Vijayan, D.J. Goodman, "Distributed Power Control in Cellular Radio Systems", *IEEE Trans. on Communications*, Vol. 42, No. 2/3/4, pp. 226-228, February 1994.

[57] G.J. Foschini, Z. Miljanic, "A Simple Distributed Autonomous Power Control Algorithm and its Convergence," *IEEE Trans. on Vehicular Technology*, pp. 641-646, Vol. 42, No. 4, November 1993.

[58] A. Lozano, *Integrated Dynamic Channel Assignment and Power Control in Mobile Wireless Communication Systems*, Ph.D. Dissertation, Stanford University, 1998.

[59] H. Panzer, R. Beck, "Adaptive Resource Allocation in metropolitan Area Cellular Mobile Radio", *40th IEEE Vehicular Technology Conference*, 1990, pp 638-645.

[60] I. Katzela, M. Naghishneh, "Channel Assignment Schemes for Cellular Mobile Telecommunications Systems", *IEEE Personal Communications Magazine*, 1997.

[61] R. Beck, H. Panzer, "Strategies for Handover and Dynamic Channel Allocation in Micro-Cellular Mobile Radio Systems", *39th IEEE Vehicular Technology Conference*, 1989, pp 178-185.

[62] J.F. Whitehead, "Performance and Capacity of Distributed Dynamic Channel Assignment and Power Control in Shadowing Fading", *IEEE International Conference on Communications*, 1993, pp. 910-914.

[63] A. Gamst, "Some Lower Bounds for a Class of Frequency Assignment Problems", *IEEE Trans. on Vehicular Technology*, vol.VT-35, pp. 8-14, February 1986.

[64] J. Zander, "Asymptotic Bounds on the Performance of a Class of Dynamic Channel Assignment Algorithms", *IEEE Journal on Selected Areas in Communications*, vol. JSAC-11, No. 6, pp. 926-933, August 1993.

[65] S.W. Halpen "Reuse Partitioning in Cellular Systems", *33th IEEE Vehicular Technology Conference*, 1983, pp 322-327.

[66] M. Serizawa, D. Goodman, "Instability and Deadlock of Distributed Dynamic Channel Allocation", *IEEE Vehicular Technology Conference*, pp.528-531, 1993.

[67] Y. Furuya, Y. Akaiwa, "Channel Segragation, a Distributed Adaptive Channel Allocation Scheme for Mobile Communication Systems", *IEICE Transactions*, Vol. E 74, No. 6, pp. 1531-1537, 1991.

[68] Y. Akaiwa, H. Andoh, "Channel Segragation - A Self-Organized Dynamic Channel Allocation Method: Application to TDMA/FDMA Microcellular System", *IEEE Journal on Selected Areas in Communications*, Vol. 11, No. 6, pp. 949-954, August 1993.

[69] G.Z. Percia, J.R.B. de Marca"A Simulation Study of the Combined Use of Power Control and Dynamic Channel Allocation Schemes", *47th IEEE Vehicular Technology Conference*, 1997, pp 1470-1474.

[70] R. Valenzuela, "Dynamic Resource Allocation in Line-of-Sight Mocrocell", *IEEE Journal on Selected Areas in Communications*, Vol. 11, No. 6, pp. 941-948, August 1993.

[71] G.J. Foschini, Z. Miljanic, "Distributed Autonomous Wireless Channel Assignment Algorithm with Power Control", *IEEE Trans. on Vehicular Technology*, vol.VT-44, No. 3. pp. 420-429, August 1995.

[72] S. Ni, "Distributed Channel Allocation Algorithm with Power Control", *IEEE 1997 PIRMC*, pp. 406-410.

[73] L.J. Cimini, G.J. Foschini, C-L, I., "Call Blocking Performance of Distributed Algorithms for Dynamic Channel Allocation in Microcells", *International Conference on Communications*, pp. 1327-1332, 1992.

[74] Y. Argyropoulos, S. Jordan, S.P.R. Kumar, "Dynamic Channel Allocation in Interference-Limited Cellular System wiht Uneven Traffic Distribution", *IEEE Trans. on Vehicular Technology*, vol.VT-48, No. 1, pp. 224-232, January 1999.

[75] F. Rashid-Farrohki, L. Tassiulas, K.J. Ray Liu, "Joint Optimal Power Control and Beamforming in Wireless Networks Using Antenna Arrays" *IEEE Trans. on Vehicular Technology*, vol.VT-46, No. 10, pp. 1313-1324, October 1998.

[76] N. Gerlich, M. Tangemann, "Towards a Channel Allocation Scheme for SDMA-based Mobile Communication Systems", *Research Report No. 104*, Institute of Computer Science, University of Würzburg, Denmark, February 1995.

[77] F. Piolini, A. Rolando, "A Channel assignment algorithms for SDMA systems" *1997 IEEE International Conference on Personal Wireless Communications*, pp. 95-99

[78] L. Chen, H. Murata, S. Yoshida, S. Hirose, "A Dynamic Channel Assignment Algorithm for Cellular System with Adaptive Array Antennas", *IEEE Vehicular Technology Conference*, 1999.

[79] T. Ohgane, Y. Ogawa, K. Itoh, "A Study on a Channel Allocation Scheme with an Adaptive Array in SDMA", *47th IEEE Vehicular Technology Conference*, 1997, pp 725-729.

[80] H-C. Lin, "Spatial Correlations in Adaptive Arrays", *IEEE Trans. on Antennas and Propagation*, Vol. AP-30, No. 2, pp. 212-223, March 1982.

[81] M. Karlsson, *Combined Interference-Based DCA & SDMA in a Narrow lobe Cellular System*, Master of Science Thesis, Royal Institute of Technology, Sweden, 1998.

[82] J.C.-I. Chuang, "Autonomous Adaptive Frequenct Assignment For TDMA Portable Radio Systems," *IEEE Transactions on Vehicular Technology*, Vol. 40, No. 3, pp. 627-635, August 1991.

[83] R. Peterson, K. Cutts, J. Haug, "System performance prediction for personal communication systems," *IEEE* 45^{th} *Vehicular Technology Conference*, pp. 749 -753, 1995.

[84] J.H.Winters, C.C. Martin, N.R. Sollemberger, "Forward Link Smart Antennas and Power Control for IS-136: Capacity Increase," *IEEE* 48^{th} *Vehicular Technology Conference*, pp. 2121-2127, 1998.

[85] G.V. Tsoulos, "Experimental and theoretical capacity analysis of space-division multiple access (SDMA) with adaptive antennas," *IEE Proc. Communications*, Vol. 146, No. 5, pp. 307-311, October 1999.

[86] C. Hartman, "Hierarchical DCA in SDMA Systems - Variations and Performance Comparison," *IEEE* 50^{th} *Vehicular Technology Conference*, pp. 721-725, 2000.

[87] A.M. Law, W.D. Kelton, *Simulation modeling and analysis*, New York: McGraw-Hill, 1982.

[88] M. M-L. Cheng, J. C-I Chuang, "Performance Evaluation of Distributed Measurement-based Dynamic Channel Assignment in Local Wireless Systems," *IEEE J. Selected Areas on Communications*, Vol 14, No. 4, pp. 698-710, May 1996.

[89] T. Kanai, "Autonomous Reuse Partitioning in cellular Systems," *IEEE 42th Vehicular Technology Conference*, pp. 782-785, 1992.

[90] M. Andersin, Z. Rosberg, J. Zander, "Distributed Discrete Power Control in Cellular PCS," *Wireless Personal Communications*, vol. 6, No. 3, pp. 211-231, March 1998.

[91] S.C. Borst, S.A. Grandhi, C.L. Kahn, K. Kumaran, B.D. Lubachevsky, D.M. Sand, "Wireless Simulation and Self-Organizing Spectrum Management," *Bell Labs Technical Journal*, pp. 81-98, Summer 1997.

[92] L. Bigler, "Performance Evaluation if Switched Beam Antennas and Downlink Power Control for IS-136," *1st Annual UCSD Conference on Wireless Communications*, pp. 172-175, 1998.

[93] C.C. Martin, N.R. Solleberger, J.H. Winters, "Field Test Results of Downlink Smart Antennas and Power Control for IS-136," *IEEE 49th Vehicular Technology Conference*, pp. 453-457, 1999.

[94] G.M. Galvan-Tejada, J.G. Gardiner, "Theoretical Blocking Probability for SDMA," it IEE Proc. Communications, Vol. 146, No. 5, pp. 303-306, October 1999.

[95] M. Karlsson, *Combined Interference Based DCA abd SDMA in a Narrow Lobe Cellular System*, Master Thesis, Royal Institute of Technology, KTH, Sweden, 1998.

[96] C. Hartman, "Hierarchical DCA in SDMA Systems - Variations and Performance Comparison," *IEEE* 50^{th} *Vehicular Technology Conference*, pp. 721-725, 2000.

[97] C. Hartman, "Dynamic Channel Allocation in Cellular Mobile Communication Systems with SDMA," *Proc EPMCC' 99*, 1999.

[98] Special Issue on Space Division Multiple Acess, *Wireless Personal Communications*, Kluwer Academic Publisers, Vol. 11, No. 1, October 1999.

[99] L.F. Fenton,"The Sum of Log-Normal Probability Distributions in Scatter Transmission Systems", *IRE Transactions on Communications Systems*, pages 57-67, March 1960.

[100] M.D. Austin, G.L. Stuber,"In-Service Signal Quality Estimation for TDMA Cellular System," *Kluwer Wireless Personal Communications*, Vol. 2, pp. 245-254, 1995.

[101] , M. Andersin, N.B. Mandayam, R.D. Yates, "Subspace Based Estimation of the Signal to Interference Ration for TDMA Cellular Systems," *IEEE* 46^{th} *Vehicular Technology Conference*, pp. 1155-1159, 1996.

[102] J.C.-I. Chuang, N. Sollenberger, "Uplink Power Control for TDMA Portable Radio Channels," *Proc. of the IEEE International Conference on Communications*, 1993.

Vita

Paulo Cardieri was born in São Paulo, Brazil, on March 15, 1964. He received the B.S. degree in Electrical Engineering from the School of Engineering Mauá, Brazil, in 1987, and the M.S. degree in Electrical Engineering from the State University of Campinas, Brazil, in 1994, where he was involved with adaptive equalization applied to digital cellular systems. Since 1987, he has been with the Research Center and Development of the Brazilian Telecommunications Company (CPqD - TELEBRÁS) (on leave), where he has been involved with cellular communications.

In 1996, he joined the Mobile and Portable Radio Research Group (MPRG) at Virginia Polytechnic Institute and State University (Virginia Tech), where he pursued his Doctoral degree. His research interests include adaptive antennas, spatial diversity, power control, channel allocation, system performance analysis. Mr. Cardieri is a member of Eta Kappa Nu.